AD-A048 448 CAMBRIDGE UNIV (ENGLAND) DEPT OF METALLURGY AND MAT--ETC F/G 11/6
SEGREGATION EFFECTS AND THE TOUGHNESS OF HIGH-STRENGTH STEELS.(U)
JUN 77 J Q CLAYTON, J F KNOTT DAJA37-74-C-1309
NL

UNCLASSIFIED

1 OF 3
ADA048448

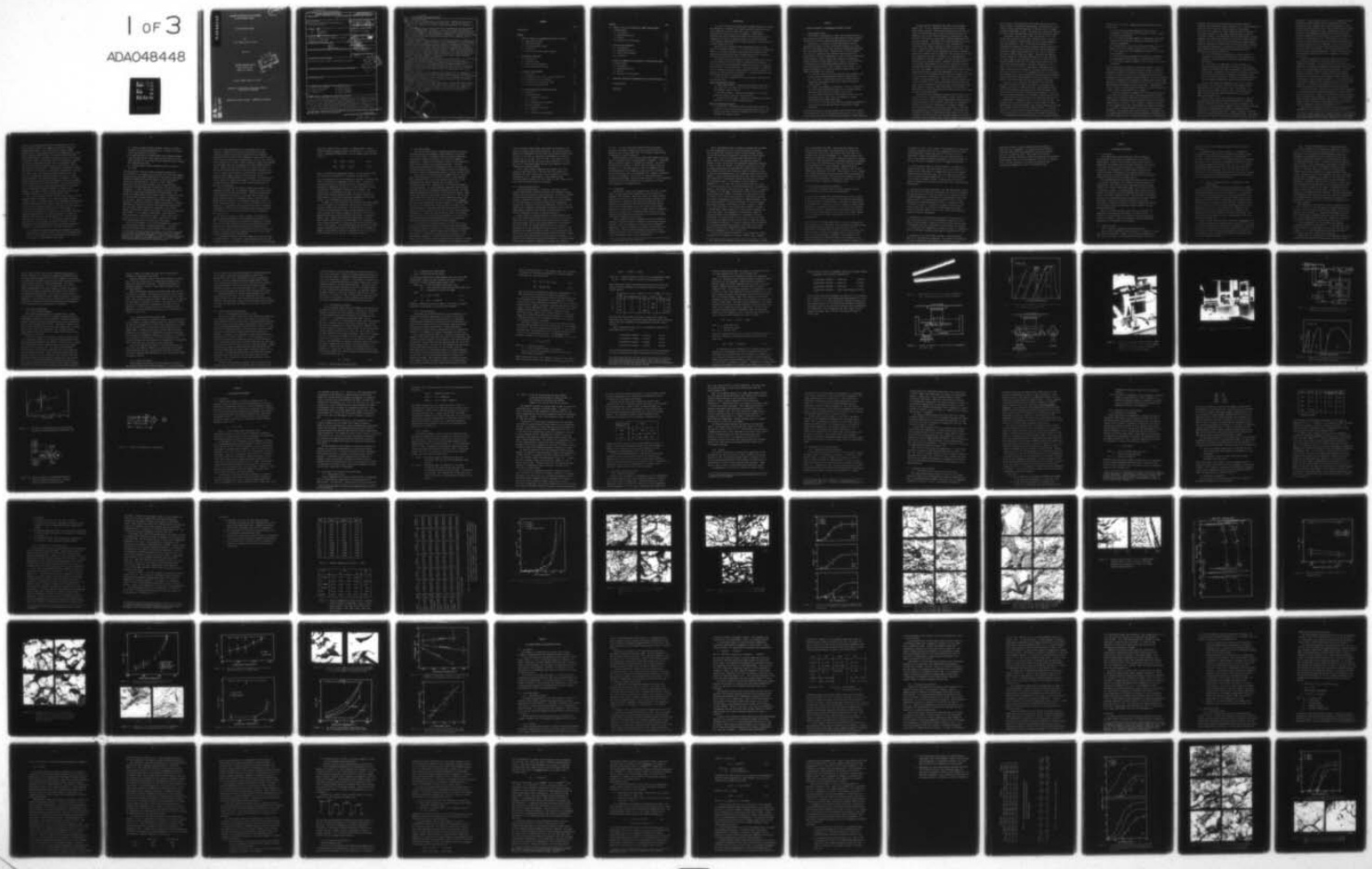

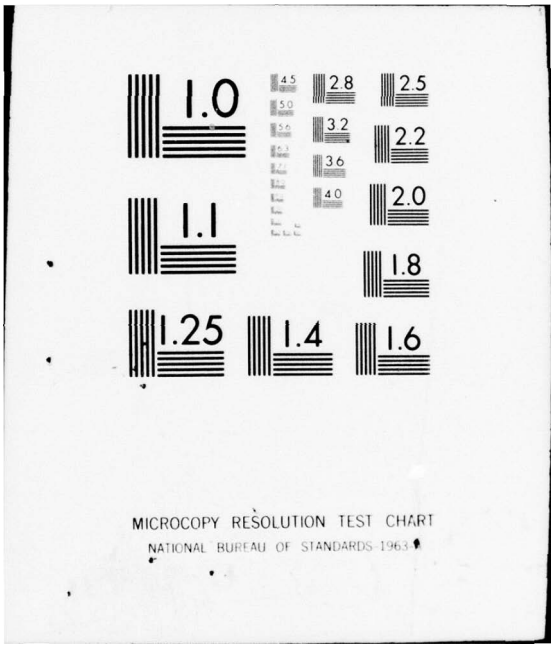
1.0
1.1
1.25
1.4
1.6
1.8
2.0
2.2
2.5
2.8
3.2
3.6
4.0
4.5
5.0
5.6
MICROCOPY RESOLUTION TEST CHART
NATIONAL BUREAU OF STANDARDS 1963-A

SEGREGATION EFFECTS AND THE TOUGHNESS OF HIGH-STRENGTH STEELS

Final Technical Report

By

J.Q. Clayton and J.F. Knott

June 1977

EUROPEAN RESEARCH OFFICE
United States Army
London W.1., England

Contract Number DAJA37-74-C-1309

390816

Department of Metallurgy and Materials Science
University of Cambridge

Approved for public release; distribution unlimited

Unclassified

SECURITY CLASSIFICATION OF THIS PAGE (When Data Entered)

REPORT DOCUMENTATION PAGE

READ INSTRUCTIONS BEFORE COMPLETING FORM

1. REPORT NUMBER

2. GOVT ACCESSION NO.

3. RECIPIENT'S CATALOG NUMBER

4. TITLE (and Subtitle)
Segregation Effects and the Toughness of High-Strength Steels.

5. TYPE OF REPORT & PERIOD COVERED
Final Technical Report
1 Oct 1973-30 Sept. 1976,

6. PERFORMING ORG. REPORT NUMBER

7. AUTHOR(s)
J.D. Clayton
J.F. Knott

8. CONTRACT OR GRANT NUMBER(s)
DAJA37-74-C-1309

9. PERFORMING ORGANIZATION NAME AND ADDRESS
Department of Metallurgy & Materials Science
University of Cambridge,
Cambridge CB2 3QZ, U.K.

10. PROGRAM ELEMENT, PROJECT, TASK AREA & WORK UNIT NUMBERS
61102A 1T161102B33D
00 398

11. CONTROLLING OFFICE NAME AND ADDRESS
USA RSG
BOX 65
FPO NY 09510

12. REPORT DATE
JUNE 1977

13. NUMBER OF PAGES
199 P.

14. MONITORING AGENCY NAME & ADDRESS (if different from Controlling Office)

15. SECURITY CLASS. (of this report)
Unclassified

15a. DECLASSIFICATION/DOWNGRADING SCHEDULE

16. DISTRIBUTION STATEMENT (of this Report)
Approved for public release; distribution unlimited

17. DISTRIBUTION STATEMENT (of the abstract entered in Block 20, if different from Report)

18. SUPPLEMENTARY NOTES

19. KEY WORDS (Continue on reverse side if necessary and identify by block number)

(U) Steel, High Strength	(U) Steel, Nickel
(U) Fracture Toughness	(U) Steel, Antimony
(U) Embrittlement	(U) Steel, Phosphorus
(U) Austenite	(U) Steel, Manganese

20. ABSTRACT (Continue on reverse side if necessary and identify by block number)

A study has been made of impurity segregation in low alloy steels and iron alloys. Various problems of practical importance have been investigated together with some of the more fundamental aspects of segregation. The general approach has been to employ simplified alloy compositions and to combine mechanical testing with Auger electron spectroscopy (AES) and scanning electron microscopy.

Segregation occurring during the austenitizing cycle has been examined in commercial and high-purity Ni-Cr steels. Low concentrations of P, Sb and Sn do not appear to embrittle as-quenched commercial Ni-Cr or Ni-Cr-Mo steels. By

over

DD FORM 1 JAN 73 1473 EDITION OF 1 NOV 65 IS OBSOLETE

Unclassified

SECURITY CLASSIFICATION OF THIS PAGE (When Data Entered)

390816

20. Abstract continued.

employing higher P concentrations it is shown that P segregation occurs at low austenitizing temperatures in Mn-free Ni-Cr steels. The main effect of Mn additions is to decrease the observed temperature dependence of P segregation in austenite.

Overheating and related effects have been investigated by fracture toughness testing and metallographic techniques. In the steels studied the effects of austenitizing temperature and overheating on the as-quenched toughness are small. Once S enters solution at high austenitizing temperatures, the precipitation of MnS at grain boundary sites during cooling is difficult to suppress. This is shown to be consistent with the observed fracture modes and the expected rates of S diffusion in austenite.

Embrittlement produced by tempering at 350C has been studied in commercial and high-purity steels. Susceptible steels show no embrittlement in the as-quenched condition, but on tempering at 350C the transition temperature increases and the brittle fracture mode changes from quasi-cleavage to intergranular cleavage. It is shown that in high-purity steels the tendency for intergranular cleavage at 350C increases with P content, and AES analyses of commercial steels show that P is present on the intergranular fracture surfaces. The critical embrittlement mechanism occurs at 350C and the results support the view that 350C embrittlement is primarily due to carbide rejection of impurities or to carbide formation at impurity embrittled interfaces. Variations in Sb content have no measurable effect on 350 embrittlement susceptibility.

Temper embrittlement has been investigated in Ni-Cr-Sb steels. It is shown that susceptibility increases with Ni content and that Ni and Sb segregate at equilibrium on the grain boundaries. Impurity-alloying element interactions are discussed in detail and it is suggested that bulk impurity content is an important variable in systems where metalloid impurities interact with alloying elements. The multilayer segregation behaviour of Sb is shown to be different from that of the nonmetallics, P and S, where the segregation limit is one monolayer or less.

A study of Sb, Ni and S segregation at free surfaces has been presented. It is shown that Sb exhibits a multilayer adsorption behaviour on Fe. Surface site competition effects between Sb and S are evaluated and compared with other studies. The Sb surface segregation kinetics are shown to be in agreement with theory. Ni segregation is observed, but no strong Ni-Sb interaction occurs within the temperature range of the experiments.

A further investigation of temper embrittlement in Ni-Cr-Mn-P steels has been included. Susceptibility to temper embrittlement increases with both Mn and P content. In the presence of Mn, steels with low P contents (eg. 70ppm) are highly susceptible to temper embrittlement. AES studies show that Mn does not measurably enhance P segregation and the embrittlement induced by Mn is attributed to Mn segregation.

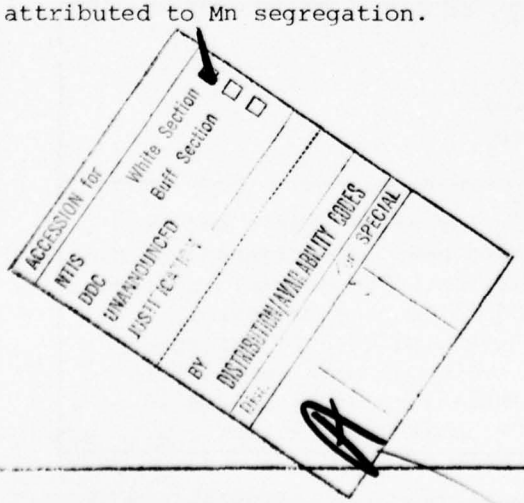

CONTENTS

		Page
INTRODUCTION		6
CHAPTER		
1.	PREVIOUS RESEARCH ON INTERGRANULAR COHESION IN STEELS	
	1.1 Temper Embrittlement	
	1.2 350C Embrittlement	17
	1.3 As-Quenched Embrittlement	18
	1.4 Overheating	19
	1.5 Conclusions and the Present Research	21
2.	EXPERIMENTAL PROCEDURES	
	2.1 Introduction	24
	2.2 Mechanical Tests	24
	2.3 Other Tests and Equipment	27
	2.4 Auger Electron Spectroscopy	29
3.	AS-QUENCHED EMBRITTLEMENT	
	3.1 Introduction	43
	3.2 The Effects of Sb in Ni-Cr and Ni-Cr-Mo Steels	44
	3.3 The Effect of P in Ni-Cr Steels	47
	3.4 The Effect of P in Ni-Cr-Mn Steels	49
	3.5 Discussion and Conclusions	50
4.	350C EMBRITTLEMENT AND OVERHEATING EFFECTS	
	4.1 Introduction	74
	4.2 350C Embrittlement	74
	4.2.1 Experimental Details	74
	4.2.2 Results	74
	4.2.3 Discussion and Conclusions	78
	4.3 Overheating Effects	81
	4.3.1 Experimental Details	81
	4.3.2 Results	83
	4.3.3 Discussion and Conclusions	86

CHAPTER		Page
5.	EFFECT OF NICKEL AND ANTIMONY ON TEMPER EMBRITTLEMENT IN ALLOY STEELS	
	5.1 Introduction	114
	5.2 Experimental Details	114
	5.3 Results	115
	5.4 Discussion and Conclusions	117
6.	FREE SURFACE SEGREGATION	
	6.1 Introduction	138
	6.2 Experimental Details	139
	6.3 Results and Discussion	142
	6.4 Conclusions	150
7.	EFFECTS OF MANGANESE AND PHOSPHORUS ON TEMPER EMBRITTLEMENT IN ALLOYS STEELS	
	7.1 Introduction	169
	7.2 Experimental Details	169
	7.3 Results	170
	7.4 Discussion and Conclusions	172
8.	CONCLUDING REMARKS AND RECOMMENDATIONS FOR FURTHER RESEARCH	190
	ACKNOWLEDGEMENTS	193
	REFERENCES	194

INTRODUCTION

It is well recognised that, during heat treatment, impurities in steels may segregate to interfaces, particularly austenite or prior austenite grain boundaries, with the result that there is a decrease in intergranular cohesion and a loss in toughness. Other material properties may also be affected and recent studies show that impurity segregation can lead to a reduced resistance to failure by fatigue {1-3}, hydrogen embrittlement {4-5}, stress corrosion {6},or fracture at elevated temperatures {7-8}.

Impurities may be present at grain boundaries either in solute form or as insoluble particles. In low alloy steels, particle segregation appears to be largely confined to the problem of overheating, which involves precipitate dissolution and redistribution, and has features substantially different from those of solute segregation.

In contrast to particle segregation, several problems seem to arise from the segregation of solute atoms at austenite grain boundaries. In past years the precise mechanisms responsible for solute segregation have successfully eluded researchers. The general problem in commercial steels is complicated because impurity elements are often individual in response and cannot be treated collectively; alloying elements may also exert pronounced effects on segregation.

In this research, segregation has been tentatively separated into the following areas:

Brittle Intergranular Fracture

1. Temper Embrittlement - observed after quenching, tempering at a high temperature (eg. 650C), then cooling or holding within the embrittlement range (375C-575C).
2. 350C Embrittlement - observed after quenching, then lightly tempering, usually within the range 250C-400C.
3. As-Quenched Embrittlement - observed in untempered steels which fracture in a brittle (smooth faceted) manner.

Ductile Intergranular Fracture

4. Overheating - intergranular facets containing microvoids are observed in steels which have been heated well above the A_3; the fracture mode may be present in quenched steels and may persist throughout the tempering range.

CHAPTER 1

PREVIOUS RESEARCH ON INTERGRANULAR COHESION IN STEELS

1.1. Temper Embrittlement

Past research on segregation in steels has concentrated mainly in this area and over recent years increased efforts and vastly improved techniques have led to a much better understanding of this problem.

Historically, the problem of temper embrittlement has been recognised for almost a century, and wherever possible alloy steels have been water quenched or rapidly cooled from tempering temperatures above the embrittlement range. Progress prior to 1944 was hampered by a failure to appreciate that mechanical tests may need to be conducted over a range of temperatures in order to detect susceptibility to embrittlement. Earlier testing was carried out by performing ambient temperature notched impact tests. However, Jolivet and Vidal {9} emphasised that temper embrittlement produced an increase in transition temperature rather than a change in shelf energy. In the review by Holloman {10} in 1946 the following characteristics of temper embrittlement were indicated:

(i) Fracture occurred along prior austenite grain boundaries and higher austenitizing temperatures increased susceptibility.

(ii) The change in impact transition was a suitable method of determining susceptibility and could be used to construct an 'embrittlement C-curve'.

(iii) Temper embrittlement was reversible; that is, an embrittled steel could be de-embrittled by heating above the embrittlement range and embrittled again by aging or slow cooling.

(iv) Plain carbon steels, with low Mn contents (<0.6%), were not susceptible, and in alloy steels, Mo prevented or reduced embrittlement over normal aging times.

(v) Mn, Cr, Ni and P were associated with increased susceptibility; high Mn or Cr steels were particularly susceptible to temper brittleness.

Hollomon was reluctant to accept evidence that increases in P content and austenite grain size could promote susceptibility {11,12}, however he did clarify the effects of changes during tempering on impact behaviour.

Although important experiments were about to be performed, Woodfine {13}, in 1953, published a subtle review of the temper embrittlement situation. Apart from confirming most of the previous points, he demonstrated that the shift in notched bar transition temperature was the most effective measure of susceptibility, and pointed out that earlier results based on ambient temperature tests could be misleading. The question of alloying elements had not been thoroughly examined at this stage, but it was concluded that embrittlement was largely restricted to steels containing Cr, Mn, Ni or Mo. Previously, McLean and Northcott {14} had shown that a 3%Ni steel (0.01%Cr, 0.02%P) was not susceptible and this was confirmed in other work by Woodfine {15} who showed that the susceptibility of 3%Ni steel depended on the steel's P content; at 0.13%P appreciable embrittlement was observed. Woodfine {13} also carefully reviewed the available data on impurity effects. Although it was known that Sb could produce embrittlement {9}, this was not unanimously accepted as temper embrittlement, probably because the effect was so severe (see {16}, for example). Variations in P content were known to produce corresponding changes in transition temperature {17,18} and at the time, P was the only impurity positively linked with temper brittleness (in the discussion of Woodfine's review, Carr {19} produced clear evidence of embrittlement by Sb). The review also drew attention to the work of Cohen et al. {20} who showed that embrittled commercial steels could be detected by etching in picric acid containing wetting agent (zephiran chloride); McLean and Northcott {14} subsequently showed that, for steels containing about 0.025%P, various etches based on picric acid were effective.

Even at this stage considerable evidence existed concerning the roles of Mn and Cr in temper embrittlement. Preece and Carter {21}, in one of the first studies of temper embrittlement using high-purity alloys, showed that; Fe-C and Fe-P-C alloys were not susceptible, pure Fe-Cr-C and Fe-Mn-C alloys (reported as <10ppm P, <200ppm Sn) were slightly susceptible, and Fe-Cr-P-C and Fe-Mn-P-C alloys were highly susceptible (all aged at 500C for 670hr). The results were interpreted in terms of an embrittling effect induced by Cr and Mn, possibly as thin carbide films, and the embrittlement in the Fe-Cr-C and Fe-Mn-C alloys, although slight, helped to support this hypothesis.

But the results indicated that Mn and Cr might interact with P and have the effect of promoting P embrittlement. Mn was puzzling in this respect, because apart from appearing to interact with P, it seemed to produce embrittlement itself. The authors also showed that additions of 0.5%Mo almost eliminated embrittlement in the Cr-P and Mn-P steels.

An important step was made in 1957, when Balajiva et al. {22} showed that a high-purity Ni-Cr steel (containing only C, Ni and Cr) was not susceptible to embrittlement, but that a similar commercial steel was susceptible. Then, in 1959, Steven and Balajiva {23} systematically examined the effects of specific impurity additions to Ni-Cr steels and were able to confirm that the four main impurities resulting in temper embrittlement are Sb, Sn, P and As (specimens were aged at 450C for 168hr and 1000hr). The most potent impurity was Sb, although the large effect observed with the steel reported to contain 10ppm Sb is questionable on the basis of more recent work. Alloying element contents were not varied, but Mn additions of up to 1.5% again produced increases in transition temperature (of up to 200C); also, Si (0.74%), had a small effect. Molybdenum (0.5%) was shown to restrict, but not eliminate, the impurity embrittlement in all cases (the result for P is in agreement with {21}, but Mo effects were examined again in later research and this conclusion was disputed). Mo also restricted Mn embrittlement, but no viable explanation of the effects of Mo could be made from the data available at the time.

Low {24}, in his review of 1959, pointed out that electron microscopy had failed to produce any evidence of extraneous grain boundary precipitates in embrittled steels. Metallographic etching was the only technique that directly associated embrittlement with a change occurring at the prior austenite grain boundaries. Low could find no enlightening proposals in the Russian literature prior to 1959.

Russian work was of the opinion that P played the decisive role in embrittlement in commercial steels. In 1963, Gruzin and Mural {25} indicated that the activation energy for the development of temper embrittlement (taken from mechanical test results) agreed more with that for P diffusion than for C or alloy element diffusion. In further work {26}, it was shown that Mn and Mo influence the diffusion of P in α-Fe and respectively raise or lower the bulk diffusion coefficient.

A comprehensive and important examination of the problem was made

by Low et al. {27} in 1968. Employing high-purity steels, the main results were:

(i) Ni-Cr steels containing 600ppm Sb or Sn are highly susceptible; similar steels in which either Cr or Ni is absent are much less susceptible.

(ii) Ni-Cr steel containing 600ppm P is considerably susceptible; Cr-free steel is much less susceptible, but Ni-free steel is almost as susceptible.

(iii) Susceptibility in Ni-Cr steels containing 530ppm As is not great, but is still reduced if either Ni or Cr is absent.

(iv) Plain carbon steels with 800ppm Sb and pure Ni-Cr steels are not susceptible.

(v) Ni-Cr iron containing 800ppm Sb (C<0.001%) is susceptible, but considerably less than that of a steel containing 0.4%C.

(vi) Ni-Cr steel containing 200ppm S (no Mn) is only very slightly susceptible.

Clearly differences in hardness or yield stress could be a factor in some of these observations (which are based on shifts in transition temperature), however the effects of Ni and Cr on the susceptibility of steels containing Sb and Sn were so pronounced that any hardness differences could be regarded as secondary effects. It was now accepted that solute segregation was responsible for embrittlement and this work suggested that impurities interacted with Ni and Cr in a complex manner. The implication for commercial steels was obvious - combinations of Ni and Cr should be avoided wherever possible, but if both elements are present, impurity levels should be at a minimum.

A review of the subject by McMahon {28} in 1968 brought attention to the fact that although electron microscopy had failed to detect abnormal grain boundary precipitates, Hill and Martin {29} had found that fracture in embrittled material appeared to take place along the cementite-ferrite interface. This interface is normally strong and the work suggested that temper embrittlement may operate by weakening the interfaces of cementite platelets lying along austenite grain boundaries. This prompted further work by Restaino and McMahon {30} who examined the ferrite-ferrite and ferrite-cementite interfaces in Fe-0.018%C-700ppm Sb alloy. The results showed that in the embrittled

condition (480C for 24hr) ferrite-ferrite and ferrite-cementite interfaces split open during tensile testing at 77K; in the de-embrittled condition (675C for 2min) no interface splitting was observed. AISI 3340 steel + 620ppm Sb was also examined by chemical analysis of the fracture surfaces; in the unembrittled condition no excess Sb was found; however, after embrittling (500C for 24hr) chemical analysis suggested that a 600 Å layer adjacent to the fracture surface contained 10 wt%Sb. This led the authors to conclude that during embrittlement, impurities segregated to ferrite-ferrite and ferrite-carbide interfaces (along austenite boundaries) and reduced their cohesive strength. The model postulated at this stage {28,30} was substantially one of equilibrium (or Gibbsian) segregation:

(i) The low solubility of impurities in austenite results in segregation at austenite grain boundaries; this segregation is retained in quenched material (for some reason martensite is not embrittled).

(ii) The solubility of impurities in ferrite is higher; at tempering temperatures above 600C the mobility of the impurity enables it to diffuse away from the interfaces; between 350C-575C the tendency to segregate is strong and the interfaces, particularly carbides along austenite grain boundaries, are preferred sites.

(iii) Below 350C the diffusivity is reduced and therefore quenching from the tempering temperature (>600C) prevents embrittlement.

At this time carbides were suspected to be the key to temper embrittlement, but the strong effect of alloying elements was not explained and more definitive work had yet to be performed. An important method of surface analysis - Auger electron spectroscopy (AES) - had been developed and was being applied to the temper embrittlement problem {31}.

Following the postulate that impurities segregate in austenite the question of when, during the heat treatment cycle, an impurity actually segregated became the subject of intensive research. Low and Smith {32} using quantitative chemical analysis of material dissolved from fracture surfaces found no evidence of segregation during austenitizing in Sb-doped 3340 steel; however, segregation of Sb was found to occur during tempering in the embrittlement range. The carbides were found to be rich in Cr and low in Ni compared with the alloy base

composition. Further research by Low et al. {33} employing both AES and fracture surface chemical analysis confirmed their earlier findings and it was concluded that no general segregation of either alloying or impurity elements (Sb) to grain boundaries occurred during austenitizing or tempering (at 650C). Tempering at 650C was shown to produce a less homogeneous distribution of alloying elements; ferrite was depleted in Cr and enriched in Ni, and the carbides were enriched in Cr but depleted in Ni. Both Ni and Sb were shown to segregate to grain boundaries during the embrittling treatment and an interaction between the two was suggested. It is worth noting that the authors found that an almost linear relationship existed between the excess weight of Sb present on the fracture surfaces and the ductile brittle transition temperature; a similar relationship was also observed by Viswanathan {34} for P segregation in embrittled Ni-Cr-P steel.

Recent French research {35-37} using Auger analysis and ion-backscattering techniques also queried the hypothesis that Sb segregated in austenite. In this case Mn steels containing up to 1300ppm Sb were studied and segregation of Mn and Sb was found to occur only in the α range during the embrittling treatments. The alloy-impurity interaction between Mn and Sb resembles that observed previously between Ni and Sb. By employing a recrystallization treatment it was shown that ferrite boundaries may be embrittled in a similar manner to prior austenite boundaries. It was suggested that in quenched and tempered steels segregation occurs at all high-angle boundaries, but austenite grain boundary fractures are favoured energetically because of their geometry and relative smoothness.

In 1972 the consensus of opinion favoured equilibrium segregation as the underlying cause of temper embrittlement, but direct proof of this was still scarce. Because of microstructural changes occurring during isothermal aging, mechanical tests alone could not distinguish between transient effects and stable embrittlement. By 1974 grain boundary analysis techniques had confirmed the equilibrium nature of impurity segregation in temper embrittlement {37-39}.

Some important aspects of the effect of Mo were examined by Schulz and McMahon {40} who showed that in the step-cooled condition* Mo

---

* Hold 1hr at 593C, furnace cool to 538C, hold 15hr, cool to 524C, hold 24hr, cool to 496C, hold 48hr, cool to 468C, hold 72hr. (accelerates embrittlement compared with isothermal treatment for the same time).

virtually eliminated embrittlement due to 600ppm Sb, Sn or As in AISI 3340 steel (0.6%Mo), but appeared to have little effect on 600ppm P embrittlement. Also, after aging at 480C for 1000hr, susceptibility in the Sb-bearing steel increased dramatically to a high level, suggesting that the effect of Mo was to retard rather than prevent embrittlement. The effects are possibly due, at least in part, to an effect of Mo on the diffusion rates of the impurities. Bearing in mind that P diffuses much faster than Sb, the apparent effect, after an arbitrary heat treatment (such as step-cooling), could be much greater for Sb than for P. Assuming that the segregation kinetics will vary with $(Dt)^{\frac{1}{2}}$ (where D is the diffusion coefficient), the effect of 0.5%Mo, based on the previously mentioned diffusion data {26}, would be to retard the P kinetics by about a factor of 4 at 480C. Schulz and McMahon also examined segregation in austenite, and Auger analyses showed that both P and S were present on the grain boundaries of brine-quenched steels, but no Sb was found. Besides discovering that Bi, Se, Ge and Te were all potentially embrittling, it was observed that 0.7%Mn produced strong embrittlement in a Mo-free steel (20ppm P; aged 300hr at 480C), consistent with the earlier findings of Preece and Carter {21}, and Steven and Balajiva {23}.

Once it was established that Sb, the most potent impurity, did not segregate except on tempering in the embrittling range, attention turned to theories of carbide growth. Schulz and McMahon had previously considered the hypothesis that impurity atoms could be rejected and piled up ahead of growing carbides and that carbide rejection together with equilibrium segregation may account for embrittlement (the relatively low susceptibility of carbon-free alloys implied that carbon played an important role). This precise hypothesis was carefully examined in the work of Rellick and McMahon {41}; Fe-0.04%C alloys were doped with either Sb, Sn, P or As and heat-treated to produce large carbides. The occurrence of interface cracking in tensile specimens was then examined quantitatively following low-temperature straining to a fixed extension (4%). The tests revealed that:

(i) Furnace cooling from the austenitizing temperature produced carbide-ferrite interface cracks in the Sb, Sn and As-doped alloys, but not in the P-doped alloy, even when cooling was interrupted by holding in the embrittlement range (480C).

(ii) Heating to 650C and water quenching eliminated interface cracking in the three embrittled alloys; cracking now occurred within the carbides in all alloys.

(iii) Reheating within the embrittlement range produced interface cracking in all alloys; these cracks were not observed at the large carbides, but on the ferrite grain boundaries which contained fine carbide precipitates.

(iv) Prolonged aging at 480C eliminated interface cracking in all alloys.

This embrittlement could not be due to equilibrium segregation; it was reversible, but unstable, and the time to reach full embrittlement seemed much less than simple diffusivity (of the impurity) would permit. The model developed by the authors, based on solute partitioning,* closely fits the observations; briefly; in Step 1 impurity partitioning occurs at large carbides; Step 2 produces carbide dissolution and outward diffusion of impurities (via matrix and grain boundaries); in Step 3 reprecipitation results in embrittled ferrite boundaries, but prolonged holding permits de-embrittlement. The absence of P embrittlement during furnace cooling is presumed to be due to its significantly greater diffusivity in ferrite, compared with Sb, Sn and As. However, the model of Rellick and McMahon cannot be transposed to describe the problem of temper embrittlement; relatively short times are required to reach the fully embrittled condition and the 'over-aging' effects emphasize the important of the alloying elements, particularly Ni and Cr which appear to slow down and stabilize embrittlement. At low tempering temperatures, where diffusion is restricted largely to interstitial elements, a model based on solute partitioning may be applicable; the authors suggest that one-step (350C) embrittlement could be largely due to this effect.

In recent work McMahon et al. {42} have examined the relevance of the carbide rejection model to temper embrittlement. In essence, electron microscopy studies in Fe+Ni+Cr+80ppm C have enabled the

---

* In the case of carbide growth, the solubility of the solute impurity in the carbide is considered negligible. If the diffusivity of the impurity in the matrix is low, compared with carbon, a high concentration (partitioning) ahead of the interface may result. Similarly, trapped solute may be partitioned behind the carbide interface.

volume of carbide precipitated, for a given aging time, to be estimated. Assuming total rejection of Ni and Sb to the grain boundaries an upper bound could be established for the expected concentrations of Ni and Sb on the boundaries. However Auger analyses seem to show that while the Ni concentration is close to that predicted, the Sb concentration is about an order of magnitude higher than predicted. It would appear then that large amounts of Sb must segregate from the matrix. McMahon {43,44} has shown that the ε-phase, (Fe, Ni)Sb, is more stable than FeSb and that Ni lowers the chemical potential of Sb in Fe, so that Sb from the matrix, by diffusing up a Ni concentration profile, diffuses down a chemical potential profile and thus stabilizes the carbide-rejected Ni at the boundary. On this basis the role of carbides in temper embrittlement is to provide an easy means of achieving a grain boundary Ni excess, thereby accelerating the approach to equilibrium.

One of the most detailed studies of temper embrittlement was conducted by Mulford {39}, who examined P segregation in Ni-Cr steels by mechanical testing and Auger analysis. Besides confirming that P and Ni segregate at equilibrium, it was shown that Ni and Cr only exert a moderate effect on P segregation (plain C steels, Mn free, showed about half the level of P segregation observed in 3.5Ni-1.7Cr steels, containing 0.06%P). From a study of the effects of Ni and Cr separately, it appears that Cr may play the major part in increasing P segregation, and thus the Cr-P interaction seems stronger than the Ni-P interaction (this is consistent with the earlier findings of Low et al. {27}).

The ability of very low C steels (0.008%C+3.5Ni+1.4Cr+Sb) to undergo temper embrittlement has been demonstrated by Ohtani et al. {45}. For both recrystallized and quenched and tempered (a lath-type structure with rough boundaries) material they showed that Ni and Sb build-up in the grain boundary and that after prolonged aging, a stable state is reached. The build-up seemed to occur in an indentical way at various aging temperatures suggesting that the Ni and Sb grain boundary concentrations are interrelated.

A thermodynamic analysis of solute interactions has been provided by Guttmann {46,47}. He considers a three-component system where two segregating solutes (eg. Ni and Sb) interact only within a two-dimensional

phase which represents the interface. The model assumes a regular solution enabling a surface interaction coefficient, α', to be derived which is independent of temperature. The free energy changes are then given as:

$$\Delta G_{13} = \Delta G^{o}_{13} + \alpha'_{12} N^{s}_{2} \qquad (1(a))$$

$$\Delta G_{23} = \Delta G^{o}_{23} + \alpha'_{12} N^{s}_{1} \qquad (1(b))$$

where 1,2 represent the segregating solutes, 3 is the solvent, and N^{s} the interfacial concentration (α' is negative for attraction).

Thus the driving-force for the segregation of component 1 depends on the surface concentration of component 2 and vice versa. Although the precise applicability of the model has yet to be determined (eg. α' may depend on temperature, N^{s}_{1}, N^{s}_{2}, etc.) it does seem that the theory is consistent with experimental observations in systems of the Sb-Ni-Fe type. In particular, when Eqns. (1(a)) and (1(b)) are substituted in standard isotherms (such as the McLean isotherm) the theory predicts a much steeper temperature dependence of N^{s} and this appears to be in agreement with experiments{39,45,46}.

To summarize, it would seem that the problem of temper embrittlement is at last beginning to be understood, mainly through the efforts of intensive research over recent years. The effectiveness of solute rejection as an embrittlement process has been demonstrated, but careful studies have enabled the cause of temper embrittlement to be separated from solute rejection and associated transient segregation effects. Until recently our theoretical understanding of temper embrittlement has been vague and the development of a thermodynamic theory, however restricted, is perhaps the most significant step in the history of the problem. The review emphasises the importance of alloy - impurity interactions and indicates the complexity of the problem in commercial steels where a variety of impurities (P, Sb, Sn, etc.) and alloying elements (Ni, Cr, Mn, etc.) are generally present.

1.2. 350C Embrittlement

This form of embrittlement is sometimes referred to as one-step embrittlement and can be observed in most commercial alloy steels. It is usually shown by a toughness trough when ambient temperature notched impact values are displayed as a function of tempering temperature. A common, but not essential, feature is for fractures at 350C to occur along the prior austenite boundaries. Although conventionally measured in fixed temperature tests, it is known that 350C embrittlement involves a shift upwards in transition temperature; this point has been confirmed experimentally by several workers {48-50}.

Early theories of 350C embrittlement suggested that it could be due to the precipitation of Fe_3C rods or plates at prior austenite grain boundaries {49,51}, or to thin ferrite layers {49}, but the decomposition of retained austenite does not appear to be a contributory factor {52}. Schrader et al. {53} showed that tempering time was important; at a given tempering temperature fracture energy decreased with time to a minimum then gradually increased. At higher tempering temperatures this process occurred much more rapidly. These effects were examined in some detail by Klingler et al. {49} who used X-ray diffraction to identify the carbides formed during aging. The authors were able to show that the onset of embrittlement coincides with the initial precipitation of plate cementite. It was also found that steels with 100% bainitic structures were not susceptible to 350C embrittlement. More recent electron microscopy studies of the tempering of Fe-C martensites {54,55} show that the initial morphology of cementite is actually an array of parallel needles, and favoured nucleation sites are at lath and grain boundaries. In the work prior to 1959, the main contribution would appear to be the association between plate cementite precipitation and embrittlement.

In 1959 Capus {56} and Capus and Mayer {57} were able to show firstly, that high purity steels were not susceptible, and secondly, that specific impurities (notably N, P and Sb) appear to be responsible for 350C embrittlement. Thus the solute rejection model of Rellick and McMahon {41} would seem to be applicable, in principle, to this embrittlement phenomenon. A similar model proposed by Kula and Anctil {58}, in which the release of impurities partitioned with carbides causes embrittlement, seems less appropriate in this temperature range

because continued carbide growth, particularly at boundaries, can prevent the escape of partitioned impurities. The work of Capus and Mayer can be questioned on the basis that the diffusion mobility of Sb at 350C is so low that no significant rearrangement of Sb atoms is possible (for 1hr at 350C, $(Dt)^{\frac{1}{2}} < 1$ Å {59}). This approach to the problem suggests that only the highly mobile impurities, N, P and S, are active in 350C embrittlement and that other impurities must be trapped within growing carbides.

There is some evidence suggesting that elements other than impurities could play a part: additions of Al are claimed to be beneficial {53}, while high levels of Mn are reported to increase susceptibility {57}. Embrittlement in this tempering range (250-375C) greatly restricts our use of steels at high strength levels and a need for further research is indicated.

1.3. As-Quenched Embrittlement

As-quenched embrittlement is revealed by low energy, smooth faceted, intergranular fractures and results from segregation during austenitizing, or conceivably, during quenching. One important problem closely associated with as-quenched embrittlement is the phenomenon of quench cracking which results, in part, from the stresses produced by the volume change in the austenite-martensite transformation. Factors such as severity of quench, M_s temperature, specimen size and geometry, etc., determine the magnitude of quenching stresses {60} and under adverse conditions these stresses are often sufficient to produce intergranular cracking in embrittled materials.

Quench cracking is commonly observed in rapidly quenched alloy steels with carbon contents greater than 0.35 to 0.4% {40,61} and it is known that at this carbon content plate martensite may be present in the microstructure (in Fe-C alloys plate martensite is not observed below about 0.6%C, but alloying elements which act to stabilize austenite (eg. Ni) may significantly lower this value {55,62}). The impingement of martensite plates can result in microcracking {63} and thus one effect of high quenching stresses could be the growth of these crack nuclei along embrittled prior austenite grain boundaries. It should be noted that plate martensite microcracking is a microstructural effect which is essentially independent of quench rate, geometry,

etc. {63}. In steels with carbon contents below 0.35%, quench cracking is not widely reported, but this is possibly due to the absence of crack nuclei, rather than to the absence of embrittlement or segregation at grain boundaries.

Previous research in the field of temper embrittlement gives some idea of the impurities that could segregate in austenite. As mentioned before, Sb does not appear to segregate in austenite; this result can possibly be extended to Sn and As which are usually similar in behaviour to Sb. The Auger results of Schulz and McMahon {40} for brinequenched AISI 3340 + 600ppm Sb (no Mn) show that S segregates during austenitizing, and in brinequenched 3340 + 600ppm P, segregation of P and S was observed. On the basis of these limited results, as-quenched embrittlement could be largely confined to S and P segregation. The effect of Mn, which precipitates S in austenite, has not been widely examined in as-quenched steels.

1.4. Overheating

Overheating is a well known phenomenon that can occur in steels heated to high austenitizing temperatures during hot working or subsequent heat treatment. When these steels are tested at ambient temperatures fracture often takes place along prior austenite grain boundaries and a deterioration of mechanical properties, such as toughness, may be observed. The facets on the fracture surfaces contain fine ductile dimples which result from a grain boundary precipitate of α-MnS* particles {64}. Studies show that overheating involves the dissolution of intragranular MnS inclusions at high temperatures and their re-precipitation at austenite grain boundary sites during subsequent cooling {64,65}.

Several workers {64,65} have demonstrated that in susceptible materials, overheating produces a decrease in resistance to ductile fracture; there is no change in the ductile-brittle transition temperature. Schulz and McMahon {66} observed the same effect in a Mn-free steel, where overheating produced a CrS austenite grain boundary precipitate (CrS is more soluble than MnS, and in Mn-free steels 'overheating' occurs at lower temperatures).

---

* A face-centred cubic form of MnS {65}.

Recent investigations seem to be mainly concerned with the extent to which overheating can lead to inferior mechanical properties. Joy and Nutting {64} showed that steels with high sulphur contents (>0.02%) did not exhibit intergranular fractures even when heated to 1400C. This is due to the relatively small proportion of S that enters solution and is precipitated on the austenite boundaries; fracture is still controlled by the unaffected intragranular sulphides. At lower S levels (eg. 0.005%) a significant proportion of the total S is reprecipitated during overheating and fracture occurs via the grain boundaries rather than through the tougher transgranular paths. Cooling rate from temperatures in the overheating range was found to be important; rapid cooling produced fine particles, while slower cooling rates resulted in a coarsening of the MnS and eventually eliminated the intergranular mode. A continuation of this research by Bodimeade et al. {67} using low S steels (0.007%S) shows that there is a critical cooling rate at which overheating effects on toughness are greatest. When cooled at the critical rate (about 6C min^{-1}), a decrease in toughness (notched impact shelf energy) of about 30% was observed. Slower cooling rates produce a coarsening of the MnS particles above a 'critical' size; faster cooling results in 'subcritical' particle sizes which are apparently less effective in reducing toughness; very fast cooling (200C min^{-1}) restricts diffusion of S to the boundaries and the grain boundary volume fraction of MnS is lowered.* O'Brien et al. {68} found that in a low sulphur steel (0.005%S) a decrease in Charpy impact energy occurred as the austenitizing temperature was raised above 1050C; this temperature coincided with a change in fracture appearance from transgranular to intergranular microvoid coalescence. The authors propose that faceted fractures occur when the spacing of boundary particles is less than $\sim$0.2 times the spacing of intragranular particles. It should be mentioned that the solubility of S in austenite depends very strongly on Mn content and in these studies the effects are interpreted in terms of the Fe-Mn-S phase diagram of Turkdogan et al. {69} or Brown {70}.

In the study of Ritchie and Knott {3}, slow cooling from 1300C to 950C produced a 35% reduction in fracture toughness (K_{IC}), compared

---

* This conclusion was modified to some extent in later work; see {68}.

with a rapid quench from 1300C. This result was obtained with material containing 0.007%S, and assuming that the cooling rate (a furnace cool) was close to the critical rate, the result is in agreement with the work of Bodimeade et al. Ritchie and Knott also showed that overheating can produce a significant reduction in fatigue resistance. Baker and Johnson {71} extensively examined the properties of two steels that displayed ductile faceting and fracture toughness tests confirmed that, in these materials, overheating had not measurably reduced the fracture toughness (whether or not the notch toughness was affected is not known). These results {3,67,71} suggest that although overheating may produce ductile facets, the presence of facets alone does not imply that the material's toughness is affected; it is only when overheating is combined with cooling close to the critical rate that a reduction in toughness occurs.

1.5. Conclusions and the Present Research

The survey of previous work in the field indicates that the following main points seem to warrant investigation.

1) In the area of temper embrittlement particular attention should be given to the interactions between alloying elements and impurities. In low-alloy steels a sound knowledge of the effects of alloy content on susceptibility is essential if we are to combat the problem without resorting to the expensive alternative of of eliminating or reducing the impurity content. A determination of the effects of Ni content on Sb segregation would appear to be a valuable step towards a method of steel selection for critical applications, which is based on susceptibility.

2) The role of Mn in temper embrittlement, although investigated by several workers, is not understood. Mn is different both metallurgically and chemically from the embrittling impurities (which are all α-stabilizers, from Groups IVB, VB or VIB of the periodic table), and thus the embrittling effect of Mn alone, which is ostensibly quite strong, is rather surprising. Perhaps even more important, with obvious implications in commercial steels, is the indication of an interaction between Mn and P. Due mainly to the work of Mulford {39},

the effect of P alone in Ni-Cr steels is now reasonably well understood. A logical extension of this work is to re-examine the earlier results, particularly those of Preece and Carter {21} in 1953, which are considered to contain the suggestion of an interaction between Mn and P. This research therefore will attempt to clarify the effects of Mn, both alone and in conjunction with P, in temper embrittlement.

3) In the literature there are very few studies of the effects of austenite grain size. The most notable work is that of Capus {72} who showed that the susceptibility of temper embrittled steels increases markedly with prior austenite grain size. The commonly held notion, that an increase in grain boundary area (ie. a fine grain size) leads to a decrease in segregant coverage, is barely plausible and some emphasis therefore will be placed on grain size, both in 350C and temper embrittlement.

4) Impurities are clearly implicated in the 350C embrittlement problem, but the effects of Sb and Sn are questionable and should be re-examined. The demonstration {56,57} that pure steels are not susceptible either at ambient temperature or -78C seems to be unquestionable proof of the impurity effect. The carbide rejection model {41} offers a viable explanation for 350C embrittlement, but this is a supposition which is difficult to prove; the problem is complex and could be due to more than one cause. Mo is known to retard temper embrittlement {23,40}, however the effects of Mo, if any, on 350C embrittlement are unknown and should be determined.

5) Segregation in the austenite phase appears to be restricted to P and S (in Mn-free steels), but no comprehensive examination of this effect has been reported. Quantitative results, indicating the extent of segregation and thus the importance of this problem, are required. It is conceivable that segregation in austenite, present in as-quenched steels, could affect subsequent embrittlement susceptibility at 350C.

6) Compared with the embrittlement problems, overheating effects appear to be reasonably well understood. The influence of overheating on notched toughness has been examined in some detail, but the

literature indicates a possible disparity between notched and sharp crack (K_{IC}) toughnesses. An examination of the effects of overheating and austenitizing temperature on fracture toughness may help to clarify this issue. Some attention will also be directed towards the conditions necessary for preventing the occurrence of overheating, since it has been suggested {73,74} that in commercial steels, fracture toughness may be improved by employing high austenitizing temperatures, within the overheating range.

CHAPTER 2

EXPERIMENTAL PROCEDURES

2.1. Introduction

Early embrittlement studies generally relied on mechanical testing methods to determine the susceptibility of a material to embrittlement. However, several factors, apart from the extent of segregation, may influence the result from a mechanical test and some of the earlier work was therefore difficult to interpret or even misleading. The introduction of surface analysis techniques has enabled the extent of segregation to be measured directly and in recent work the most successful studies have been those which combine mechanical testing with grain boundary analysis.

The standard mechanical test chosen for the embrittlement studies in the present investigation was a modified transition temperature determination. This type of test has been used successfully by many workers in the field of temper embrittlement {27,33,34,39,40,45} and, as mentioned in Chapter 1, an approximately linear relationship exists between the increase in transition temperature (ΔTT) and the impurity excess on the grain boundaries {33,34}. The tests have the advantages that they can be performed quickly and require only very small amounts of material. Because of the obvious limitations of the tests, particularly in dissimilar materials, transition temperatures measured in the present work have been related, wherever possible, to grain boundary compositions.

Most of the steels and other alloys used in the research were designed to investigate specific effects. The details of the materials will be described in the chapters in which the particular effects are examined. Only the more generally applied experimental procedures will be discussed in this Chapter.

2.2. Mechanical Tests

2.2.1. Transition Temperature Tests-Specimen Details

The transition temperature method was used for 'as-quenched', '350C', and 'temper embrittlement' studies. The specimen configuration was the same in all studies, but the experimental apparatus used for the

temper embrittlement work differed slightly and will be described in Section 2.2.3.

The specimen design is shown in Figure 2.1; the specimens were 100mm long x 6.25mm diam and were notched every 20mm to a depth of 1.0mm. A carbide-tipped thread-forming tool (truncated UNC) was used to machine the notches; this ensured that the notch geometry was identical in all specimens. The specimens are basically similar to the single specimens first used by Low et al. {27}. In comparison the segmented design saves about 40% in material and assists with machining and other operations. Low et al. {27} have shown that the shift in transition temperature obtained with these small specimens is essentially the same as that measured in the Charpy notched impact test, for tempered martensite microstructures.

2.2.2. Transition Temperature Tests - As-Quenched and 350C Embrittlement

All transition temperature testing was performed with a 5000Kg Instron testing machine. The test apparatus used for the as-quenched and 350C embrittlement tests is shown in Figure 2.2. The specimens were tested in cantilever bending at a crosshead displacement rate of 2mm min^{-1} and load-displacement curves were recorded using a chart magnification factor of 100X. The specimen bath was thermostatically controlled over the temperature range -160C/250C. Isopentane cooled by coils within the bath was used below room temperature and at high temperatures silicone oil could be heated by an immersion heater. Nitrogen gas agitation was employed and the test temperature was determined from an chart recording of the thermocouple output. The control system is basically the same as that described later for the temper embrittlement tests.

Figure 2.3 shows the method used to determine an approximate value of the energy absorbed by the specimen prior to fracture. In all cases the elastic loading line was extrapolated to maximum load; the offset at this load (corresponding to the plastic displacement) was then used to calculate the energy absorbed by multiplying by the maximum load. In preliminary tests, using mild steel specimens, the apparatus gave accurately reproducible results.

2.2.3. Transition Temperature Tests - Temper Embrittlement

During the course of this research the specimen bath shown in Figure 2.2 was found to be slow and inconvenient to use. For these reasons only the as-quenched and 350C embrittlement tests were performed in the isopentane bath and a different testing device, designed to dispense with heating or cooling liquids, was used for all temper embrittlement tests. A drawing of the testing device is shown in Figure 2.4 and a photograph of the apparatus attached to the Instron crosshead (as used in low temperature tests) is shown in Figure 2.5. Basically the device consists of a hardened steel specimen holder silver-soldered into a copper heating or cooling jacket. The device relies on heat conduction to or from the specimen and the control thermocouples are situated on the jacket rather than the specimen to provide a damping effect; the test temperature is measured by a thermocouple bead held in the notch by a tension spring. The thermocouple bead was tapered to fit the specimen notch and was used to locate the specimen in the holder; the specimen was then fixed in position with the locking screw. The apparatus could be operated in the temperature range -185C/250C. Tests with thermocouples soft-soldered onto the specimen showed that steady-state temperatures were achieved quickly and that the temperatures at positions of $\pm$ 2mm from the notch were within $\pm$ 3C of the notch temperature over the range -150C/150C.

The experimental lay-out for the transition temperature tests is shown in Figure 2.6; the thermostatic controlling apparatus is at the lower left of the Figure and a schematic diagram of the control system is shown in Figure 2.7. Temperature measurements were made with a Comark digital thermometer which had a specified accuracy of 0.1% $\pm$ 1C and sampling rate of about 5Hz. Temperature variations at the specimen notch during a test were always less than $\pm$ 3C.

In most experiments tests were conducted at a standard crosshead displacement rate of 2mm min^{-1}; in experiments with very ductile materials the displacement rate was raised, for convenience, to 5mm min^{-1}. The chart magnification factors used with these displacement rates were, respectively, 50X and 20X.

Compared with the 'as-quenched' and '350C tempered' materials, the 'temper embrittled' materials had much higher upper shelf energies

and the ductile-brittle transition was consequently much easier to detect. Therefore, in the transition temperature determinations for the temper embrittled materials, the elastic component of the system was ignored and the change in the total area under the load-displacement curve was used to define a transition temperature. The method used is shown in Figure 2.8. It is obvious that there is a zero offset corresponding to the elastic component, but for the purposes of defining a transition temperature this effect can be ignored. In all temper embrittlement tests an area under the load-displacement corresponding to 4J energy was used to define the material's transition temperature. The relationship of this energy level to the transition curves and the accuracy of the transition temperature determinations will be mentioned with the presentation of the results.

2.3. Other Tests and Equipment

2.3.1. Heat Treatment Equipment

Most austenitizing treatments were performed under a dynamic vacuum and three furnaces capable of covering the temperature range 850C-1600C were employed in the investigation. Transition temperature, fracture toughness and Hounsfield specimens were usually austenitized under a vacuum somewhat below 10^{-2}torr. Occasionally, specimens that were to be machined after heat treatment were austenitized in a sealed furnace under a pure argon atmosphere. Small specimens used for metallographic studies (about 10 x 10 x 10mm) were austenitized under a vacuum below 1×10^{-5}torr.

In the heat treatment of the fracture toughness specimens (used in the overheating studies) it was desirable to quench specimens from the austenitizing temperature very rapidly. To achieve this, a furnace was designed which enabled a specimen, under vacuum, to be dropped directly into the quenching bath. The furnace was constructed vertically with a central mullite tube heated by a single concentric Crusilite element (5cm diam). After isolating the rotary pump, the specimen, held in the tube by a fuse-wire, was released electrically and would drop down the tube through an aluminium foil seal into the quench bath. A thyristor proportional controller was used and the thermocouple was situated inside the mullite tube, beside the specimen. Because of the risk of fracturing the mullite tube (and the expensive

Crusilite element) the furnace was only used for austenitizing treatments at temperatures above 1150C.

Tempering treatments (distinct from aging treatments) at either 650C or 625C were carried out in a vacuum furnace equipped with a solid-state proportional controller. Fluidized beds, capable of temperature control to within ± 3C were used for tempering within the range 100C-500C.

Temper embrittlement specimens were aged at 480C, 520C and 590C for times up to 10,000hr. For aging times of 20hr or longer, specimen blanks were skim-machined after tempering and sealed in silica tubes either under vacuum or a partial pressure (70mm) of argon. The capsules were then aged in a Carbolite air furnace; the furnace had a large hot-zone and was fitted with a proportional controller for these experiments. Short-term aging was done in the tempering furnace. Temperatures were spot-checked during aging and are considered to be accurate to within ± 3C.

2.3.2. Scanning Electron Microscopy (SEM)

A Cambridge Scientific Instruments Stereoscan was used extensively in this research to examine fracture surfaces and indentify inclusions. The particular instrument could achieve useful magnifications of about 10K and was fitted with a Nuclear Diodes energy dispersive X-ray system (EDAX). For Auger spectroscopy and other work quantitative estimates of the proportion of intergranular fracture were required. This was done by photographing randomly selected areas of the fracture at a convenient low magnification. The non-intergranular areas (usually cleavage) were then shaded on the photographs and a transparent 10 x 10 grid was used to estimate the total shaded area.

Many of the specimens were broken at low temperatures and, as a rule, these were warmed by immersion in alcohol, dried, then coated with RS protective lacquer. The specimens could then be stored in air and for subsequent SEM examination the lacquer was readily removed by washing in acetone.

2.3.3. Optical Microscopy

Metallographic specimens were usually prepared by hot-mounting and standard grinding and polishing techniques. In the embrittlement

studies, samples were occasionally prepared to check microstructures and the depth of hardening after quenching, but most of the metallographic work in this investigation related to overheating effects. To reveal overheating and grain boundary detail several etching reagents were tried, but the most effective etch was found to be an equal mixture of 10% nitric acid and 10% sulphuric acid (sometimes referred to as 10% nitrosulphuric acid). To improve contrast these specimens were usually lightly polished after etching.

Prepared specimens were examined and photographed with a Carl Zeiss projection microscope. For the determination of prior austenite grain sizes, the linear intercept method was used and grain boundaries were delineated by etching in warm saturated aqueous solution of picric acid containing a few drops of wetting agent (sodium alkyl sulphate).

2.4. Auger Electron Spectroscopy (AES)

2.4.1. The Development and Principles of AES

The emission of Auger electrons was first discovered and explained in 1925 by Pierre Auger {75} and in 1953 Lander {76} obtained N(E) curves depicting the energy distribution of emitted secondary electrons. The N(E) curves contain small Auger electron peaks, but the peaks are on a slowly changing background and are difficult to resolve. In 1968, Harris {77,78} demonstrated that a high sensitivity could be obtained by using the electronically differentiated energy distribution, $dN(E)/dE$. An example of the improvement in sensitivity produced by differentiation is shown in Figure 2.9. In 1969, Palmberg et al. {79} showed that sensitivity and resolution could be further improved by using a cylindrical mirror electron analyser (CMA) and since that stage the application of AES to surface studies has developed rapidly. Modern systems usually combine ion-sputtering facilities with AES and the trend is towards combining several surface techniques together in the one system. Electron beam diameters are being reduced and Scanning Auger Microprobe (SAM) systems with high lateral resolution are available. A block diagram of a typical AES system using a CMA is shown in Figure 2.10.

The AES technique employs an electron beam to ionize the inner electron shells of atoms in the specimen. Atoms, thus excited, may

relax by dropping an electron down from an outer shell to fill the hole in the inner shell. There is an energy release associated with this transition which is imparted to another outer shell electron (or it may be emitted as a photon); if the energy is sufficient the electron is ejected from the atom as an Auger electron with a kinetic energy determined by the particular transition. In practice only a few of the many possible transitions occur and individual elements are easily identified on the energy spectra. An important property of Auger electrons is their short inelastic mean free path, which is typically in the range 3 to 30 Å, allowing just the atom layers near the surface to be analysed. Several informative reviews of AES principles and equipment have been published recently {80,81}.

2.4.2. AES Operation Procedures

All grain boundary Auger work was performed in the same Physical Electronics cylindrical analyser system; in general, the calibration standards referred to were also analysed in this system. In one run the equipment would accept 8 specimens of the dimensions shown in Figure 2.11. The specimens were fractured under a vacuum, typically $<1 \times 10^{-10}$ torr, at temperatures of about -100C, and generally about 8-10 different areas of each fracture surface were analysed. The system was operated with a primary beam energy of 2000eV, a beam current of 50μA and a beam size of about 0.5mm. An AC technique, with a lock-in amplifier modulation of 6 volts, was used to obtain the derivative dN(E)/dE of the energy distribution. After first recording the entire spectrum from 0-1000eV, the desired peaks were retraced, usually with a sensitivity of 10μV and a time constant of 300ms. Because slight differences in operating conditions, sample positioning and surface roughness may all influence the signal strength it is customary to express the peak-heights of the elements present as a proportion of a major peak. In common with other embrittlement work, the procedure adopted was to always normalize peak-heights with respect to the Fe-703eV peak, that is:

$$A'_p = H_s/H_{Fe} \qquad (2.1)$$

where A'_p = measured Auger peak-height ratio

H_s = segregant peak-to-peak height

H_{Fe} = Fe-703eV peak-to-peak height.

The fractures obtained with the AES specimens were not usually 100% intergranular cleavage and where necessary the values of A_p' were corrected in a manner assuming simple mixing {39,45}.

Taking A_p = 100% intergranular peak-height ratio

A_b = bulk (cleavage or deep-sputtered) peak-height ratio

X = intergranular fraction (from SEM)

Then:

$$A_p' = X.A_p + (1-X)A_b \qquad (2.2)$$

and

$$A_p = (A_p' - (1-X)A_b)/X \qquad (2.3)$$

Hereafter, peak-height ratios will refer to this value, A_p (usually expressed as a percentage), unless mentioned otherwise.

2.4.3. AES Calibrations

The primary aim of the AES studies in this investigation is to determine the chemical composition of the material at the grain boundary. Qualitative grain boundary analysis is a reasonably straightforward procedure, but determining actual concentrations is difficult and at present there is no universally applied technique. In this work an attempt has been made to express AES results quantitatively, however there are uncertainties in this approach and therefore, for reference, the original measurements are also given.

For a species deposited evenly on a substrate by evaporation the adsorbate peak-to-peak height (and less strictly, the peak-height ratio) increases in direct proportion to the number of atoms excited and thus the coverage. This has been confirmed experimentally {82} and can be deduced theoretically. Of course, at high coverages (many monolayers) the adsorbate peak-to-peak height will be constant, while the peak-height ratio will tend toward infinity at a coverage dependent on the substrate and the attenuation length of its Auger electrons in the adsorbate (ie. the substrate peak-height will decrease will increasing coverage). The attenuation length or inelastic mean free path of Auger electrons is largely controlled by the energy level of the particular electrons emitted, rather than the material through

which the electrons travel. In the simplest terms, for a coverage of thickness z, the adsorbate peak-height, H_a, and the substrate peak-height, H_b, are given by {81}:

$$H_a^z = H_a^\infty (1 - \exp(-z/L_a)) \qquad (2.4)$$

$$H_b^z = H_b^o \exp(-z/L_b) \qquad (2.5)$$

where L_a and L_b are the attenuation lengths in the adsorbate for the Auger electrons of the adsorbate and substrate respectively.

For Fe or similar substrates the decay of the high energy peaks with coverages up to a few monolayers is not expected to be great. For the case of known coverages of Sn condensed on Fe {83} the peak-to-background ratio (simply a different normalizing procedure) for Sn_{430}/Fe_{598} is, within experimental error, linear with coverage up to the maximum value measured of 1.6 monolayers. The Auger electrons producing the Fe_{703} peak will have a greater attenuation length than Fe_{598} electrons and it seems satisfactory therefore to seek simple calibration constants that will enable peak-height ratios, X/Fe_{703}, to be converted directly to coverages.

Calibration constants for P, Sn, Sb and Ni were determined from published AES measurements of binary solid solutions of these elements in Fe {45,84}. The solute Auger electron intensity in a binary alloy is derived from a depth determined by the attenuation length, in the solvent, of the solute Auger electrons. The <u>equivalent</u> surface monolayer coverage, θ, for solute atoms on a pure solvent base is {83}:

$$\theta = X_c L_c (C_c/C_s) \qquad (2.6)$$

where, X_c = solute atom fraction

L_c = solute attenuation length (in monolayers)

C_c and C_s are the cross-sectional areas of the solute and solvent atoms respectively

Atomic areas should refer to the 'effective' atom area in Fe; this is usually described in terms of the volume size factor, Ω_{SF}, given by:

$$\Omega_{SF}(\%) = 100(\Omega_B^* - \Omega_A)/\Omega_A \qquad (2.7)$$

where, Ω_B^* = effective volume of solute B in A, extrapolated to 100%B.

Ω_A, Ω_B = atomic volumes of solvent and solute respectively.

Auger attenuation lengths were estimated from the work of Powell {85} and are shown below together with calculated values of C_c/C_s from several sources:

	Peak (eV)	L (Fe monolayers)	C_c/C_s Ω^*{86}	Ω^*{45}	Fe_3P	Ω
P	120	2.5	0.91	-	<u>1.10</u>	1.26
Sn	430	5.5	1.41	<u>1.44</u>	-	1.77
Sb	454	5.7	1.23	<u>1.47</u>	-	1.87
Ni	849	7.0	<u>1.03</u>	-	-	0.95

Apart from the values based on the atomic volumes of the solutes in their pure form, the C_c/C_s ratios are in fair agreement and the underlined values, which are considered to be representative, have been used in this work.

Then, substituting in Eqn. (2.6), the calibration constants**, for peak-height ratios in %, are:

$$\theta_P \text{ (monolayer coverage)} = 0.0055.A_p \qquad (2.8(a))$$

$$\theta_{Sn} \text{(monolayer coverage)} = 0.022.A_p \qquad (2.8(b))$$

$$\theta_{Sb} \text{(monolayer coverage)} = 0.028.A_p \qquad (2.8(c))$$

$$\theta_{Ni} \text{(monolayer coverage)} = 0.073.A_p \qquad (2.8(d))$$

In the previously mentioned studies of Sn on Fe {83} the Sn calibration constant was determined by several techniques and correcting for the

---

** The AES measurements for the binary alloys {45,84} show two curves for each alloy system, obtained by using different time constant settings. The calibration constants were derived from the more sensitive measurements, recorded with the shorter time constant setting.

different normalizing procedure the constant is 0.020 $\pm$ 0.002, which is in good agreement with the Sn value obtained here.

In the application of calibration constants to a segregated surface it is necessary to make assumptions about the profile or depth distribution of the segregants. Sputter profiles, although not precise, suggest that strong segregants such as Sb, Sn, P and S are largely confined to within one or two atom layers of the grain boundary {45,87}. For calibration purposes it is reasonable, at least initially, to treat these segregants as being confined solely to the grain boundary or surface (from published results {39,45} Ni appears to show a more gradual profile, unlike that expected for equilibrium segregation to grain boundary sites, but a correction for this can be made at a later stage). For grain boundary segregation, the Ni Auger electrons from the bulk will also contribute to the Auger signal (this effect can be ignored for the trace impurities); this bulk signal should be subtracted before Ni segregation levels are determined. Assuming that the segregation of Ni is confined to the surface atom layer, then the surface concentration signal is simply:

$$Ni^S = Ni(m) - Ni(X_c) + Ni^S(X_c)$$

where S = surface AES signal

m = measured AES signal

and X_c = bulk AES signal

Since the attenuation length of Ni is taken as 7 Fe monolayers, 6/7 of the bulk Ni signal will be derived from layers below the surface layer, ie.:

$$Ni^S = Ni(m) - 0.87Ni(X_c) \qquad (2.9)$$

The final factor to be considered is the fracture process itself. Assuming that the segregant lies along the precise fracture path, then during the fracture process, the total amount of segregant will be divided evenly between the fracture surfaces. The grain boundary Auger concentrations should therefore include a factor, k, which allows for the division of segregant by fracture. Depending on the concentration profile at the boundary k will normally vary between one, for a very

gradual profile, and two, for segregant confined to the grain boundary.

To summarize, the calibration constants are:

$$\theta_P \text{ (monolayer coverage)} = 0.0055.k.A_p \qquad (2.10(a))$$

$$\theta_{Sn} \text{(monolayer coverage)} = 0.022.k.A_p \qquad (2.10(b))$$

$$\theta_{Sb} \text{(monolayer coverage)} = 0.028.k.A_p \qquad (2.10(c))$$

$$\theta_{Ni} \text{(monolayer coverage)} = 0.073.k.(A_p - 0.87A_p(X_c)) \qquad (2.10(d))$$

For the reasons previously discussed, the value of k in this research will be taken as 2 for grain boundary Auger measurements of P, Sn and Sb; a value of $k = 1.5$, which provides an arbitrary correction for a more gradual profile, will be used for grain boundary Ni segregation. The precise errors in the calibration constants cannot be determined, but consideration of the assumptions made would suggest that for adsorbate coverages Eqns. (2.8(a-d)) are probably accurate to within $\pm$ 20%.

Figure 2.1. Segmented specimens used for transition temperature tests (specimen dimensions are given in the text).

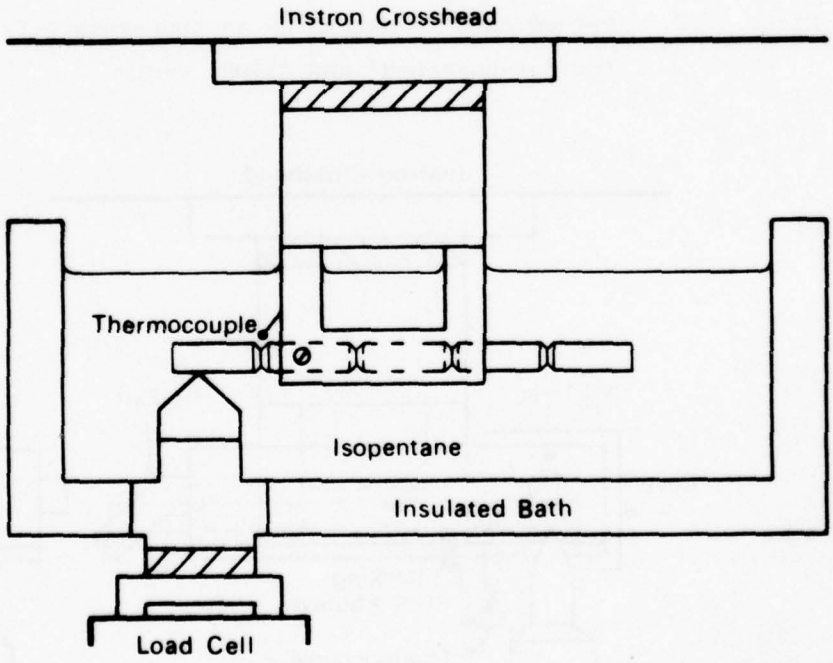

Figure 2.2. Transition temperature apparatus used for 'as-quenched' and '350C' tests.

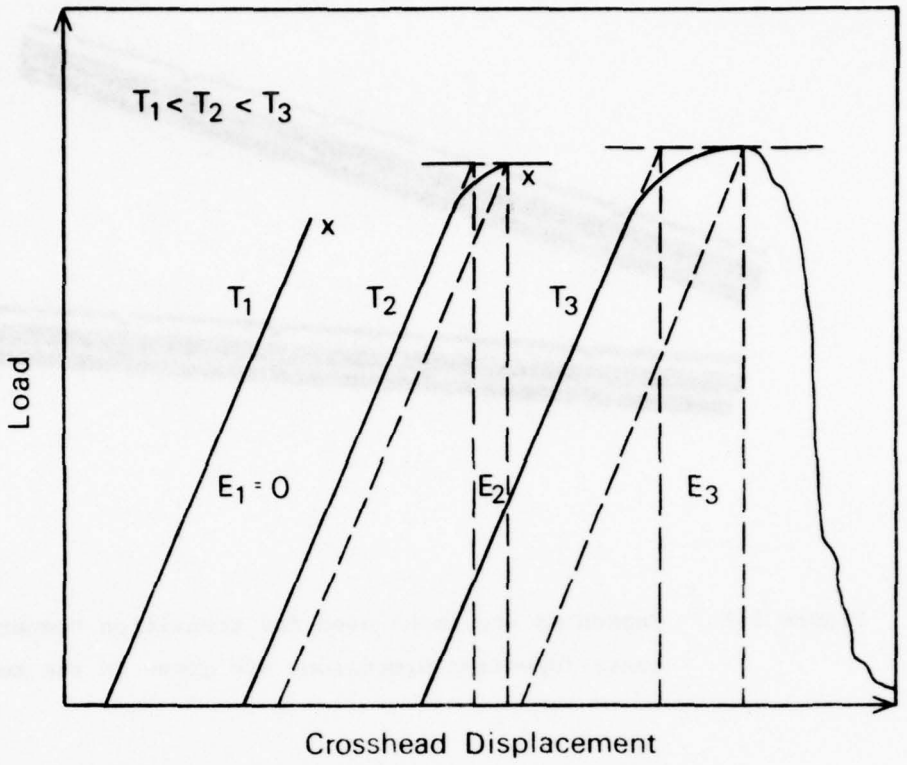

Figure 2.3. Method used to determine an approximate fracture energy for 'as-quenched' and '350C' tests.

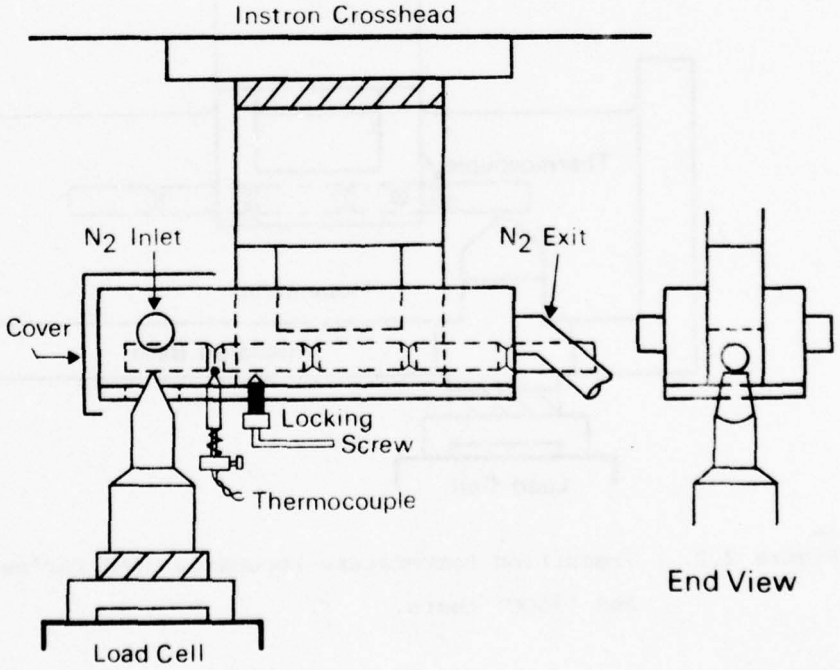

Figure 2.4. Transition temperature apparatus used for temper embrittlement tests.

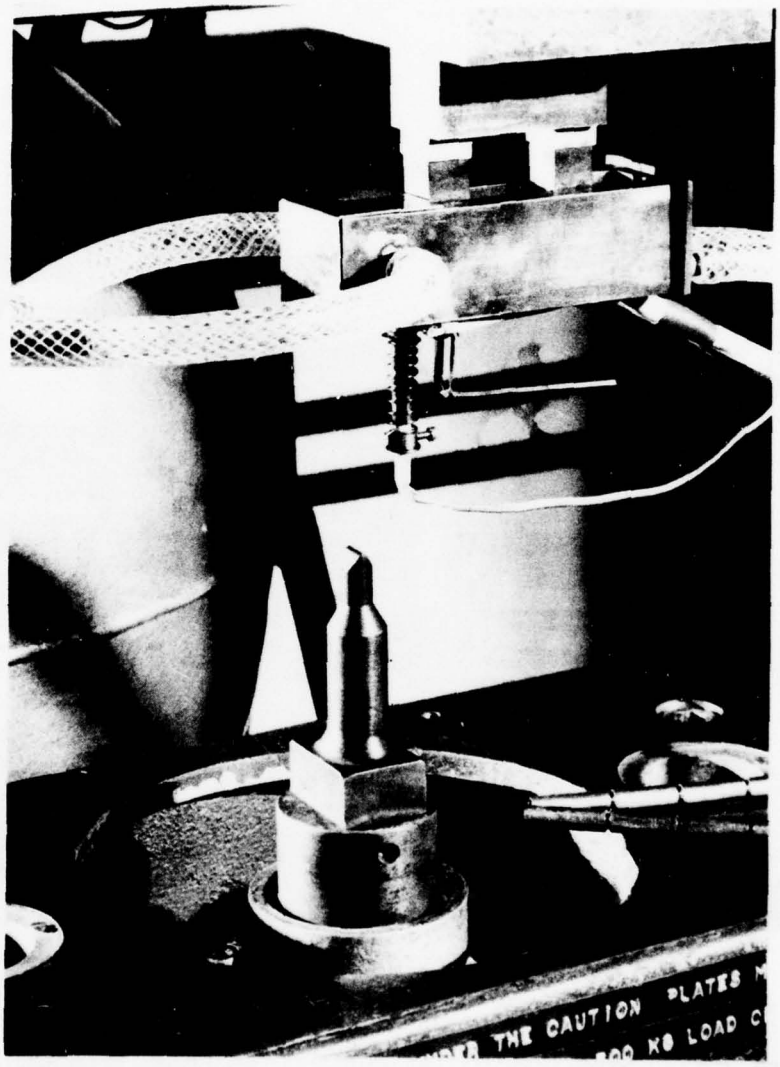

Figure 2.5. Transition temperature apparatus used for temper embrittlement tests. For testing above ambient temperature the liquid nitrogen cooling was replaced by a plug-in heating element.

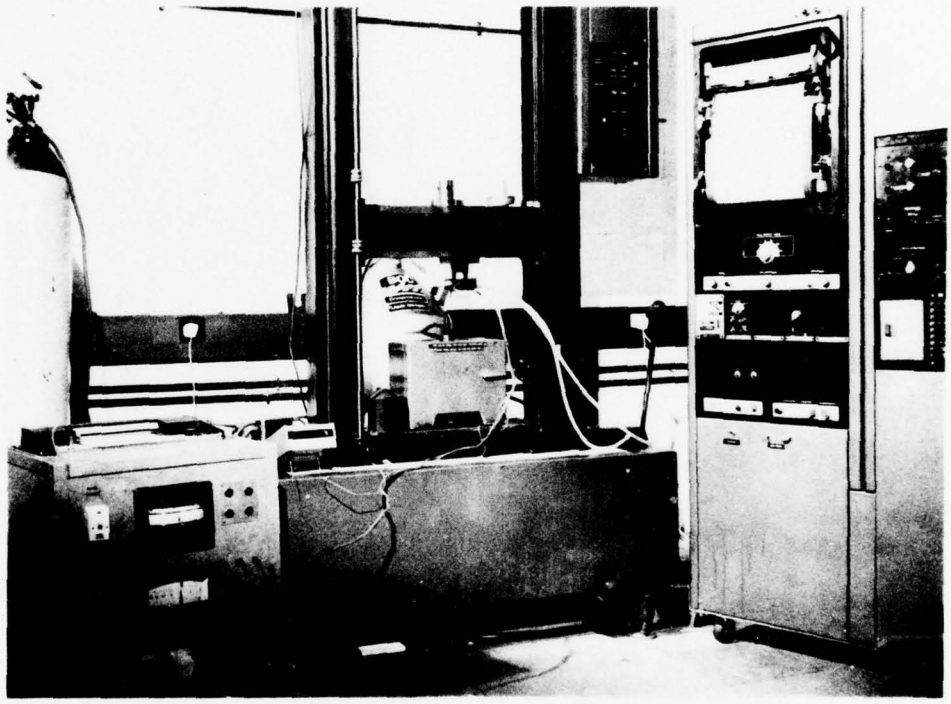

Figure 2.6. Experimental lay-out for the transition temperature tests.

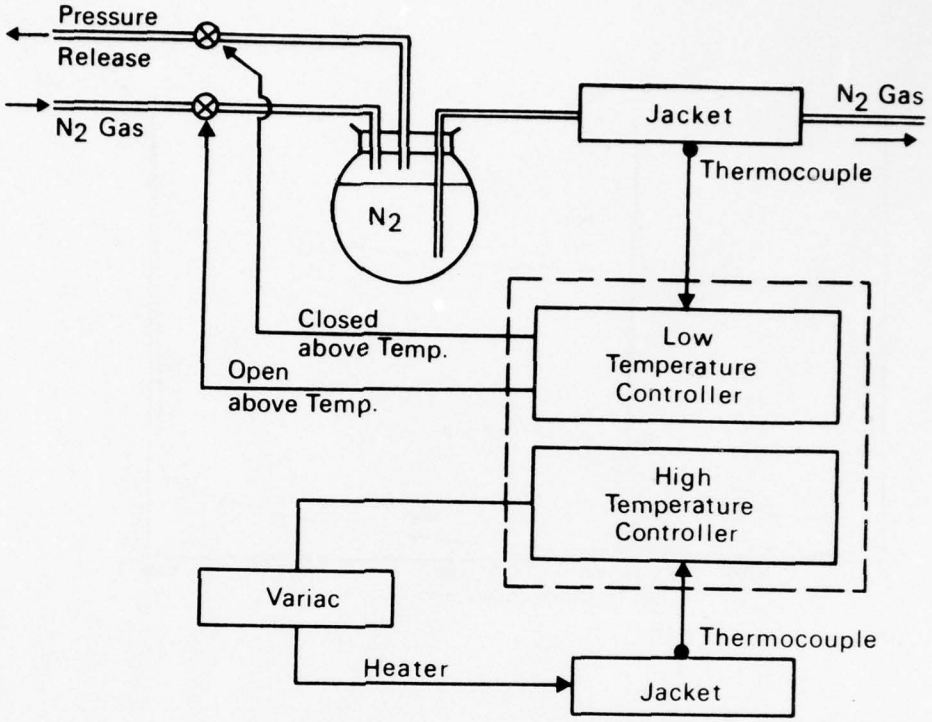

Figure 2.7. Temperature control system employed for transition temperature testing over the range -180/250C.

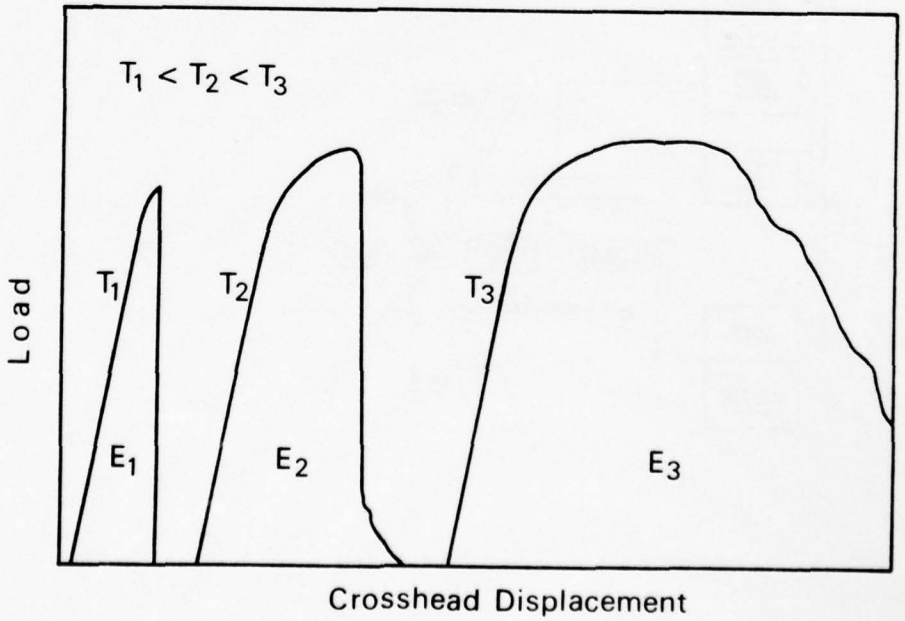

Figure 2.8. Method used to determine an approximate fracture energy for temper embrittlement tests.

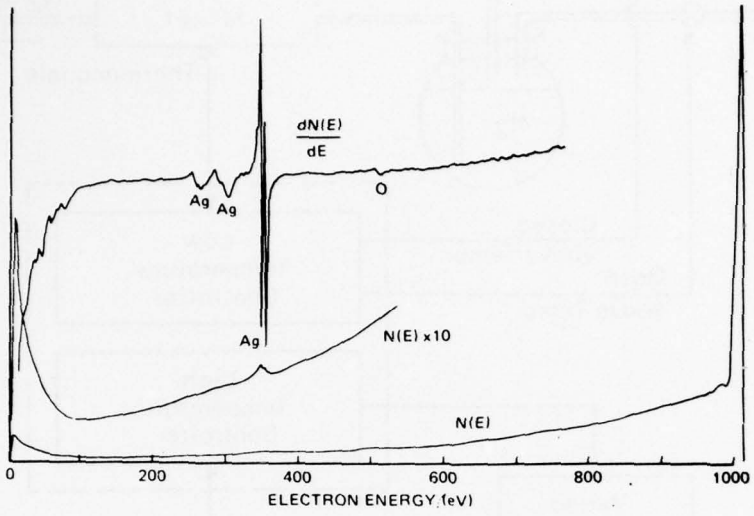

Figure 2.9. The effect of differentiation on the AES spectrum (courtesy of Physical Electronics Industries, USA).

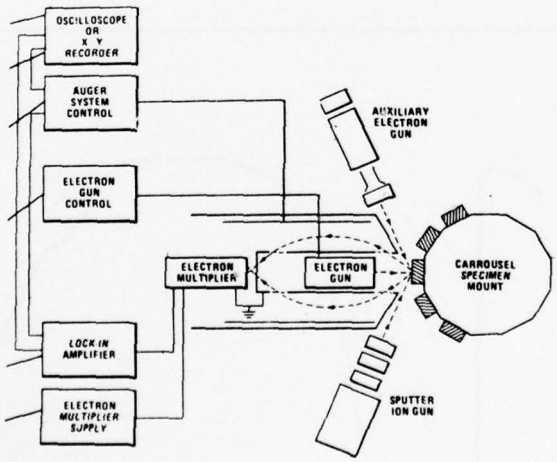

Figure 2.10. Schematic diagram of an AES system showing two possible electron gun orientations (courtesy Physical Electronics Industries, USA).

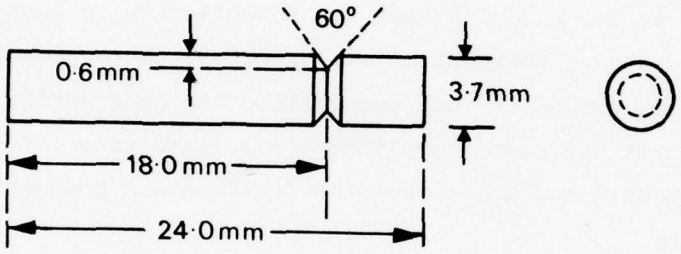

Figure 2.11. Geometry and dimensions of AES specimen.

CHAPTER 3

AS-QUENCHED EMBRITTLEMENT

3.1. Introduction

In temper embrittlement, the concept of segregation in the austenite phase arose originally from the knowledge that the inverse solubility is approximately related to a solute's segregation tendency. Since impurities such as Sb, Sn and P have low solubilities in austenite (a few wt%) moderately strong segregation was expected. More recently the relationship between solubility and segregation has been refined and extended {87,88}; it has been shown that for a large range of systems, the atomic solubility, X_o, is related to the grain boundary enrichment ratio, β, by:

$$\beta = (1 \text{ to } 10)/X_o \qquad (3.1)$$

where β = molar boundary concn./molar bulk concn.
Thus solutes such as Sb, Sn and P would be expected to segregate in austenite, but whether or not the levels of segregation are appreciable and influence mechanical properties is another matter.

The segregation of Sb in austenite has been examined in relation to the temper embrittlement problem and several workers {32,33,37,40} have found that Sb does not seem to segregate to a level detectable by either AES or ion-backscattering analysis. In addition no appreciable segregation of Ni or Cr {32,33}, or Mn {37} has been found, using such techniques. These latter observations would appear to be in conflict with earlier work based on interfacial energy measurements in binary alloys {89}, where the grain boundary enrichment ratios for Ni, Cr and Mn were all found to be greater than 10 at 1200C. These alloying elements have unlimited solubility in austenite and on the basis of Eqn. (3.1) these enrichment ratios are rather high. However it is also possible that segregation effects are modified in complex steels, where a number of solutes are present together.

Several workers have indicated that P segregates in austenite, but this is based on limited data and there has been no attempt to quantify P segregation in steels. Interfacial energy results {89} give a P enrichment ratio of about 200 for the Fe-P binary alloy, which

is in agreement with Eqn. (3.1). Inoue et al. {90} found appreciable P segregation in AES studies of a 3Mn+0.02P steel and Schulz and McMahon {40} obtained similar evidence of segregation in a sample of 3.5Ni+1.7Cr+0.06P steel, brine quenched from 1250C. But Krahe and Guttmann {36} and Guttmann et al. {37} claim that there is no evidence of P segregation in their 1.92Mn+0.013P steel, water quenched from 1200C and tempered at 350C (to produce an intergranular fracture). Their published AES spectrum {36} does however show a small P peak and with an enrichment ratio of about 200 the fracture surface concentration would be less than 0.03 monolayers, which is difficult to detect by AES.

In a different approach Clark et al. {91} studied the quench cracking susceptibility of an En30A steel (290ppm P, 80ppm Sn, 50ppm Sb) by water quenching from a range of austenitizing temperatures between 900C and 1300C. Intergranular quench-cracking was found in specimens quenched from 900C and 1000C, but not in those quenched from higher temperatures. The tendency for grain boundary grooving, indicated by a standard etch in a picric acid solution, decreased correspondingly with austenitizing temperature and this led the authors to propose that impurities segregate more strongly at austenitizing temperatures below 1100C.

The work described in this Chapter was initiated to examine the tendency for as-quenched embrittlement in a typical high-strength commercial-purity steel. To explore the effects of steel composition and austenite grain size a variation in Sb and Mo content has been employed. In subsequent Sections mechanical test and AES grain boundary results are presented, indicating the extent to which P segregates during the austenitizing cycle in Ni-Cr and Ni-Cr-Mn steels. The importance of variables such as austenitizing temperature, quench rate and steel composition is investigated.

3.2. The Effects of Sb in Ni-Cr and Ni-Cr-Mo Steels

3.2.1. Experimental Details

In these experiments the aim was to employ transition temperature tests to investigate the susceptibility of as-quenched steels to embrittlement. A Mo-free En25 Specification* was chosen as the base

---

* The 3 steels had higher C contents than planned and were closer to En26 specification.

composition and 3 steels were melted to give the following compositional variations:

Steel 1 : Commercial purity (C.P.)

Steel 2 : C.P. + 120ppm Sb

Steel 3 : C.P. + 0.5%Mo + 120ppm Sb

The chemical compositions of the steels are given in Table 3.1 (the steels were analysed by two laboratories and the results were in good agreement). Melts of about 50kg were supplied in the form of hot-rolled 25mm diam. bars. Several bars were then hot-forged, hot-swaged and machined to give rods of 8.0mm diam. The rods were all austenitized in vacuum at temperatures of either 950C, 1150C or 1350C and quenched in either 5% brine or oil. Transition temperature specimens were then produced from the rods by centre-grinding and notching with a carbide tool.

3.2.2. Results

The original intention in these tests was to quench from the austenitizing temperature in brine, because this would give less time for alterations in grain boundary composition to occur during the quenching process. Tests for the brine quenched condition, after austenitizing at 950C, are shown in Figure 3.1. At room temperature, there was almost no measurable energy absorbed during fracture and although the energy level began to increase at 100C, a conventional energy shelf could not be detected. The fractures were examined by SEM, with main observations as follows:

1) Steel 1 : The fracture mode was transgranular microvoid coalescence (TMC) over the testing temperature range 25C-210C.

2) Steel 2 : The fracture mode at temperatures in the range 25C-200C was TMC mixed with what appeared to be intergranular microvoid coalescence (IMC). No distinctly brittle facets were observed, but the IMC facets were clean, unlike those in overheated steels (Figures 3.2(a) and (b)).

3) Steel 3 : At 25C the fracture mode was quasi-cleavage (cleavage through martensite) mixed with TMC; at 65C and above the fractures were 100%TMC (Figures 3.2(c) and (d) show the 25C fracture).

The anomalous increase in fracture energy at 100C is clearly not associated with a transition in fracture modes; a specimen of Steel 1 fractured at -196C showed that the fracture mode was 100% quasi-cleavage and thus the fracture appearance transition temperature was below 25C. Figures 3.3(a-c) show fractures in Steel 1 obtained at -196C, 25C and 150C.

Consideration of these results suggested that brine quenching could restrict carbon diffusion during quenching (ie. autotempering) and that a rearrangement of carbon atoms during testing produced the observed increase in fracture energy at temperatures above 100C. It is well known that autotempering involves the segregation of carbon to lattice defects {54,55}. Depending on the quench rate and M_s temperature, autotempering may also involve carbon clustering and some ε-carbide precipitation. The prevention of autotempering, either by very rapid quenching in steels with high M_s temperatures, or by employing steels with M_s temperatures too low for C diffusion to occur is known to affect the strength and hardness of martensite {92-94}.

To check the hypothesis that carbon segregation during testing produced the increase in fracture energy at high testing temperatures, a sample of Steel 1 was aged at 250C for 10 minutes and tested at 25C; the fracture energy increased markedly (Figure 3.1). A similar increase in fracture energy was observed for a sample of Steel 2, aged at 100C for 24hr. Subsequent tests with oil-quenched specimens revealed a low-temperature energy transition, coincident with a transition in fracture modes.

The results for oil-quenched specimens, austenitized at 950C (1hr), 1150C(2hr) and 1350C(2hr) are shown in Figure 3.4. The energy transition is not very abrupt and a crosshead displacement of only a few hundred microns separates the lower and upper shelf energies. In view of the high oil-quenched hardness values (which were all within 630 $\pm$ 10VPN/20kg), the transition temperatures are low, and their are no obvious differences between the results for the three materials.

At higher austenitizing temperatures there is a trend towards a higher transition temperature and an increase in the experimental scatter (or differences in the upper shelf energy).

Fracture surfaces from above and below the transition were examined by SEM. The low energy fractures were entirely quasi-cleavage; the only exception was in Steel 2 where, at 950C and 1150C, the fractures showed a few splits, perpendicular to the fracture plane, and occasional intergranular facets (less than 1-2% of the fracture surface). The high energy fractures varied considerably with austenitizing temperature and this behaviour is summarized below:

Austenitizing Temperature	Steel 1	Steel 2	Steel 3
950C	TMC	TMC	TMC
1150C	IMC	TMC + IMC	TMC + IMC
1350C	IMC	TMC + IMC	IMC

Ductile and brittle fractures for the 950C treatment are shown in Figures 3.5(a-f) and corresponding fractures for 1150C are shown in Figures 3.6(a-f) (apart from a grain size difference the 1150C fractographs are representative of the 1350C fractures).

A more detailed SEM examination of the IMC facets showed that although the facets were apparently ductile and contained fine dimples (Figure 3.7(a)), particles were not particularly prevalent. One of the exceptional areas is shown in Figure 3.7(b); an examination of particles such as these by EDAX generally indicated Mn and S, although in some analyses Si and Cr were also present.

3.3. The Effect of P in Ni-Cr Steels

3.3.1. Experimental Details

Because of the difficulties in determining transition temperatures in rapidly quenched specimens it was decided to introduce a different test for the study of P segregation. The method chosen was to make comparative tests of the effect of P additions on the low-temperature fracture appearance of a Ni-Cr steel. Preliminary tests showed that

Steel 4 was ideal for use as a base for remelting; this steel could be quenched from 900C or 1300C to give fractures that were 100% quasi-cleavage at 77K.

Steel 4 was prepared (primarily for temper embrittlement studies) as a 15kg ingot by melting electrolytic iron together with high-purity alloying elements (details of the hot-working are given in Chapter 5) to give a nominal composition of 0.3C+2.5Ni+1.4Cr (see Table 3.2). Remelting was done in an electric-arc furnace, using a Cu hearth and an argon atmosphere. The P additions were made by remelting 70gm samples with high-purity iron phosphide to give P contents of 1200ppm. After the initial melting each sample was cut into two lengths which were laid side-by-side and remelted; this procedure was repeated about 4 or 5 times to ensure that the P distribution was homogeneous. Chemical analysis checks on 3 samples gave P contents of 1140, 1190 and 1230ppm.

Two Hounsfield impact specimens were machined from each 70gm sample. The specimens were heat-treated under vacuum ($<10^{-5}$torr), quenched into either 5% brine or oil,* and fractures were produced by a standard impact test at 77K. Specimens of the control steel (Steel 4) were heat treated together with those of the P-containing steel (referred to as Steel 4+P). All specimens were tested in the as-quenched condition and notches were machined after heat treatment; specimens for Auger analysis were prepared from the broken halves of the impact specimens.

3.3.2. Results

Following the first tests at austenitizing temperatures of 900C and 1000C it was clear that Steel 4+P readily produced intergranular fractures at 77K. As shown by the Auger spectra in Figures 3.8(a-b) (for the brine-quenched condition) the fractures are associated with concentrations of P on the prior austenite grain boundaries. Apart from very small S peaks, no other embrittling elements are present.

At temperatures in the vicinity of 900C P can diffuse rapidly

---

* Unless mentioned otherwise, austenitizing treatments were for 1hr, followed by a 5% brine quench.

in austenite {95} and the presence of P segregation* in as-quenched steels cannot necessarily be taken as proof that P segregates in the stable austenite phase (ie. above the A_3). The influence of a difference in quench rate on the fracture appearance is shown in Figure 3.9. It is clear that less severe quenching does not significantly alter the fracture appearance; this would support the view that a major part of the observed P segregation occurs above the A_3. Typical fractures produced in the two steels after quenching from 900C and 1000C are shown in Figures 3.10(a-d).

The AES results (given in Table 3.3) show that P segregation decreases as the austenitizing temperature is raised from 900C to 1000C. This is consistent with the small, but measurable, change in fracture appearance found in the mechanical tests. The effect of austenitizing temperature on the fracture appearance is shown in Figure 3.11; when quenched from 1300C in either brine or oil Steel 4+P gave fractures that were almost 100% quasi-cleavage (shown in Figures 3.12(a-b)). These results show that the observed decrease in the level of P segregation between 900C and 1000C is part of a general trend which continues to 1300C, where P has no detectable effect.

3.4. The Effect of P in Ni-Cr-Mn Steels

3.4.1. Experimental Details and Results

The technique described in Section 3.3.1 was also used to examine the effect of Mn on P segregation in austenite. In this case a melt of steel (Steel 5) similar in composition to Steel 4, but with a lower P content, was chosen as remelting stock. Steel 5 is a pure melt of 2.5Ni+1.4Cr steel with P analyses varying between 5 and 15ppm (Table 3.2). Comparatively large austenite grain-sizes were obtained in the stock material and fracture tests produced partly intergranular fractures over a range of austenitizing temperatures. It seemed

---

* It is assumed that the P is present as a solute segregant; in subsequent work (SEM, etc.) there was no indication of any form of phosphide precipitate.

unlikely that P was responsible because Steel 4 had a much higher P content (50ppm), but showed almost no tendency for intergranular fracture. Further tests, using a remelted version of Steel 5 containing 0.6%Mn (5+Mn), showed that the Mn addition eliminated the intergranular fracture mode (the results are shown in Figure 3.13). These factors suggested that the intergranular weakness in Steel 5 was due to S or possibly N segregation (this is supported by results obtained in Chapter 4, where the effect of tempering on the fracture mode of Steel 5 is examined).

The effect of remelting Steel 5+Mn with 0.12%P (Steel 5+Mn+P) is shown in Figure 3.14. Mn and P in combination produce very smooth-faceted fractures and even at an austenitizing temperature of 1350C the fracture was mostly intergranular (fractures for 1200C and 1350C are shown in Figures 3.15(a-b)).

It seems that one effect of Mn is to stabilize embrittlement at high austenitizing temperatures. To check that Mn really altered the fracture behaviour in steel treated at 1300C, samples of Steel 4, the steel used in preceding section, were remelted with the usual amount of P and just 500ppm Mn(Steel 4+0.05Mn+P). After austenitizing for either 1 or 2hr at 1300C this amount of Mn produced fractures that were about 30% intergranular; the results are shown in a plot of the combined data for Mn and P (Figure 3.16).

AES results for these steels are given Table 3.3 and are shown plotted as a function of austenitizing temperature in Figure 3.17. The AES results are broadly consistent with the changes in fracture appearance and it seems that, in the Ni-Cr steels examined, Mn alters the extent and temperature dependence of P segregation in austenite. In the Ni-Cr-Mn steels, AES did not detect any Mn segregation at the grain-boundaries.

3.5. Discussion and Conclusions

3.5.1. The Effects of Sb in Ni-Cr and Ni-Cr-Mo Steels

From temper embrittlement studies, Sb is known to be a potent embrittling element and the measurement of transition temperatures in hard, as-quenched material provides a severe test for any appreciable segregation in Steels 1, 2 and 3. No significant variations in

transition temperature were found, either between steels, or with austenitizing temperature variations. Apart from Steel 2, which appeared to show a slight degree of intergranular weakness, the low temperature fractures were wholly quasi-cleavage. It seems reasonable to conclude that the presence of 50ppm P, 120ppm Sb and 50ppm Sn does not embrittle Ni-Cr or Ni-Cr-Mo steels in the as-quenched condition. It was indicated in the Introduction that these elements would be expected to segregate during the austenitizing cycle, but it appears that the extent of segregation is insufficient to reduce the intergranular fracture resistance to a level below that of the transgranular resistance. The absence of any measurable effect of Sb content is in good agreement with other work {32,33,37,40} and it seems that this is a general result applicable to many steels.

The presence of IMC fractures in oil-quenched steels is rather interesting because the steels were not overheated in the conventional sense (ie. slowly cooled within the high austenitizing temperature range). The particles responsible for the fractures appear to be MnS which, for a Fe-Mn-S alloy containing about 0.6%Mn, will begin to enter solution in appreciable amounts at temperatures above about 1100C {70}. This would agree with the observed effect of austenitizing temperature on the occurrence of IMC fractures (see Table in Section 3.2.2.). Thus either the precipitation of MnS is difficult to suppress on another process is contributing to the formation of these fractures. Bearing in mind that S is a very strong segregant in Fe {88,96} one possibility to be considered is that the particles could result from S segregation. It should be noted that for a given amount of S in solution, the effect of Mn will be to increase S segregation; this follows directly from theory of Guttmann for interacting solutes {46,47} (Guttmann's estimate of the Mn-S surface interaction coefficient indicates that these elements will have a marked tendency to enhance each other's segregation in austenite). A more detailed study of possible factors contributing to IMC fractures is made in Chapter 4.

Conclusions:

i) Low concentrations of P(50ppm), Sb(120ppm) and Sn(50ppm) do not embrittle as-quenched Ni-Cr or Ni-Cr-Mo steels.

ii) In the three steels examined, oil-quenching from austenitizing temperatures above 1100C produced ductile

intergranular fractures in tests in the as-quenched condition.

iii) The particles responsible for the intergranular fractures appear to contain Mn and S; once in solution, S is expected to segregate strongly in austenite, but whether or not the particles result from the precipitation of segregated S remains to be determined.

3.5.2. The Effects of P in Ni-Cr Steels

1) The Importance of Cooling-Rate

Unless measurements of P segregation in austenite are made at temperature, some account must be taken of the extent to which P redistribution may occur during the quenching process. The results indicate that an increase in quench-rate from oil to brine does not significantly change the tendency for P to segregate to austenite grain boundaries, but it is still possible that adjustments in grain boundary composition occur so rapidly that they are essentially complete even during a brine quench. These effects can be analysed by assuming that P segregation in austenite will approximately obey the McLean isotherm {97}, then, at constant temperature, the time, t, for segregation to reach the half-way mark is given by:

$$t = 9.a^2.d^2\ (64D)^{-1} \qquad (3.2)$$

where a = equilib. boundary concn./bulk conc.
d = width of the grain boundary
and D = diffusion coefficient

Taking the equilibrium grain boundary concentration as 0.5 monolayers, d as 8 Å, and the diffusion coefficients for P in austenite from the work of Mural and Gruzin {95}, the times to reach 0.25 monolayers (about the level observed) are*:

---

* These times rely on P segregation in austenite obeying the assumptions of McLean segregation. Simple diffusional flow to the boundary gives shorter times, but as shown in Chapter 5, P segregation in α-Fe conforms to the McLean isotherm and it seems reasonable to assume that P will conform to this isotherm in γ.

700C : 20s
900C : 0.3s
1100C : 0.02s
1300C : 0.002s

The alloying elements Ni, Cr and C do not appear to greatly affect the diffusion of P in austenite {95}, but the diffusion coefficients will contain a component from grain boundary diffusion which cannot really contribute to grain boundary segregation and these times are possibly less than those actually required. For the specimen size used, the quench rate in brine is estimated to be in the vicinity of 500C s^{-1} and on the basis of the above figures, segregation during brine quenching from 900C may be ignored. In the case of oil-quenching (quench rate approximately 100C s^{-1}) there is sufficient time for some adjustment in grain boundary composition between 900C and about 800C, but the similarity in fracture behaviour between brine and oil quenched conditions indicates that this effect is small.

The intriguing observation is the complete absence of embrittlement in specimens either brine or oil quenched from 1300C; on cooling from 1300C there would appear to be ample time for full embrittlement in the temperature range 1100C-800C. Basically there are two possibilities:

a) P does not segregate significantly at 1300C and the above times underestimate those required for segregation at lower temperatures.

b) P segregates at 1300C, but some unknown process causes desegregation during cooling.

This latter process would, however, involve a movement away from equilibrium (since it has been shown that P segregates at equilibrium at 900C). Such an effect is unreasonable and the general consistency of the results obtained for both fast and slow quenching from 900C, 1000C and 1300C supports the former possibility.

2) The Extent of Segregation

The AES results for the Ni-Cr steels (Table 3.3), converted to monolayer P coverages (θ_P), are shown below:

T(C)	$^{*}\theta_P$	β	Fracture Test (%IG)	
			Brine	Oil
900	0.27	135	85 ± 5	80 ± 5
1000	0.19	95	80 ± 5	70 ± 5
1300	-	-	8 ± 5	5 ± 5
(1300)	0.078	39	-	-

* weighted coverage

The P coverage at 900C and 1000C corresponds to a free energy of segregation of $\Delta G = -2.75 kJ.mol^{-1}$; the coverage at 1300C, calculated using this free energy, is shown at the base of the table. The results show that at constant ΔG, the P coverage expected at 1300C would be about one third of the coverage at 900C.

The fracture tests indicate that the level of P segregation is probably more temperature dependent than that shown by the calculated result for 1300C. Kaneko et al. {98} have examined the effects of Ni, Cr and C on P solubility in Fe-X-P austenites and although Ni has only a small effect, both Cr and C strongly reduce the P solubility limit. By interaction with P, Ni and Cr will strengthen the temperature dependence of P solubility and hence increase the temperature dependence of segregation {99}. In steels there is another factor which may tend to offset this effect. As austenitizing temperature (and time) increases, the dissolution of Cr carbide will increase the Cr and C content of the matrix and the net effect will be to decrease the otherwise steeper temperature dependence of P segregation. In Ni-Cr-P steels, Cr has a similar effect on P solubility in both the α and γ phases {98} and the Cr-P interaction would seem to be the most important solute interaction in both phases. In the γ phase the presence of C in solution (in appreciable amounts) is an additional complication, but apart from the solubility data very little is known about the effect of C on P segregation.

3) Conclusions

i) P additions (0.12 wt%) to a pure steel containing 0.3C-2.5Ni-1.4Cr show that P segregates to austenite grain boundaries in the low temperature austenite range (below 1100C).

ii) The measured segregation levels for austenitizing temperatures of 900C and 1000C correspond to a free energy of P segregation of $-2.8 kJ.mol^{-1}$.

iii) P segregation decreases with austenitizing temperature and at 1300C only a slight segregation tendency remains.

3.5.3. The Effects of P in Ni-Cr-Mn Steels

The main effects of Mn are to increase and stabilize P segregation over the temperature range 900C-1200C. The AES results (Table 3.3) show that grain boundary P, C, and Cr all tend to increase with quenching temperature and at 1000C the P and Cr peak-height ratios are significantly higher than those observed in the Ni-Cr steel. A careful AES examination failed to detect any Mn segregation, but the Mn and Cr Auger peaks almost overlap and the presence of Cr (both as a segregant and in the bulk) may obscure low levels of Mn segregation.*

In all three steels examined (Mn-free, 0.05Mn and 0.6Mn) the P segregation levels appear to follow those of Cr; this is shown in Figure 3.18. It seems that the level of P segregation is decided primarily by the Cr-P surface interaction and this is in agreement with other work {98,99}, where it has been shown that the Cr-P interaction is considerably stronger than the Mn-P interaction. The result in Figure 3.18 seems to suggest that the effect of Mn is associated with a complex 3-way interaction between Mn, Cr and P. In this respect it should be noted that there appears to be thermodynamic evidence supporting a strong Mn-Cr interaction, and therefore it cannot be assumed that the effect of Mn is due simply to the Mn-P interaction. The Mn-Cr binary system has not been studied in any detail thermodynamically, but the phase diagram {100} shows that Mn and Cr form compounds of an $MnCr_x$ type (the heats of formation are

---

* This seems to be the case in temper embrittled steels as well; see Chapter 7.

not known). Perhaps the most relevant study is that of Kirchner and Uhrenius {101} who have evaluated the bulk ternary interaction coefficients (describing the excess free energy) for the Fe-Mn-Cr system. Their results for dilute γ-Fe at 900C show that the interaction of Mn and Cr together in Fe is much stronger than their individual reactions with Fe. It seems that in solution these elements may tend to enhance each other's segregation, and hence that of P.

The fracture test results and the AES results both suggest that the P coverage does not decrease, as might be expected, over the temperature range 900C-1200C. Why Mn should have such an effect on the temperature dependence is not clear; one possibility to be considered is the dissolution of Cr-carbides as mentioned above, although it seems unlikely that Mn itself will alter their dissolution behaviour. An alternative interpretation of the effect of austenitizing temperature is that the true temperature dependence resembles that of the Mn-free steel. Due to the higher segregation levels in the Ni-Cr-Mn steels, significantly greater amounts of P may segregate during the quenching process*. Inoue et al. {90} also found that the P segregation levels (in a steel containing 3%Mn+0.02%P) were similar after water quenching from either 1300C or 850C, but their specimens were large (apparently 13 x 13 x 70mm impact specimens) and the effect of segregation during quenching is not known.

As shown in Table 3.3, the grain boundary C concentration tends to follow that of Cr. The C levels are considerably higher than those observed from as-quenched transgranular fractures and show that C segregates to the grain boundaries. This seems to be a subsidiary effect of Cr and the high diffusion coefficient of C will allow this process to occur at low temperatures (possibly below the M_s temperature).

In the AES specimens there was no indication of a variation in the Ni level. The mean peak-height ratio was 2.50% which gives a Ni enrichment ratio in austenite of 4 ± 2.

---

* Although Mn increases the diffusion mobility of P in α-Fe, it does not appear to affect P diffusion in austenitic Fe-Mn-P alloys {95}; presumably Mn has a similar effect in Fe-C-Ni-Cr-P alloys.

Conclusions:

1) P additions (0.12 wt%) to a pure steel containing 0.3C+2.5Ni+1.4Cr+0.6Mn show that P segregates over a wide austenitizing temperature range. Compared with Mn-free Ni-Cr steels, Mn increases the level of P segregation.
2) The P enrichment ratio was found to be within 190 $\pm$ 30 for all temperatures between 900C and 1200C.
3) In both Ni-Cr and Ni-Cr-Mn steels the extent of P segregation seems to be related to the grain boundary Cr concentration.
4) It is suggested that the effect of Mn on P segregation in austenite is primarily due to Mn-P and/or Mn-Cr solute interactions.

Wt%	Steel 1	Steel 2	Steel 3
C	0.38	0.38	0.38
Si	0.26	0.27	0.27
Mn	0.62	0.66	0.63
Ni	2.72	2.78	2.39
Cr	0.79	0.83	0.51
Mo	<0.01	<0.01	0.50
V	<0.01	<0.01	<0.01
Cu	0.015	0.020	0.020
S	0.005	0.006	0.007
P	0.006	0.006	0.007
Sb	0.002	0.012	0.013
Sn	0.005	0.006	0.005
As	<0.005	<0.005	<0.005

Table 3.1. Chemical compositions of Steels 1, 2 and 3.

Steel	Wt%				ppm
	C	Ni	Cr	Mn	P
4 (stock)	0.29	2.46	1.26	(0.005)	50
4+P	(0.29)	(2.46)	(1.26)	(0.005)	1190±50
4+0.05Mn+P	(0.29)	(2.46)	(1.26)	(0.05)	(1200)
5 (stock)	0.30	2.50	1.37	0.01	10±5
5+Mn	(0.30)	(2.50)	(1.37)	0.6	(10±5)
5+Mn+P	(0.30)	(2.50)	(1.37)	(0.6)	(1200)

Table 3.2. Chemical compositions of Steels 4 and 5. Expected values are shown in parentheses. Impurity levels (ppm) for Steel 4 are; 30S, Sb<10, Sn<20, As<20, and for Steel 5; 30S, 300Si, 360xy, 120N, 10Sb, Sn<20, As<10.

Steel	%IG	P-120eV	S-150eV	C-270eV	Cr-489eV	O-510eV	Ni-848eV
4+P Brine Q. 900C	90	21.88±1.27(12)	2.00±1.52(4)	14.74±0.27(12)	2.11±0.34(12)	2.97±0.85(12)	2.53±0.08(12)
4+P Brine Q.1000C	96	16.80±1.29(8)	2.81±0.08(2)	16.68±0.48(8)	1.85±0.16(8)	5.44±1.76(8)	2.47±0.04(8)
4+0.05Mn+P Brine Q.1300C	100*	21.87±4.97(6)	4.89±1.17(3)	17.22±0.78(6)	2.00±0.14(5)	7.44±2.95(5)	2.48±0.06(6)
5+Mn+P Brine Q. 900C	83	28.54±5.63(10)	1.24±1.17(2)	15.46±7.29(2)	2.53±0.20(10)	3.49±1.01(10)	2.45±0.17(10)
5+Mn+P Brine Q.1000C	97	33.40±3.12(10)	0.84±0.81(2)	22.72±2.11(10)	2.66±0.11(9)	2.34±0.42(10)	2.48±0.15(9)
5+Mn+P Brine Q.1200C	100	40.00±7.69(8)	1.57±0.16(2)	28.57±2.42(7)	2.94±0.45(4)	6.00±0.91(7)	2.51±0.19(4)

* in area of measurement

Table 3.3. AES data for Steels 4 and 5 in the as-quenched condition, expressed as the peak-height ± std. deviation (no. of measurements). Peak-heights are not weighted. Measurements for Steel 4+0.05Mn+P were obtained from the intergranular area of a specimen containing ∿50% cleavage.

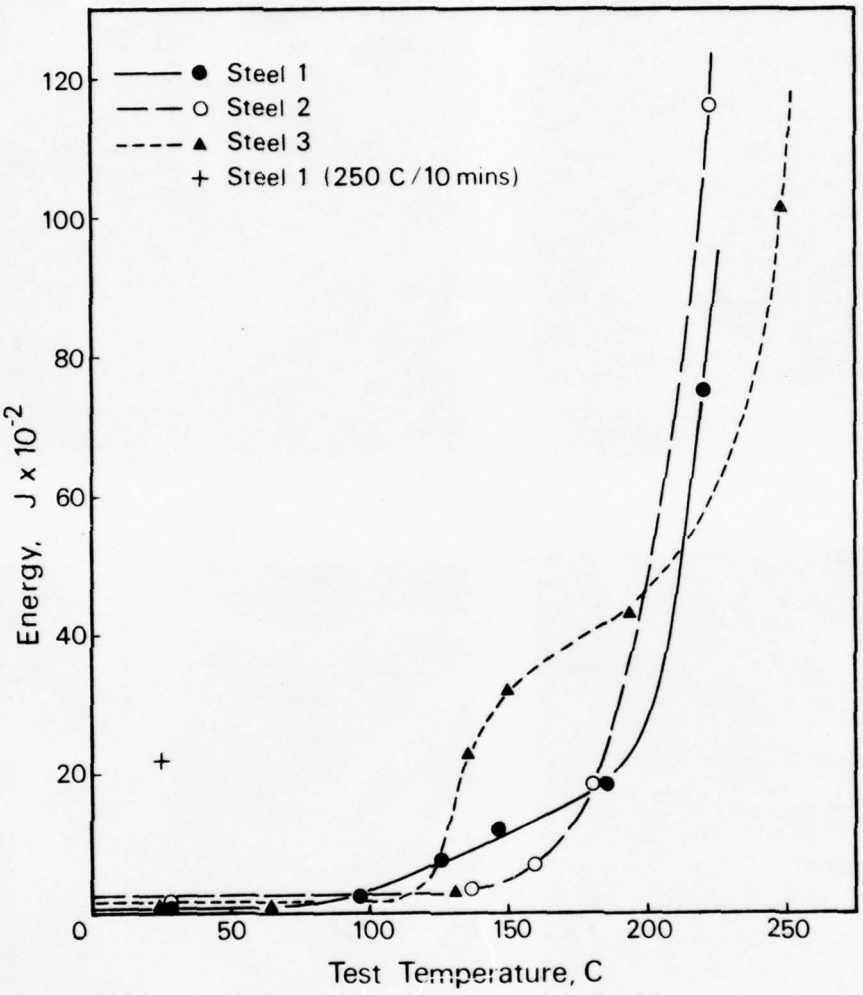

Figure 3.1. Variation in fracture energy with test temperature for Steels 1-3, brine quenched from 950C.

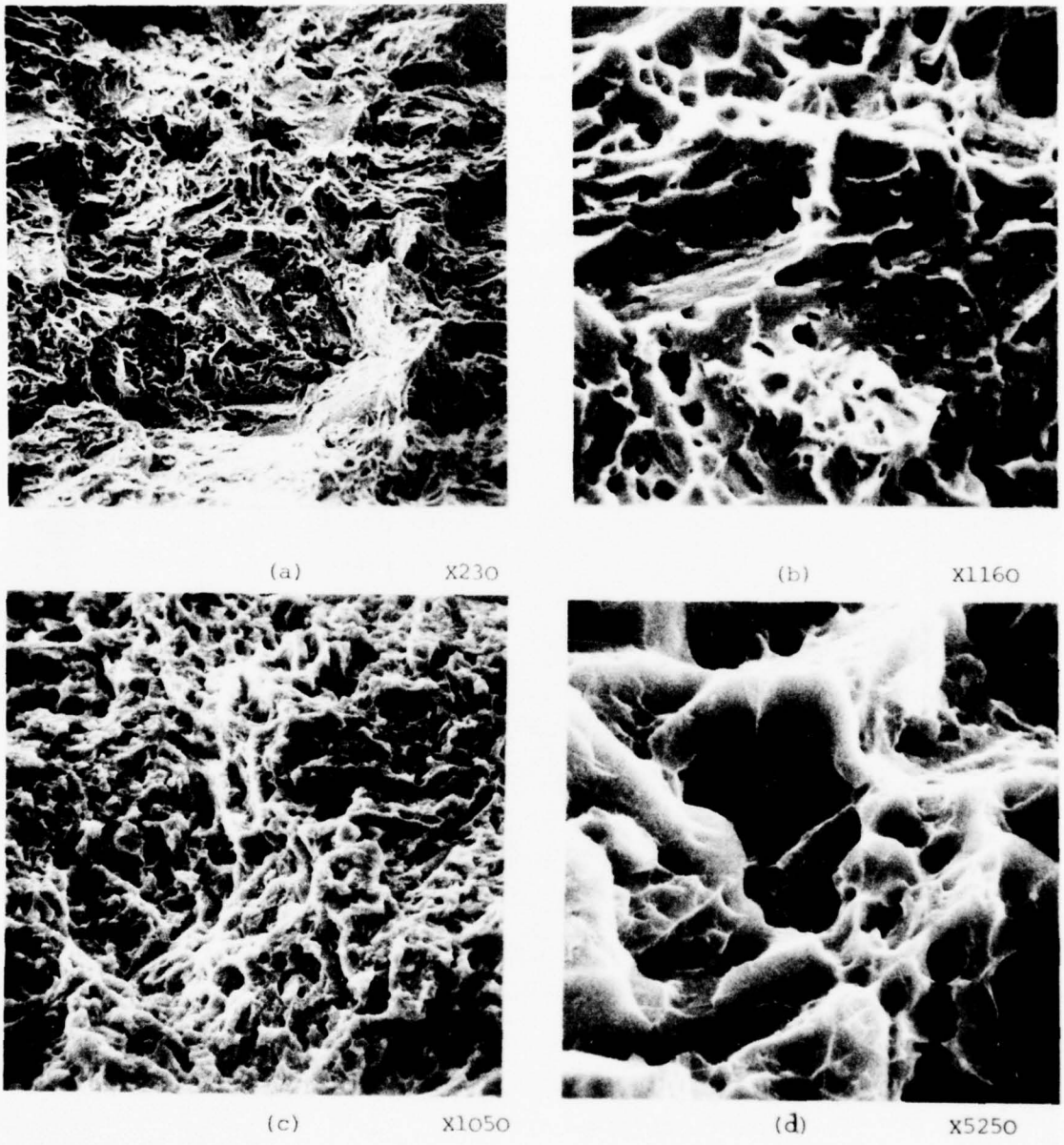

Figure 3.2. Fracture surfaces obtained after brine quenching from 950C and testing at 25C; (a)-(b), Steel 2; (c)-(d), Steel 3.

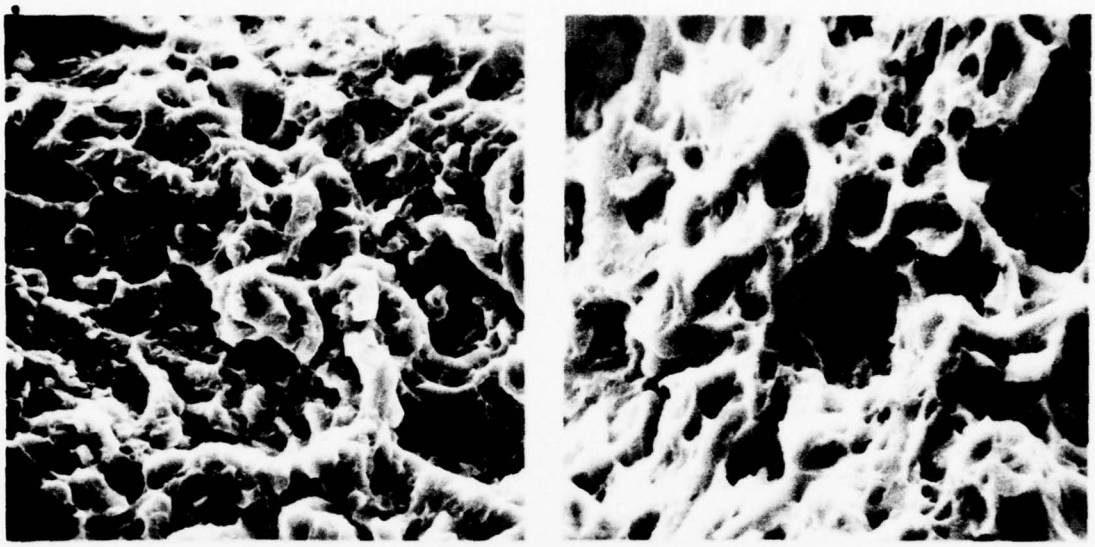

(a) X1950 (b) X2330

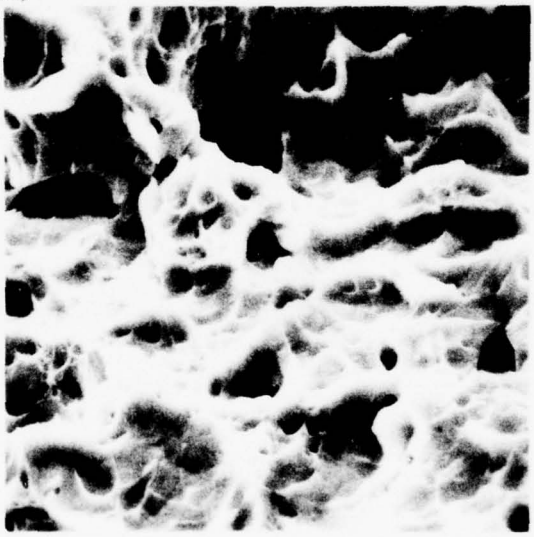

(c) X2400

Figure 3.3. Fracture surfaces of Steel 1 after brine quenching from 950C and testing at (a) -196C, (b) 25C, and (c) 140C.

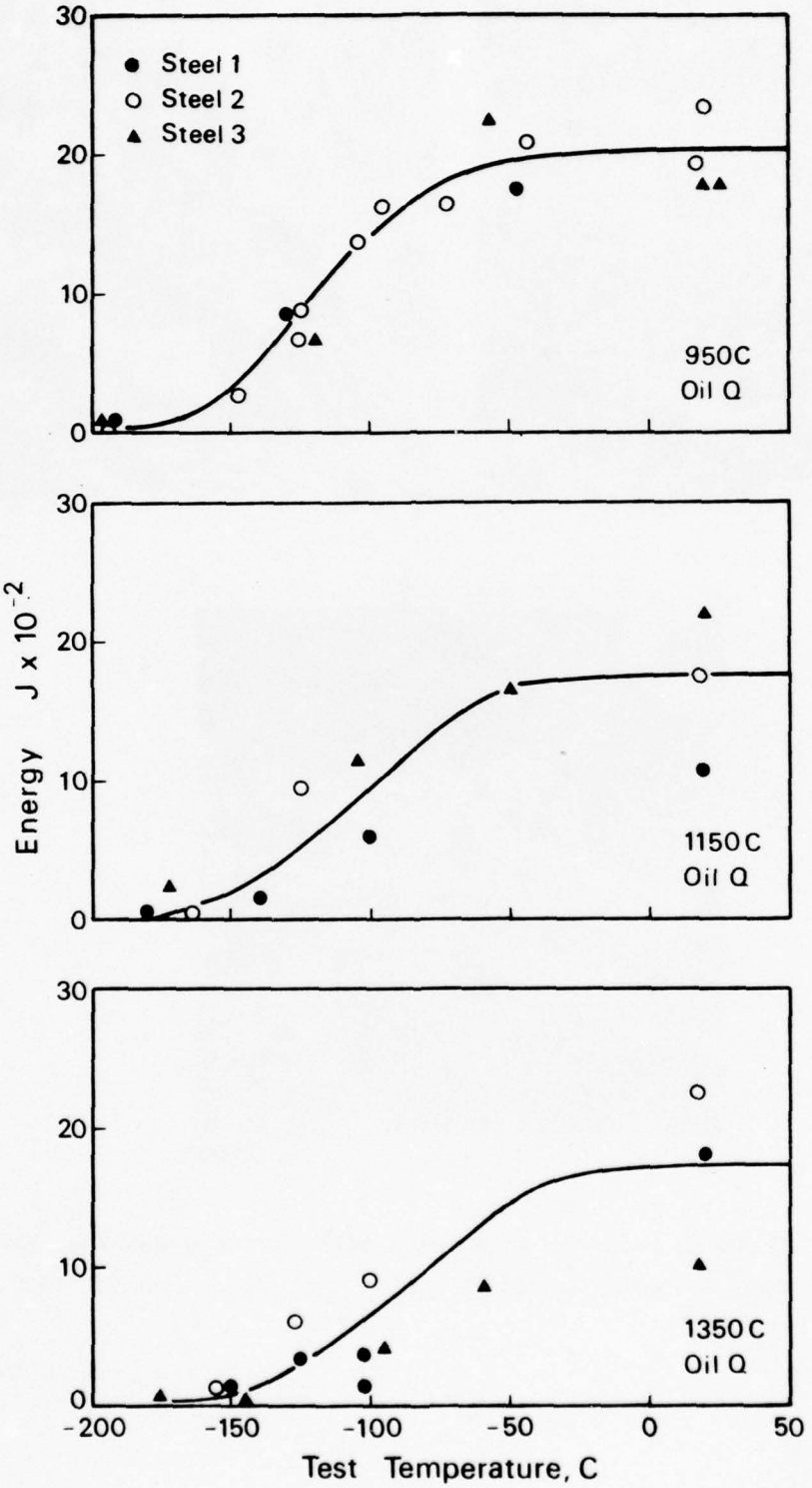

Figure 3.4. Variation in fracture energy with test temperature for Steels 1-3, oil quenched from different austenitizing temperatures.

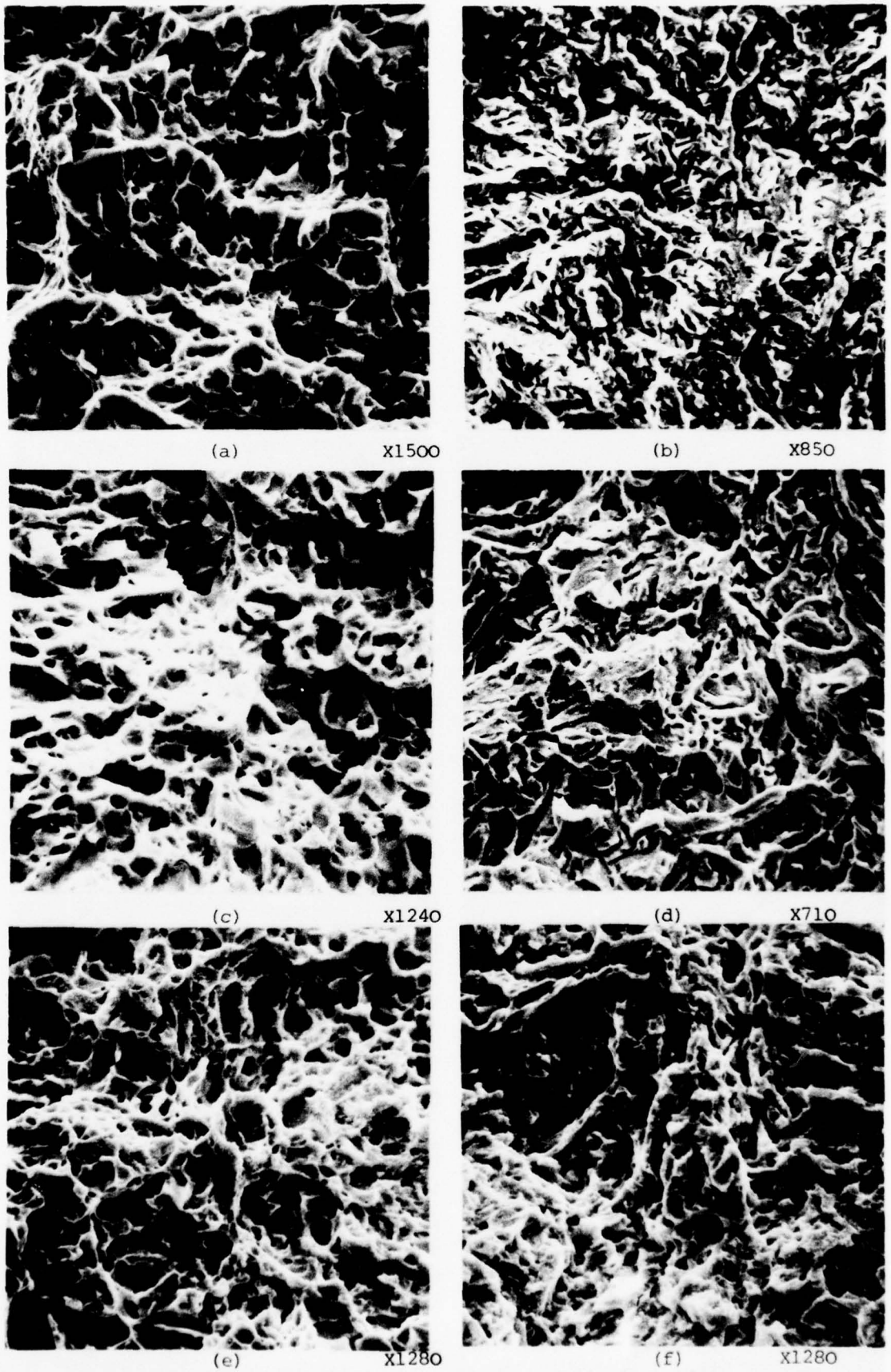

Figure 3.5. Fractures obtained after oil quenching from 950C; (a)-(b), Steel 1 tested at 25C and -196C, respectively; (c)-(d), Steel 2 tested at 17C and -196C, respectively; (e)-(f), Steel 3 tested at 25C and -196C, respectively.

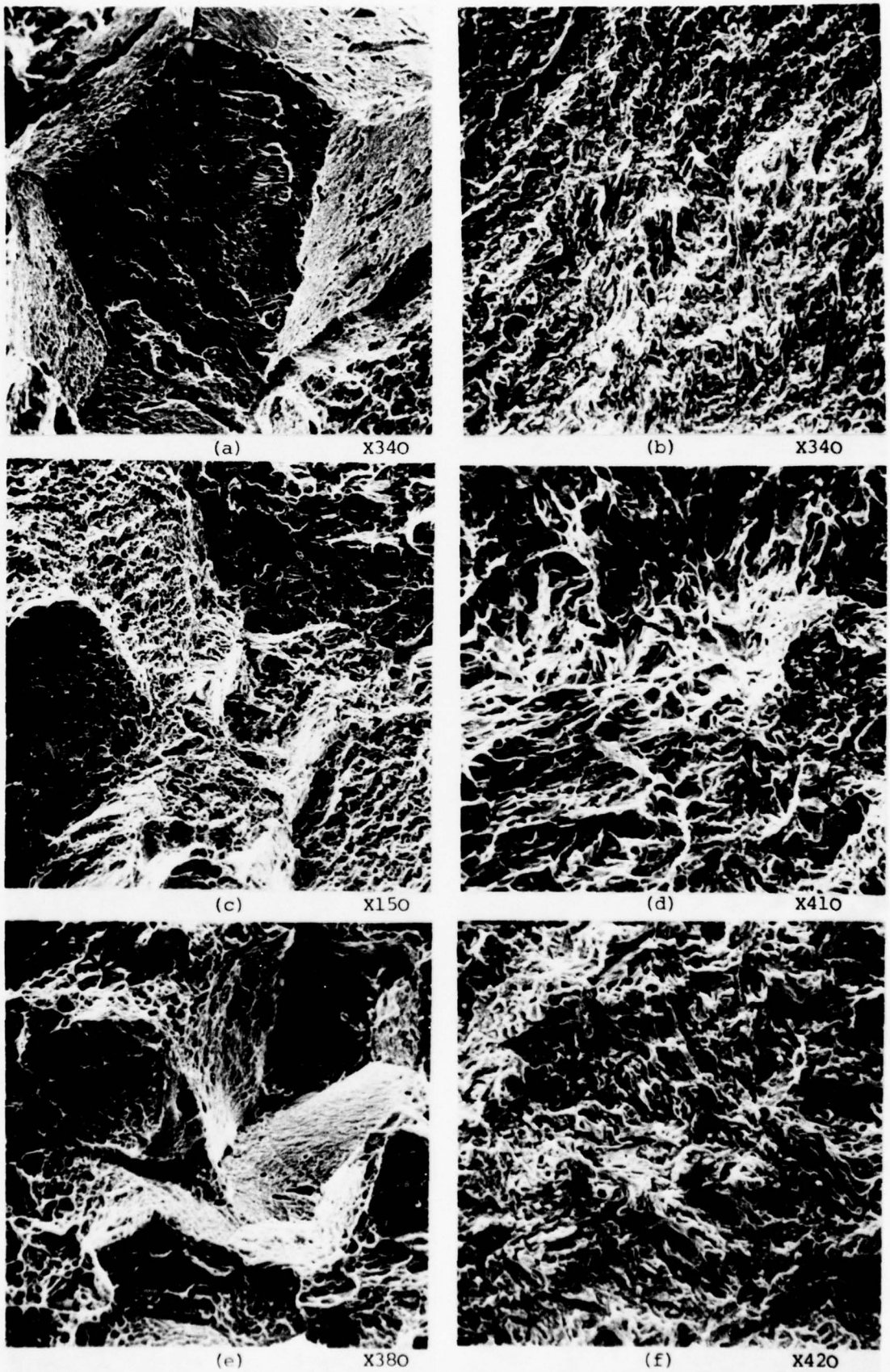

Figure 3.6. Fractures obtained after oil quenching from 1150C; (a)-(b), Steel 1 tested at 18C and -180C, respectively; (c)-(d), Steel 2 tested at 18C and -165C, respectively; (e)-(f), Steel 3 tested at 18C and -170C, respectively.

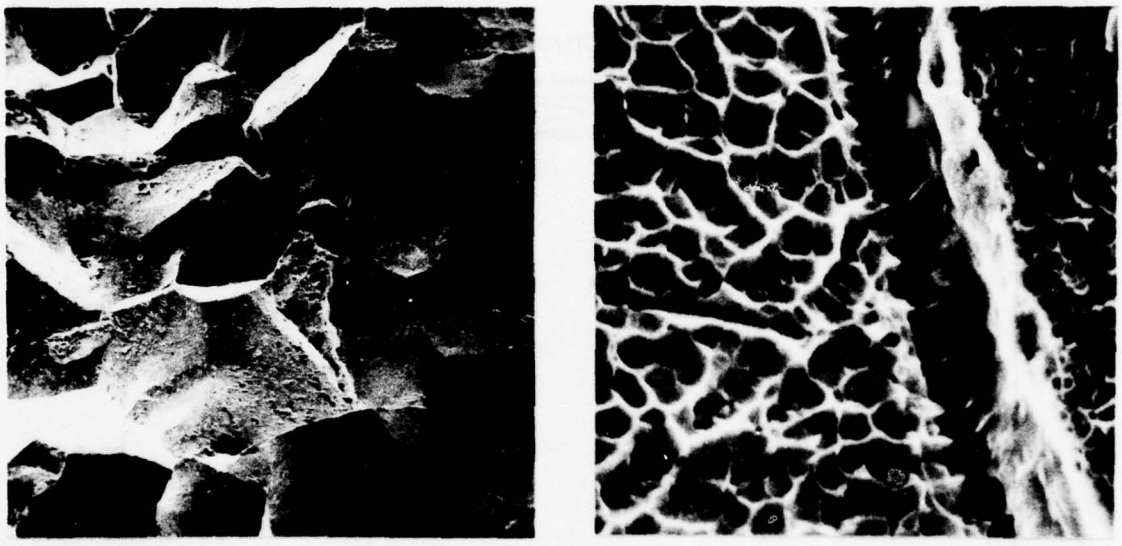

(a) X64 (b) X3100

Figure 3.7. Fracture surface of Steel 3 after oil quenching from 1350C and testing at 18C; (a) fracture along prior austenite grain boundaries, (b) detail of a region between neighbouring grains.

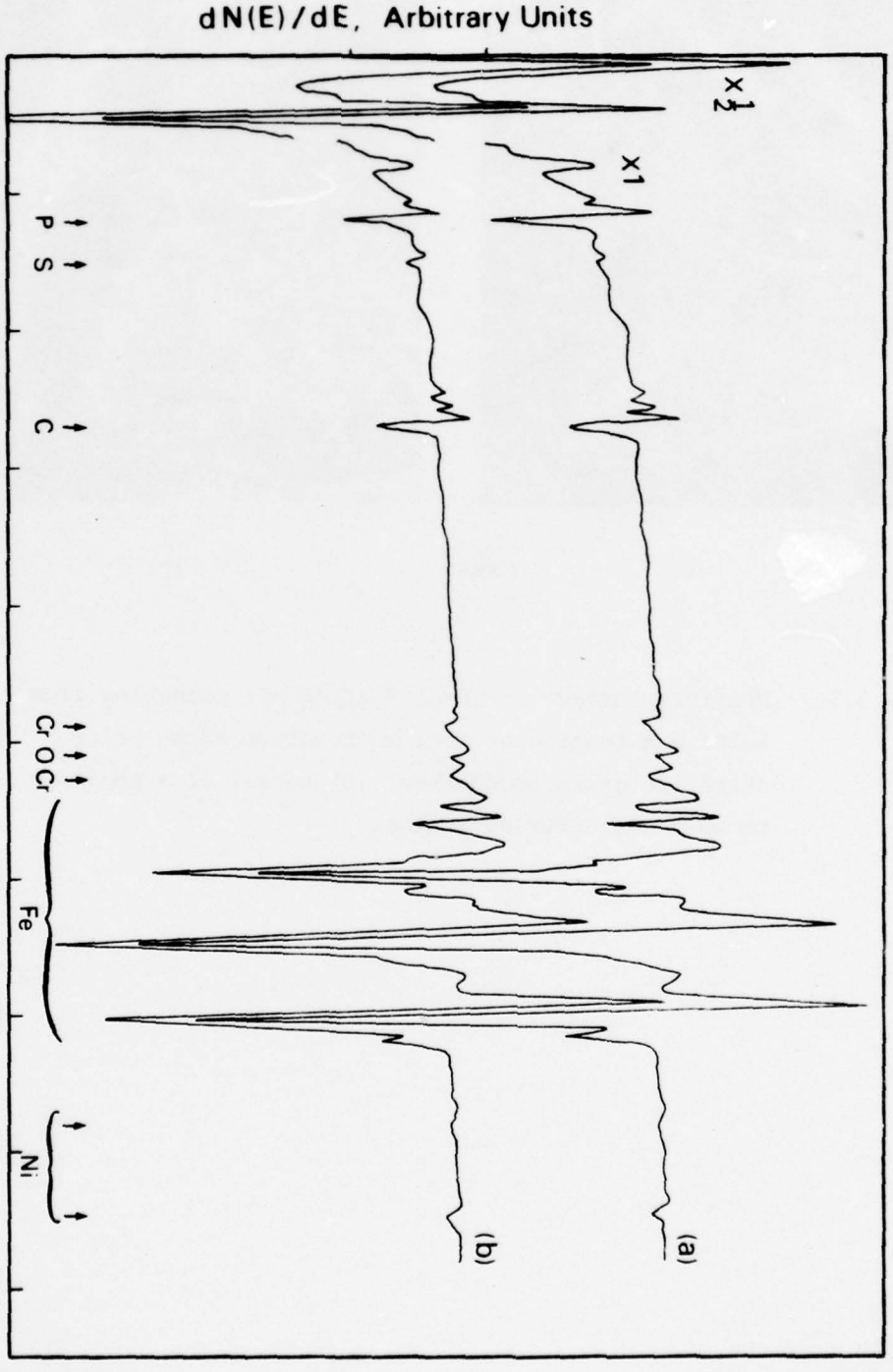

Figure 3.8. Examples of AES spectra obtained from Steel 4+P; (a) after brine quenching from 900C, (b) after brine quenching from 1000C.

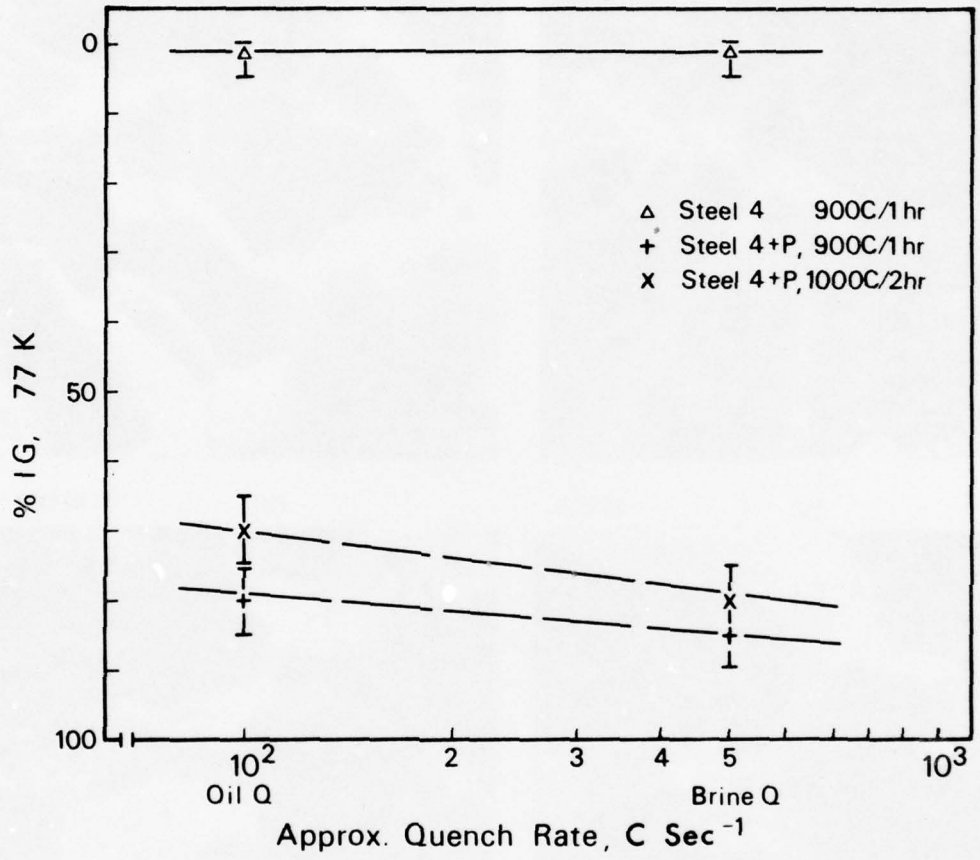

Figure 3.9. Effect of quench rate on fracture appearance in as-quenched steels.

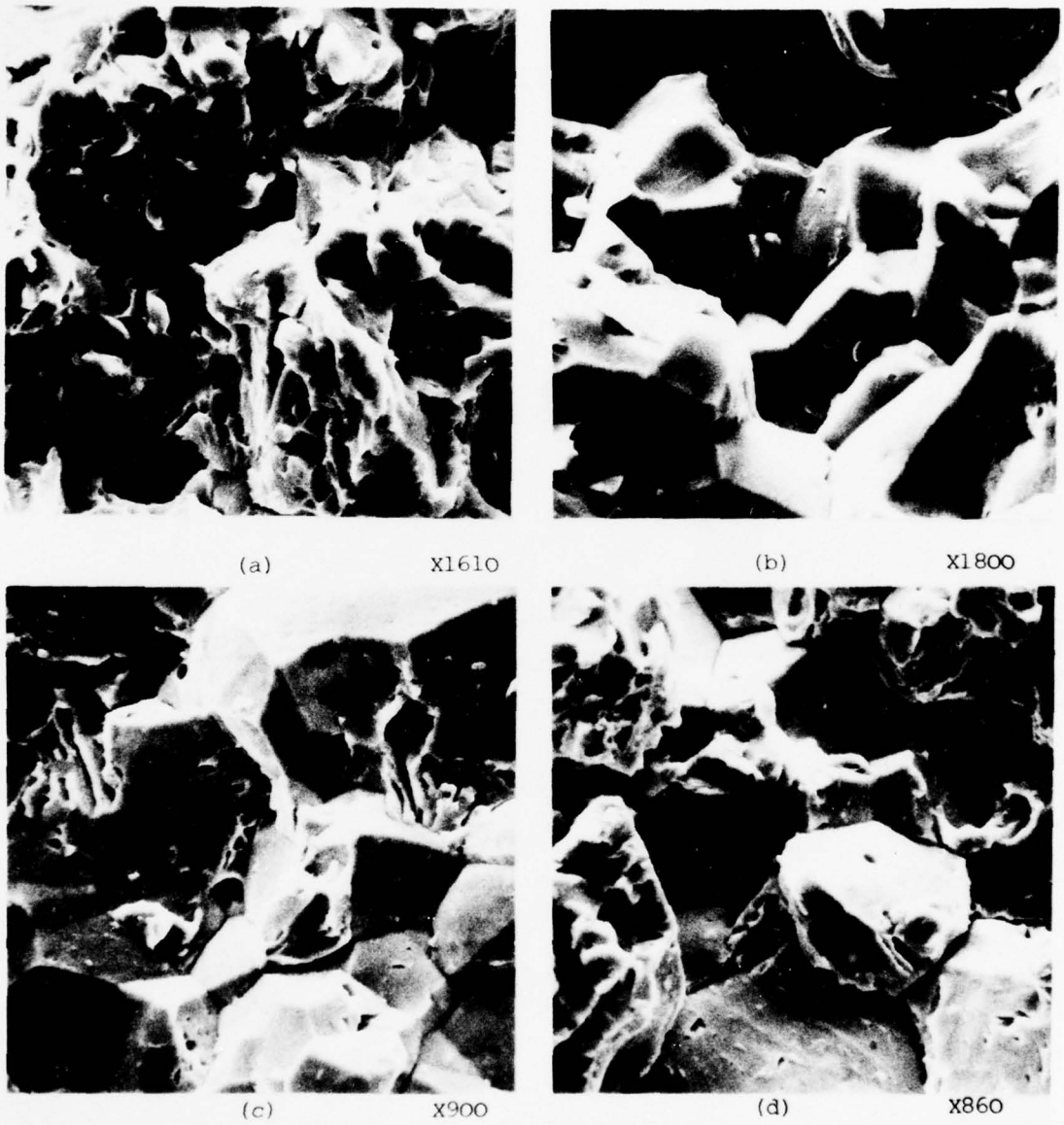

Figure 3.10. Fractures obtained after quenching from the austenitizing temperature and testing at 77K; (a) Steel 4 brine quenched from 900C, (b) Steel 4+P brine quenched from 900C, (c) Steel 4+P oil quenched from 1000C, and (d) Steel 4+P brine quenched from 1000C.

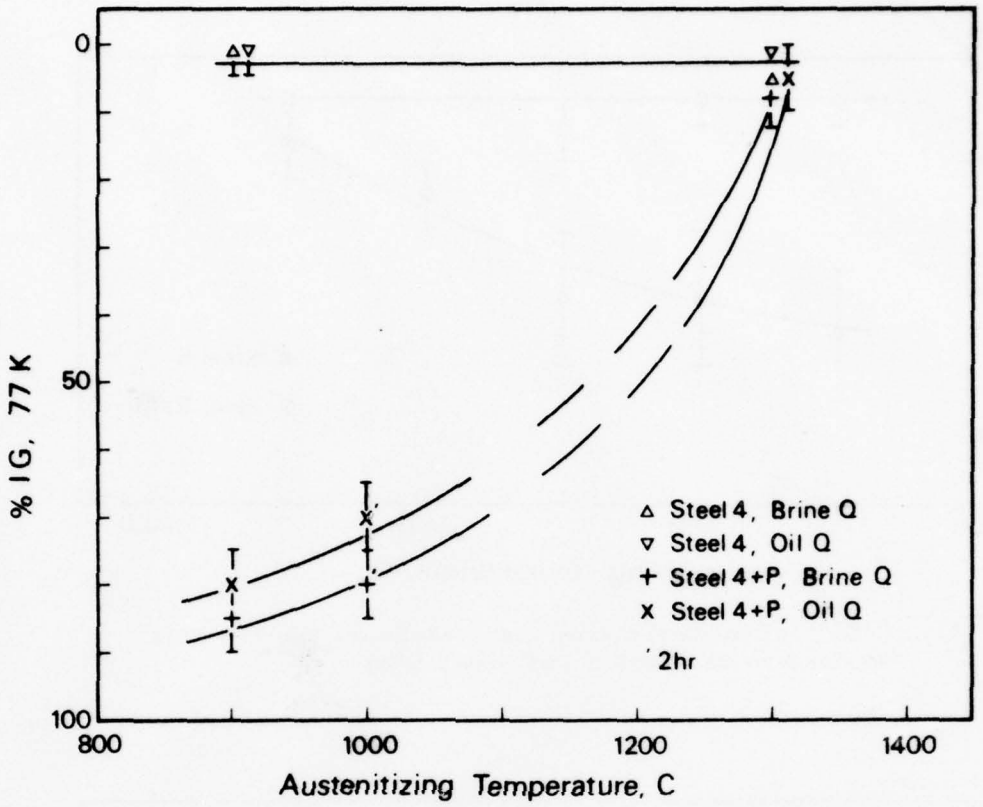

Figure 3.11. Effect of austenitizing temperature on fracture appearance in as-quenched Ni-Cr steels.

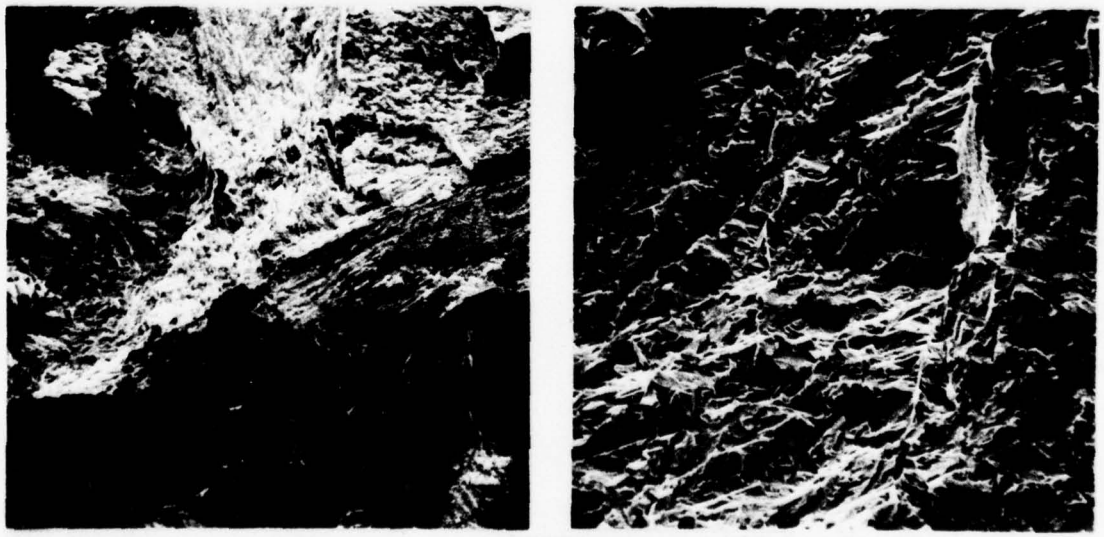

(a) X32 (b) X190

Figure 3.12. Fractures in Steel 4+P after quenching from 1300C and testing at 77K; (a) brine quench, (b) oil quench.

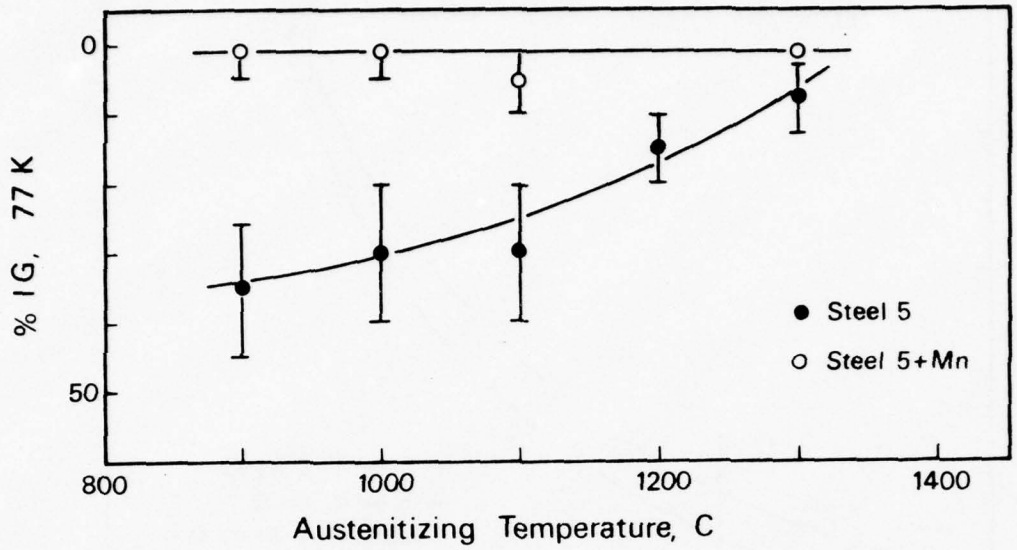

Figure 3.13. Effect of austenitizing temperature on the fracture appearance of Steel 5 and Steel 5+Mn.

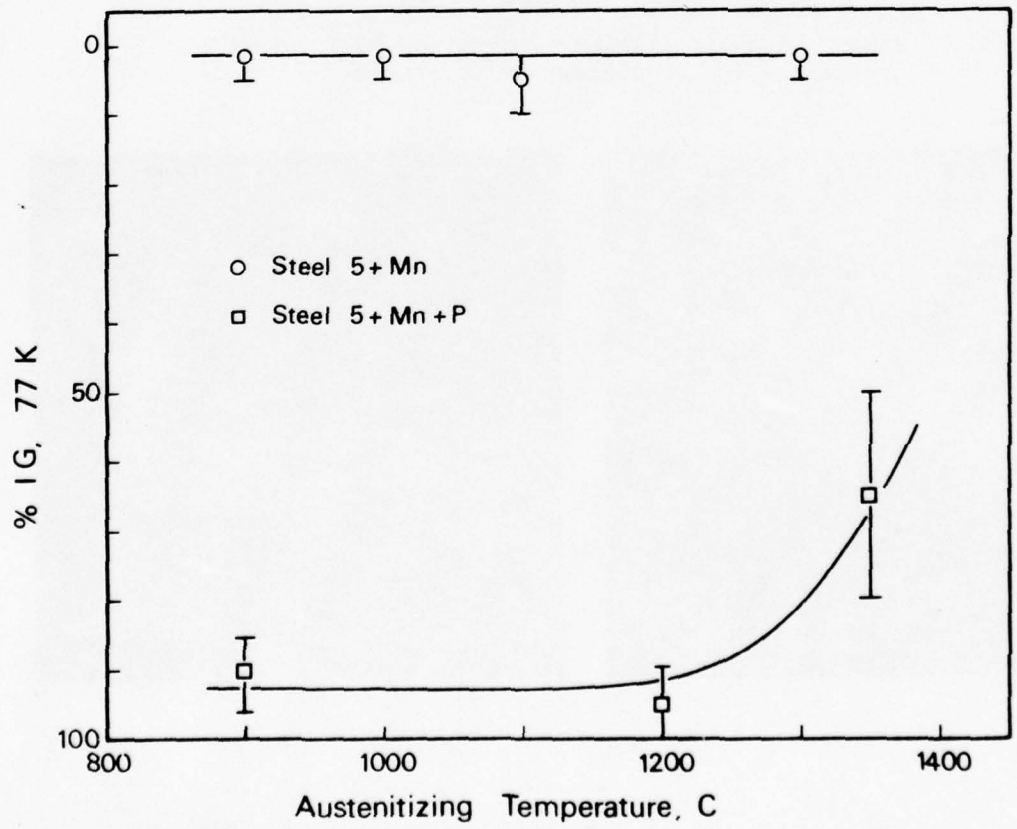

Figure 3.14. Effect of P on the fracture appearance of Steel 5+Mn.

Figure 3.15. Fractures in Steel 5+Mn+P obtained after brine quenching from the austenitizing temperature and testing at 77K; (a) quenched from 1200C, (b) quenched from 1350C.

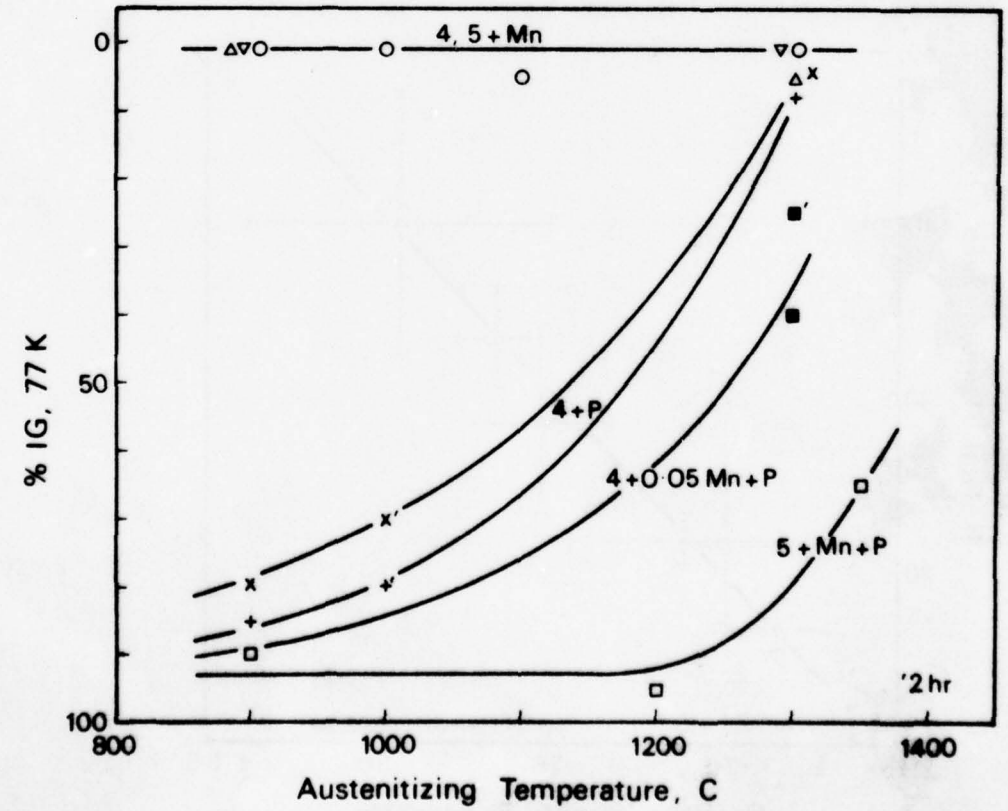

Figure 3.16. The effect of austenitizing temperature on the fracture appearance of Ni-Cr and Ni-Cr-Mn steels.

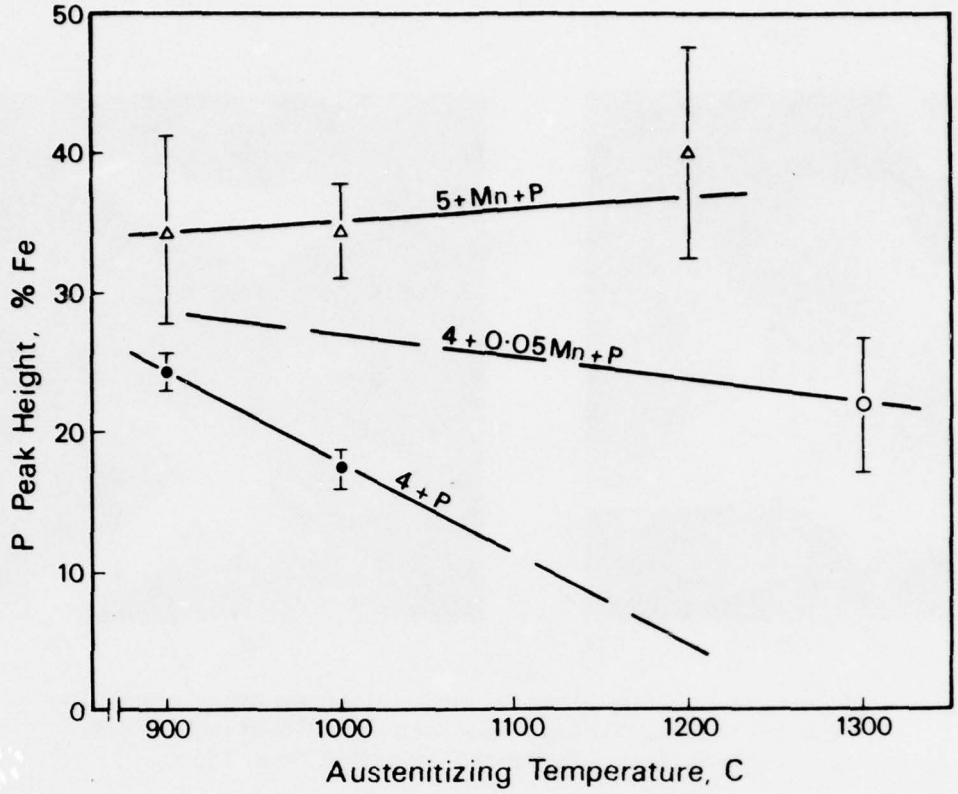

Figure 3.17. Phosphorus peak height as a function of austenitizing temperature. Peak heights have been weighted for the proportion of intergranular cleavage (Table 3.3).

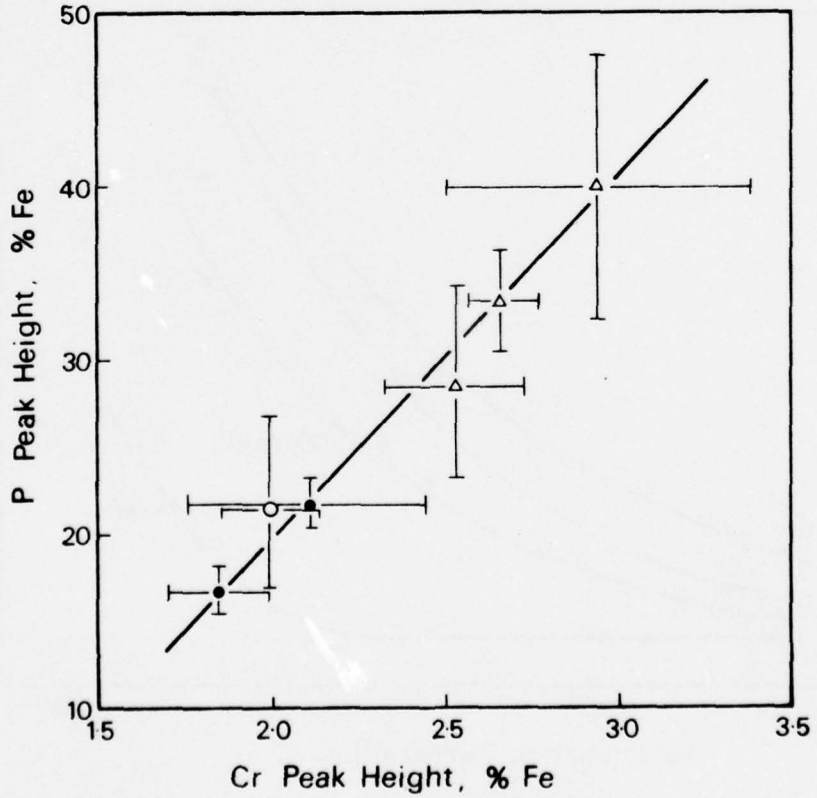

Figure 3.18. Relationship between P peak height and Cr peak height in Ni-Cr and Ni-Cr-Mn steels (from Table 3.3). Peak heights are not weighted.

CHAPTER 4

350C EMBRITTLEMENT AND OVERHEATING EFFECTS

4.1. Introduction

This Chapter is divided into two sections, both of which re-examine or extend some of the observations made in Chapter 3.

In the first section the susceptibility of the commercial purity steels (Steels 1, 2 and 3) to 350C embrittlement is examined. To enable a comparison to be made between results obtained in Chapter 3 and the results obtained in this Chapter, the same mechanical testing techniques have been employed. The effect of impurities on 350C embrittlement is investigated using steels with controlled variations in impurity content.

In Chapter 3 it was shown that Steels 1, 2 and 3 fractured by intergranular microvoid coalescence (IMC) when oil-quenched from high austenitizing temperatures. In the second section of this Chapter the factors responsible for IMC fractures are investigated, and the effects of austenitizing temperature and overheating on fracture toughness are determined in typical high strength steels.

4.2. 350C Embrittlement

4.2.1. Experimental Details

The chemical compositions of the steels are given in Table 3.1. Specimen blanks 8.00mm in diameter were austenitized in vacuum at temperatures of either 950C(1hr), 1150C(2hr) or 1350C(2hr) and quenched into either 5% brine (for the 950C treatments) or oil (treatments at 1150C and 1350C). The specimen blanks were tempered at 350C for either 1hr or 4hr and transition temperature specimens were then machined from the blanks.

AES specimens were machined from each steel, austenitized in vacuum at 1100C for 2hr, oil quenched, and tempered at 350C for 1hr.

4.2.2. Results

Transition temperature results for a 950C austenitizing treatment, followed by tempering for 1hr or 4hr, are shown in Figures 4.1(a-b). It is obvious from Figure 4.1(a) that Steel 3 (0.5%Mo) has a much lower

transition temperature than either Steel 1 or 2. Tempering for 4hr seems to produce a small increase in transition temperature for Steel 3 and a decrease in transition temperature for the other steels. The longer tempering time also reduces the experimental scatter in fracture energies.

SEM examination showed that all high energy fractures were transgranular microvoid coalescence (TMC). For both tempering times the low energy fractures for Steel 3 were 100% quasi-cleavage, as shown in Figures 4.2(a-b). In both Steels 1 and 2 the low energy fractures were mixed quasi-cleavage and intergranular cleavage, and there was no apparent effect of tempering time on the fracture appearance. Typical fractures for these steels are shown in Figures 4.2(c-f).

Transition temperature results for an 1150C austenitizing treatment followed by a 1hr temper are shown in Figure 4.3. Steels 1 and 2 show little change in behaviour from that observed for the 950C austenitizing treatment, but the energy transition for Steel 3 clearly increases in temperature. Also noticeable, particularly for Steel 3, is a decrease in upper shelf energy.

An examination of the fractures showed that the high energy fracture mode was generally IMC in all steels. The detail on the intergranular facets was found to vary from a deeply dimpled form to a smooth and almost featureless form. The smooth faceted form (referred to as mode IGS) was observed only in Steels 1 and 2, and only on a small proportion of the facets. Examples of the IMC and IGS fracture modes are shown in Figures 4.4(a-b). In all steels, fractures below the transition showed intergranular cleavage, present in the approximate amounts; Steel 1 - 95%, Steel 2 - 50% and Steel 3 - 10% (Figures 4.5(a-c)).

In Steels 1 and 2, reliable transition temperature tests could not be carried out on specimens austenitized at 1350C. This was an effect associated with the very large austenite grain size which introduced a wide scatter in fracture energies for specimens broken above the energy transition. An examination of the fractures suggested that at large austenite grain sizes (>notch radius) the fracture energy increases when there is no favourably orientated boundary beneath the notch. This effect reduces with austenite grain size, and at finer grain sizes (<notch radius), where there is always a grain boundary below the notch,

the fracture energy is reasonably constant. This phenomenon also occurred, but to a lesser degree, in tests on as-quenched steels.

It was possible however, to obtain transition temperature results for austenitization treatments at 1350C in Steel 3, which contained 0.5%Mo. Two austenitization treatments were investigated:

a) 1350C(2hr) + 350C(1hr)

and b) 1350C(2hr), furnace cool to 850C(2hr) + 350C(1hr)

The results are shown in Figure 4.6 and for comparison the results obtained for 950C and 1150C are included (tempered at 350C for 1hr in all cases). The austenitizing treatment has a pronounced effect on the susceptibility of Steel 3 to 350C embrittlement; at an energy of 5×10^{-2}J a transition temperature increase of 125C is produced by treatment b) above. For both 1350C heat treatments the high energy fractures were substantially IMC, and in treatment a) there were also areas of the IGS mode (Figure 4.7(a)). The low energy fractures in both cases were mixed intergranular and quasi-cleavage (Figures 4.7(b-c)).

The prior austenite grain sizes were determined from metallographic sections and are shown as a function of austenitizing temperature in Figure 4.8 (the grain size is plotted as the mean value $\pm$ std. deviation).

AES specimens of Steel 2 and 3 were fractured at about -90C and analysed. The fractures obtained were only partly intergranular and the approximate proportions of intergranular cleavage were 50% and 25%, for Steel 2 and 3, respectively. About 5 areas were analysed on each specimen and the spectra consistently showed a small P peak (around $1\%Fe_{703}$), and occasionally a small S peak (around $3\%Fe_{703}$); no other impurity elements were found. Due to the low proportions of intergranular fracture, the results have not been weighted or treated quantitatively, but a typical spectrum from Steel 2 is shown in Figure 4.9.

Because of the association between impurities and 350C embrittlement reported in the literature it was decided to examine the relative susceptibility of a set of 6 steels containing variations in P and Mn content. These steels were melted primarily for a detailed study of the temper embrittlement problem and their chemical compositions, etc. are given in Chapter 7. Hounsfield impact specimens were

austenitized at 900C(1hr), brine quenched, tempered for 30min at temperatures up to 500C, and tested at -30 ± 2C; the results are shown in Figure 4.10. The fractures from specimens tempered at 100C, 200C and 350C were examined by SEM and the fracture modes, in order of decreasing proportions, are given in the following table:

Steel	100C	200C	350C
5(10ppm P)	QC + IGC	IGC + TMC	IGC + QC
5 + Mn	QC(<5%IGC)	TMC(<10%IGC)	QC + IGC
6(70ppm P)	TMC + QC	TMC(100%)	QC + TMC
6 + Mn	"	"	"
7(200ppm P)	TMC + QC(<1%IGC)	"	QC + TMC + 5%IGC
7 + Mn	TMC + QC(<2%IGC)	"	50%IGC + QC + TMC

(Tested at -30C) where QC = quasi-cleavage
IGC = intergranular cleavage

A chemical analysis check of the residual impurities in the 10ppm P steels showed that P, S, Sb, Sn and As were all 30ppm or less, but the N level was found to be 120ppm. These two steels were of separate origin to the others; their inferior impact properties (Figure 4.10) and intergranular fracture modes are apparently due to their high N contents. For some reason Mn tends to reduce and eliminate N embrittlement. Judging by the fracture appearance the effect of N seems to become progressively stronger with tempering temperature up to 350C, after which the properties begin to improve dramatically (as shown in Chapter 7, tempering at 625C totally eliminates N embrittlement; this tempering effect is presumably due to scavenging by Cr).

The four higher P steels were melted as one batch from the same stock material and thus provide a sound basis for comparison. In these steels the 100C cleavage mode (typically 50%QC) disappears on tempering at 200C, where the only fracture mode observed was transgranular microvoid coalescence, but returns either as intergranular-

or quasi-cleavage at 350C (Figures 4.11(a-d) show fractures for 350C in the four steels).

The fractures clearly show that apart from a few splits there is no detectable tendency for intergranular cleavage in the two 70ppm P steels (tempered at 350C). However, both 200ppm P steels show intergranular cleavage and it would seem that an increase in P from 70ppm to 200ppm increases the proportion of intergranular cleavage. This is particularly obvious in the two Mn-bearing steels where the proportion of intergranular cleavage increases from almost nil to about 50% (Figures 4.11(b) and (d)).

Differences in C content make precise mechanical test comparisons difficult, but the magnitude of the embrittlement trough seems to increase with P content. In Steel 7 there is a continuous decrease in fracture energy in the tempering range 200C-300C and it is interesting that this effect is less apparent in Steel 7+Mn. In the presence of 200ppm P, Mn appears to displace the embrittlement trough upwards in temperature, and compared with the other steels Mn reduces the fracture energy at tempering temperatures above 350C.

4.2.3. Discussion and Conclusions

To enable an interpretation to be made of results obtained in the commercial purity steels it is desirable to define a transition temperature which indicates the embrittlement present after a given heat treatment. To avoid problems associated with variations in the upper shelf energy, a fracture energy, close to the NDT (nil-ductility temperature), of 5×10^{-2} J was selected for comparison. These transition temperatures, obtained by inspection of the results, are shown in Table 4.1. Because of the experimental scatter an error band of $\pm$ 15C, considered to be representative of the majority of the data, has been applied to the transition temperatures.

A plot of the results for the 950C austenitization, as a function of tempering time at 350C, is shown in Figure 4.12. The as-quenched fractures in all steels are virtually 100% quasi-cleavage (Chapter 3) and the increase in transition temperature in Steels 1 and 2 corresponds to the appearance of intergranular fractures (Figures 4.2(c-f)). As shown by the hardness values, the increase in transition temperature occurs despite a 200VPN decrease in hardness. For Steel 3 the behaviour

at 350C, after tempering for 1hr, is rather different from that of Steels 1 and 2. In this case there is a sharp decrease in transition temperature, corresponding to the hardness decrease, and the fracture mode remains 100% quasi-cleavage (Figure 4.2(a)). An aging treatment of 4hr seems slightly to reduce the embrittlement in Steels 1 and 2, but the fractures still show a similar amount of intergranular cleavage (Figures 4.2(c-f)). The decrease in transition temperature is consistent with a hardness decrease or, in terms of a carbide rejection process, a decrease in the rate of grain boundary carbide growth. In Steel 3 there appears to be a slight increase in susceptibility with aging time between 1hr and 4hr indicating that Mo may retard the embrittlement kinetics, however this is based on limited data and there are no signs of intergranular fracture after 4hr at 350C (Figure 4.2(b)).

The results for an austenitizing temperature of 1150C are also shown in Figure 4.12. In Steels 1 and 2 austenitization at 1150C produces much the same effects as those observed at 950C, but in Steel 3 there is a marked change in transition behaviour coincident with a slight, but distinct, tendency for intergranular cleavage (Figure 4.5(c)).

These observations suggest that the susceptibility of Steel 3 to 350C embrittlement is related to austenite grain size and a plot of the results as a function of grain size is shown in Figure 4.13. Austenite grain sizes above about 100μm have little effect on the measured transition temperatures but, in Steel 3, the very fine grain size appears to produce a low transition temperature. In these steels the effect of austenitizing temperature per se is small, as shown by the result obtained for the 1350/850C treatment in Steel 3. Figure 4.13 also shows that Sb content has no measurable effect on 350C embrittlement.

In the three commercial steels studied, the highest transition temperatures are clearly related to the heat treatments producing the larger proportions of intergranular cleavage. However the proportion of intergranular cleavage alone is not a satisfactory indication of susceptibility because the transition temperature increases abruptly before the low energy fractures show more than a few per cent of intergranular cleavage. This non-linear relationship between fracture appearance and transition temperature suggests that the primary role

of an embrittled boundary (prior austenite, lath, carbide-ferrite, etc.) is to facilitate the initiation of a crack which can spread by quasi-cleavage. This could be associated with a tendency for some boundaries to embrittle more than others. It is only at high embrittlement levels (or at large grain sizes) that the crack propagates by intergranular cleavage.

Commercial Ni-Cr high strength steels are conventionally austenitized at temperatures such as 830C or 850C and the prior austenite grain sizes are typically in the range 30-60μm. In an impact energy/tempering temperature test these fine-grained steels show an energy trough at about 350C, indicating that several factors such as impurity content, alloy content and the type of test (strain rate, test temperature, etc.) probably affect the relationship between grain size and susceptibility.

In Figure 4.10(c) it is shown that, at high P levels, Mn appears to displace the embrittlement trough upwards in temperature. Based on the diffusion equation obtained from studies in ferrite at 700C-900C {25}, 0.6%Mn will increase P diffusion at 350C by a very large factor (500-1000). Assuming that Mn will exert a similar effect in dislocated ferrite, this trough displacement can be interpreted in terms of Mn increasing the diffusion of P in Fe. In the temperature range 200C-300C an increased P mobility will tend to lower the concentrations at carbide-ferrite interfaces by P diffusion into the matrix. At higher temperatures of 300C-400C, Fe_3C begins to form in appreciable amounts along the prior austenite grain boundaries, but the rejected P can now rapidly escape via the boundaries as an equilibrium segregant, producing a decrease in toughness (Figure 4.10(c)), and intergranular fractures (Figure 4.11(d)). The relatively poor impact properties of Steel 7+Mn at temperatures above 350C seem to be due to an acceleration of the temper embrittlement kinetics by Mn (see Chapter 7).

Conclusions*

The results obtained in this investigation support the view that 350C embrittlement is primarily due to carbide rejection of impurities

---

* Because yield stress, work hardening, carbide formation, etc. all vary with tempering temperature there is no reason to assume that a pure steel will not show a tendency towards embrittlement at some stage during tempering. The conclusions obtained here refer particularly to the magnitude of the problem in commercial low alloy steels.

or to carbide formation at impurity embrittled interfaces; the principal impurity responsible appears to be P. In summary, the main points, consistent with this conclusion, are:

1. In three commercial purity Ni-Cr and Ni-Cr-Mo steels, a high 350C susceptibility (as measured by a transition temperature test) is related to an increased tendency for low-temperature fractures to occur by intergranular cleavage, rather than by quasi-cleavage.
2. AES analyses show that P is present on the intergranular cleavage fracture surfaces. The P level (around 1-2%Fe_{703}) corresponds to a grain boundary P enrichment (for the steels examined, the enrichment factor is in the vicinity of 200).
3. The critical embrittlement mechanism occurs <u>at</u> 350C; susceptible steels show no embrittlement in the as-quenched condition. On tempering at 350C the transition temperature increases and the brittle fracture mode tends to change from 100% quasi-cleavage to intergranular cleavage.
4. In high-purity steels, impact test results suggest that the proportion of intergranular cleavage and the embrittlement trough (between 200C-400C) both increase with P content. Mn, which is known to affect P diffusion in recrystallized ferrite alters the shape of the trough.
5. Limited results indicate that N also produces intergranular embrittlement at low tempering temperatures (<400C), but rather than creating a trough, N seems to cause general embrittlement at all temperatures up to 400C.
6. Variations in Sb content between 20 and 120ppm have no measurable effect on 350C embrittlement susceptibility.

4.3. Overheating Effects

4.3.1. Experimental Details

Initially it was proposed to examine overheating effects in Steels 1, 2 and 3. However tests showed that these steels tended to quench-crack when rapidly quenched in the large specimen sizes required for fracture toughness tests. Two new steels, referred to as Steels 8 and 9, were therefore introduced for this study. These steels have lower carbon contents than Steels 1, 2 and 3, and are basically two

commercial melts of En25 specification.

The main difference between Steels 8 and 9 is in the steelmaking technique. Steel 8 is a double-slag electric air melt and Steel 9 is a vacuum melt; both steels were produced from the same melting stock and their chemical compositions are given in Table 4.2.

The steels were supplied as 35kg billets which were sawn into sections, then hot-forged to give 25mm square bars. Fracture toughness (K_{IC}) specimens, 20mm square x 100mm long were machined from the bars. Most of the specimens were centrally notched (60^{o}) to a depth of 5.0mm prior to heat treatment, but to avoid cracking on quenching, notches in severely quenched specimens were cut after heat treatment with a 0.15mm thick silicon carbide slitting wheel. The specimens were austenitized for 2hr in vacuum and either brine or oil quenched; some specimens were tempered for 1hr at 300C in a fluidized bed. After heat treatment all specimens were precracked on a Mand servohydraulic testing machine under displacement control, at a frequency of 100Hz. The specimens were then tested in four-point bend according to the provisional BSI procedure for fracture toughness measurement {102}. Concerning the BSI procedure, the following validity checks were applied:

1. Deviation at $0.8P_Q \leq$ 25% Deviation at P_Q
2. $P_{max} \leq 1.1P_Q$
3. Crack geometry requirements.
4. $(a, W-a, B) > 2.5(K_Q/\sigma_y)^2$

where P_Q = 5% offset load.
a = crack length
W = specimen width
B = specimen thickness
$W-a$ = uncracked ligament depth

All specimens satisfied the Validity Checks 1-3 (except one specimen containing a 0.38mm notch, where the deviation at $0.8P_Q$ was 40% of the deviation at P_Q). In Check 4 all specimens satisfied the dimensional requirements for B, but the requirements for a and W-a (both about 0.5B)

were only met strictly at values of fracture toughness below 90MNm$^{-3/2}$.

4.3.2. Results

The fracture toughness of Steel 8, measured in the as-quenched condition for various austenitizing treatments is shown in Figure 4.14. Austenitizing (2hr) at temperatures in the range 850C-1300C, followed by oil quenching, produced only small variations in fracture toughness; brine quenching from 1300C produced a slight increase in toughness compared with the oil quenched condition. The effect of a conventional overheating treatment is also shown in Figure 4.14. These specimens were austenitized at 1300C for 2hr, furnace cooled at about 10C min^{-1} to 850C, held for 2hr, then either brine- or oil-quenched. The overheated materials showed slightly higher toughnesses than material austenitized at 850C.

SEM examination showed that fractures from specimens austenitized at 850C and 1000C were 100%TMC; at 1150C the fracture was similar, but with slight tendency for IMC. Both brine- and oil-quenching from 1300C resulted in a change of fracture mode to a high proportion of IMC. As expected, the overheated material also produced IMC fractures. These IMC fractures were superficially identical, but close examination showed that the particles nucleating the dimples were much larger and more obvious in the overheated materials; the dimple spacing was also larger. These features are shown in Figures 4.15(a-d). EDAX examination of the particle compositions was carried out in the following manner. Firstly the particles were analysed to give a fixed Fe count, then the background was analysed (on line scan) to give the same Fe count. By subtracting the background count, the elements present in the particle could be determined. In this way it was possible to show, for example, that the Cr signal obtained during the analysis of a very small particle was generally a contribution from the background, rather than from the particle itself. This procedure was applied specifically to two specimens of Steel 8, one brine-quenched from 1300C, and the other brine-quenched from 850C after slow cooling from 1300C. The EDAX analyses showed that the particles on the facets of the directly quenched specimen (typically 0.2-0.6μm) usually contained Mn and S; Al and Cr were occasionally present and in a few

cases the particles showed only Al. In the overheated material the particles (typically 1-3μm) almost invariably contained just Mn and S.

The influence of austenitizing temperature on the as-quenched, and quenched and lightly tempered toughness of Steel 9 is shown in Figure 4.16. Up to 1150C the results and fractures were similar to those obtained in Steel 8, but at 1300C the toughness increased and the fracture mode changed to mixed TMC and IMC (Figures 4.17(a-b)). The austenite grain size increased greatly between 1150C and 1300C and this appeared to be associated with the increase in fracture toughness. An 8hr austenitizing treatment at 1300C produced a slight decrease in the proportion of IMC fracture, but the value of fracture toughness was not affected. The notched toughness of the material austenitized at 1300C was measured using a 0.38mm notch and the specimen was tested under normal fracture toughness conditions. Although this method invalidated the fracture toughness procedures, the result indicated that the notch fracture resistance of the material was not significantly higher than the sharp crack resistance (for the same heat treatment and a/W ratio, the maximum load for the notched specimen was 7% higher than the sharp crack load). Figure 4.16 also shows the fracture toughness after tempering for 1hr at 300C. The increase in toughness on tempering is most marked for low austenitizing temperatures; again the fracture mode for 1150C and below was TMC, and at 1300C the fracture was mixed TMC, IMC and intergranular cleavage.

The occurrence of IMC fractures agreed with the observations in Chapter 3, but it was surprising to find that, in the fracture toughness specimens, the effect appeared to be independent of quenching media (brine or oil). Since the IMC fractures were only observed in these two materials after heat treatment at 1300C, it was decided, as a preliminary check, to ensure that the materials had not been previously overheated. The approximate forging temperatures used in the preparation of the fracture toughness specimens are shown below:

	Max. Temp.	Finishing Temp.
Steel 8	1200C	1000C
Steel 9	1100C	900C

Under forging conditions, these temperatures did not seem to be sufficiently high to produce conventional overheating effects. A a fracture test a specimen of Steel 8 was prepared from half of a fracture toughness specimen previously austenitized at 850C. This specimen was tempered to a tough condition (600C/1hr) and when fractured produced 100%TMC. Etching (in 10% nitric + 10% sulphuric acid) showed no grain boundary delineation (tempered or untempered conditions). These tests confirmed that the materials had not been overheated and that the IMC fractures resulted from the last austenitization treatment.

Metallographic specimens were prepared from part of the fracture toughness testpiece of Steel 8, austenitized at 1300C (oil quench). In the as-quenched condition etching tests revealed a slight tendency for fine pitting around the austenite grain boundaries. After tempering this pitting effect was much clearer suggesting that fine MnS-bearing particles were present on the grain boundaries (it was shown in later work that the need for tempering was largely to produce a ferritic microstructure and thereby provide improved etching conditions).

In the next experiments the main aim was to determine whether or not the particles were on the austenite grain boundaries prior to quenching. The specimens used in these metallographic studies were 10 x 10 x 10mm samples of Steel 8. Heat treatment was under a vacuum of $<10^{-5}$ torr and specimens were rapidly water-quenched after the austenitizing treatment.

The metallographic samples were subjected to a variety of heat treatments in the austenite range; about 15 heat treatment variations were employed at temperatures between 1150C and 1410C. These included isothermal heat treatment, isothermal combined with slow heating, and slow heating alone (the latter two heat treatments were to simulate the austenitization of a larger specimen). Because sectioning and etching in the as-quenched condition rarely showed any effect, tempering at 600-650C was adopted as a standard procedure. In summary, the main results were:

1) In most specimens clearly resolvable particles were found on the grain boundaries, particularly after heating or holding within the range 1250C-1350C.
2) The particles were part of a general distribution that extended throughout the interior of the samples.

3) Prolonged heating (at 1270C, for 15-25hr) appeared to reduce the grain boundary particle population.

4) Heating at 1400 for 2½hr eliminated most of the particles, but increased the delineation of the boundaries by etching.

Examples of the particles, for two different heat treatments, are shown in Figures 4.18(a-d); in all cases heating was at 1C min^{-1}. Figure 4.19(a) shows the persistence of these particles (from the treatment shown in Figures 4.18(c-d)) after a second, low temperature (900C/1hr), austenitizing treatment. Most specimens showed a surface region, less than 100μm in depth, which contained a very high particle density. Unlike the grain boundary particles described above, these particles were clearly visible in the unetched condition. Figure 4.19(b) shows a typical surface region; this effect is presumably due to O, or N penetration.

The particles in Figure 4.19(a) were only obvious at the steps marked P in the following heat treatment cycle:

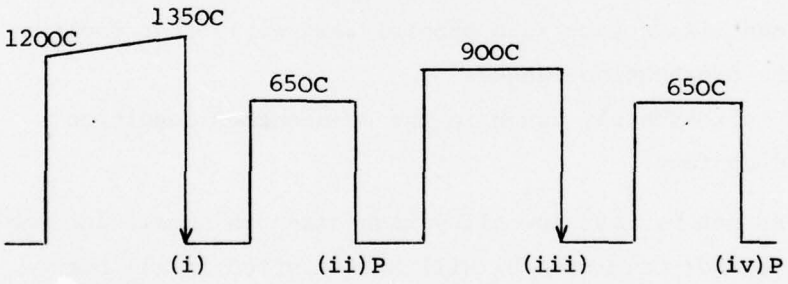

The fact that the same particle distribution was found at Steps (ii) and (iv) confirmed that tempering only affected the observation of particles. Finally, for comparison, the particle distribution produced by a conventional overheating treatment (1270C/1hr, cool at about 10C min^{-1} to 900C, hold 1hr, water quench) is shown in Figures 4.20(a-b); it is clear that slow cooling does not greatly increase the grain boundary volume fraction.

4.3.3. Discussion and Conclusions

Fracture Toughness Tests

In both steels oil quenching from austenitizing temperatures up to 1150C produced as-quenched fractures that were fully ductile and generally 100% transgranular (the only exception was in specimens

quenched from 1150C, where there was a very slight tendency for IMC). The fracture mode is primarily of the zig-zag type, commonly observed in a steel matrix of high yield stress and low work-hardening capacity {103}. As indicated by the fracture mode, the values of K_{IC} did not vary significantly with austenitizing temperature over this range, and the two materials showed almost identical toughnesses. In Steel 8, brine quenching from 850C, compared with oil quenching, produced a measurable decrease in K_{IC}. This effect is presumably due to a restriction of autotempering (similar to the decrease in toughness observed in Chapter 3) and possibly a higher level of residual stress.

The change in fracture mode at 1300C to either 100%IMC (Steel 8) or mixed IMC and TMC (Steel 9) substantiates the results obtained in Chapter 3. This effect has been observed in five steels and it appears that high austenitizing temperatures (>1150C) will generally produce IMC fractures in the as-quenched condition when:

a) The S content renders the steel susceptible to overheating.
b) The specimen size/quench rate prohibit extremely fast cooling through the overheating range.
c) The steel is reasonably tough in the as-quenched condition (ie. low C content).

Condition a) will be met by most low alloy high strength steels and the experiments indicate that Condition b) will be satisfied in all but minute specimens (this is discussed below).

The K_{IC} measurements show that the toughness of Steel 8 is unaffected by austenitization at 1300C, but the toughness of Steel 9 is increased by about 30%. The similarily between the notched and precracked toughnesses indicates that the microstructural dimension controlling the toughness of Steel 9 is greater than the notch root diameter (380μm). The two steels are almost identical except for a difference in S content and the results suggest an interpretation of the toughness differences arising primarily from the effect of S on pinning austenite grain growth at 1300C. The austenite grain sizes, measured in specimens quenched from 1300C(2hr) are:

Steel 8 (Air melt)	210 $\pm$ 50μm
Steel 9 (Vac. melt)	1240 $\pm$ 400μm

In the propagation of a ductile crack, the plastic zone, surrounding the crack tip, will confine the region in which the fracture process occurs. Under plane strain deformation, for a crack in an infinite continuum, the finite element results of Rice and Tracey {104} show that the plastic zone is of maximum extent, R_y, at about $\pm$ 70° to the crack, where:

$$R_y = 0.155(K/\sigma_y)^2 \qquad (4.1)$$

Taking the yield stress, σ_y, as 1418MNm^{-2} {105}, K as 80MNm$^{-3/2}$ then R_y = 490μm. It is clear that in Steel 9, the plastic zone is of insufficient size to envelop a single grain, and to follow the grain boundaries the crack would be required to deviate appreciably from the general (macroscopic) plane of propagation. The mixed IMC and TMC mode (Figure 4.17(b)) shows that although the grain boundaries are weaker, it is energetically easier in many cases for the crack to propagate through the tough interiors of the grains, than around the grain boundaries. It seems that provided the fracture remains ductile, the net effect of an increase in grain size is to increase the crack path length and hence the toughness. These conclusions are consistent with the work of Baker and Johnson {71} who showed that in an overheated Ni-Cr-Mo steel, the proportions of IMC to TMC increase with tempering temperature (ie. with decreasing yield stress and increasing plastic zone size).

The results obtained in this investigation cannot be directly compared with other work {73,74,106} in which the use of high austenitizing temperatures has been shown to produce a large increase in the as-quenched, ambient temperature fracture toughness. The reason for this is that the beneficial effects of high austenitizing temperatures have been studied in higher carbon steels (eg. AISI 4340) where there is a change in fracture mode from quasi-cleavage to IMC* with increasing austenitization temperature (in this investigation, fractures are fully ductile for all austenitizing temperatures); such results should be treated with caution. Although the authors {74} claim there are no

---

* At higher S contents {74} the fracture mode is described as largely TMC, but the results of {106} show mainly IMC, and indicate the difficulty in avoiding IMC fractures at lower S contents.

undissolved carbides in material austenitized at 870C it would seem that the effect is largely one of an anomalously low toughness in material austenitized at 870C (ie. 30/40MNm$^{-3/2}$), rather than a particularly high toughness produced by higher austenitizing temperatures (ie. 70-90MNm$^{-3/2}$). Steels are rarely used in the as-quenched condition and the results of this investigation (Figure 4.16) show that the improvement in toughness after tempering is more marked in material austenitized at lower temperatures.

Metallographic Tests

The principal observation in these tests is that approximately similar volume fractions of MnS particles were found at the grain boundaries in the following two treatments:

a) Water quench from 1250C/1350C; cooling rate in the vicinity of 2 x 10^{4}C min^{-1} (330C s^{-1})*.

b) Furnace cool from 1275C to 900C; cooling rate in the vicinity of 10C min^{-1} (0.2C s^{-1}).

In a homogeneous solid solution the precipitation of MnS at the grain boundaries will be limited by the diffusion distance for S (which is present only in very dilute concentrations, compared with Mn). The published diffusion data for S in γ-iron {108}, determined in the temperature range 1200C-1350C, give the diffusion equation as:

$$D_S = 1.35 \exp(-202.6/RT) \qquad (4.2)$$

where R is in kJ mol^{-1} K^{-1}

At a typical temperature of 1300C, the solubility determinations for Fe-Mn-S alloys show that the amount of S in solution is expected to be about 50ppm {69,70}. For a temperature decrease S will tend to precipitate as MnS, but to calculate an approximate upper limit for the grain boundary MnS volume fraction it will be assumed that S can only diffuse to precipitation sites at grain boundaries (ie. there is no intragranular precipitation). For diffusional flow, the amount of solute that can be supplied to a free surface ({109}, see also

---

* Cooling rates are estimated from specimen size and quenching media data in {107}.

Chapter 6) is given by:

$$A_S = 2 A_o (Dt/\pi)^{\frac{1}{2}} \quad (4.3)$$

where, A_S = solute supplied
A_o = solute concentration

Calculating the atomic volume of S in Fe from FeS and remembering to double the amount supplied to a grain boundary, then for a bulk concentration of 50ppm (0.0085 at%)S:

$$\theta_S(m/l) = 1.16 \times 10^4 (Dt)^{\frac{1}{2}} \quad (4.4)$$

From Eqn. (4.2), at 1300C;

$$\theta_S(m/l) = 5.8\, t^{\frac{1}{2}} \quad (4.5)$$

where t is in seconds and θ in monolayers.

On the basis of Eqn. (4.5) it is clear that S can be supplied to the grain boundary (and precipitated as MnS) at a very rapid rate. The total S in solution (50ppm) is capable of producing the equivalent of 35 monolayers of S (as MnS, for a grain size of 200μm); quench times or delays of even a few seconds will enable a large fraction of this S to be precipitated at the boundaries. It would seem reasonable to conclude that in most practical situations, quench rates over the range 1350C-1250C will be too slow to prevent appreciable grain boundary MnS precipitation.

In recent work O'Brien et al. {68} have reached similar conclusions regarding MnS precipitation. The authors quote a more recent determination of S diffusion in austenite, but suggest that the diffusion of S must be faster than previously supposed to account for their high measured volume fractions of MnS precipitate.

The metallographic studies showed that the majority of the finer intragranular sulphide particles could be removed from the microstructure by austenitizing for 1-2hr at 1350C. This is in qualitative agreement with the solubility determinations {69,70}, but presumably particle coarsening will also contribute to the dissolution of finer particles,

as demonstrated by Granamuthu {110}. There is some indication that once the finer sulphides are in solution (either by heating at very high temperatures, or for long times), then the particle density at the boundaries also reduces for rapid cooling rates. This may however, be a morphological change produced by the dissolution of fine grain boundary (pinning) sulphides which act as growth or nucleation sites during cooling. This is suggested, for example, by quenching from 1400C, where the particle density is much reduced, but the general delineation of the boundaries seems to increase.

As mentioned in Chapter 3, strong S solute segregation is expected in austenite, but S, like P, will probably show a segregation limit of 1 monolayer or less (McLean segregation); this appears to be true for S segregation in α-Fe {88}. This coverage is too small to contribute markedly to the general phenomenon of overheating, but it is worth mentioning that high transient coverages have been reported in α-iron {111}. Scavenging of fine particles by grain boundary migration is another factor which might contribute to measured volume fractions.

In summary it may be said that large variations in cooling rate do not significantly alter the volume fraction of MnS precipitated at prior austenite grain boundaries (ie. within a factor of 2-3). Because S is at the solubility limit and diffuses very rapidly, it seems that once undercooling occurs, S precipitation at grain boundaries cannot be avoided unless abnormally high quench rates are employed. The main effect of quench rate appears to be one of changing the morphology of the precipitate.

Conclusions:

1) In an air-melted En25 steel there is no significant effect of austenitizing temperature on the as-quenched fracture toughness (K_{IC}). Slow cooling (10C min^{-1}) through the overheating range produced no measurable decrease in K_{IC}.

2) A vacuum-melted En25 steel shows similar K_{IC} values to the air-melted steel, except for an austenitizing temperature of 1300C, where the toughness increased by about 30%. This effect is attributed to an abnormal increase in austenite grain size.

3) All fractures were fully ductile, but austenitizing at temperatures above 1150C produced a change in fracture mode from transgranular to intergranular rupture. The intergranular mode was not eliminated by brine quenching.

4) Experiments with small metallographic specimens show that once S enters solution in the overheating range, the subsequent precipitation of MnS at grain boundaries is very difficult to suppress. This is shown to be consistent with the expected rates of S diffusion to the grain boundaries.

	As-Quenched			350C/1hr				350C/4hr
Steel	950C	1150C	1350C	950C	1150C	1350C	1350-850C	950C
1	-140	-110	-105	- 80	- 75	-	-	- 95
2	-140	-135	-130	-105	- 85	-	-	-130
3	-135	-145	- 90	-200	-130	-110	-75	-165

Table 4.1. Slow-bend transition temperatures of Steels 1-3 (in C, ±15C), for various austenitizing and tempering treatments.

Steel	C	Si	Mn	Ni	Cr	Mo	S	P	Sb	Sn	As
8	0.31	0.20	0.67	2.65	0.64	0.54	0.010	0.008	0.005	0.013	0.019
9	0.30	0.31	0.58	2.71	0.73	0.58	0.007	0.006	0.003	0.005	0.016

Table 4.2. Chemical compositions (wt%) of Steels 8 and 9.

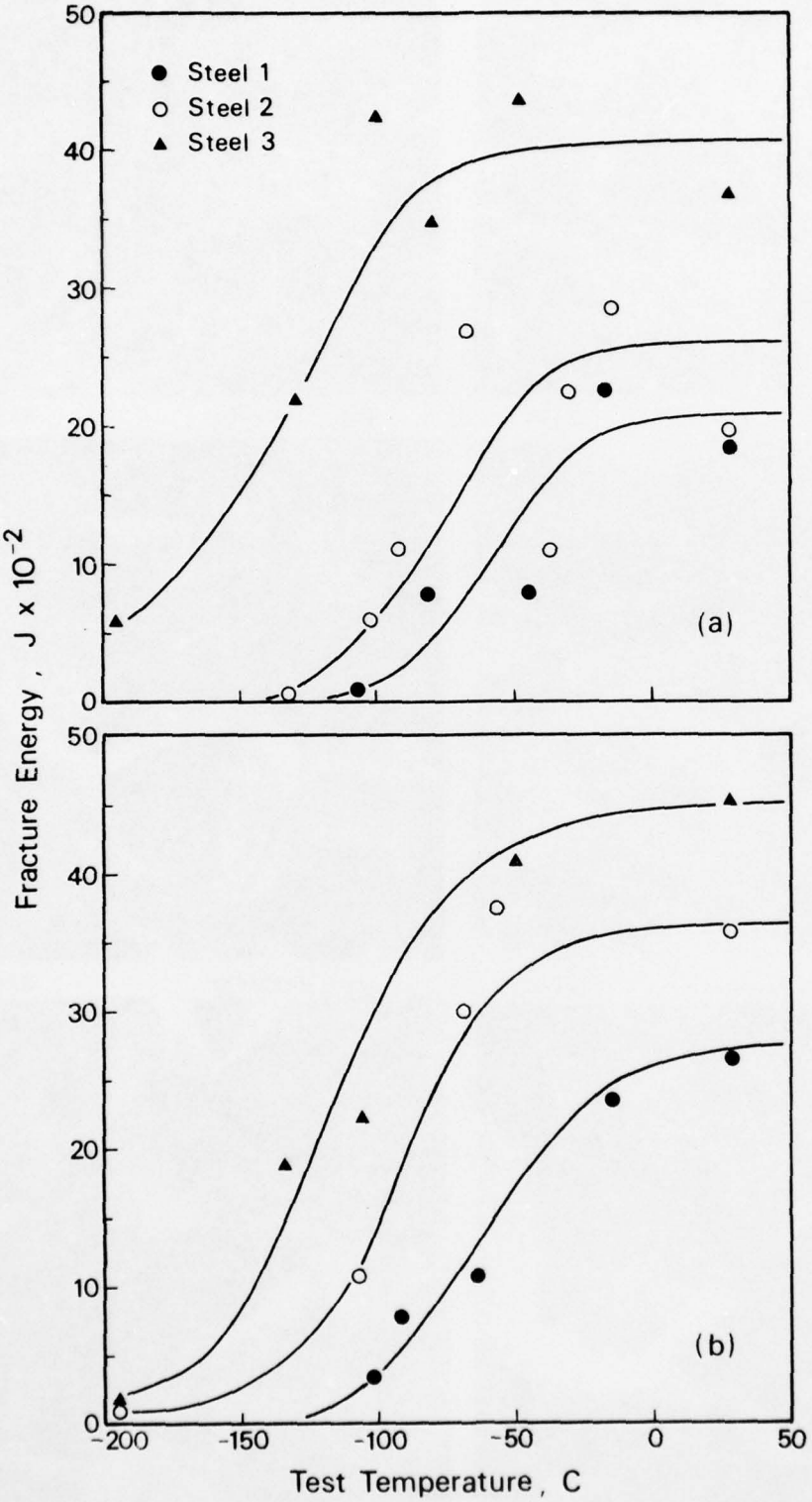

Figure 4.1. Slow-bend transition temperature results for Steels 1-3; (a) austenitized at 950C and tempered for 1hr at 350C, (b) austenitized at 950C and tempered for 4hr at 350C.

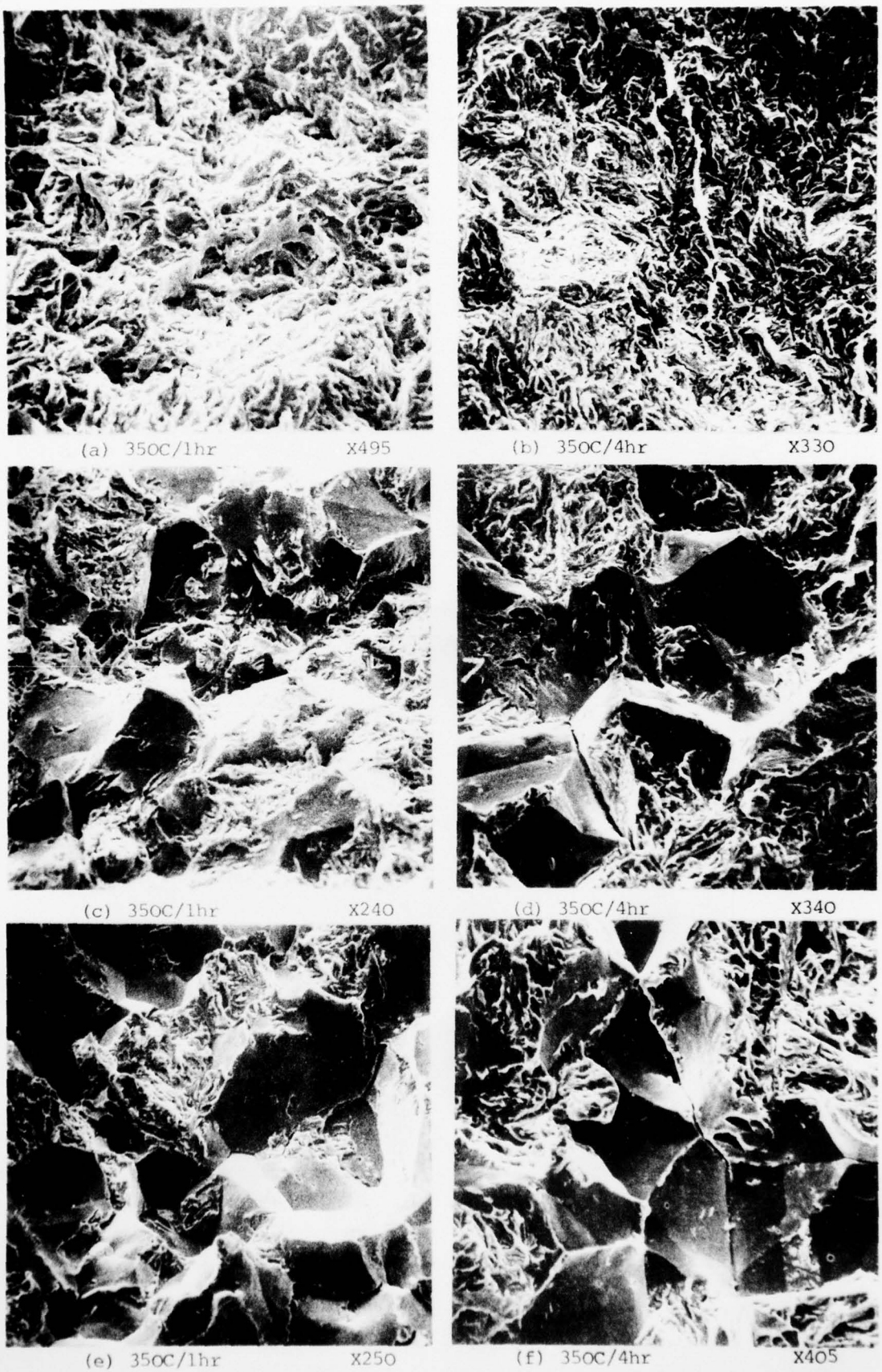

(a) 350C/1hr X495 (b) 350C/4hr X330

(c) 350C/1hr X240 (d) 350C/4hr X340

(e) 350C/1hr X250 (f) 350C/4hr X405

Figure 4.2. Brittle fractures after austenitizing at 950C and tempering at 350C for times shown; (a)-(b) Steel 3 tested at -196C; (c)-(d) Steel 1 tested at -100C and -102C, respectively; (e)-(f) Steel 2 tested at -130C and -196C, respectively.

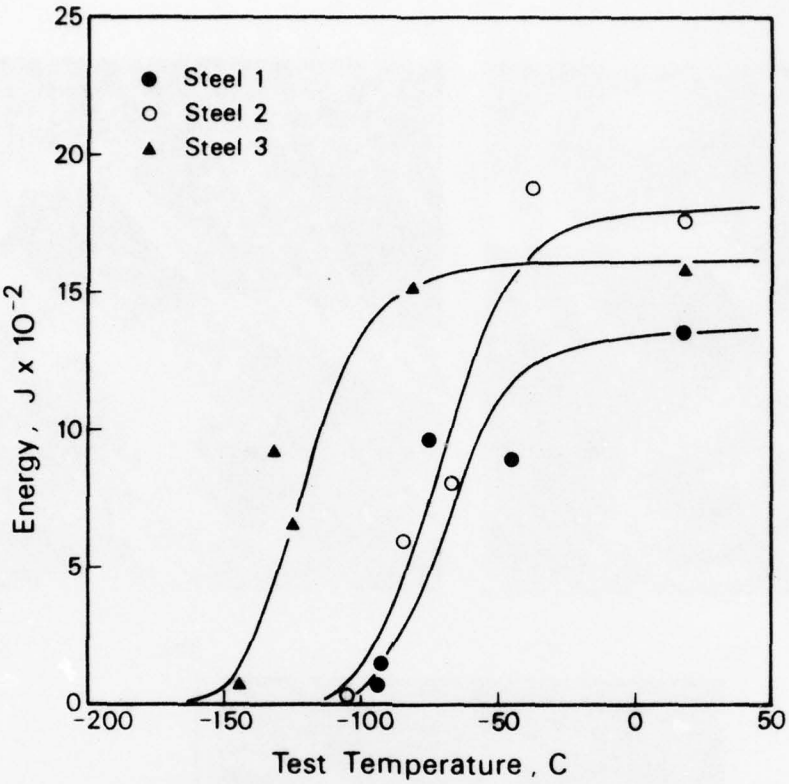

Figure 4.3. Slow-bend transition temperature results for Steels 1-3 austenitized at 1150C and tempered for 1hr at 350C.

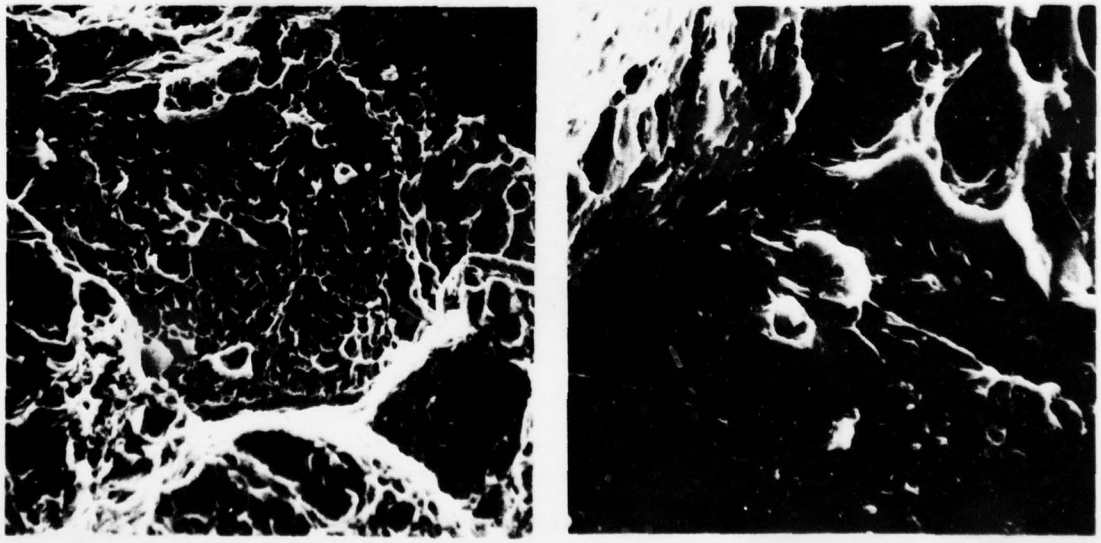

(a) X705 (b) X2680

Figure 4.4. Ductile fractures after austenitizing at 1150C and tempering for 1hr at 350C; (a) Steel 3 showing IMC mode, (b) Steel 1 showing IGS mode (both tested at 18C).

AD-A048 448 CAMBRIDGE UNIV (ENGLAND) DEPT OF METALLURGY AND MAT--ETC F/G 11/6
SEGREGATION EFFECTS AND THE TOUGHNESS OF HIGH-STRENGTH STEELS.(U)
JUN 77 J Q CLAYTON, J F KNOTT DAJA37-74-C-1309
NL

UNCLASSIFIED

2 OF 3
ADA048448

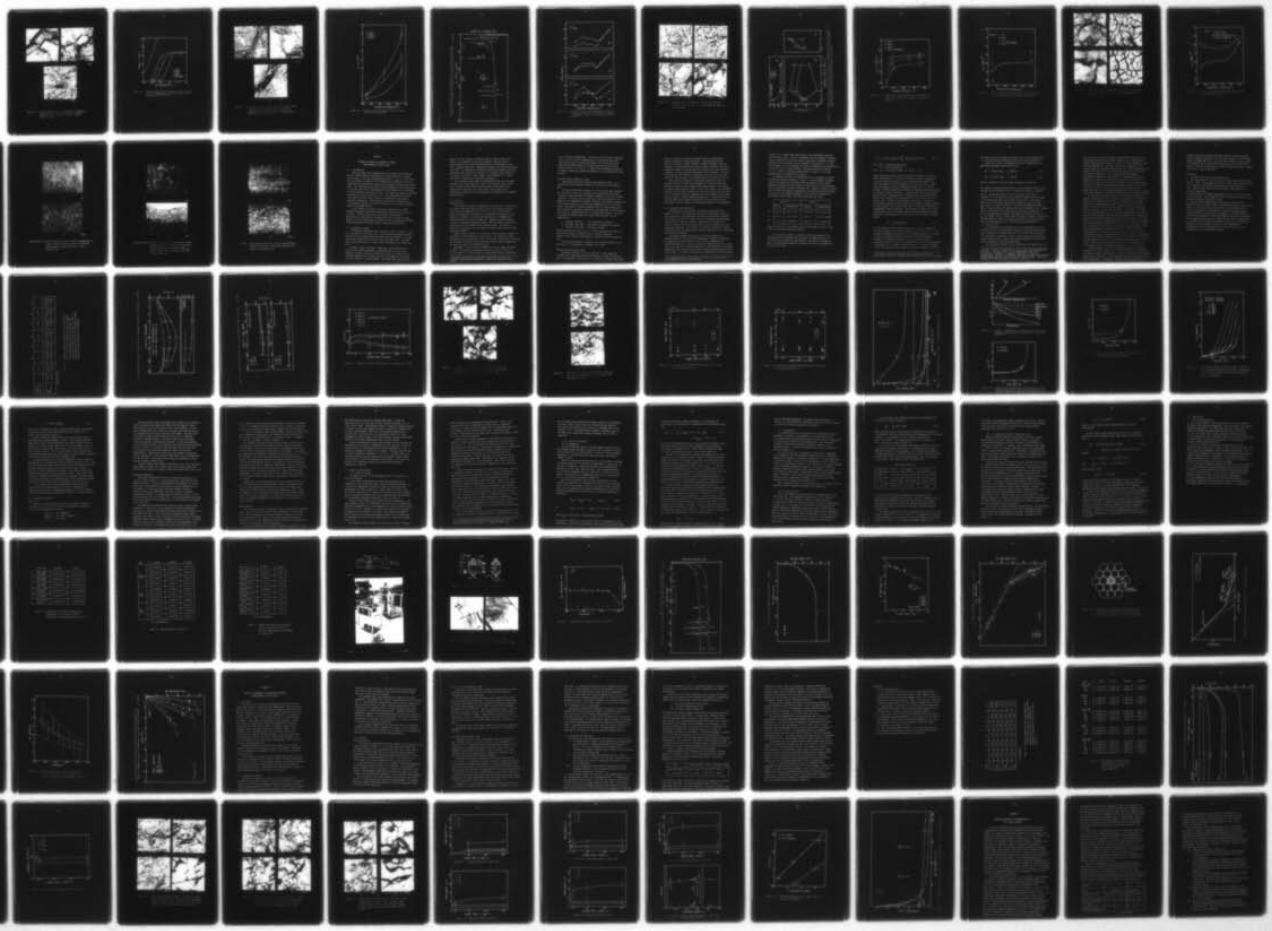

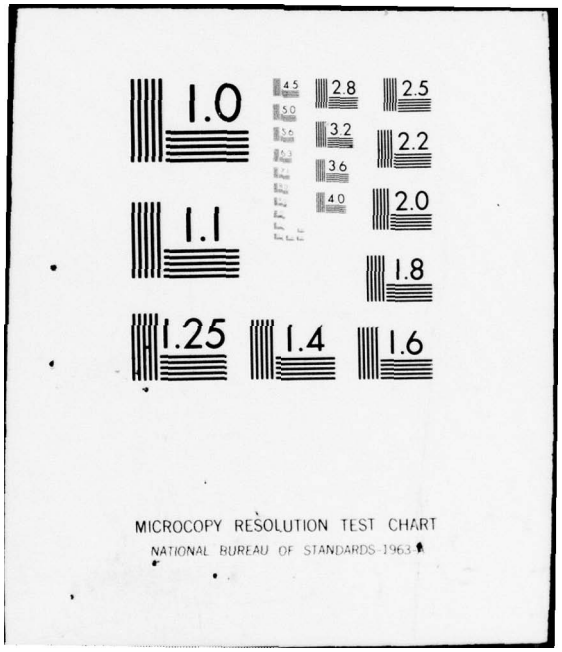
1.0
1.1
1.25
1.4
1.6
1.8
2.0
2.2
2.5
2.8
3.2
3.6
4.0
4.5
5.0
5.6
6.3
MICROCOPY RESOLUTION TEST CHART
NATIONAL BUREAU OF STANDARDS-1963-A

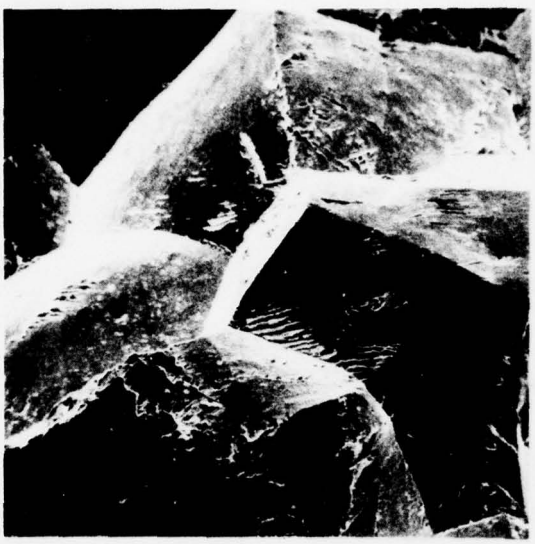

(a) X130

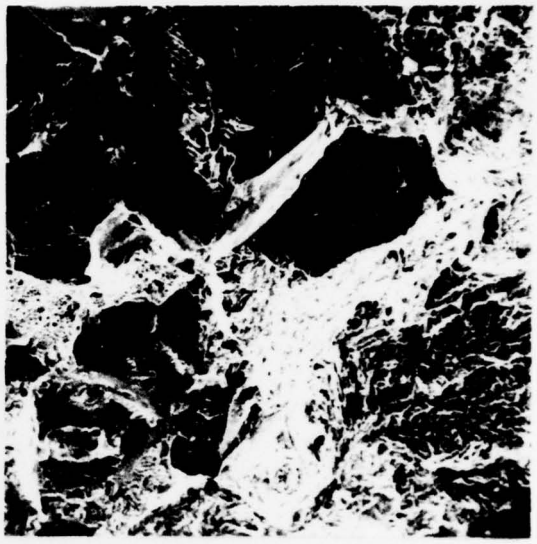

(b) X140

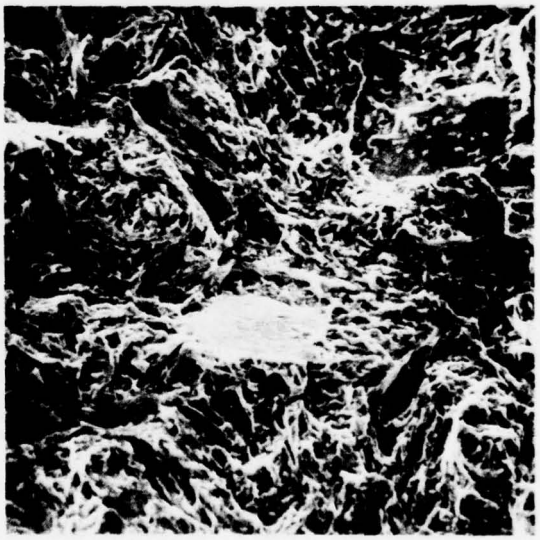

(c) X400

Figure 4.5. Brittle fractures after austenitizing at 1150C and tempering for 1hr at 350C; (a) Steel 1 tested at -96C, (b) Steel 2 tested at -104C, (c) Steel 3 tested at -145C.

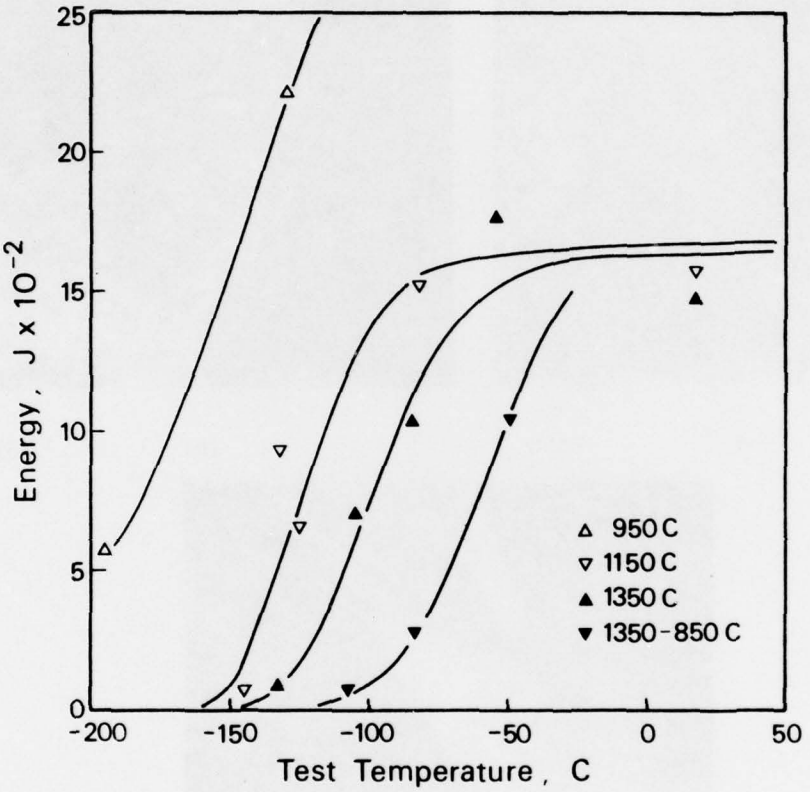

Figure 4.6. Effect of austenitizing treatment on the slow-bend transition temperature of Steel 3, measured after tempering for 1hr at 350C.

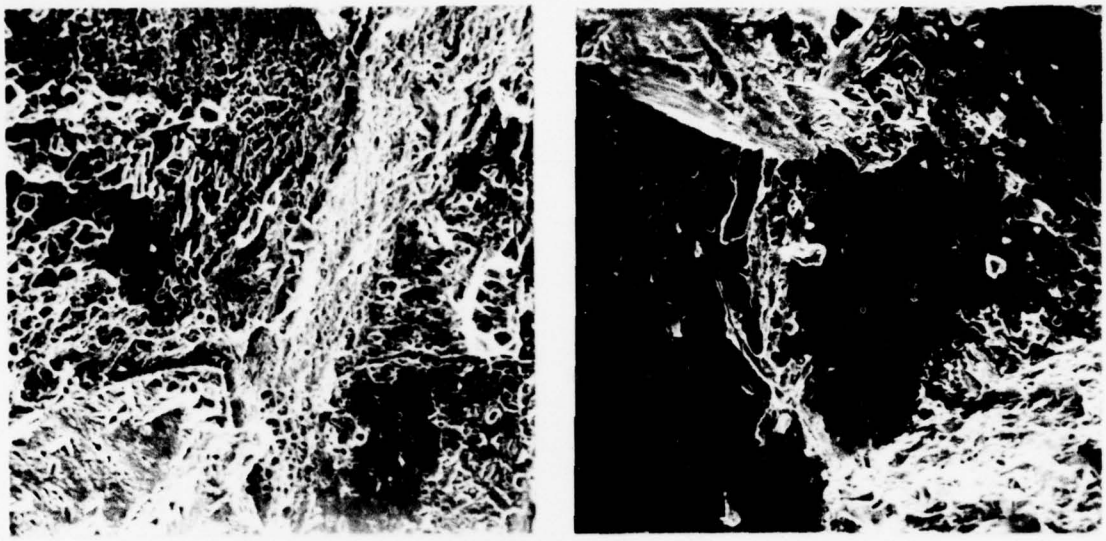

(a) X350 (b) X315

(c) X170

Figure 4.7. Fractures in Steel 3 after tempering for 1hr at 350C; (a) austenitized at 1350C and tested at 18C; (b) austenitized at 1350C and tested at -133C; (c) austenitized at 1350C (2hr) furnace cooled to 850C (held 2hr) and tested at -106C.

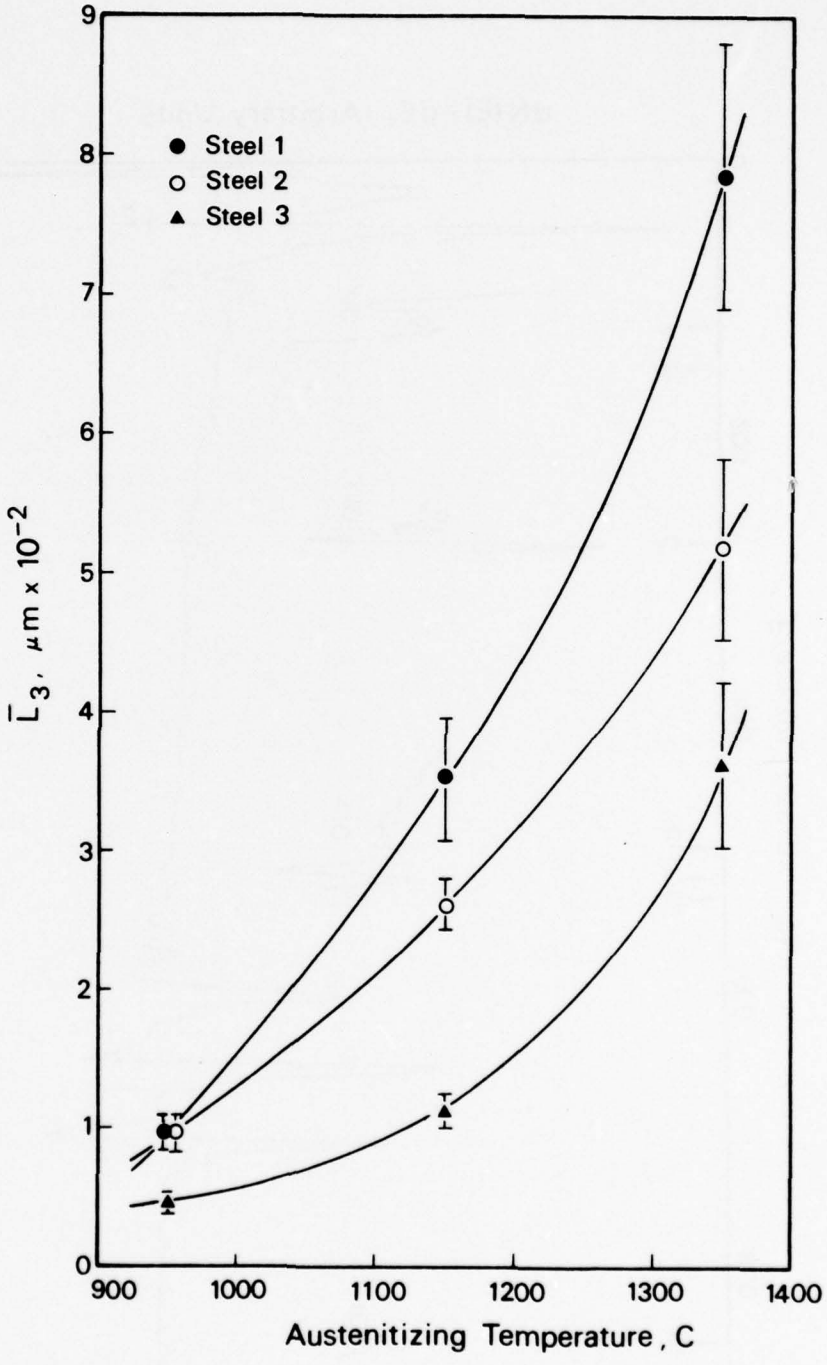

Figure 4.8. Variation in prior austenite grain size with austenitizing temperature.

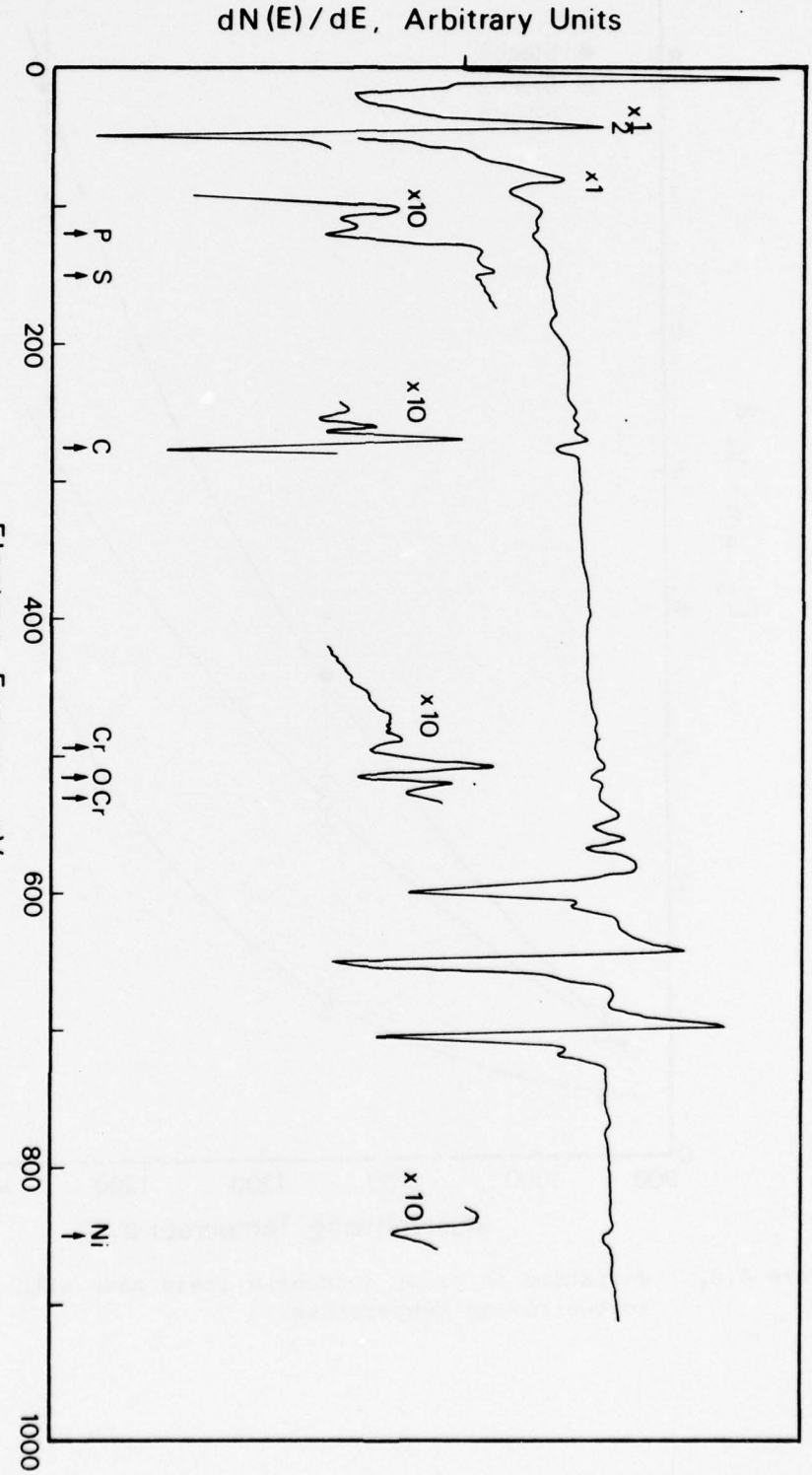

Figure 4.9. Typical AES spectrum from Steel 2 obtained after tempering for 1hr at 350C (specimen fractured at -90C to give approximately 50% intergranular cleavage).

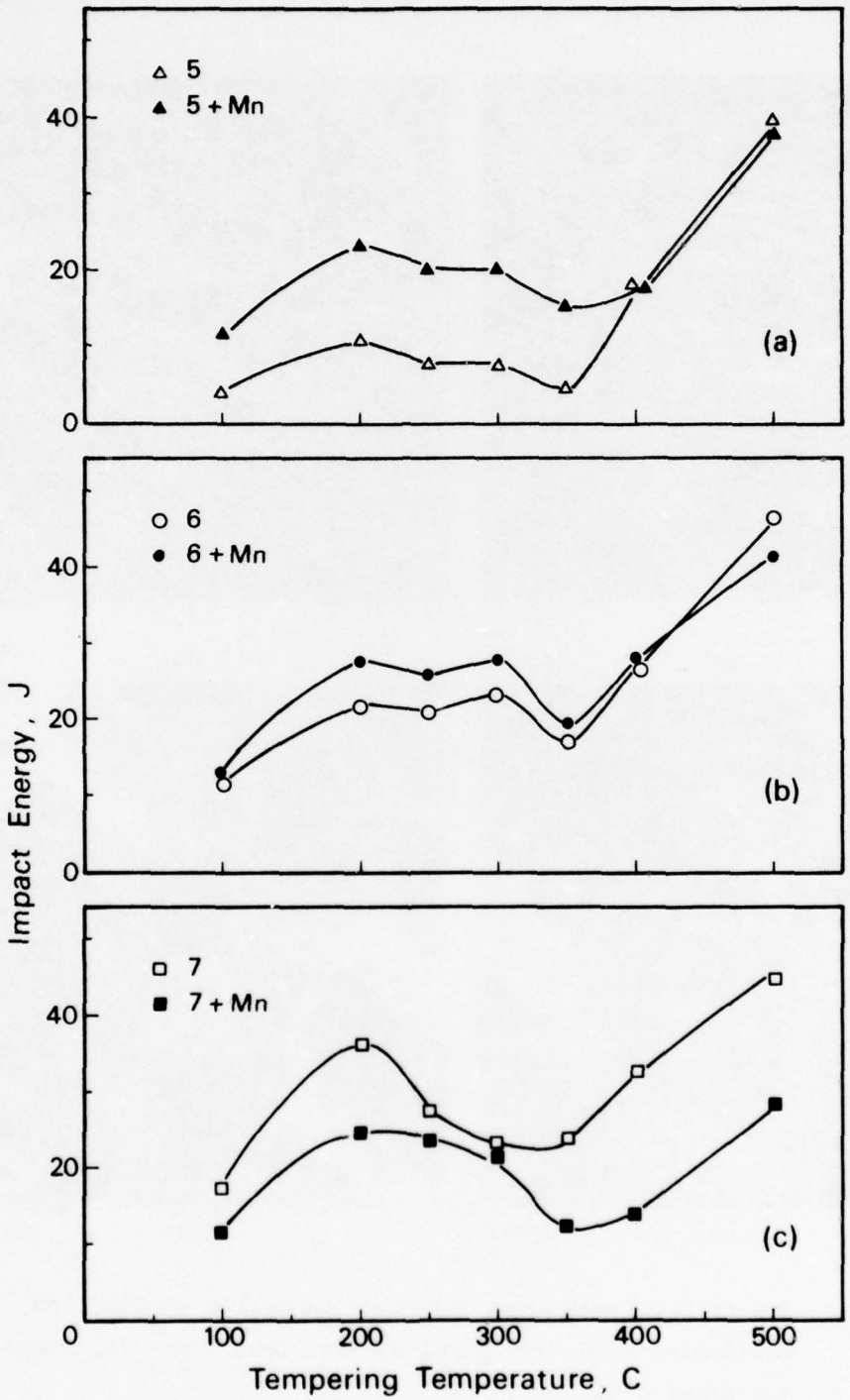

Figure 4.10. Variation in notched impact energy at -30C with tempering temperature; (a) 10ppm P, (b) 70ppm P, (c) 200ppm P. Chemical compositions are given in Table 7.1.

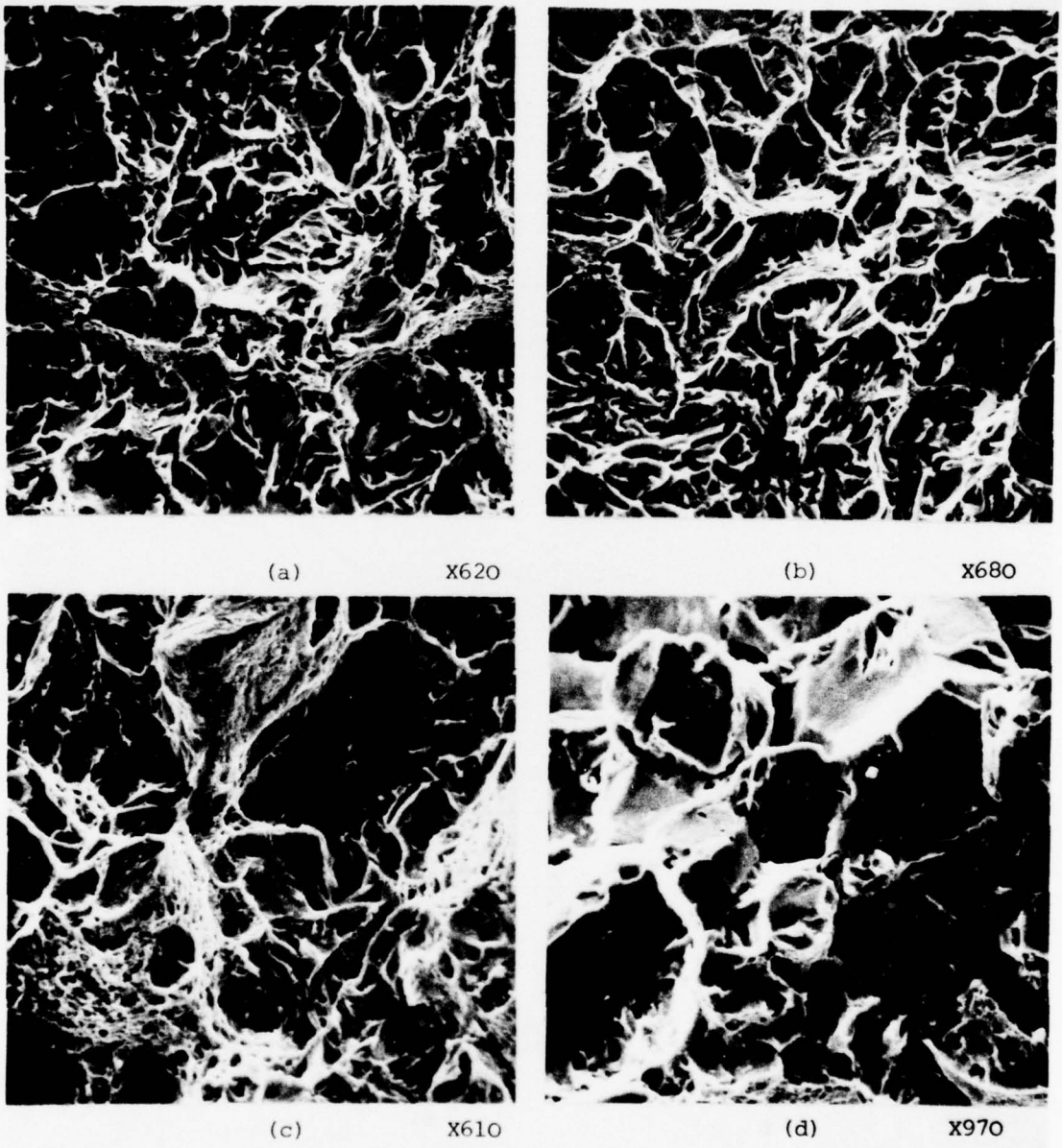

Figure 4.11. Impact fractures observed after tempering at 350C and testing at -30C; (a) Steel 6, (b) Steel 6+Mn, (c) Steel 7, (d) Steel 7+Mn.

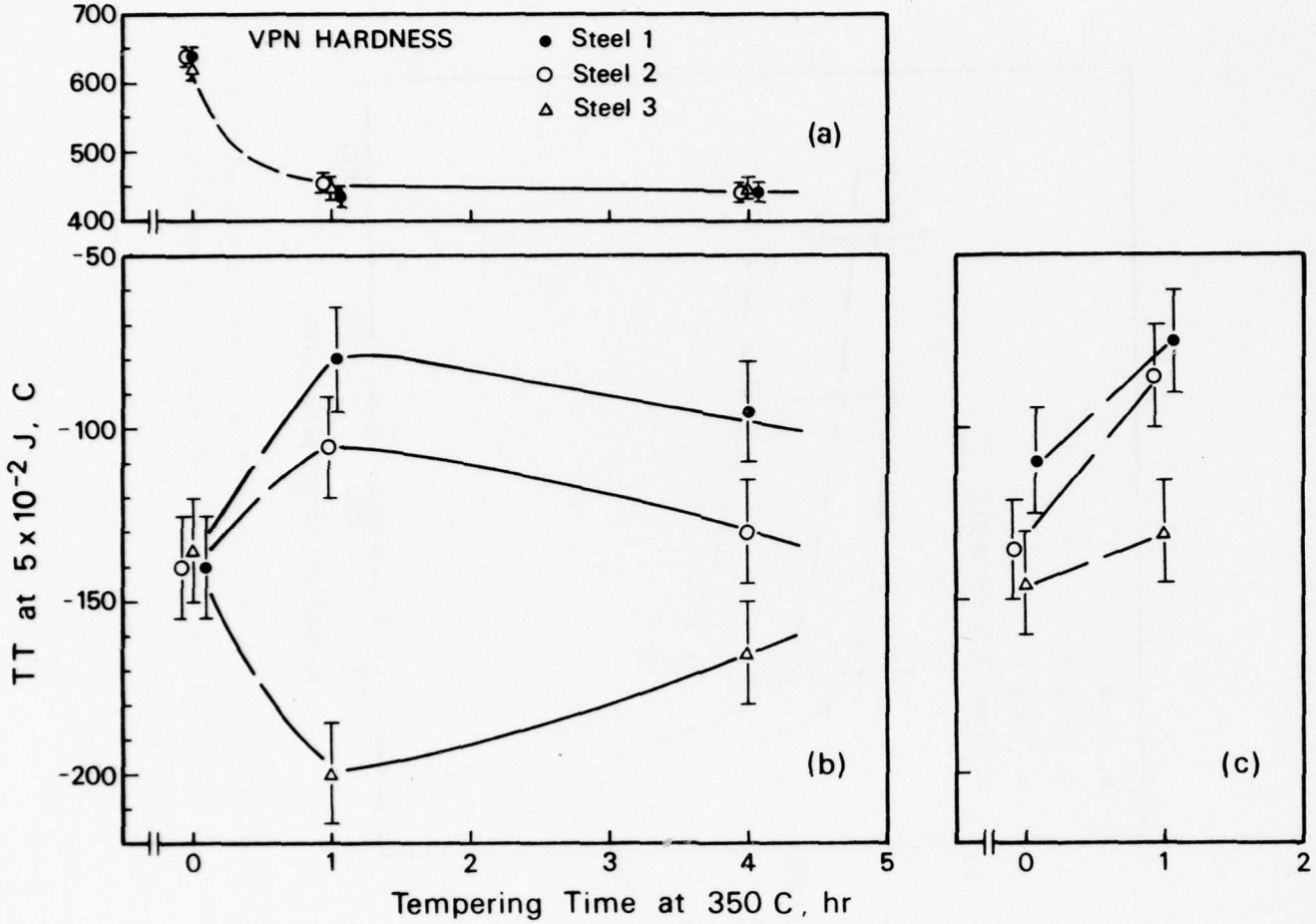

Figure 4.12. Effect of tempering time at 350C on the transition temperature and hardness of Steels 1-3; (a) hardness changes after 950C austenitization, (b) and (c), transition temperature changes after 950C and 1150C austenitizing treatments, respectively.

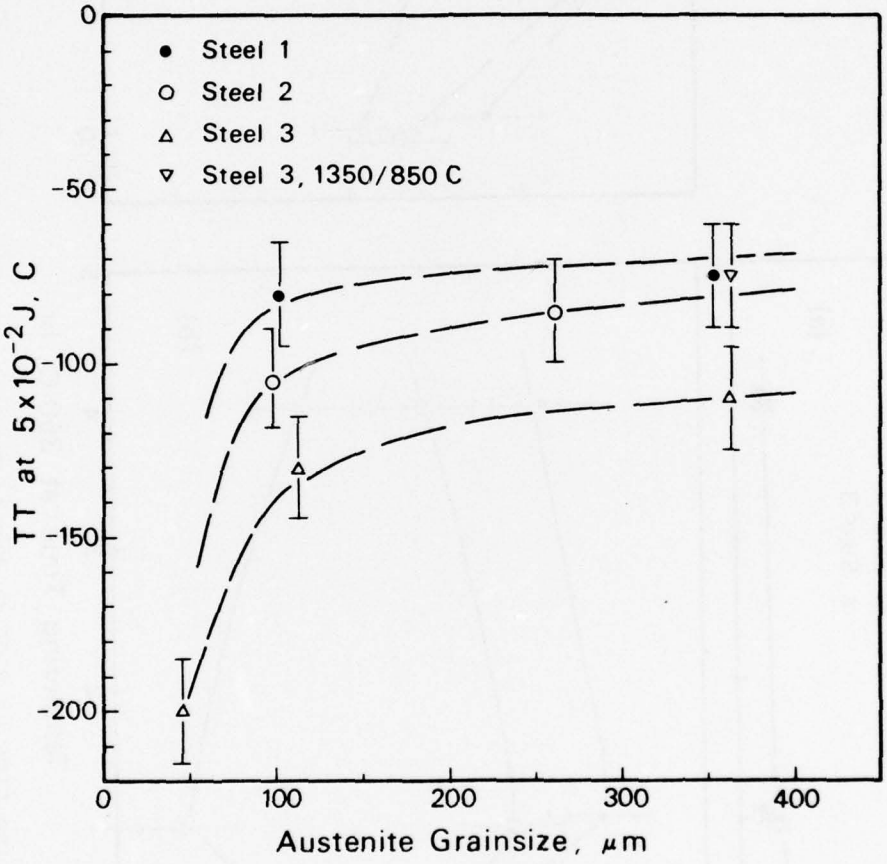

Figure 4.13. Variation in transition temperature, measured after tempering for 1hr at 350C, with prior austenite grain size.

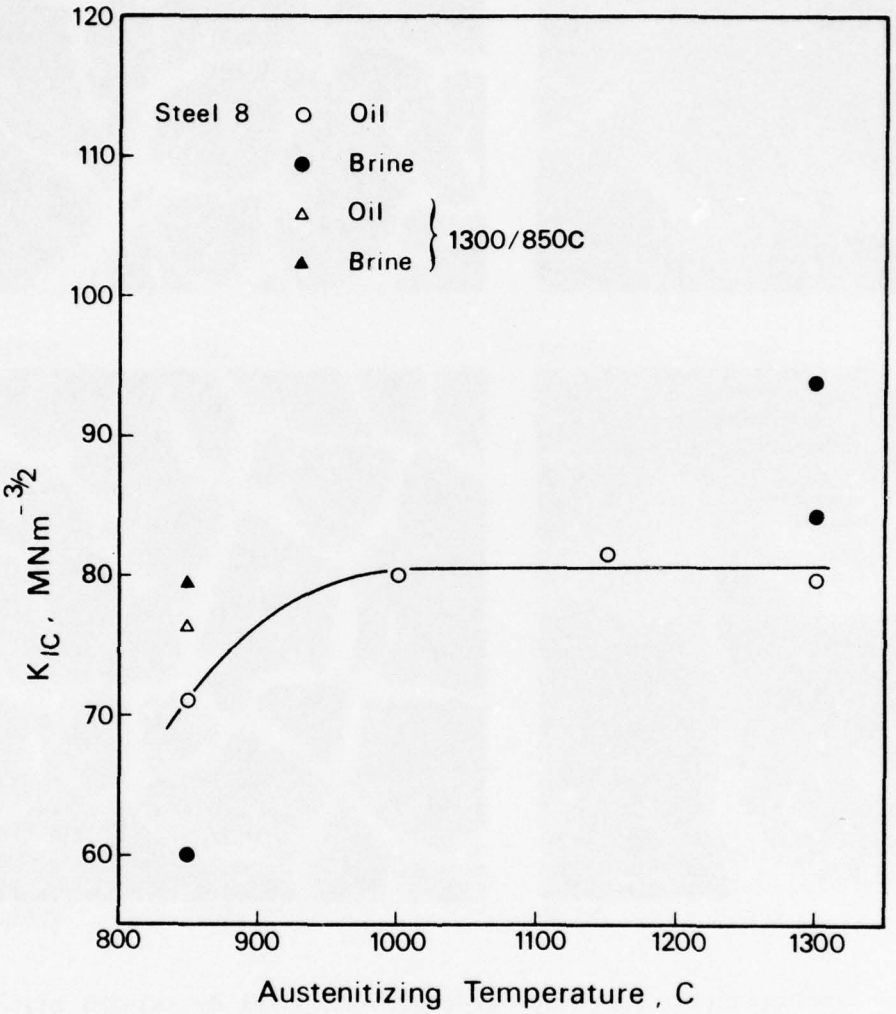

Figure 4.14. Effect of austenitizing treatment and quenching medium on the as-quenched fracture toughness of Steel 8.

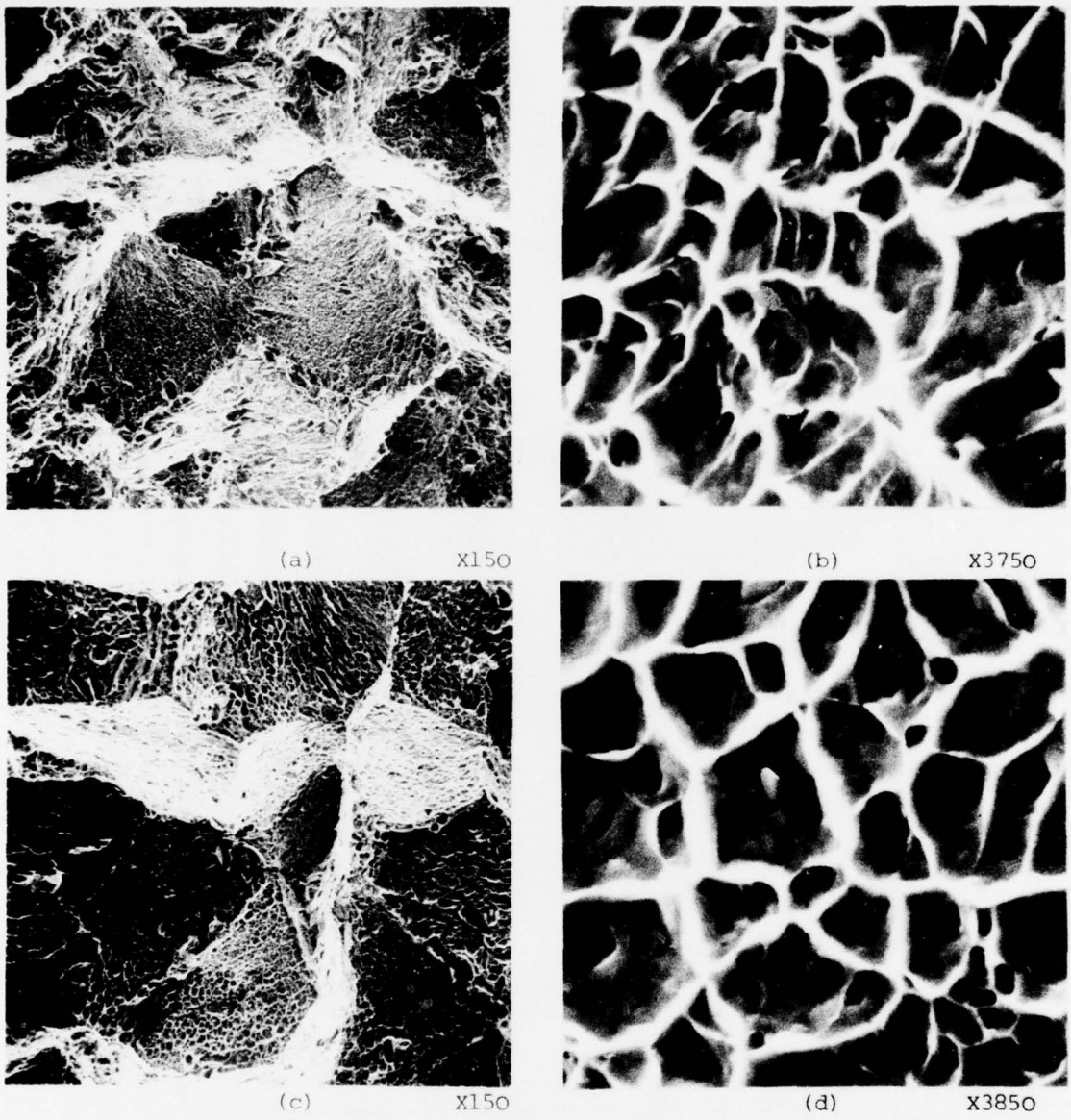

Figure 4.15. Intergranular microvoid fractures in Steel 8; (a)-(b) brine quench from 1300C; (c)-(d) 2hr at 1300C, furnace cool to 850C, brine quench.

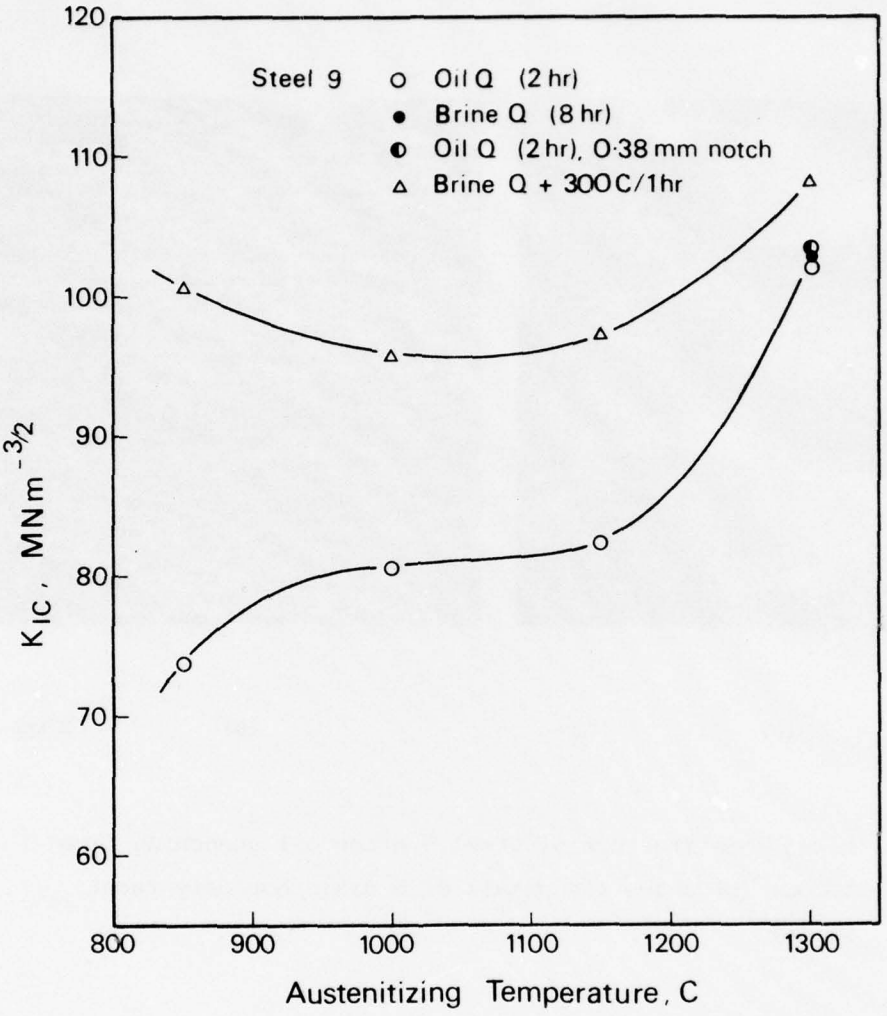

Figure 4.16. The as-quenched and quenched and lightly tempered fracture toughness of Steel 9.

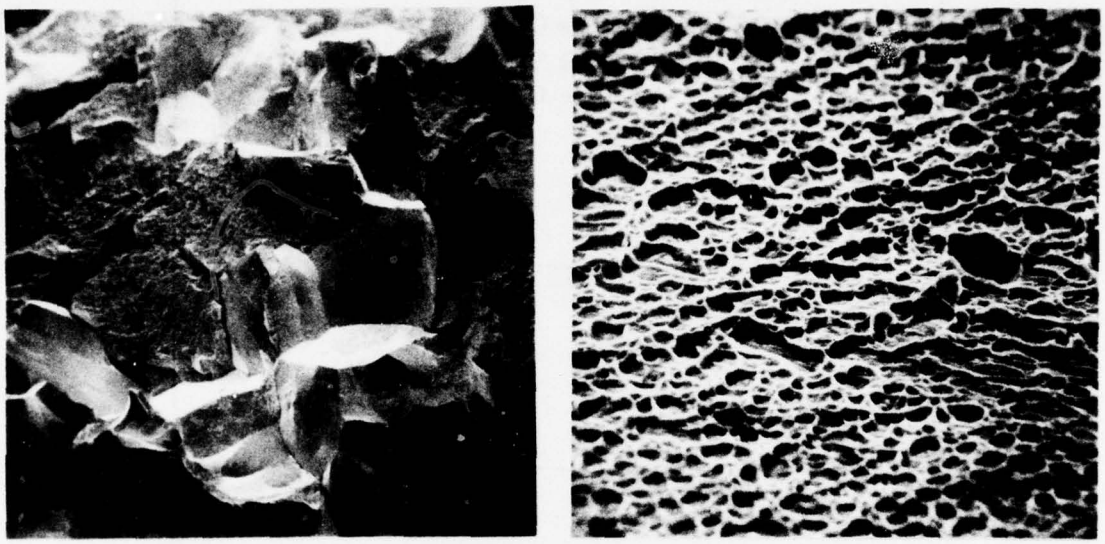

(a) X14 (b) X705

Figure 4.17. Mixed mode fracture of Steel 9 after oil quenching from 1300C; (b) shows the detail of a grain boundary facet in (a).

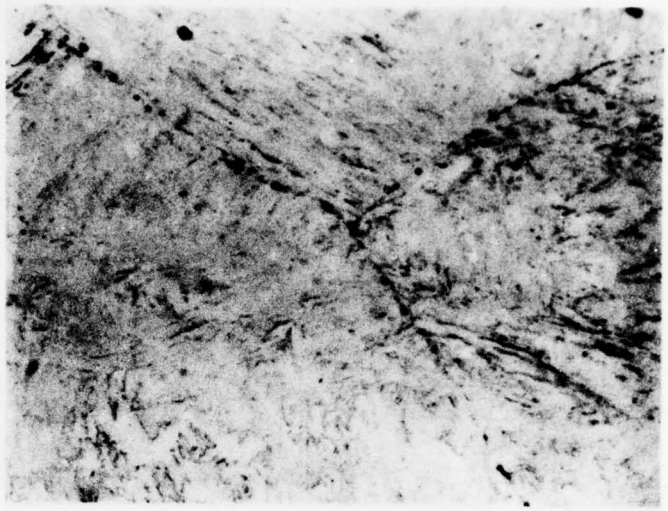

(a) X680

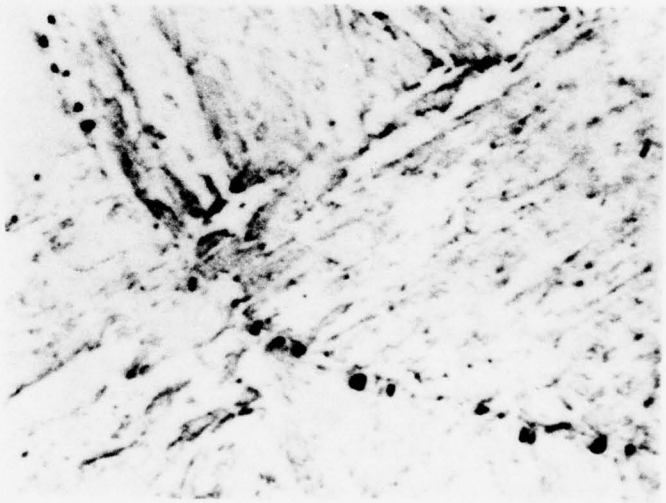

(b) X1700

Figs.4.18(a)-(b). Grain boundary particles in Steel 8 (austenitized at 1300C for 1hr, heated at 1C.min^{-1} to 1350C and and water quenched). Etched in 10% nitric + 10% sulphuric acid.

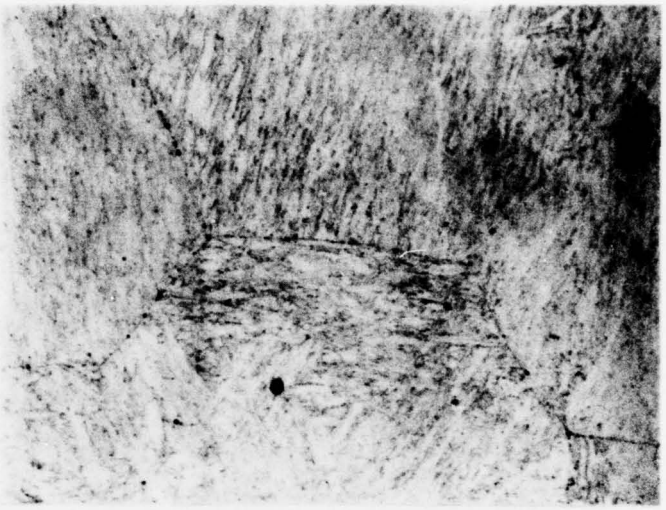

(c) X312

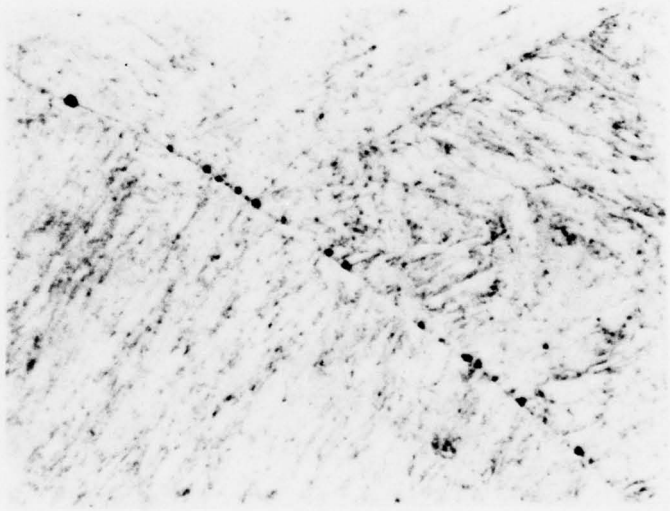

(d) X1050

Figs.4.18(c)-(d). Grain boundary particles in Steel 8 (austenitized at 1200C for 10min, heated at 1C.min^{-1} to 1350C and water quenched). Etched in 10% nitric + 10% sulphuric acid.

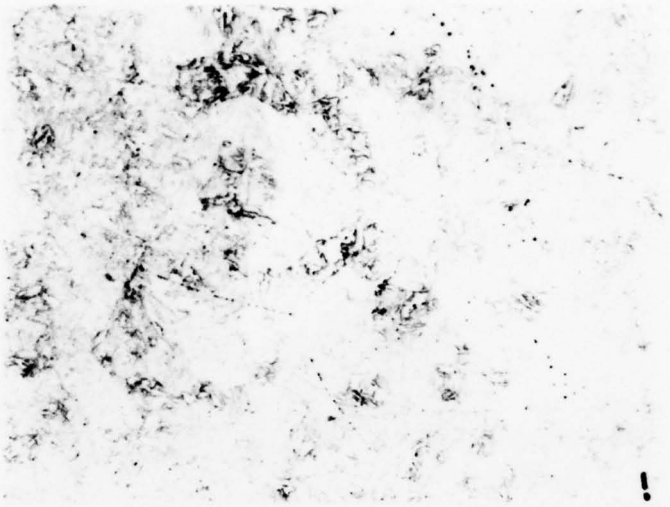

(a) X270

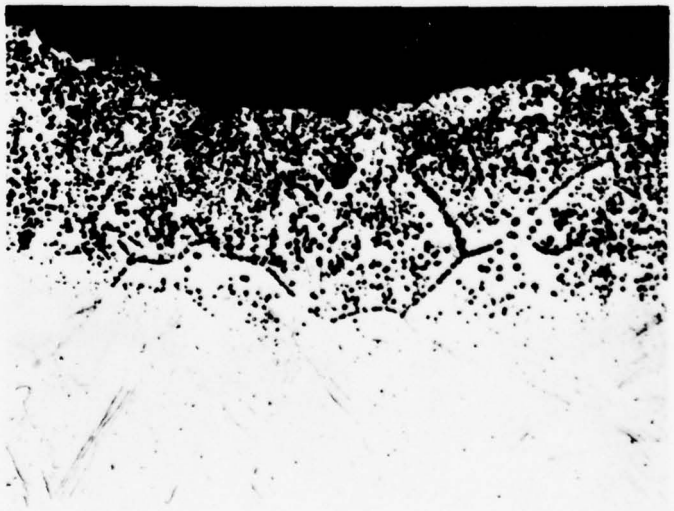

(b) X270

Figs.4.19(a)-(b). Particles in Steel 8; (a) persistence of grain boundary particles in Figs.4.18(c)-(d) after a second austenitizing treatment at 900C; (b) typical surface region. Etched in 10% nitric + 10% sulphuric acid.

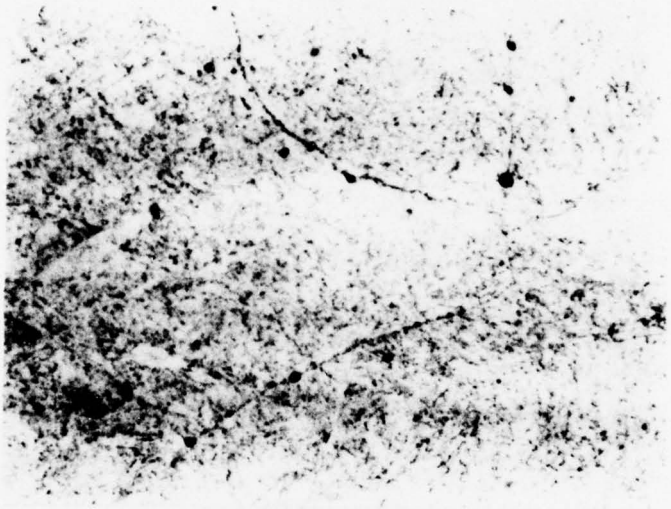

(a) X680

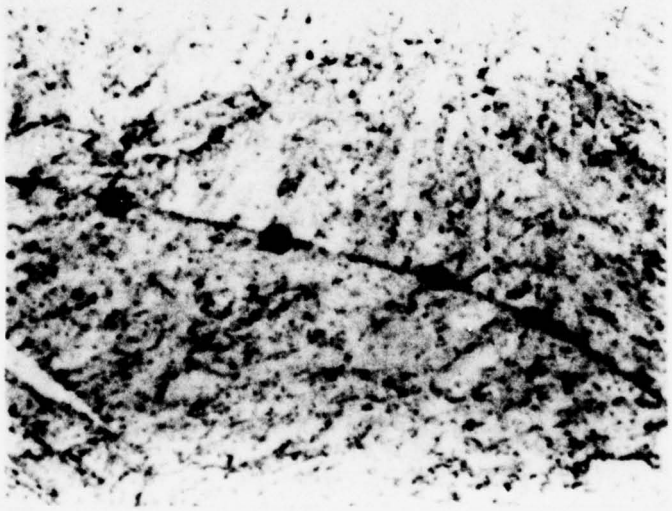

(b) X1700

re 4.20. Grain boundary particles in Steel 8 observed after furnace cooling from 1270C to 900C. Etched in 10% nitric + 10% sulphuric acid.

CHAPTER 5

EFFECTS OF NICKEL AND ANTIMONY ON TEMPER EMBRITTLEMENT IN ALLOY STEELS

5.1. Introduction

Previous studies have suggested that alloy content is an important factor in determining the susceptibility of Ni-Cr-Sb steels to temper embrittlement. This was first demonstrated by Low et al. {27} who showed that the removal of either Ni and Cr dramatically reduced the transition temperature shift produced by step-cooling through the temper embrittlement range. The observation that both Ni and Sb segregated to grain boundaries in Ni-Cr-Sb steels led to the proposal of an enrichment of the interfaces by a Ni-Sb chemical interaction {32,33}. Such alloy and impurity interfacial concentrations (Ni-Sb, Mn-Sb, Ni-P, etc.) have subsequently been shown to be stable {37,39,45} and are thus in accordance with equilibrium (Gibbsian) segregation. These general observations are consistent with a thermodynamic analysis of solute interactions at an interface, proposed recently by Guttmann {46,47}.

In this Chapter the nature of the Ni-Sb interaction is further examined by employing controlled variations of the Ni and Sb content in the steel. Previous studies have been largely concerned with embrittlement at high bulk Sb concentrations, and to extend the range, emphasis in this investigation is placed on lower Sb concentrations, more closely approaching the values found in commercial alloy steels.

5.2. Experimental Details

The chemical compositions of the alloys are given in Table 5.1, and will be referred to as Steels 10-14. The alloys were prepared by melting electrolytic iron together with high-purity alloying elements. The 15kg ingots were forged and hot-rolled to give 15mm square bars. The bars were softened (650C/24hr) in vacuum, then cold swaged to give 10mm diam bars.

Specimens blanks, 10mm diam x 100mm long, were austenitized at 1100C for 2hr (argon atmosphere), end-quenched into 5% brine, then tempered at 650C in vacuum for either 3hr or 30hr. The reason for the long-term tempering was to enable results to be compared at two levels of matrix hardness (ie. yield stress). The blanks were skim-machined,

sealed in silica capsules, and aged at 520C or 590C for times up to 3000hr*. The temperature of 520C corresponds to the nose of the embrittlement C-curve, where the maximum rate of embrittlement occurs {45}. Segmented transition temperature specimens were then machined from the blanks. The specimens were tested as described in Chapter 2 and the load-displacement curves were recorded at a crosshead rate of 2mm min^{-1} (3hr temper) or 5mm min^{-1} (30hr temper). Two specimens (ie. 8 tests) were used to establish each transition temperature.

Grain boundary compositions were determined by AES using specimens machined from the bend specimens. About 8-10 different areas of each fracture surface were analysed and the measured peak-heights were normalized and weighted in the usual manner (the proportions of intergranular fracture in the SEM specimens were determined by subsequent SEM examination).

5.3. Results

Mechanical Tests

The changes in transition temperature with aging time at 520C for the two steels containing 5Ni+Sb (Steels 12 and 13) are shown in Figure 5.1. In the materials tempered for 3hr there is an initial rapid rise in transition temperature followed by a slow decrease corresponding to the decrease in hardness. The transition temperatures for 200ppm Sb are clearly greater than those for 100ppm Sb. Tempering for 30hr produces a constant transition temperature between 300hr and 1000hr, followed by a decrease, again associated with the hardness change. The effect of Sb content, observed for the 3hr temper, is almost absent with the longer tempering treatment.

Aging curves for Steels 10, 11 and 14 at 520C are shown in Figure 5.2. The effect of the Sb additions is very slight; the curves are, within experimental error, identical to that of the Sb-free curve (Steel 14), which was included to check any effects that might result from the segregation of impurities other than Sb(P,Sn,As and S).

Specimens of the five steels, tempered for 30hr at 650C, were aged at 590C. The transition temperature results are shown in Figure 5.3. For the Steels 10, 11 and 14 there is no measurable effect of aging time

---

* Specimens were aged for longer times at 520C, but due to the low transition temperatures encountered at 3000hr these specimens were not tested.

on the transition temperatures. In Steels 12 and 13 there is possibly a small rise in transition temperature for aging times under 100hr (the zero time point is taken from Figure 5.1), but the transition temperatures between 100hr and 1750hr are very low and well below those of Steels 10, 11 and 14. It seems that the toughening effect of Ni tends to govern the transition behaviour at aging times beyond 100hr at 590C.

Fracture Surface Examination (SEM)

Representative fracture surfaces were examined by SEM. In all materials and heat treatment conditions the ductile fracture mode was TMC.

The brittle fractures in Steels 10, 11 and 14 were quasi-cleavage, but in Steels 12 and 13 the fractures varied from almost 100% quasi-cleavage to 100% intergranular cleavage, depending on the heat treatment condition. In general, for fractures just below the transition, the proportion of intergranular cleavage increased with transition temperature, then decreased again as the transition temperature fell at long aging times. The effect of increased tempering time (or aging temperature), which lowered the transition temperature, was observable on the fractures, which showed a reduced proportion of intergranular cleavage. For these two steels the fracture modes, for aging times over 5hrs, can be summarised as:

1. 650C/3hr, aged 520C : >75% intergranular cleavage
2. 650C/30hr, aged 520C : mixed quasi-/intergranular cleavage
3. 650C/30hr, aged 590C : >90% quasi-cleavage.

Typical fractures for Steel 13 (No. 1, above) indicating the effect of aging time are shown in Figures 5.4(a-c), and for comparison Figures 5.5(a-b) show the same material, tempered for 30hr and aged at 590C.

The fractures obtained in specimens with fracture energies of ∿4J were (quasi- or intergranular) cleavage in all cases.

Fracture Surface Analysis (AES)

Specimens from Steels 12 and 13 (aged 520C; short tempering treatment) were analysed by AES and the results are shown in Figures 5.6 and 5.7 respectively. Except for Cr, all values are weighted peak-height

ratios (but the top scale shows the proportions of intergranular fracture produced in the AES specimens). The peak-height ratios refer to : P-120eV, S-150eV, Sb-454eV, Cr-489eV, Ni-849eV. With the exception of carbon these were the only elements detected at the grain boundaries (oxygen was also present on the spectra, but the peak-height increased with time, indicating adsorption from the system). Two sets of data points were obtained by taking mean values for the first and second 4-5 areas analysed (all AES measurements are given in Table 5.2).

Depth profiles, obtained by controlled sputtering with Ar ions indicated that Ni, Sb and P were segregated at the grain boundaries, but with Ni showing a more gradual profile than either Sb or P (Figure 5.8 shows a depth profile in Steel 13 after 20hr aging*). With prolonged sputtering (many 100 Å) S decreased to zero and an even slower decrease in the Cr peak was observed, suggesting that these elements were present, partly or wholly, as grain boundary precipitates. Profiles taken after 20hr and 1000hr were compared and showed that aging beyond 20hr did not produce any major change in the depth distribution of the segregants.

5.4. Discussion and Conclusions

The AES results show that over the range of aging times little variation occurs in the peak-height ratios of the impurities Sb and P. These peak-height ratios represent equilibrium concentrations achieved within 100hr or even 20hr at 520C. This is confirmed by the mechanical tests which show that the transition temperature rises steeply (at constant hardness) during the first 100hr, but then gradually falls with increasing aging time. The decrease in transition temperature observed after 100hr occurs at constant grain boundary composition and is associated with decreasing hardness.

The general mechanical test results show that hardness has a pronounced effect on the transition temperature of embrittled material, but comparatively little effect on the transition temperature of unembrittled material. Figure 5.2 shows that tempering Steels 10, 11 and 14 for a further 27hr at 650C produces only a small decrease in transition temperature, and the values remain almost unaltered during aging at either 520C or 590C. In contrast, the transition temperatures of Steels 13 and 14

---

* The residual Sb level is probably not genuine and could be due to a small underlying Cr peak close to 454eV.

(Figure 5.1), at aging times beyond 100hr, vary considerably depending on the hardness level. This is in agreement with the findings of Mulford {39} who showed that in Ni-Cr-P steels, sensitivity to hardness increased markedly with prior austenite grain boundary P concentration. It seems that hardness is also an important variable in determining the susceptibility of Ni-Cr-Sb steels to embrittlement. The general effect of hardness (or yield stress) is explained schematically in Figure 5.9, for grain boundary impurity concentrations $C_3 > C_2 > C_1$.

To examine the results in further detail it is necessary to convert the AES peak-heights in Figures 5.6 and 5.7 to grain boundary coverages. It may be observed from the Figures that Ni appears to show a slight decrease with aging time up to 300hr and this could be a non-equilibrium effect associated with carbide rejection {42}. Because of this uncertainty only the 300hr and 1000hr Ni peak-heights are taken as equilibrium values to calculate grain boundary coverages. For P and Sb, coverages have been taken from the 100hr, 300hr and 1000hr results, to give:

	Steel 12		Steel 13	
	Mean A_p	θ (monolayers)	Mean A_p	θ (monolayers)
Ni	7.45 ± 0.2	0.42 ± 0.02	9.36 ± 0.2	0.62 ± 0.02
P	9.08 ± 1	0.10 ± 0.01	10.17 ± 1	0.11 ± 0.01
Sb	1.29 ± 0.2	0.072 ± 0.01	1.84 ± 0.2	0.103 ± 0.01

(Errors refer only to the standard deviation in Figures 5.6 and 5.7, and do not include Auger calibration errors).

For the Fe-Ni-Sb system, the effect of bulk Sb concentration on segregation may be estimated from the theory of Guttmann {46,47}. In his derivation, Guttmann has considered the case where the segregants obey the limited-side assumptions of McLean {112} and the isotherms are written in the form:

$$N_i^s = N_i^b \exp(-\Delta G_i/RT)\left[1+\sum_{j=1}^{n-1} N_j^b \left(\exp(-\Delta G_j/RT)-1\right)\right]^{-1} \qquad (5.1)$$

where N^s = boundary concentration,

N^b = bulk concentration,

and ΔG = free energy change, for solute i = 1,2,...

McLean segregation applies where the maximum coverage is limited to unity (one monolayer or less) and in a dilute solution the summation term above effectively allows for the decrease in free sites as the total segregation of solutes approaches the saturation level. Apart from the assumptions of the thermodynamic theory, Eq. (5.1) cannot provide a complete description of metalloid segregation because coverages are known to exceed one monolayer. This has been shown for the Fe-Sn system, where a coverage of about 3 monolayers has been observed {87}, and as will be shown below, Sb segregation in Ni-Cr steels may reach a similar value. Ideally, a description of segregation in systems of the Fe-Ni-Sb type would require a multilayer isotherm, perhaps resembling the BET analogue* of the Fe-Sn system {88}, but which also embodies the thermodynamic theory of Guttmann. The multilayer isotherm of the Fe-Sn system, which is the only system where multilayer segregation has been analysed, is approximated at low coverages, by both the McLean isotherm and by:

$$N_i^s = N_i^b \exp(-\Delta G_i/RT) \qquad (5.2)$$

For the purposes of this simplified analysis it will be assumed that the true isotherms of the Fe-Ni-Sb system are given by Eq. (5.2). This isotherm is reasonably accurate up to 0.5 monolayers which is sufficient to cover the important range over which the Ni-Sb grain boundary interaction is expected to develop. In Eq. (5.2) the Sb and Ni segregation levels are taken to be independent as far as site availability is concerned, but it should be noted that there is no reason to assume *a priori* that Sb and Ni will compete for sites (for example, S and Sn do

---

* This theory allows for both multilayer segregation and eventual precipitation at the grain boundary, when the solubility limit is reached.

not compete for grain boundary sites {88}, and at a free surface there is no indication of site competition between Ni and Sb (Chapter 6)).

Taking Sb, Ni and Fe as components 1, 2 and 3 respectively, the approximate segregation equations are then:

$$N_1^s = N_1^b \exp[-(\Delta G_{13}^o + \alpha' N_2^s)/RT] \quad (5.3)$$

$$N_2^s = N_2^b \exp[-(\Delta G_{23}^o + \alpha' N_1^s(/RT] \quad (5.4)$$

where α' represents the Sb-Ni surface interaction coefficient.

The problem in applying these equations is that measured values of ΔG_{13}^o and ΔG_{23}^o are not available and it is necessary to resort to estimated values. The measured value of ΔG for Sn in Fe at 793K (520C) is $-44 kJ\ mol^{-1}$ {113} and because of the similarity between Sn and Sb atoms it is reasoned that ΔG_{13}^o will be close to this value. Free surface studies of Ni segregation (described in Chapter 6), show that ΔG_{23}^o, at a free surface, is about $-15.5 kJ\ mol^{-1}$ and for this approximate analysis ΔG_{23}^o at a grain boundary is taken as half the free surface value. Setting the Ni in solution at 4 at% and using the interaction coefficient α' as the only adjustable parameter, the graphical solutions obtained for β_{Sb} (ie. N_1^s/N_1^b), and β_{Ni} at 793K (520C) are shown in Figures 5.10 and 5.11. The experimental points at Sb concentrations above 0.025 at% are drawn from the literature {45,114}*, and the fit shown corresponds to $\alpha' = -15 kJ\ mol^{-1} m/l^{-1}$.

In a quaternary system with Ni+Cr+Sb, the interactions of Cr with Sb and Ni should also be considered. However it has been shown that the Ni-Sb interaction is stronger than that of Cr-Sb {39} and the effect of Cr in enhancing Sb segregation seems to result largely from the strong Cr-Ni interaction {99}. Thus in the preceding equations the effect of Cr may be considered as entering through ΔG_{23}^o.

This approximate analysis allows a prediction to be made only up to

---

* Figures 5.10 and 5.11 show data for a Ni-Cr steel containing 500ppm Sb (0.023 at%). This alloy (Steel 15) was prepared following the main investigation, specifically to examine these effects. The same austenitizing (1100C/2hr) and tempering (650C/3hr) treatments were employed and AES samples were aged at 793K (520C) for 140hr and 640hr. The steel composition and AES measurements are given in Table 5.3

the solute range where the interaction terms become large and the Sb coverage begins to increase rapidly. However, it is interesting to compare the predictions of Eqns. (5.3) and (5.4) with experimental data at other temperatures. Taking the same values of ΔG^{o}_{23} and α', and correcting ΔG^{o}_{13} for entropy changes (based on the Fe-Sn system, where the entropy term is 44J mol^{-1} K^{-1}), the results shown in Figure 5.12 are obtained for temperatures in the range 673K-833K (400C-560C). Unfortunately, apart from 793K, there are no experimental points for comparison at <u>low</u> bulk Sb concentrations, where the isotherms are expected to be more accurate, but the changes in the positions of the curves clearly agree with the known experimental data for Ni-Cr steels. It should be noted that similar results can be obtained using the McLean isotherm as a low-coverage approximation and in this case the fit to the data requires an interaction coefficient of about -24kJ $mol^{-1}m/l^{-1}$.

The effect of Ni content at low Sb concentrations is difficult to assess. The solutions shown in Figure 5.12 suggest that Ni content may exert only a modest effect for bulk Sb concentrations below 200ppm (0.009 at%). The AES measured value of ΔG_{Sb} (793K) for the two 5Ni steels is -47kJ mol^{-1} which is very close to the value of -44kJ mol^{-1} for Sn in pure Fe. On this basis the effect of Ni appears to be small (about a two-fold increase in grain boundary concentration), but due to the lack of thermodynamic data the precise components of Sb segregation resulting from the Fe-Sb and Ni-Sb interactions are unknown. The clear variation in transition temperature with Sb content (Figure 5.1) and the lack of measureable embrittlement in the 2.5Ni and 0.5Ni steels suggest that the effect of Ni could be somewhat greater than the adopted values for the thermodynamic constants would predict. However it should be remembered that in the 5Ni steels, Ni will interact with Sb and to a lesser extent with P (as shown elsewhere {39,99}, the Ni-Sb interaction is stronger than the Ni-P interaction), but the total effect is really one of P+Sb interacting with Ni. The P coverages are appreciable and the observed transition temperature shifts may be partly associated with P segregation (which is presumably higher than in the 0.5Ni steels).

A combined plot of the known equilibrium coverages for P and Sb segregation is shown in Figure 5.13. There are important differences in the effect of impurity concentration. Due to the strong Ni-Sb interaction and multilayer segregation, the Sb coverage builds up exponentially with bulk concentration. In contrast P appears to show site saturation at

saturation at about 0.9 monolayers which indicates the firm restraint imposed by McLean segregation. Thus the behaviour of P in this respect seems to resemble that of S in Fe, where site saturation occurs at about 0.5 monolayers {88}. The P results in Figure 5.13 are for AISI 3340 steel {39} and can be described to within $\pm$ 20% using the McLean isotherm and a value of ΔG_P of -52kJ mol^{-1}.

Conclusions

The main points of this investigation are:

1) The susceptibility of Ni-Cr-Sb steels to temper embrittlement varies with Ni content. After tempering for 3hr at 650C, 0.5Ni steels containing up to 200ppm Sb show almost no susceptibility to embrittlement at 520C. Under the same conditions 5Ni steels show about 100C rise in transition temperature:

2) Equilibrium grain boundary segregation of Sb, P and Ni was observed in the 5Ni steels. At the 200ppm Sb level equilibrium concentrations are achieved for aging times $\geq$100hr at 520C.

3). Limited results suggest that bulk impurity content may be an important variable in systems where alloy/metalloid impurity interactions occur. In the case of Sb a large increase in the enrichment factor may occur at high bulk concentrations. Because of the approximately linear dependence of the transition temperature on the grain boundary concentration (References {32,45}, for example), high bulk concentrations may be proportionately much more embrittling than lower concentrations.

4) The effect of Sb content on segregation seems to be in qualitative agreement with the Guttmann analysis, but more comprehensive thermodynamic data will be required if the effects of Ni and Sb on segregation are to be determined in detail.

Steel	Wt%			ppm			
	C	Ni	Cr	Sb	Mn	P	S
10	0.24	0.47	1.43	105	50	40	45
11	0.28	0.51	1.40	190	(50)	50	(45)
12	0.26	4.82	1.52	125	(50)	60	(45)
13	0.28	4.90	1.38	200	(50)	50	(45)
14	0.29	2.46	1.26	<10	(50)	50	(30)

Table 5.1. Chemical compositions of Steels 10-14. The steels were melted as one batch and check analyses (Steel 14) showed Sn<20ppm, As<20ppm. Expected values are shown in parentheses.

		P	S	Sb	C	Cr_{489}	Cr_{529}	O	Ni
Steel 12									
20hr	(1)	6.77	2.16	0.86	-	1.96	-	-	7.46
"	(2)	5.77	1.73	0.76	-	2.10	-	-	8.33
W	(1)	9.03	2.88	1.15					8.58
"	(2)	7.69	2.31	1.01					9.74
100hr	(1)	7.06	1.95	0.92	6.38	2.46	4.33	1.85	7.88
"	(2)	8.47	2.18	1.27	7.78	2.66	4.67	2.80	8.41
W	(1)	7.67	2.12	1.00					8.21
"	(2)	9.21	2.37	1.38					8.78
300hr	(1)	8.10	2.20	1.21	6.40	2.50	-	-	6.95
W	(1)	9.52	2.59	1.42					7.45
1000hr	(1)	6.87	1.89	0.89	7.00	2.13	-	-	6.35
"	(2)	6.04	2.02	0.92	-	2.10	-	-	6.33
W	(1)	10.10	2.78	1.31					7.40
"	(2)	8.88	2.97	1.35					7.37
Steel 13									
20hr	(1)	7.76	2.33	1.39	7.05	2.45	4.61	4.02	8.51
"	(2)	8.26	3.12	1.53	8.90	2.83	4.53	9.41	9.24
W	(1)	9.95	2.99	1.78					9.75
"	(2)	10.59	3.99	1.96					10.69
100hr	(1)	8.04	2.35	1.47	7.76	2.74	4.73	1.79	8.39
"	(2)	7.84	2.22	1.67	7.43	2.40	4.29	2.22	8.28
W	(1)	10.05	2.94	1.84					9.46
"	(2)	9.80	2.78	2.09					9.32
300hr	(1)	8.68	2.07	1.56	8.25	2.62	4.75	1.53	8.42
"	(2)	8.46	2.03	1.43	9.02	2.33	4.36	3.11	8.29
W	(1)	10.85	2.59	1.95					9.50
"	(2)	10.56	2.54	1.79					9.34
1000hr	(1)	5.87	1.52	0.93	8.64	2.01	-	-	7.44
"	(2)	6.38	1.72	1.16	8.04	2.04	-	-	7.20
W	(1)	9.47	2.45	1.50					9.48
"	(2)	10.29	2.77	1.87					9.10

Table 5.2. AES peak-heights for Steels 12 and 13 (aged 520C). Each value is the mean of 4-5 measurements made on different areas of the specimen. Peak-heights for P, S, Sb and Ni have been weighted (denoted by W).

	C	Ni	Cr	Sb	S	P	O
Chemical Comp. (wt%)	0.30*	4.11	1.4*	0.050	0.005*	0.005*	-
AES Results (i) 140hr	8.14±1.35 (7)	9.14±0.90 (7)	2.69±0.16 (7)	3.27±0.36 (7)	1.91±0.27 (7)	7.29±1.11 (7)	4.29±1.50 (7)
(ii) 640hr	8.33±1.21 (6)	9.67±0.82 (6)	2.67±0.32 (6)	4.28±0.90 (6)	1.84±0.40 (5)	5.67±1.03 (6)	6.17±2.32 (6)

* *nominal values*

Table 5.3. Chemical composition and AES results for Steel 15. The C, Cr, S and P contents are based on analyses of the stock material (prior to melting). AES specimens were aged at 520C for 140hr and 640hr to give fractures of 92% and 83% intergranular cleavage respectively (peak-heights are not weighted).

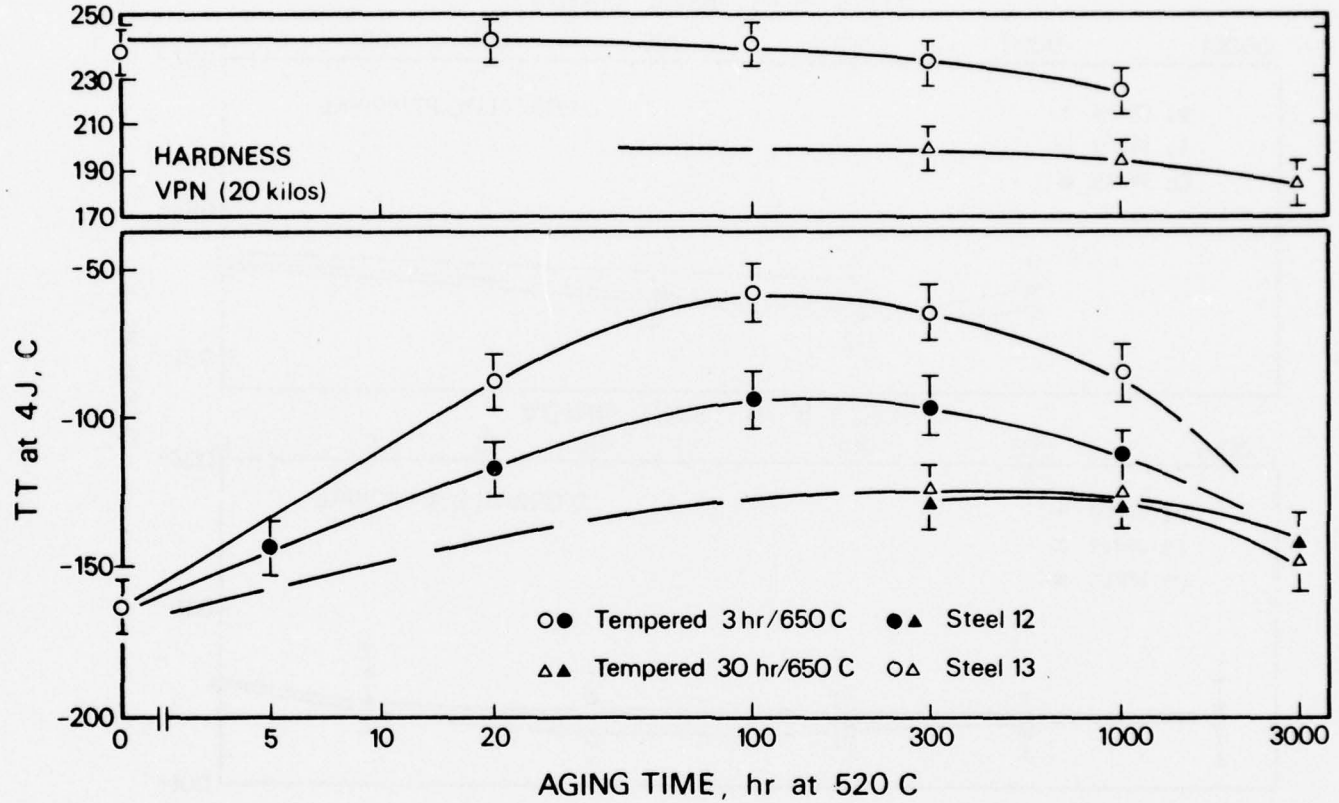

Figure 5.1. Variation in transition temperature with aging time at 520C for Steels 12 and 13.

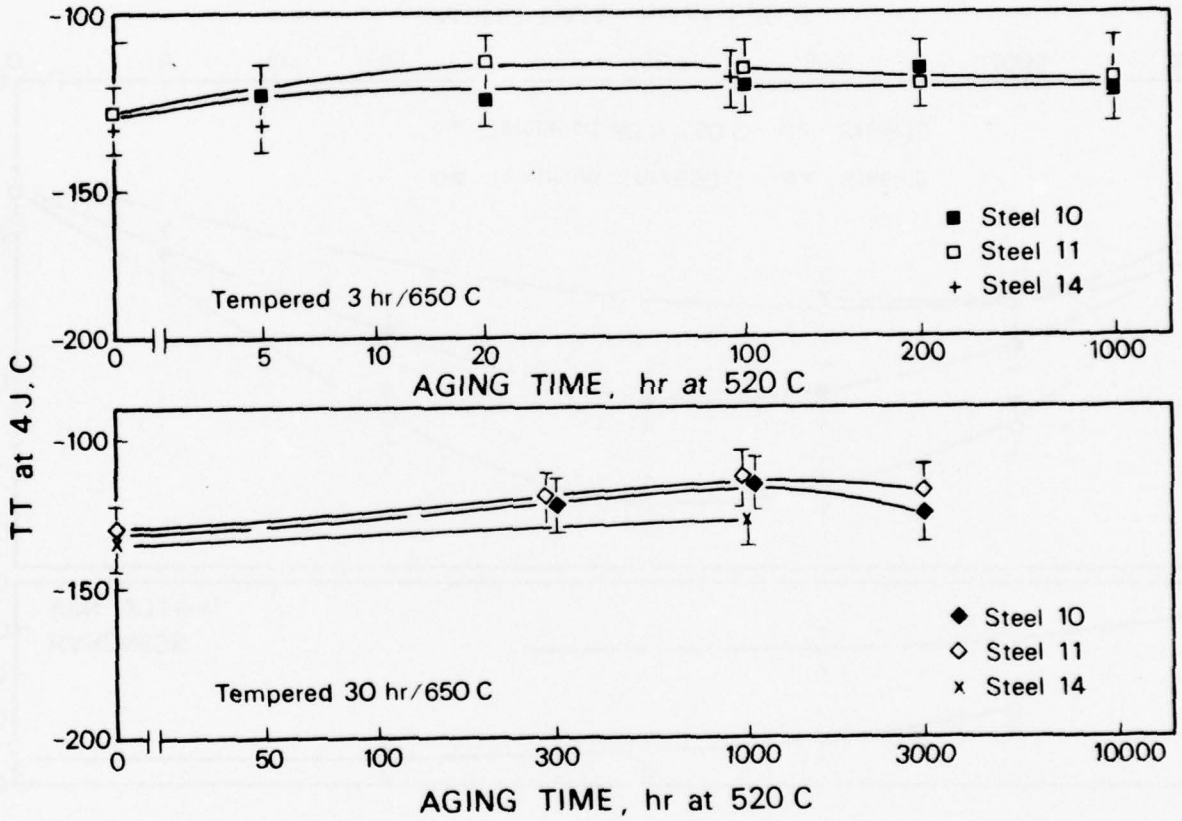

Figure 5.2. Variation in transition temperature with aging time at 520C for Steels 10, 11 and 14.

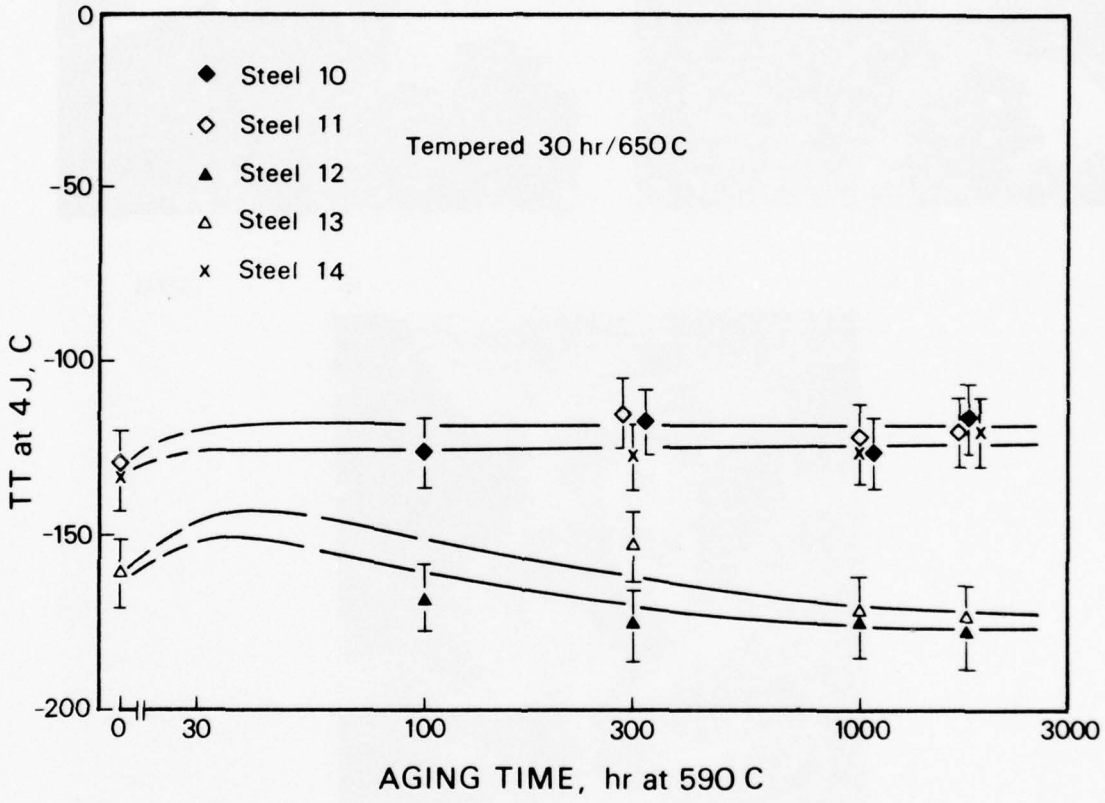

Figure 5.3. Variation in transition temperature with aging time at 590C.

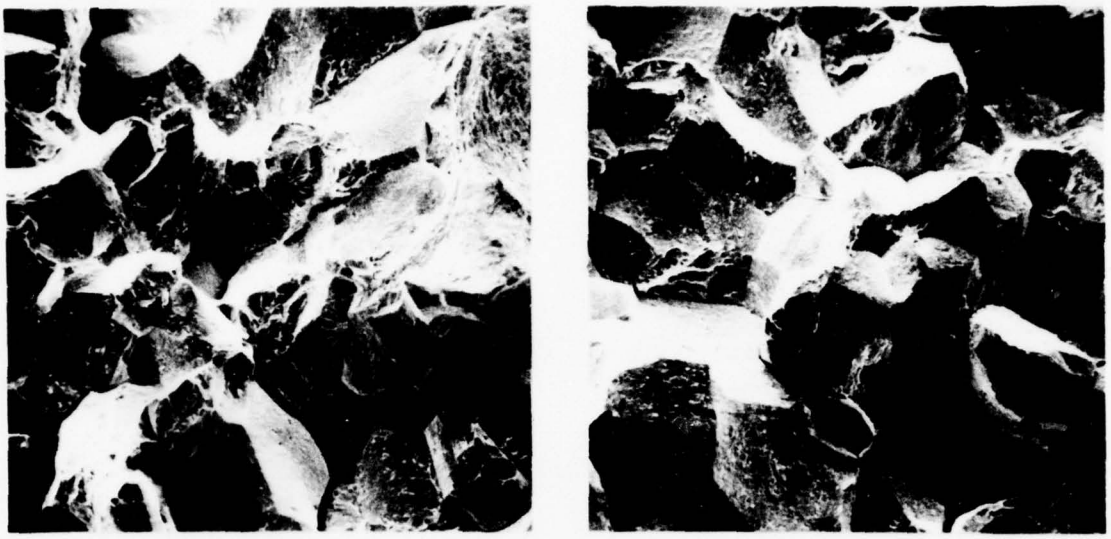

(a) X160 (b) X160

(c) X150

Figure 5.4. Fracture modes in Steel 13 after aging at 520C; (a) aged 20hr and fractured at -99C, (b) aged 100hr and fractured at -101C, (c) aged 1000hr and fractured at -96C.

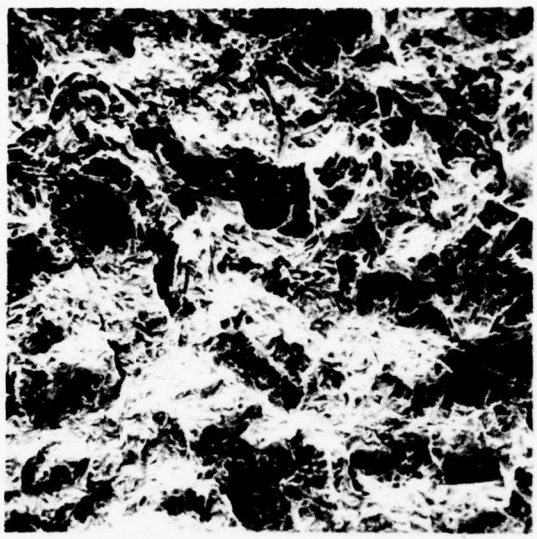

(a) X150

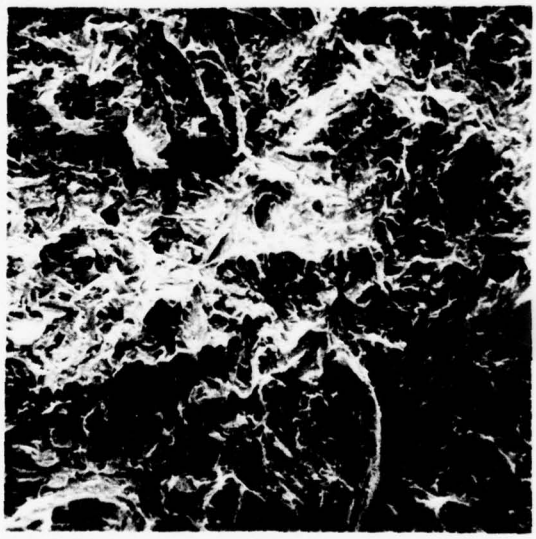

(b) X150

Figure 5.5. Fracture modes in Steel 13 after aging at 590C; (a) aged 300hr and fractured at -153C, (b) aged 1750hr and fractured at -171C.

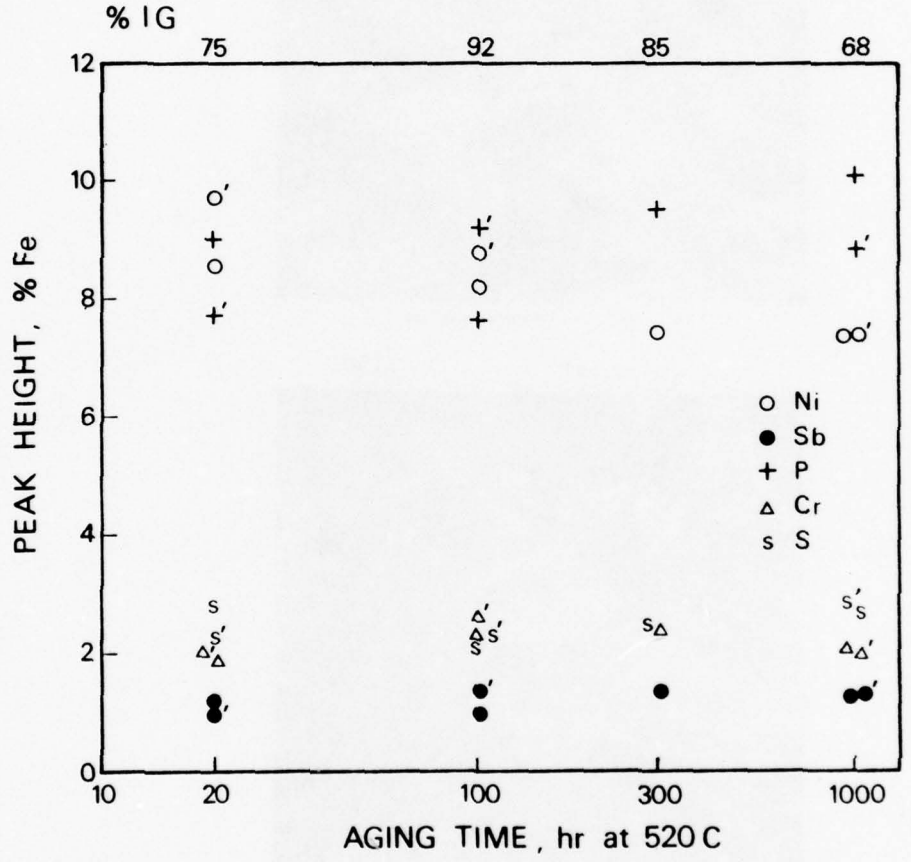

Figure 5.6. Normalized and weighted AES peak-heights as a function of aging time for Steel 12.

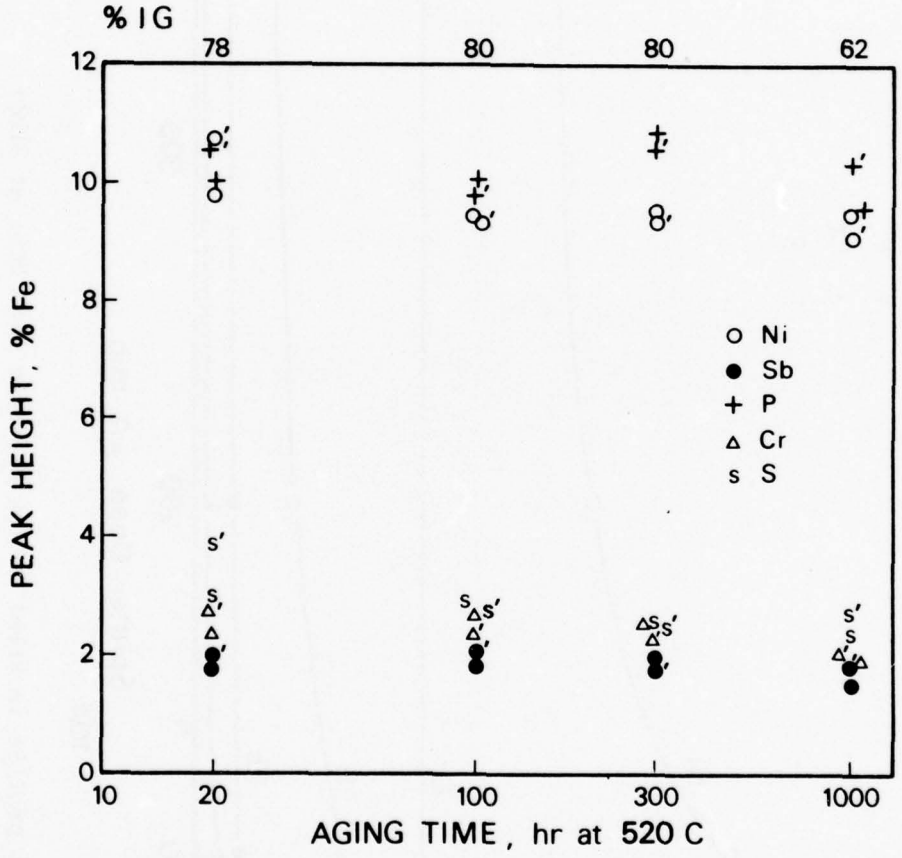

Figure 5.7. Normalized and weighted AES peak-heights as a function of aging time for Steel 13.

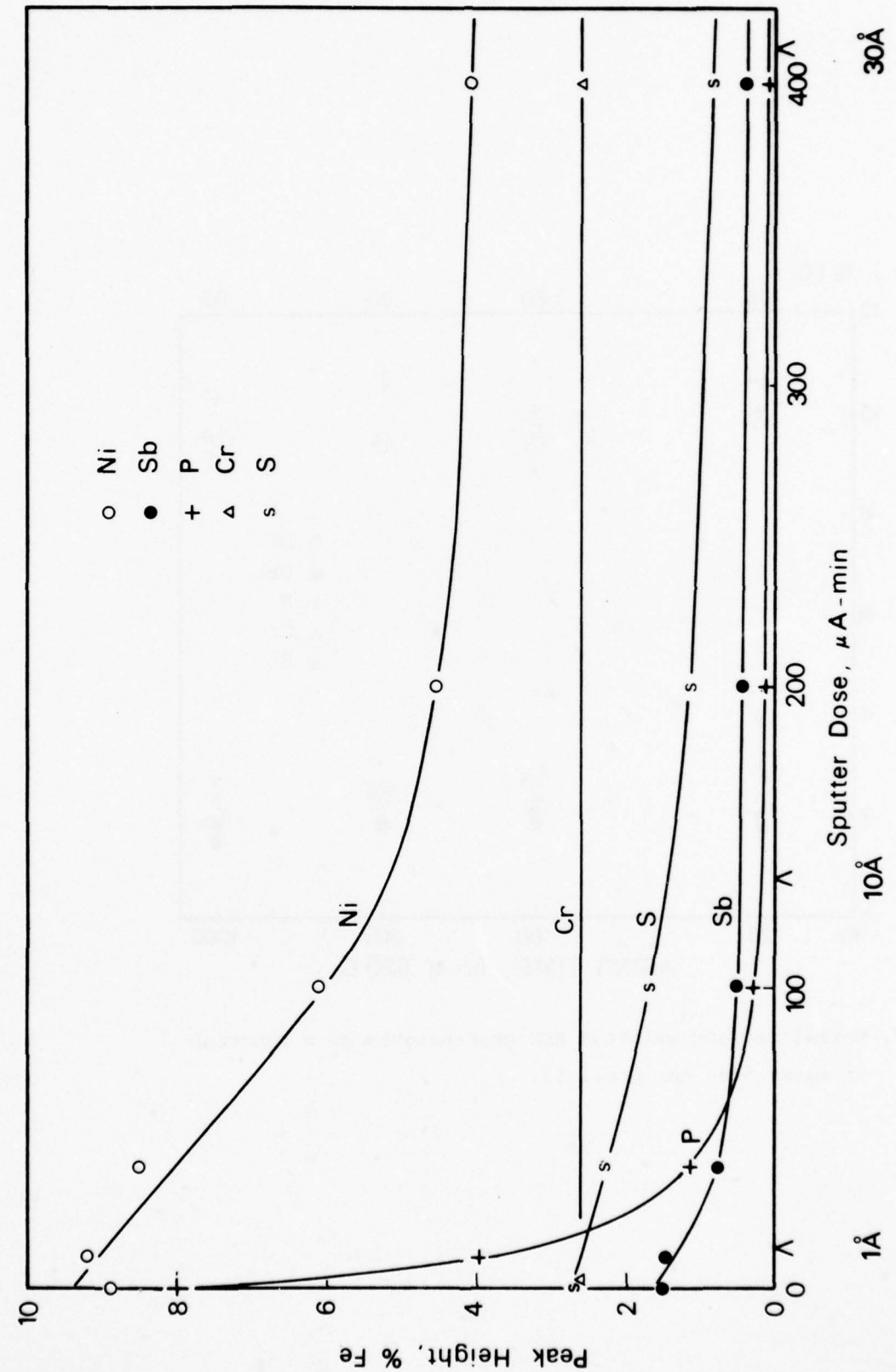

Figure 5.8. Segregant depth profile in Steel 13 (in specimen aged 20hr at 520C).

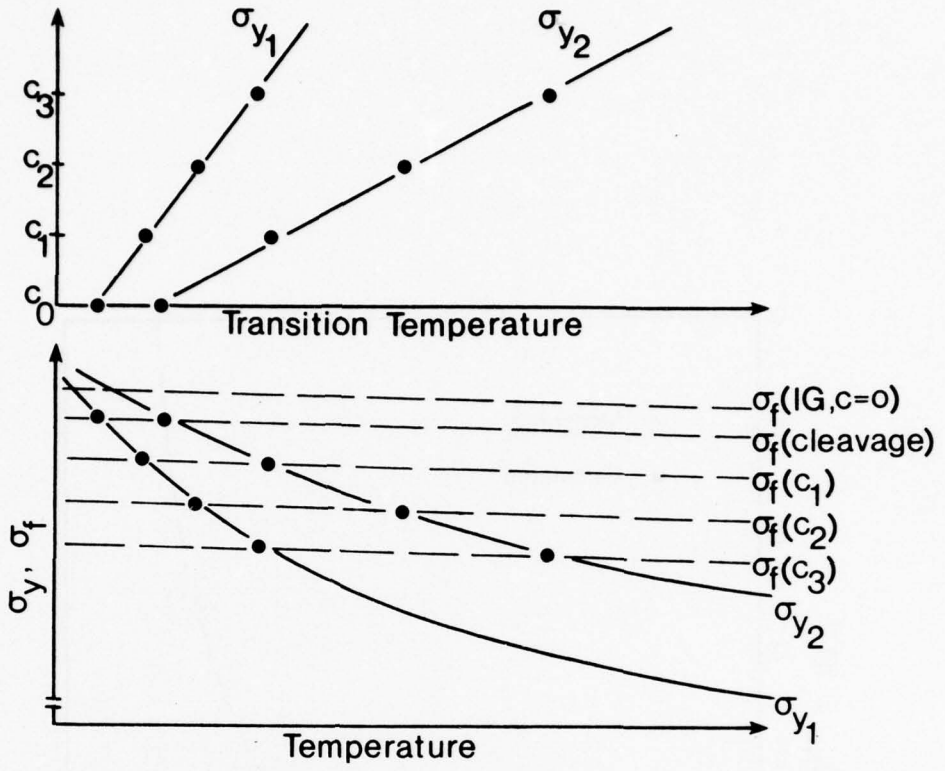

Figure 5.9. Schematic representation of the effects of yield stress and grain boundary impurity concentration on transition temperature.

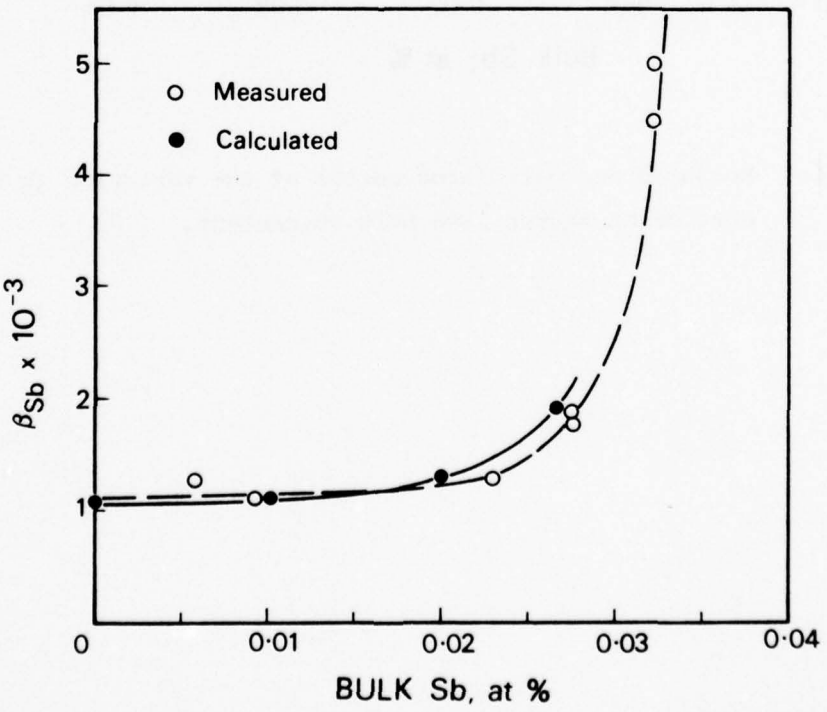

Figure 5.10. Measured and calculated curves of the variation in Sb enrichment factor with bulk Sb content. Results for Sb contents >0.025at% are drawn from the literature {45,114}.

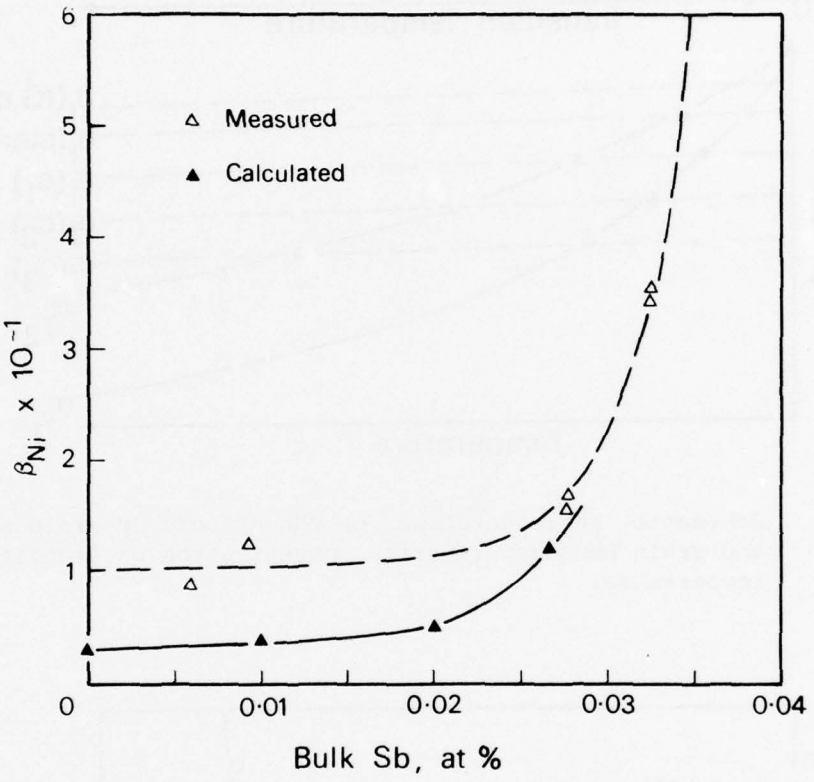

Figure 5.11. Measured and calculated curves of the variation in Ni enrichment factor with bulk Sb content.

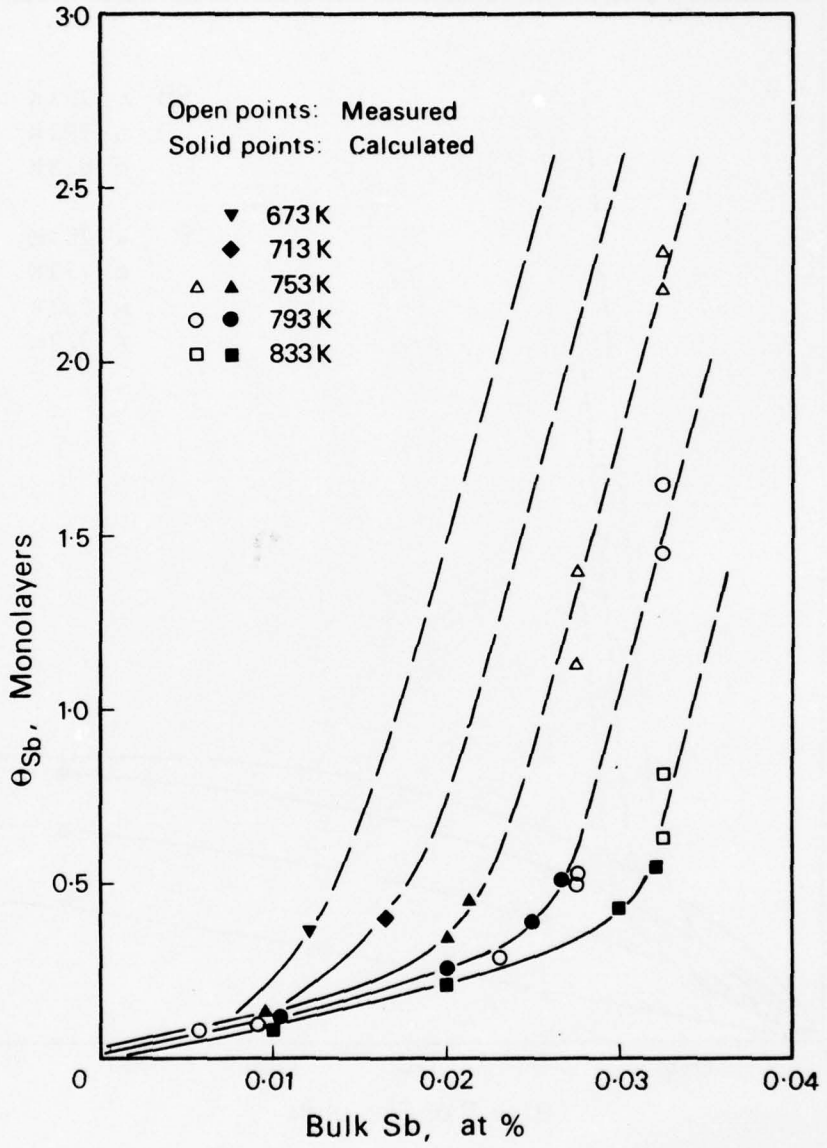

Figure 5.12. Equilibrium Sb coverage in Ni-Cr steels as a function of aging temperature and bulk Sb content. Experimental points are shown together with coverages calculated up to 0.5 monolayers.

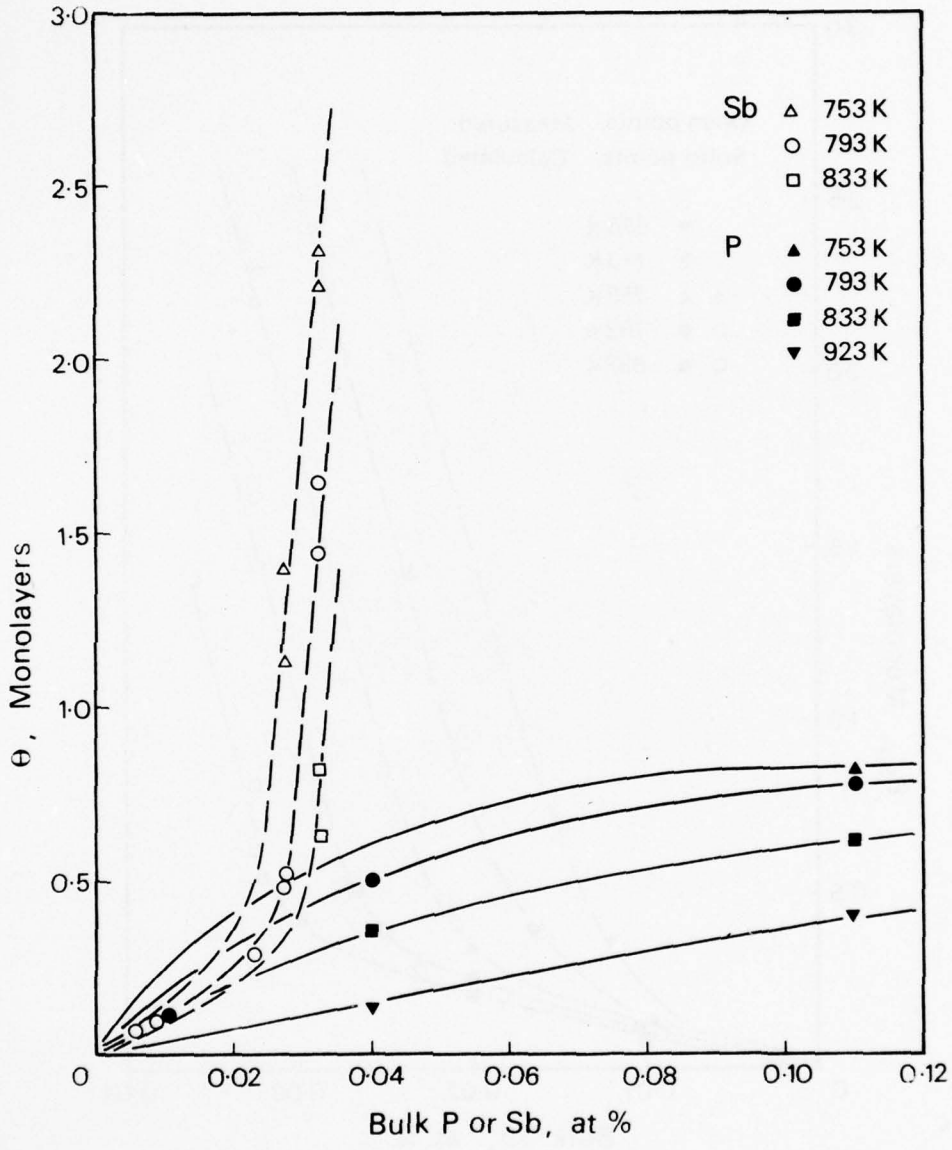

Figure 5.13. Experimental results for P and Sb equilibrium segregation in Ni-Cr steels.

CHAPTER 6

FREE SURFACE SEGREGATION

6.1. Introduction

If surface analysis techniques are to be employed in the study of the diffusion of solutes to grain boundaries, then it is necessary to fracture the material to expose the solute at the boundaries. Thus a segregating solute must be both embrittling and present at the grain boundaries in appreciable amounts, before any measurements can be made. Since solutes tend to segregate at all low energy sites, one method which can be used to overcome these limitations is the study of free surface segregation, where the solute accumulation can be observed in situ.

The earlier work on surface and grain boundary segregation relied on the indirect methods of surface and interfacial energy measurement. The general expression for the change in free energy (surface or grain boundary) in a multicomponent system is {115}:

$$d\gamma = VdP - SdT - \sum_i \Gamma_i \, d\mu_i \qquad (6.1)$$

where V and S are the specific volume and entropy, respectively, and Γ_i is the excess of species i per unit area, having a chemical potential μ_i. For a binary solution, where i = 1 and 2 for the solvent and solute respectively, the above equation can be simplified by applying the Gibbs-Duhem equation at constant temperature and pressure:

$$d\gamma = [-\Gamma_2 + \Gamma_1 X_2/(1-X_2)]d\mu_2 \qquad (6.2)$$

where X_2 is the mole fraction of solute.

Assuming that the solute obeys Henry's Law and taking the solute activity as a_2, then for $X_2 \ll 1$:

$$d\mu_2 = RT \, d \ln a_2 = RT \, d \ln X_2 = RT \, d X_2/X_2 \qquad (6.3)$$

From Eqns. (6.2) and (6.3) a dilute approximation of Gibbs' adsorption isotherm is obtained:

$$\Gamma_2 = - X_2(RT)^{-1}(d\gamma/dX_2) \qquad (6.4)$$

Prior to the introduction of AES and other surface analysis techniques this equation was the basis for determining grain boundary and free surface solute segregation levels.

For most metals the surface energy, γ_s, is about three times the high-angle grain boundary energy, γ_b, {89}. In Fe-X binary systems at temperatures close to the melting point, the rates of change of these energies with solute content (which are as a rule, negative), have also been shown to be about three times greater at a free surface than at a grain boundary {89,116}. Eq. (6.4) then leads to the conclusion that, at temperatures approaching the melting point, the free surface segregation level is about three times the grain boundary level.

Of the more recent work on surface segregation, the most important contribution is the study of the Fe-Sn system by Seah and Lea {113}. Using AES, the authors have shown that the ratio between free surface and grain boundary segregation levels can increase by well over an order of magnitude at lower temperatures (eg. 550C). This effect is due to the entropy terms associated with the different states. Apart from showing that solute elements can accumulate at free surfaces, other AES studies have been limited mainly to a determination of the P saturation coverage on Fe {117}, and the free energy of segregation of Au in Ni {118}.

In this Chapter free surface segregation in Fe-Sb, Fe-Ni and Fe-Ni-Sb alloys is investigated with the aims of determining the tendencies for Sb and Ni to segregate seperately in Fe, and to examine their segregation behaviour when present together in a ternary solution.

6.2. Experimental Details

Materials

The Fe-Sb, Fe-Ni-Sb and Fe-Ni alloys, which will be referred to respectively, as Alloys 16, 17 and 18, were prepared as laboratory melts to the following specifications:

Alloy 16 : Fe + 200ppm Sb
Alloy 17 : Fe + 4%Ni + 200ppm Sb
Alloy 18 : Fe + 4%Ni

Because impurities tend to segregate very strongly at free surfaces, special procedures were employed to ensure that the impurity content (particularly S and P) of the alloys was as low as possible. Battelle iron of composition given in Table 6.1 was used as the melting base and the alloying metals were 5N Ni and 6N Sb (Koch-Light). The melts were about 10gm in weight and melting was carried out in a Cu-hearthed horizontal induction furnace. Initially a master alloy containing 1.5%Sb was prepared, homogenized and analysed. To avoid any problems of Sb loss during melting, this alloy was used to provide the Sb additions to Alloys 16 and 17. The melting time for each alloy was about 1min and the melts were inverted and remelted 3 times to assist with homogenization. After melting, the alloys were wrapped in high-purity Ta foil, sealed-off in silica capsules under 70mm of Ar, and homogenized at 1225C for 50hr. To provide a grain coarsening treatment the alloys were then heated at 650C for 20hr.

Chemical analysis checks showed that Alloys 16 and 17 both contained 190 $\pm$ 10ppm Sb (0.0087 at%). Weight losses during melting were <10mg and thus the Ni contents in Alloys 17 and 18 are within 4%(3.8 at%) $\pm$ 0.1%.

AES Heating Apparatus

The specimen configuration used for the studies of Alloys 16, 17 and 18 is shown in Figure 6.1. The specimens were 0.2mm thick and were heated resistively. Various specimen designs were examined, but it was found that if the thermocouple was placed on the main heating strip of the specimen, the heating current invariably created a potential difference across the thermocouple spot-weld, leading to erroneous thermocouple readings. The thermocouple was therefore placed on a small tag spot-welded to the main heating strip. The AES measurements were made on the tag, adjacent to the thermocouple, which was welded to the reverse side of the tag.

The temperature was measured and controlled using a chromel-alumel thermocouple. The control circuit employed a thyristor proportional controller, the 240V AC output being rectified and divided to operate a 12V high-speed reed relay. A 50 A resistively-programmable power supply, operating under current control, provided the heating power and the supply produced constant current pulses as demanded by the reed relay. A high-low system was used and the switchable current was varied depending on the temperature required. The temperature stability was better that $\pm$ 2C

and as temperatures were continuously monitored by a digital thermometer (<± 2C), the temperature accuracy was within ± 4C. Figure 6.2 shows the controller, thermometer and power supply, together with the AES system.

To hold the specimens inside the AES chamber a special carousel, which could accommodate two specimens, was constructed from stainless steel. The specimens were held 180^{o} apart in a horizontal circle. A diagram of one half of the carousel is shown in Figure 6.3.

The specimens were sliced from the ingots using a silicon carbide slitting blade, then ground and polished to 1μm. After spot-welding the thermocouple and tag to the main strip, the specimens were cleaned in trichlorethylene, then acetone, and mounted in the carousel. The system was pumped down and baked out to establish a base pressure of 2×10^{-10} torr. The specimen to be examined was then cleaned by ion sputtering prior to heating. By successively comparing the absolute Sb and Fe peak-heights in the heated and quenched states it was found that reliable AES spectra could be recorded with the specimen at temperature. The only observable difference between the two states was a very slight reduction in the high-energy noise level for spectra recorded cold. Thus by performing the measurements on the tag, rather than on the heating strip, the magnetic field interference effects, mentioned by other workers {113,118}, could be avoided.

Spectra were only recorded from one area of the specimen tag, but as the electron beam was of large diameter (∿500μ), measurements made with the beam positioned centrally on the tag (of width 1000μ) were assumed to be representative of the general segregation levels. After the completion of the experiments, the specimens were examined by SEM; Figure 6.4(a) shows a specimen at low magnification and in Figure 6.4(b) the ion-etched grain boundaries of the material, in the area studied, can be resolved.

AES Procedures

Each specimen was used to determine a number of segregation isotherms over a temperature range, generally between 900K-1200K. The isotherms were usually investigated in order of ascending temperature and both the segregation kinetics (for Sb) and the equilibrium coverages were measured. Prior to the commencement of each isotherm the accumulation of segregants was removed by deep ion sputtering.

As will be shown below, the practical temperature range for in situ

AES experiments was found to be between 900K-1200K. At 900K the diffusion of Sb is so slow that the time to reach equilibrium, t_e, is >24hr, and at 1200K Sb evaporation begins to affect the surface coverages. In Alloys 17 and 18 this temperature range is expected to encompass the α-γ phase transformation {100}, but with increasing temperature no discontinuity in either the Ni or Sb segregation levels was found. Presumably the phase change, if and when occurring, has only second-order effects on the surface segregation levels of these elements.

Despite the precautions taken in the selection of the materials and preparation of the alloys, S segregation was still observed. Because of the possibility of S interfering with Ni and Sb segregation, it was necessary to examine the effect of S in detail. The AES system was free of system contaminants (adsorbed O, C, Cl, etc.), and apart from S, no extraneous elements could be detected on the specimen surfaces (after ion sputtering, in which the system was filled with 1×10^{-5} torr of Ar, minute O and C peaks were present, but these peaks disappeared immediately on heating).

6.3. Results and Discussion

6.3.1. Alloy 16 (Fe-Sb)

Two samples of Alloy 16 were examined and will be referred to as Alloys 16A and 16B.

In Alloy 16A, Sb segregation isotherms were determined for 11 temperatures in the range 923K-1203K. The equilibrium peak-heights, as a function of temperature are shown in Figure 6.5 and the detailed measurements are given in Table 6.2. Typical spectra from Alloy 16A are shown in Figure 6.6(a-b); Figure 6.6(a) shows a spectrum recorded prior to heating and Figure 6.6(b) shows a spectrum after equilibration. The corresponding segregation isotherm is given in Figure 6.7.

Figure 6.5 also shows the Sb segregation level in monolayers; the high segregation level ($\sim$1.3 monolayers) and the lack of any appreciable temperature dependence are in good agreement with results obtained recently for Sn on Fe {113}. Although it is clear that Sb must have a high heat of adsorption on Fe (similar to Sn on Fe), this cannot be determined quantitively from the present experiments, because the Sb coverage must be examined as a function of bulk concentration, as required by the BET theory {113}.

The measured S levels (Figure 6.5) were generally close to 10%Fe$_{703}$

which corresponds to a coverage of 0.045 monolayers*. While it was suspected that S and Sb competed for surface sites, no systematic variation in S level, which would enable the site competition effects to be evaluated, could be obtained in Alloy 16A. Despite prolonged holding at temperatures between 900K-1125K no appreciable change in either the S or Sb levels was observed.

Sulphur could be made to segregate to high levels by heating above 1150K, but strong Sb evaporation also occurred above this temperature (see Figure 6.5). This led eventually to depletion of Sb in the near surface region of the specimen. Significant Sb evaporation at temperatures above 1150C was shown most clearly by a gradual retardation of the segregation kinetics (the kinetics will be discussed later) with increasing temperature. This was opposite to the effect observed at temperatures between 900K-1100K. The presence of a depleted zone was confirmed by reheating at a lower temperature, where it was found that the segregation kinetics were retarded, compared with those determined initially.

Alloy 16A was heated initially at temperatures below 923K, where the Sb segregation kinetics were found to be too slow to be determined. High S levels were observed below 923K and a significant amount of S was removed from the specimen (by ion sputtering) prior to the experiments in the temperature range 923K-1203K. However, Alloy 16B was heated initially at 923K and the S level was about 3 times higher than that in Alloy 16A. With increasing temperature (and S removed by ion sputtering) the S level decreased to much the same level as that in Alloy 16A. These results, for temperatures in the range 923K-1053K, are shown in Figure 6.8 and in Table 6.3. Remembering that, at constant S, the Sb segregation level is almost independent of temperature (Figure 6.5), the result shows that the effect of S may be accounted for if one S atom displaces approximately 3 Sb atoms from the surface. The results for the two samples (the Sb equilibrium levels and segregation kinetics) were in good agreement.

Due to the removal of S by ion-sputtering (and evaporation) it was not possible to accurately determine the heat of adsorption for S on Fe.

---

* A S calibration was determined from that quoted in Reference {113}. After correcting for the different normalizing procedures, the S calibration arrived at was, $\theta_S(m/l) = 0.0045(\pm 0.001)\ k\ A_p$.

The Fe melting base contained only 0.2ppm S (Table 6.1) and assuming that the S level in the bulk was not increased during remelting, the higher levels observed would require an enrichment ratio in the vicinity of 10^6. The measured grain boundary S enrichment ratio is $>10^4$ {88}, and a higher free surface enrichment ratio of $\sim 10^6$ is reasonable.

6.3.2. Alloy 17 (Fe-Ni-Sb)

a) Sb Segregation

The two Ni-bearing alloys (17 and 18) showed S levels that were considerably higher than those of Alloy 16 (this is thought to be due to the presence of S in the Ni pellet). In Alloy 17 this provided an opportunity to evaluate Sb:S site competition over a wide range of surface S levels.

Because S diffuses much faster than Sb, it was possible to deplete the surface region of S by subjecting the specimen to a very short ion sputter at temperature. Using this procedure low-S isotherms were determined at 923K, 963K, 1023K and 1113K. With prolonged holding at 1113K, S slowly segregated again to a high level. In this way it was possible to follow Sb:S site competition from <0.1m/l S up to almost 1m/l S; these results are shown in Figure 6.9.

Apart from the present study, the only investigation of free surface site competition is the recent work at N.P.L. by Lea and Seah {119}, on the Fe-Sn-S system. Because of the similar size of Sn and S atoms, and the comparatively high heat of adsorption of S on Fe {88}, the authors propose that S will replace Sn in the first monolayer, on the basis:

$$\theta_{Sn} = \theta_{Sn(e)} (1 - \theta_S) \qquad \theta_{Sn(e)} < 1 \qquad (6.5)$$

or

$$\theta_{Sn} = 1 - \theta_S \qquad \theta_{Sn(e)} > 1, \quad \theta_S > 0.22 \qquad (6.6)$$

where $\theta_{Sn(e)}$ is the S-free, Sn equilibrium coverage.

To explain the effect of S (in the first layer) on Sn adsorption in the second layer, the statistical probability of Sn filling close-packed sites

around a first-layer S atom is considered. A site reduction of 4.5Sn atoms in the second layer is proposed for every adsorbed S atom. Thus:

$$\theta_{Sn} = (1 - \theta_S) + (\theta_{Sn(e)} - 1)(1 - 3\theta_S - 3p\theta_S) \qquad (6.7)$$

$$\text{for } \theta_{Sn(e)} > 1,\ \theta_S < 0.22$$

The second term represents the site losses around the adsorbed S atom, and p is the probability of filling intermediate sites surrounding the S atom (p is taken as 0.5). This is shown in Figure 6.10 where p = 0 for sites labelled A, and p = 0.5 for those labelled B.

Firstly, it is interesting to compare Sb:S competition with Sn:S competition, at low surface S levels. Figure 6.11 shows the averaged results for Alloy 17 (see Table 6.4) and Alloy 16B (from Figure 6.8), combined with those of the Fe-Sn system {119}. It is clear that all results show good agreement with Eqns. (6.6) and (6.7). In Alloy 16 the S-free Sb segregation level is close to 1.5 monolayers, and it seems that in Alloy 17 the Sb levels are significantly higher (and have a steeper temperature dependence). Segregation levels in Alloy 17 rely on a long extrapolation and cannot be determined precisely. A further uncertainly is in the position of the point X (fixed by the value of p in Eq. (6.7)), which will be dependent on temperature {119}.

At high S levels, the present results suggest that in the Fe-Ni-Sb-S system, Sb:S competition is different from that described by the theory above. From Eq. (6.6), for one monolayer coverage of Sb, each S atom will replace one Sb atom up to a monolayer of S; this was shown for Alloy 17 at 1113K in Figure 6.11. Antimony (like Sn) will have a high heat of adsorption for both the first and second monolayers. One way in which the free energy of the system can be reduced is by the formation of Sb clusters (or islands). This will reduce the proportion of high energy sites (with p = 0 and p = ½) and increase the proportion of normal second layer sites (with p = 1). For Sn and Sb, the upper limit for clustering (represented by a fully divided surface) is:

$$\theta_{Sb} = 2(1 - \theta_S) \qquad (6.8)$$

Clustering will therefore produce a deviation from Eq. (6.6) towards Eq. (6.8) and because this effect is one of configurational entropy it

must be temperature dependent. The high-S results for Alloy 17 (Table 6.4), obtained over the temperature range 923K-1113K, are shown in Figure 6.12 and are attributed to clustering.

b) Ni Segregation

In comparison with Sb, Ni did not show any pronounced changes in behaviour. In general, Ni segregated to a low equilibrium level (0.3-0.5monolayers) and because of the high Ni bulk content, equilibrium was achieved well before Sb reached equilibrium. The subsequent Sb increase to equilibrium produced no observable change in the Ni segregation level. A typical isotherm showing Ni and Sb segregation is given in Figure 6.13.

The results show that Ni segregation is essentially independent of Sb segregation over the temperature range 923K-1113K. Although the presence of Ni appears to increase Sb segregation to a level approaching the adsorption limit, there is no clear indication of Ni:Sb 'coupling' (kinetic or equilibrium), similar to that observed in the Guttmann analysis of grain boundary segregation (Chapter 5). The lack of a strong free surface interaction is possibly due to entropy effects, which cause Ni-Sb bonding to break down at temperatures above the temper embrittlement range ($\sim$713K-863K). Other factors which may be important are the different states (surface-grain boundary), and the high level of Sb segregation in the absence of Ni (Figure 6.11).

The S segregation level, which was varied over a wide range in these experiments, had no detectable influence on Ni segregation.

6.3.3. Alloy 18 (Fe-Ni)

Alloy 18 was examined by equilibration at 8 temperatures over the range 773K-1123K. The measurements obtained are shown in Table 6.5.

The Ni calibration derived in Chapter 2 yields the surface concentrations in Table 6.5, which are shown as a function of temperature in Figure 6.14. Ni segregation only increases the Ni peak-height by 30-100% depending on temperature, and the Ni signal from the bulk is always a significant proportion of the signal measured after segregation. Bearing in mind also that the total Ni peak-height is just 5-10% of the Fe_{703} peak-height, the cumulative errors involved in the determination of Ni on the surface are quite high (as shown by the error bars in Figure 6.14).

The free energy of Ni segregation has been calculated from the low-coverage isotherm (Chapter 5),

$$N_{Ni}^{S} = N_{Ni}^{b} \exp(-\Delta G/RT) \qquad (6.9)$$

which approximates mono- and multilayer isotherms up to coverages of 0.5 monolayers (the true isotherm describing Ni segregation is, of course, unknown). A satisfactory fit to the results is obtained with $\Delta G_{Ni} = -15.5 kJ\ mol^{-1}$. For comparison the effect of a variation in ΔG of $\pm$ 3kJ mol^{-1} is shown in Figure 6.14.

A S level of 0.1-0.5 monolayers was commonly observed in Alloy 18, however detailed studies showed that the S segregation level had no detectable influence on Ni segregation. This conclusion was reached following experiments at 773K and 873K, where the Ni coverage approached an equilibrium level well before any appreciable level of S appeared on the surface. Some typical results are shown below:

873K Isotherm (Alloy 18)

t (min)	5-23	74-104	5-104
$\bar{x}$ (A_p^S)	5.9 $\pm$ 5(4)	59.8 $\pm$ 6.2(4)	38.1 $\pm$ 23.1(17)
$\bar{x}$ (A_p^{Ni})	9.98$\pm$ 1.2(4)	9.55$\pm$ 0.93(4)	9.17$\pm$ 1.17(17)
θ_S (m/1)	0.03$\pm$ 0.03	0.3 $\pm$ 0.03	varying

It is clear that the ensuing S segregation, building up to 0.3 monolayers, has no effect on the Ni level. This is in agreement with the available thermodynamic data {47} which show that the standard enthalpies of formation of FeS and NiS are about the same, and the Ni-S surface interaction coefficient calculated from the enthalpies is almost zero.

The results demonstrate that Ni is surface active in Fe, with a free energy of segregation of -15.5 $\pm$ 3kJ mol^{-1}. This supports the view that Ni will segregate, in the absence of Sb or other elements, to the grain boundaries in steels. In the temper embrittlement range, at say

773K (500C), the measured Ni surface enrichment ratio is ∿12. Bearing in mind that surface segregation levels are >3 times the grain boundary levels {89,116}, this gives an estimate of the Ni grain boundary enrichment ratio in Fe of 2.5 $\pm$ 1.5.

6.3.4. Sb Segregation Kinetics (Alloys 16A, 16B)

Because a complete spectrum, from S-120eV to Fe-703eV, required several minutes to record, the most suitable range for accurately determining the segregation kinetics was found to be 900K-1050K. At temperatures below 900K, t_e > 1000min, and at temperatures above 1050K, t_e < 10min, so that at the higher temperatures only a few measurements could be recorded before equilibrium. Furthermore, Sb evaporation from the specimen surface became increasingly important at temperatures above 1050K. The results and discussion will therefore be limited to the region between 900K and 1050K.

In the initial stage of segregation, Sb will diffuse from just below the surface and thus create a depleted zone or 'well' which will in turn be supplied by down-hill diffusion from the bulk. The characteristics of the solute 'well' depend on the system studied and in particular on time, diffusion rate and evaporation rate. Analytical expressions have recently been derived {120} which extend McLean's original kinetic theory {97} by incorporating the effects of both strong adsorption and evaporation. In essence, McLean has considered the case where the surface (or grain boundary) concentration is proportional to the solute concentration just below the surface (albeit depleted). However, in systems of the Fe-Sb/Fe-Sn type the surface concentration is fairly insensitive to the bulk concentration, except at very low bulk concentrations {113}. When the kinetics are plotted against $t^{\frac{1}{2}}$, this effect is expected to increase the linearity of the kinetics compared with the McLean theory {120}. As will be shown below, results for the Fe-Sb system are consistent with this prediction.

If, in the Fe-Sb system, the surface concentration is not particularly sensitive to the bulk concentration, the initial segregation kinetics should correspond to diffusional flow from below the surface into an infinite sink. The relevant diffusion equation, attributed to Crank {109}, is:

$$A_S = 2 A_o (Dt/\pi)^{\frac{1}{2}} \qquad (6.10)$$

where A_S is the amount of solute supplied and A_o the solute concentration.

The most recent volume diffusion data for Sb in Fe (although determined in the paramagnetic range, above 1070K) are described by {59}:

$$D_{Sb} = 440 \pm 200 \exp [(-270 \pm 7)/RT] \qquad (6.11)$$

where R is in kJ mol^{-1} K^{-1} and D in cm^2 s^{-1}.

Taking,

$$A_o = 0.0087 \text{ at\%} = 7.40 \times 10^{18} \text{ at } cm^{-3}$$

and $$\theta_{Sb} = 1 \text{ (m/1)} = 1.01 \times 10^{15} \text{ at } cm^{-2}$$

Then, from Eq. (6.10):

$$\theta_{Sb} \text{ (m/1)} = 8278 (Dt)^{\frac{1}{2}} \qquad (6.12)$$

A plot of Eq. (6.12) against the experimental results is shown in Figure 6.15, where in all cases, the higher values of D_{Sb} have been chosen in Eq. (6.11). For each temperature Eq. (6.12) provides agreement with the measured surface concentrations to within a factor of 2. In view of the assumptions made and the lack of precise ferromagnetic diffusion data, this agreement is good. By replotting the results at 963K, it was shown that the kinetic curve is of identical shape to that predicted by the analysis given by Lea and Seah {120}, in which t is given on a log scale. It seems that for strong metalloid adsorbants like Sb and Sn, which do not obey the assumptions of McLean segregation, Eq. (6.10) will describe the surface segregation kinetics fairly accurately. However, at very low bulk concentrations (<0.01 at%), or in the presence of evaporation, a more detailed kinetic analysis {120} will be required.

6.4. Conclusions

The main conclusions are:

1) In the Fe-Sb system a bulk concentration of 0.01 at%Sb produces multilayer free surface Sb segregation. The Sb coverage is not strongly temperature dependent in the range 920K-1150K and it seems that Sb exhibits a BET-type adsorption behaviour very similar to Sn on Fe.

2) In an Fe-4 at%Ni alloy, surface segregation of Ni was observed over the temperature range 770K-1120K. Within this range the Ni coverage is described by a free energy of segregation of $-15.5 \pm 3 kJ\ mol^{-1}$ (subject to AES calibration errors).

3) In an Fe-4 at%Ni-0.01 at%Sb alloy, Ni segregation over the temperature range 920K-1120K is similar to that in the binary Fe-Ni alloy, and is essentially independent of the Sb surface concentration. The S-corrected Sb segregation level appears to be increased from the binary coverage (approximately 1.5 monolayers) to a level approaching the expected adsorption limit (2 monolayers). No kinetic or equilibrium coupling was found between the Ni and Sb coverages.

4) In Fe, Ni does not appear to compete for surface sites with either Sb or S. Site competition was observed between Sb and S and the results obtained are in general agreement with recently proposed models based on simple site substitution. Sb clustering is introduced to explain anomalous behaviour at higher S levels and lower temperatures.

5) The Sb segregation kinetics do not show the slow approach to equilibrium suggested by the McLean kinetic theory, but conform closely to a simple diffusional flow of solute from the bulk to the surface.

Resistivity Ratio	No magnetic field	Max. with a magnetic field
$\rho 297 \pm 1.5/\rho 4.2K$	170	920

Nonmetallic Impurities	
Oxygen	1.7
Nitrogen	
Vacuum Fusion	<0.1
Internal Friction	N<0.1
Hydrogen	0.07
Carbon	
Combustion-Conduc.	7
Internal Friction	3.2
Sulphur	
Mass Spectrometer	0.2

Total nonmetallic impurities 6 (Includes internal friction values for nitrogen and carbon and mass spectrometer or colorometric values for sulphur.)

Metallic Impurities often detected with the Mass Spectrometer
(Impurities not detected are denoted N together with the estimated detection limits)

Aluminium	----	Nickel	1
Arsenic	N<0.1	Phosphorus	0.05
Boron	N<0.002	Potassium	0.07
Calcium	0.04	Silicon	N<1.5
Chromium	0.1	Sodium	≤ 0.1
Cobalt	2	Tantalum	N<0.1
Columbium	N<0.06	Tin	≤ 0.06
Copper	2	Titanium	N<0.1
Germanium	N<0.1	Tungsten	N<0.03
Magnesium	N<0.1	Vanadium	N<0.1
Manganese	0.3	Zinc	N<0.6
Molybdenum	N<0.2	Zirconium	N<0.1

Total detected metallic impurities 8 (Includes values marked ≤ except germanium, and values underlined below plus an arbitrary 2ppm aluminium.)

Metallic Impurities not usually detected with the Mass Spectrometer
(Impurities detected in this bar are underlined)

Antimony	≤ 0.04	Holmium	N<0.01	Rubidium	N<0.07
Barium	N<0.03	Indium	N<0.06	Ruthenium	N<0.2
Beryllium	N<0.0005	Iodine	N<0.02	Samarium	N<0.03
Bismuth	N<0.01	Iridium	N<0.02	Scandium	N<0.08
Bromine	N<0.01	Lanthanum	N<0.01	Selenium	N<0.1
Cadmium	N<0.25	Lead	N<0.04	Silver	N<0.1
Cerium	N<0.01	Lithium	N<0.003	Strontium	N<0.05
Cesium	N<0.03	Lutetium	N<0.01	Tellurium	N<0.2
Dysprosium	N<0.03	Mercury	N<0.1	Terbium	N<0.01
Erbium	N<0.03	Neodymium	N<0.03	Thallium	N<0.02
Europium	N<0.02	Osmium	N<0.02	Thorium	N<0.01
Gadolinium	N<0.03	Palladium	N<0.08	Thulium	N<0.01
Gallium	N<0.6	Platinum	N<0.04	Uranium	N<0.01
Gold	N<0.4	Praseodymium	N<0.01	Ytterbium	N<0.03
Hafnium	N<0.01	Rhenium	N<0.02	Yttrium	N<0.06
		Rhodium	N<0.06		

Table 6.1. Analysis of pure Fe (Bar 111) quoted by Battelle Memorial Institute. All analyses are ppm by weight.

Temp./Time	Sb-454eV	S-150ev
650C (923K) 1310-2220min	44.54±1.73(7)	12.66±1.58(7)
690C (963K) 110-225min	44.62±1.50(6)	8.85±1.38(6)
720C (993K) 25-65min	48.90±0.96(3)	2.63±0.76(3)
735C (1008K) 100-150min	43.25±1.30(8)	7.45±0.62(8)
750C (1023K) 25-32min	41.07±0.80(3)	4.77±0.49(3)
780C (1053K) 13-22min	41.71±0.71(5)	4.35±0.92(2)
810C (1083K)	46.89±1.13(8)	13.14+1.38(8)
840C (1113K)	43.86±1.45(7)	7.27±2.56(7)
870C (1143K)	45.20±1.32(7)	7.83±2.46(7)
900C (1173K)	31.18±1.31(5)	18.34±2.23(5)
930C (1203K)	15.79±2.79(6)	49.47±5.00(6)

Table 6.2. AES results for Alloy 16A after equilibration at temperatures in the range 923-1203K. No correction has been applied for site competition.

Temp./Time	Sb-454eV	S-150ev
650C (923K) 860-900min	37.01±1.26(8)	34.43±1.27(8)
690C (963K) 603-638min	45.88±1.66(8)	22.43±0.80(8)
720C (993K) 120-155min	45.54±0.98(7)	22.55±0.91(7)
(a) 750C (1023K) 49-105min	49.07±0.96(12)	11.53±1.00(12)
(b) 750C (1023K) 173-250min	48.06±1.05(6)	14.12±0.49(6)
780C (1053K) 14-61min	50.75±1.90(10)	4.38±1.39(10)

Table 6.3. AES results for Alloy 16B equilibrated at temperatures in the range 923-1053K. Peak-heights are shown plotted in Figure 6.8.

Temp.	n*	S-150eV	Sb-454eV	Ni-848eV
750C (1023K)	14	20.67±2.05	46.64±1.92	7.26±1.08
	3	80.17±0.65	23.63±1.86	5.20±0.78
	4	97.93±6.37	22.93±0.54	5.03±1.69
	6	155.62±3.32	14.07±1.77	5.47±1.94
690C (963K)	7	16.66±1.68	52.14±1.87	9.91±0.91
	3	81.07±0.81	26.77±0.74	5.93±1.00
	6	158.07±3.63	16.70±1.84	7.83±2.40
650C (923K)	7	31.10±1.76	49.66±1.21	10.26±1.13
	4	86.00±2.14	29.83±2.01	9.03±0.96
	9	147.9±3.33	21.20±1.64	8.24±1.77

* No. of measurements

Table 6.4. AES peak-heights for Alloy 17.

Temp./Time	n*	Ni-848eV	θ_{Ni} (m/l)
500C (773K) 270-350min	10	10.36±1.15	0.48
550C (823K) 5-120min	20	8.55±1.05	0.34
600C (873K) 5-105min	17	9.17±1.17	0.39
650C (923K) 10-70min	11	8.20±0.98	0.32
700C (973K) 7-100min	15	6.57±0.76	0.20
750C (1023K) 7-65min	10	7.07±0.84	0.24
800C (1073K) 6-75min	12	5.90±1.22	0.15
850C (1123K) 7-60min	10	5.70±1.03	0.14

* No. of measurements

Table 6.5. Nickel peak-heights and calculated surface coverages for Alloy 18. The bulk (deep-sputtered) peak-height is 4.41±0.5(16).

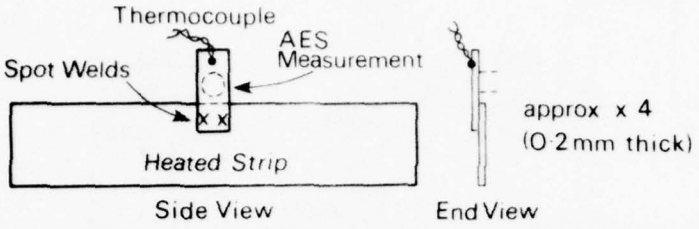

Figure 6.1. Design of surface segregation specimen.

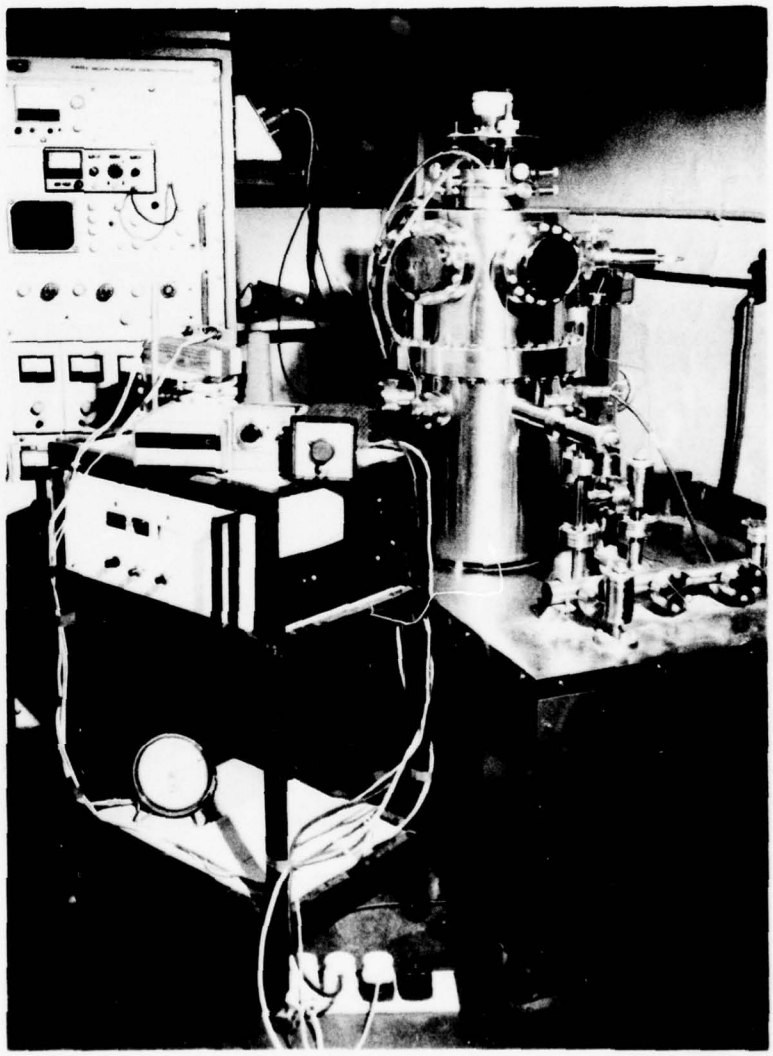

Figure 6.2. Auger system together with specimen heating equipment.

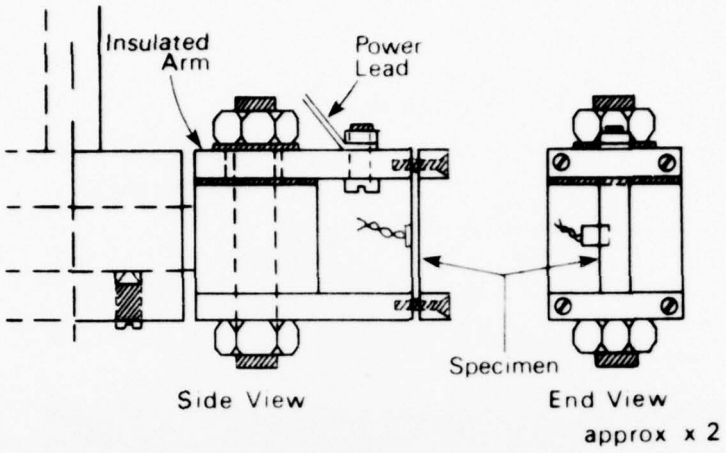

Figure 6.3. Carousel used to resistively heat specimen.

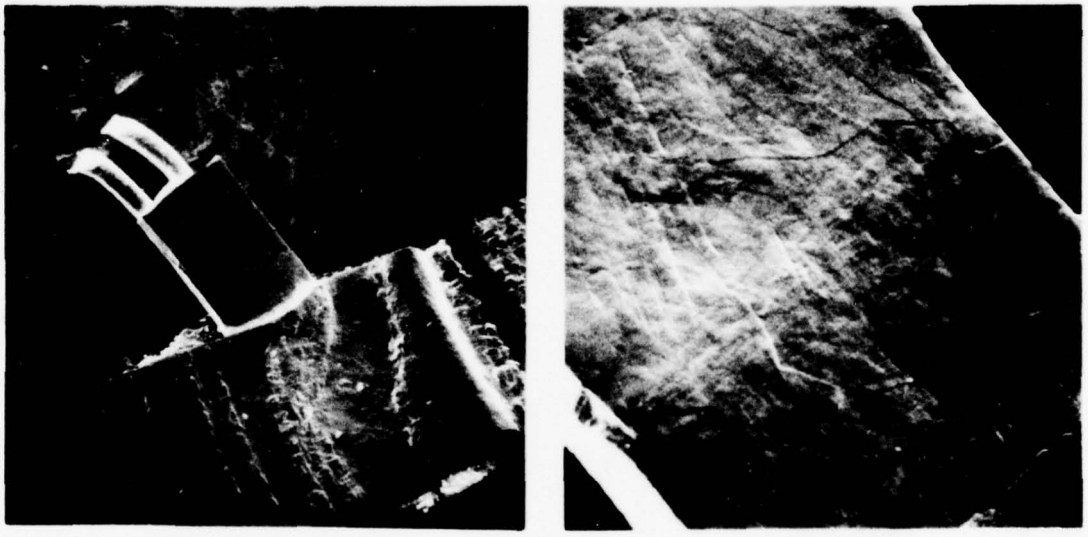

(a) X17 (b) X83

Figure 6.4. Specimen of Fe-0.02%Sb after segregation studies; (a) heating strip and tag, (b) surface of tag in area studied.

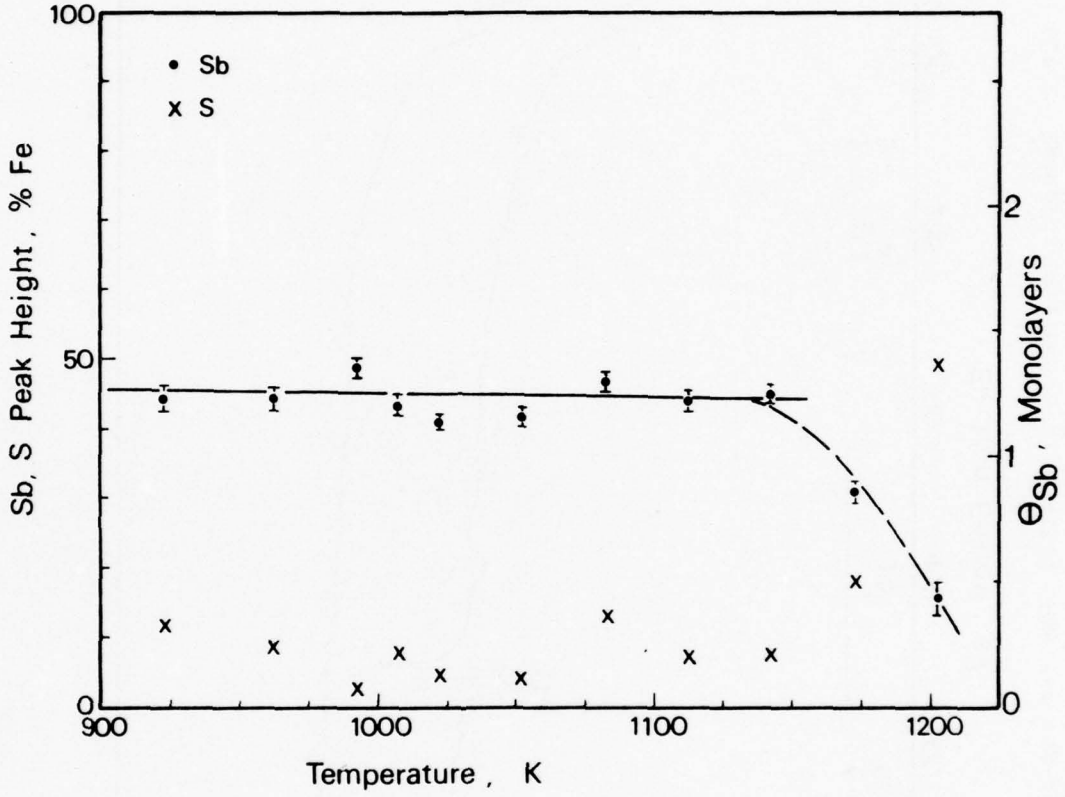

Figure 6.5. Antimony and S segregation levels in Alloy 16A.

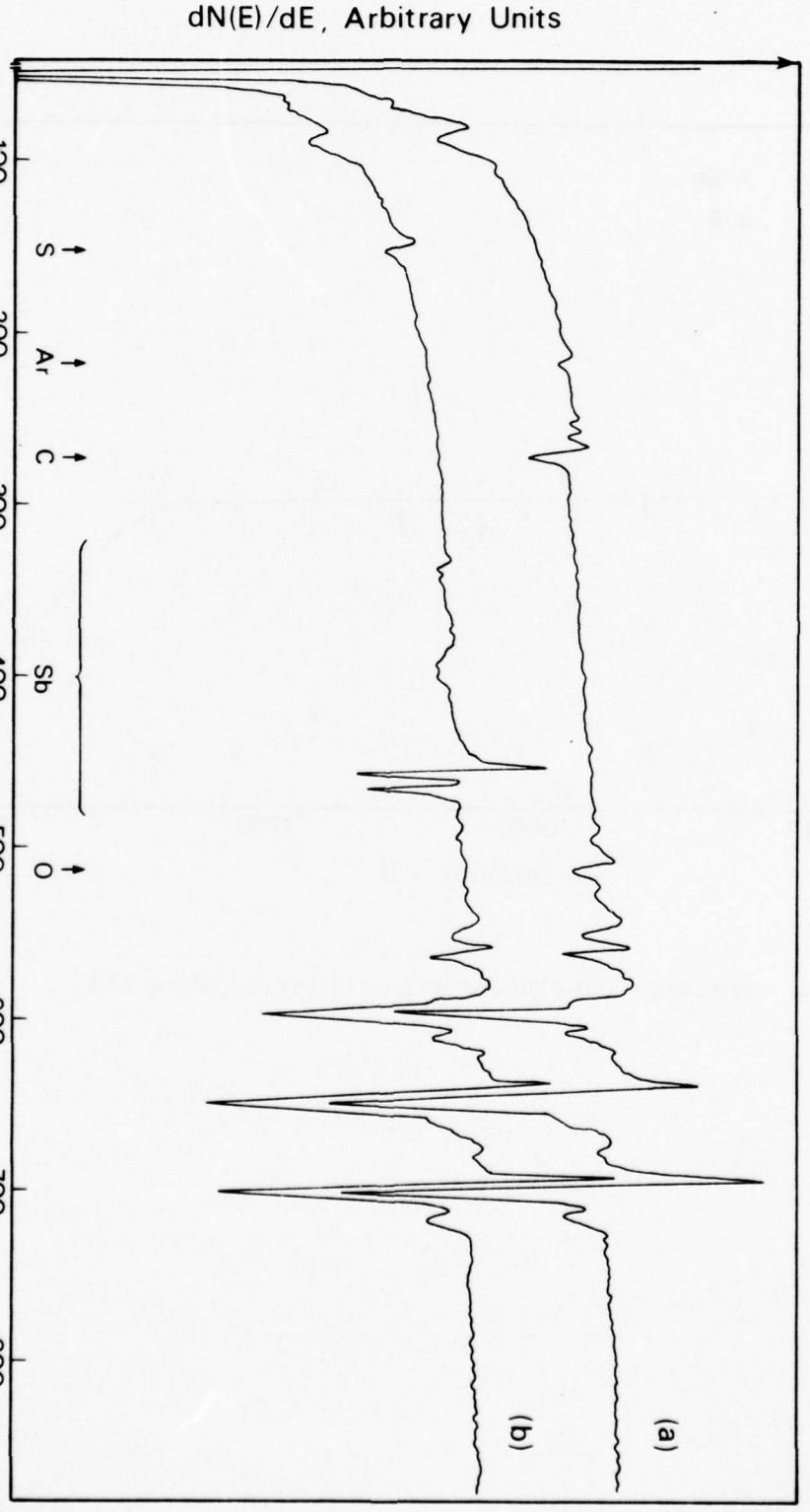

Figure 6.6. Examples of spectra from Alloy 16A; (a) ion-sputtered surface prior to heating, (b) Sb and S peaks after equilibration at 963K.

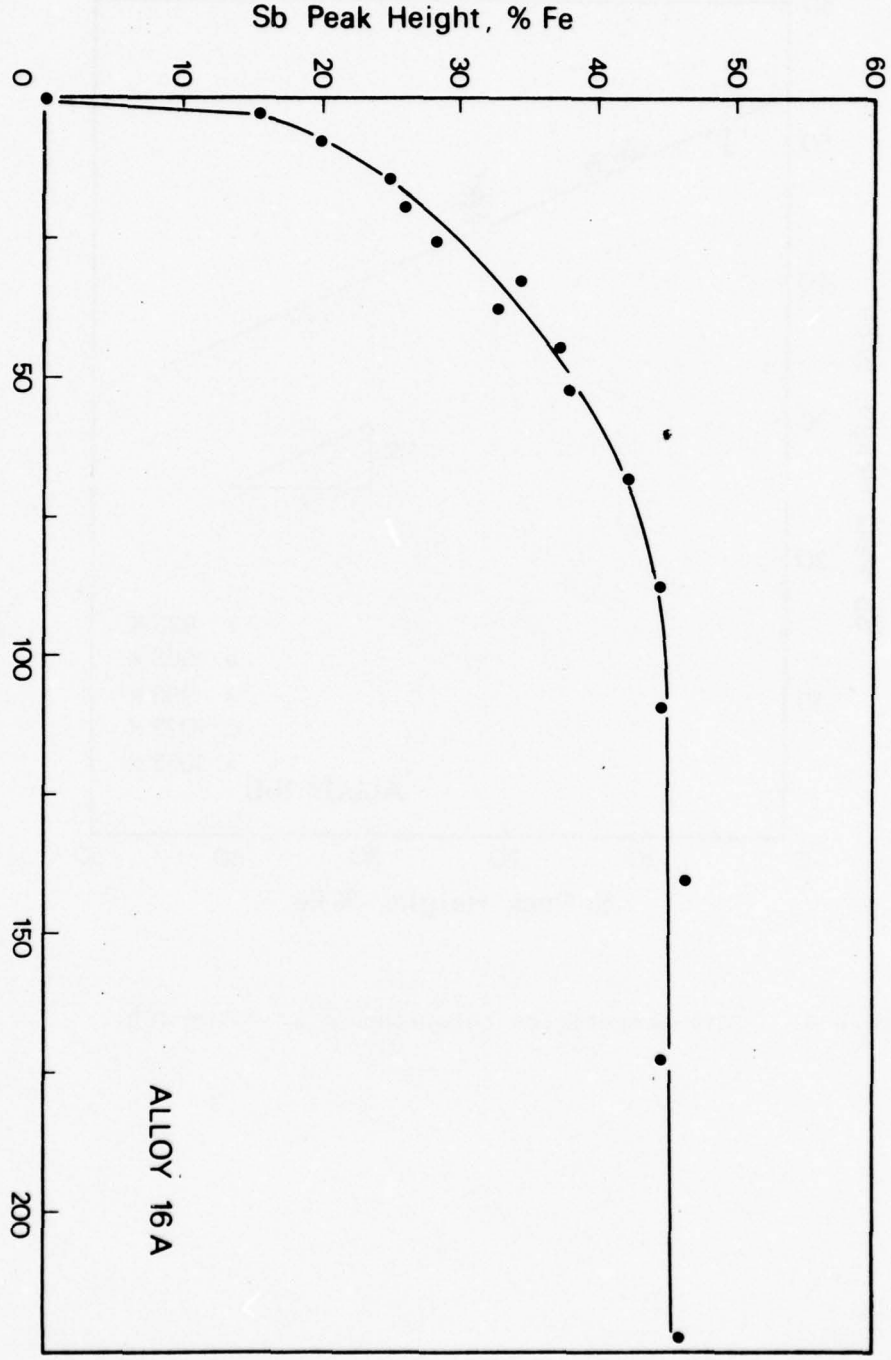

Figure 6.7. Antimony surface segregation isotherm at 963K.

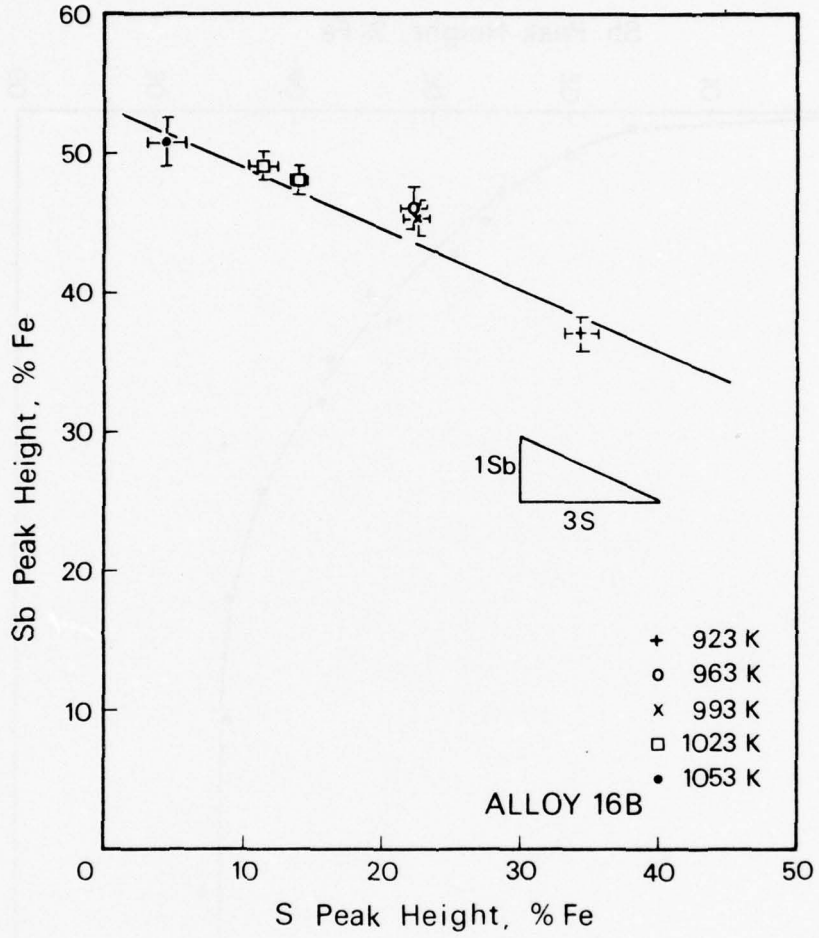

Figure 6.8. Site competition relationship in Alloy 16B.

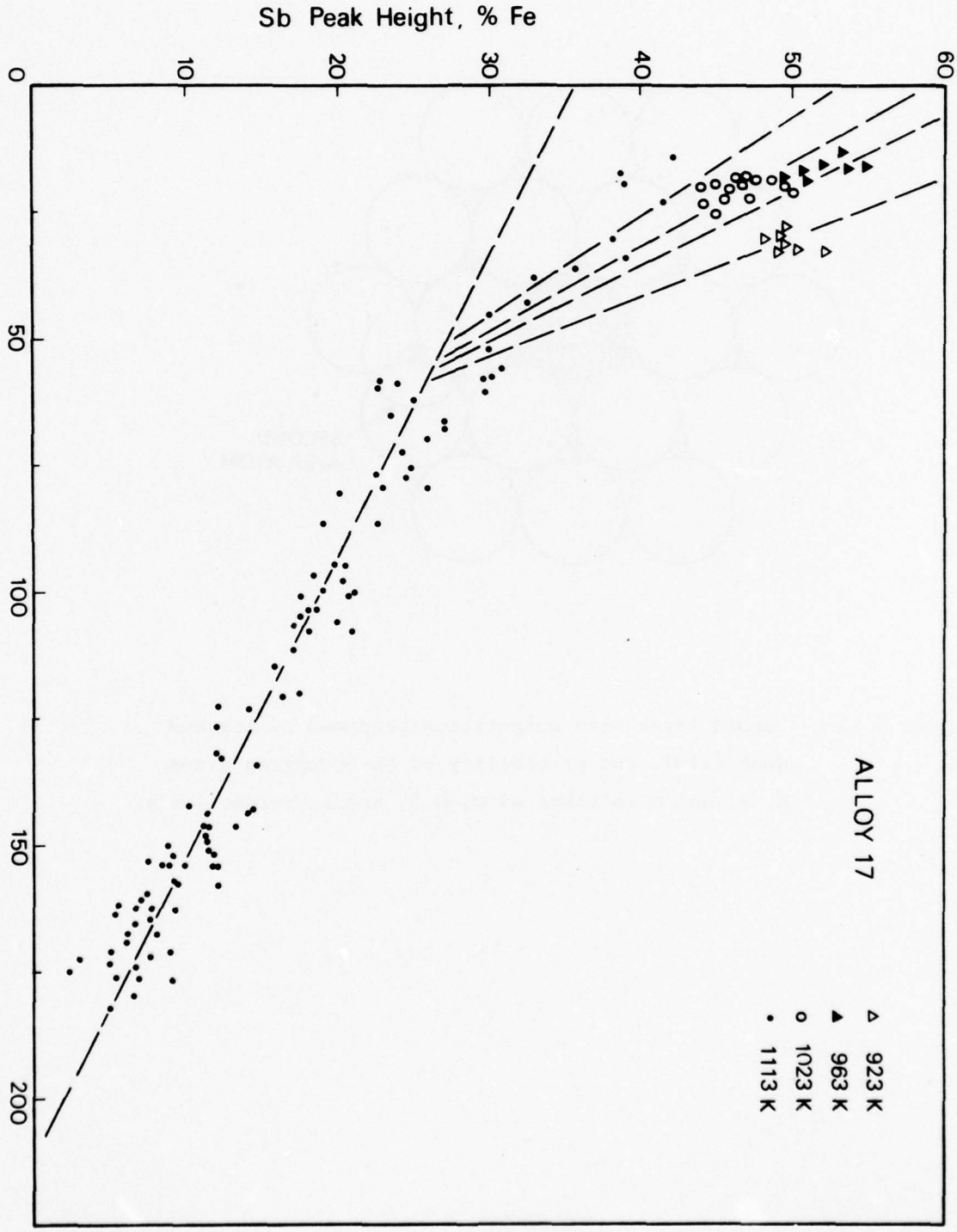

Figure 6.9. Sulphur and Sb site competition in Alloy 17.

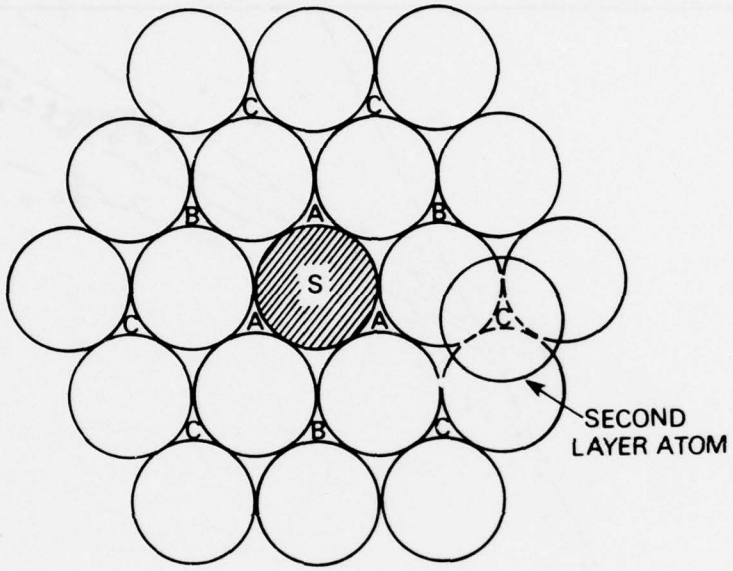

Figure 6.10. Second layer site competition proposed by Lea and Seah {119}. The probability of Sn occupying sites A, B, and C is taken as 0, 0.5, and 1, respectively.

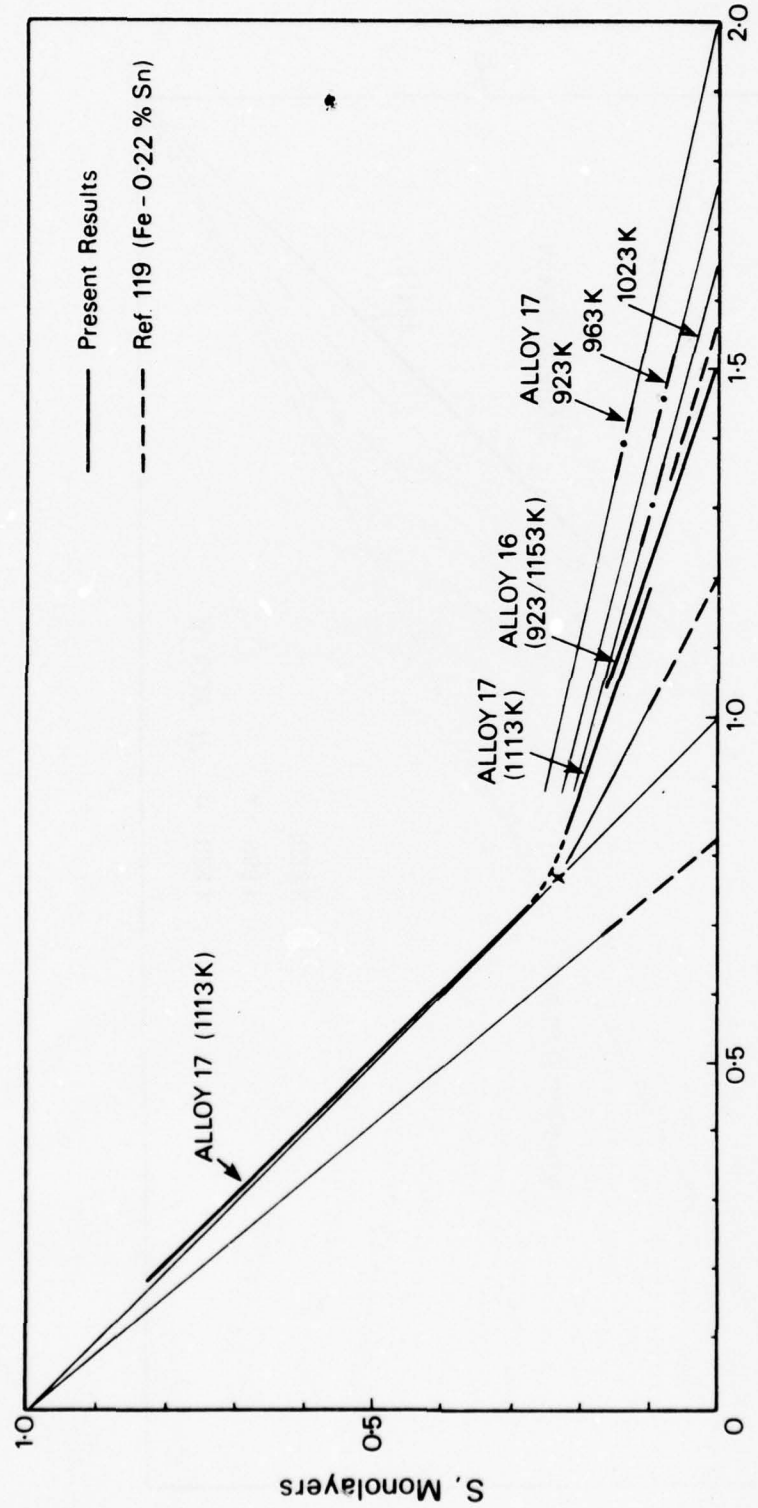

Figure 6.11. Low-S site competition in Alloys 16, 17 and the Fe-Sn-S system.

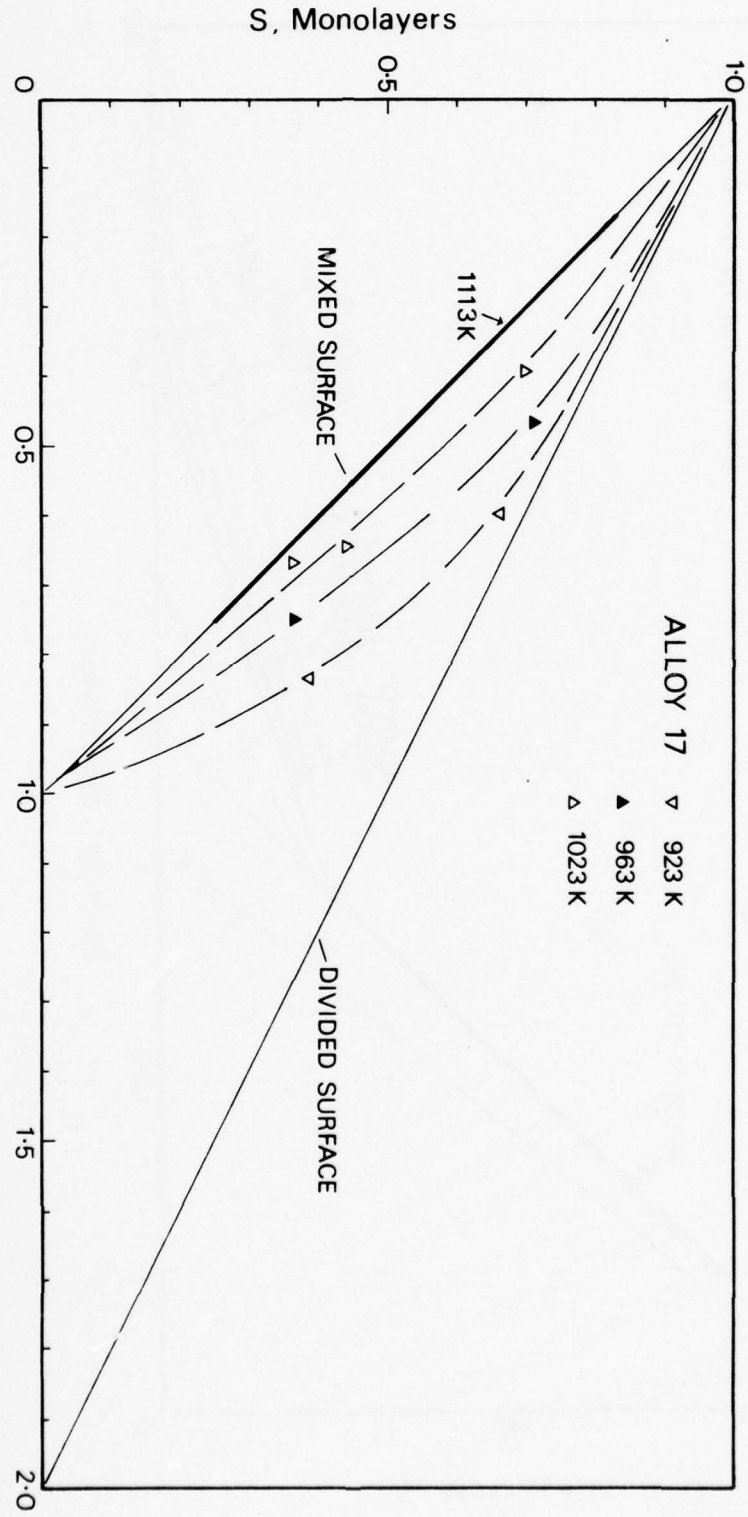

Figure 6.12. High-S site competition in Alloy 17.

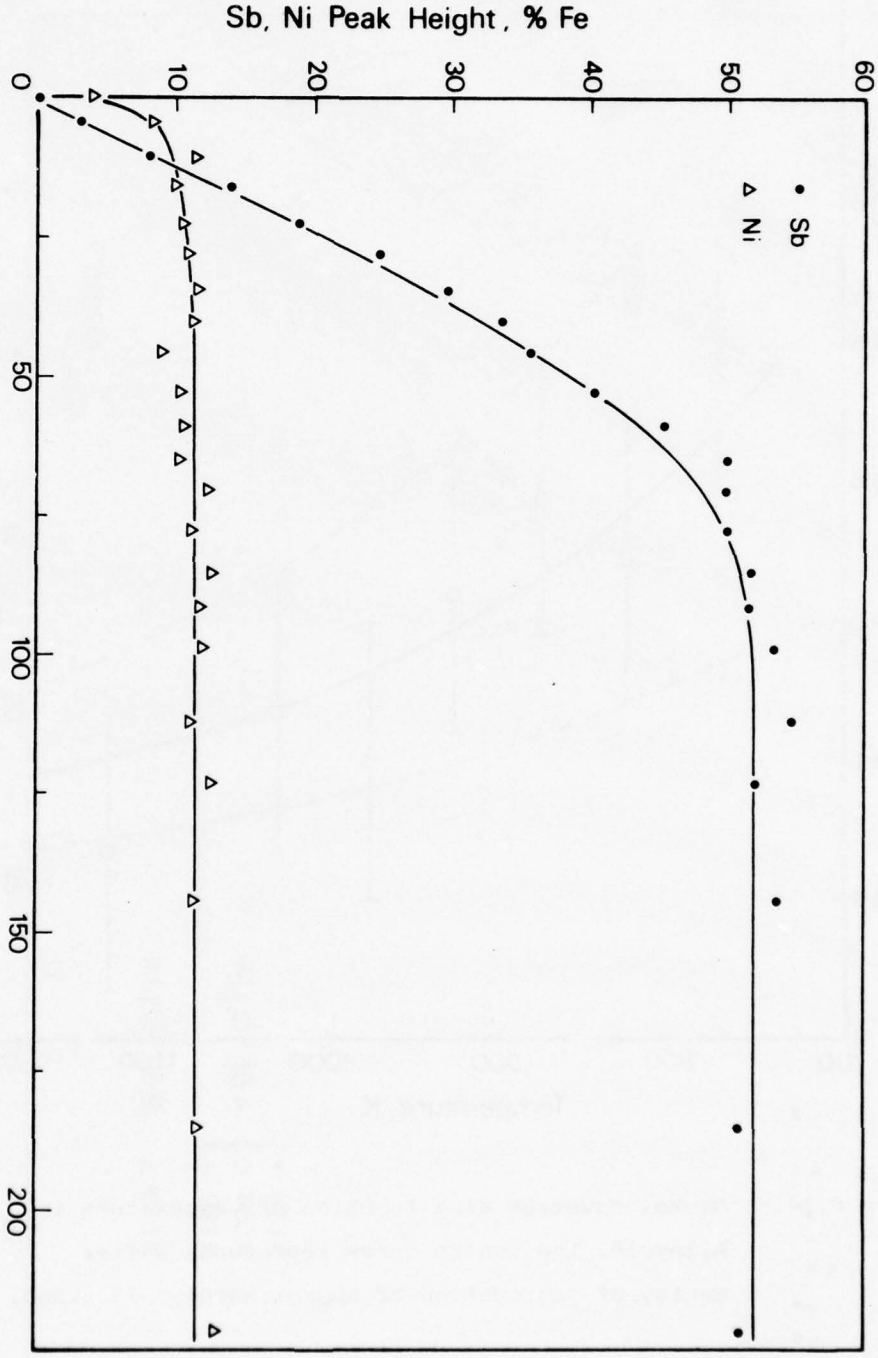

Figure 6.13. Nickel and Sb segregation at 963K in Alloy 17.

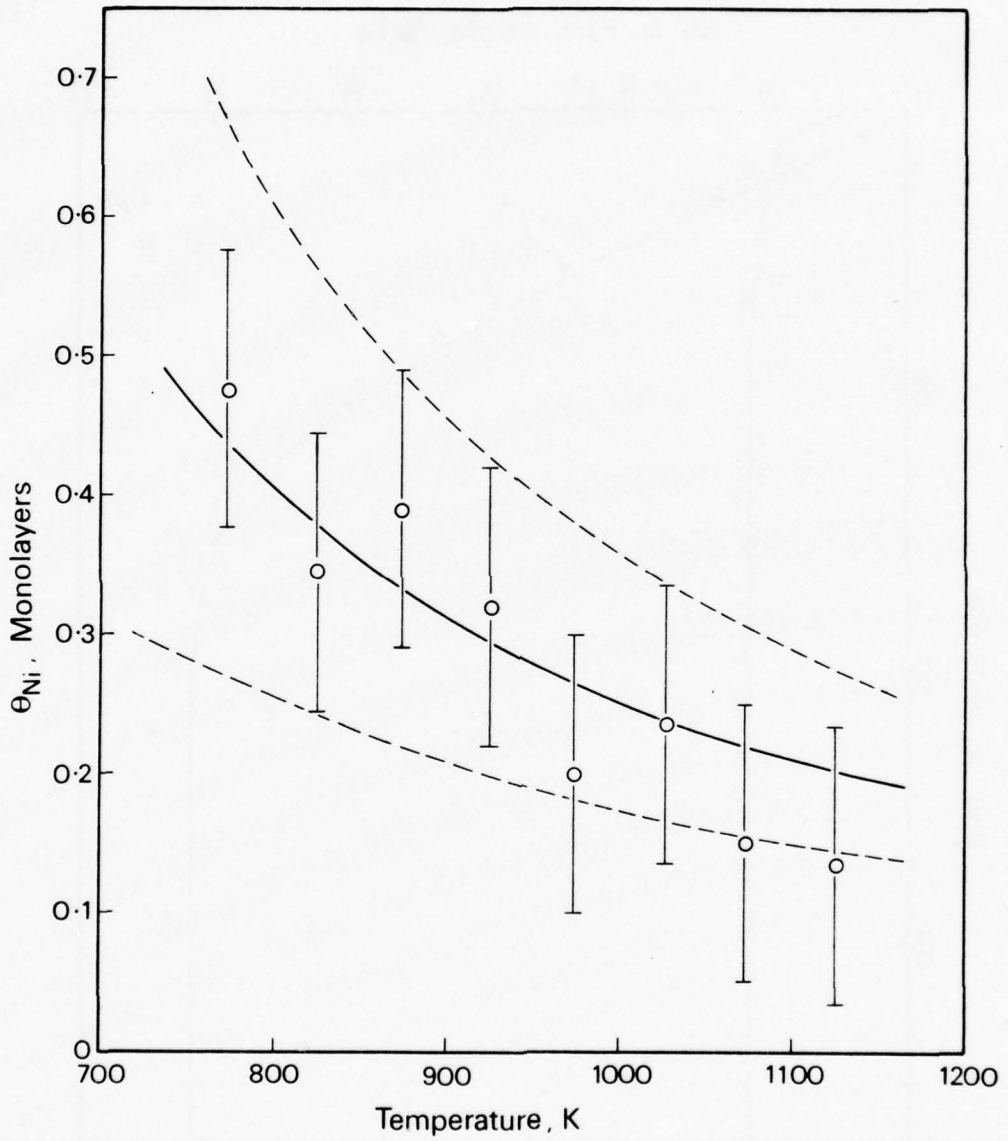

Figure 6.14. Nickel coverage as a function of temperature in Alloy 18. The centre curve represents a free energy of segregation of approximately -15.5kJmol^{-1}.

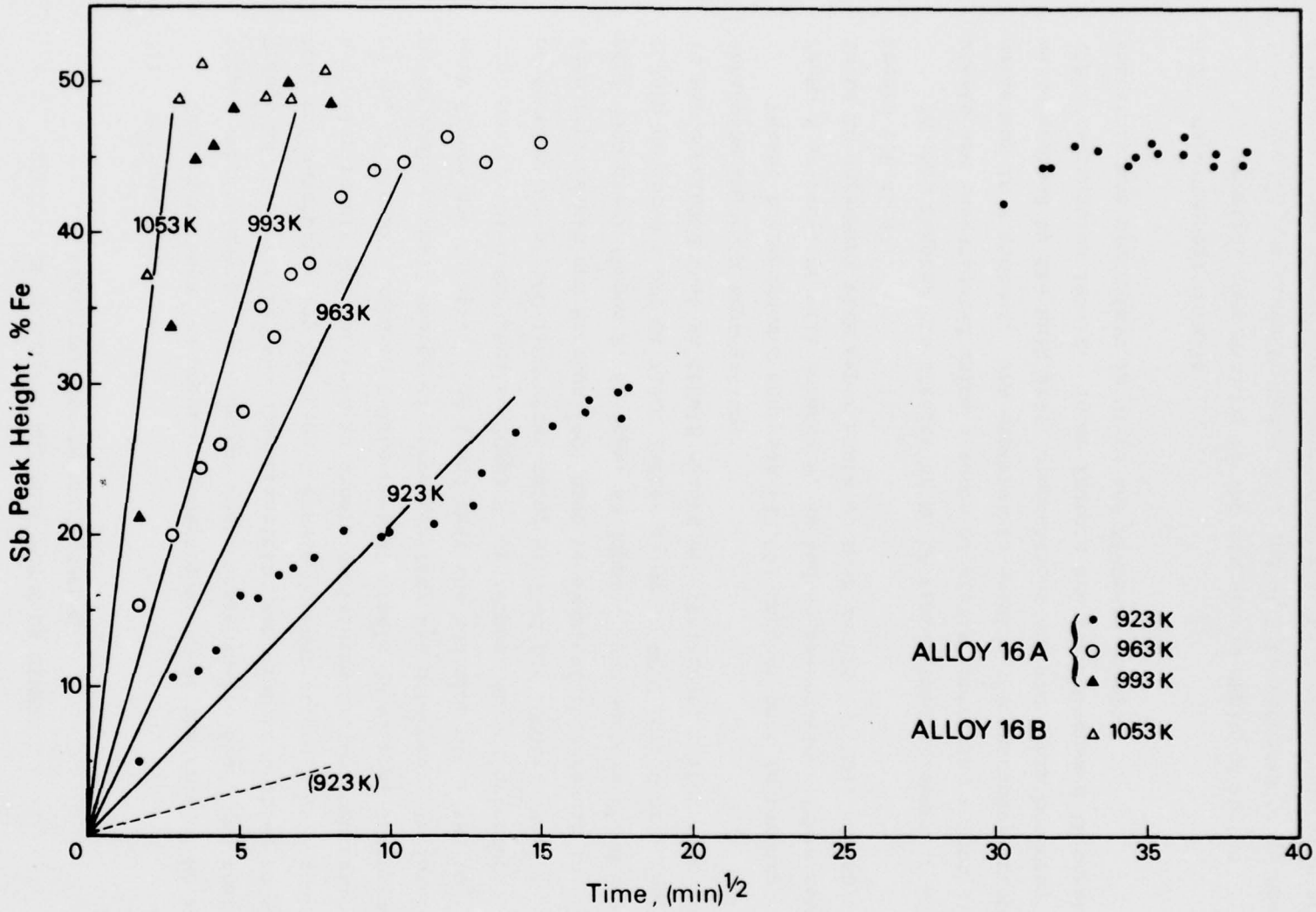

Figure 6.15. Antimony segregation kinetics in the temperature range 923K-1053K. The broken line indicates the calculated Sb increase at 923K with D_{Sb} minimized (Eq.(6.11)).

CHAPTER 7

EFFECTS OF MANGANESE AND PHOSPHORUS ON TEMPER EMBRITTLEMENT IN ALLOY STEELS

7.1. Introduction

There have been few previous investigations of the role of Mn in temper embrittlement. Perhaps the most comprehensive study was that of Preece and Carter {21}, who used transition temperature testing to show that the susceptibility of Fe-Mn-C steels depends strongly on P content. A similar result was obtained in steels containing Cr, or combinations of Mn, Cr and Ni. Even in P-free Fe-Mn-C steels (P <10ppm, Sb<50ppm, Sn<200ppm), a small degree of susceptibility was detected. In later work Steven and Balajiva {23} found that the addition of 0.7%Mn to high-purity 3Ni-0.8Cr steels (20ppm P, Sn<100ppm, Sb not detected) produced a ΔTT of 80C-110C after aging at 450C for 1000hr. More recently, Schulz and McMahon {40} have re-examined this result in AISI 3340 steel (20ppm P, Sb<5ppm, Sn<20ppm). The authors found that 0.7%Mn produced a ΔTT of >150C (after aging at 480C for 300hr), and it was concluded that Mn itself causes embrittlement, rather than just enhancing impurity segregation.

Recent thermodynamic analyses {47,99} suggest that in ternary Fe-Mn-X systems, Mn will enhance P, Sb and Sn segregation. This seems to be in agreement with experiments on Mn-P steels {21,90}, and Mn-Sb steels {36,46,47}.

In this Chapter the effects of Mn on temper embrittlement in Ni-Cr steels are investigated using a range of steels containing a controlled variation in P content. The experiments examine the mechanical properties as determined by the bulk steel compositions and the grain boundary (AES) segregation levels. These factors are then discussed in terms of embrittlement mechanisms in Ni-Cr and Ni-Cr-Mn steels.

7.2. Experimental Details

The chemical compositions of the six steels employed in the investigation are given in Table 7.1, and will be referred to as Steels 5, 5+Mn, etc. The alloys were prepared by melting electrolytic iron and adding high-purity alloying elements. Steels 5 and 5+Mn were of separate origin to the others and special procedures were used to reduce their P

contents to a very low level. The ingots of ∿15kg were forged and hot-rolled to give 13mm diameter bars, from which specimen blanks, 10mm diam x 100mm long, were machined.

The specimen blanks were austenitized at 1100C for 2hr (argon atmosphere), end-quenched into 5% brine, then tempered at 625C in vacuum for 1hr. The blanks were skim-machined, sealed in silica capsules, and aged at 480C for times up to 300hr. Previous experiments with AISI 3340+P steels {39} suggested that this aging treatment would enable P segregation to achieve equilibrium levels. Segmented transition temperature specimens were then machined from the blanks and tested as described in Chapter 2. The load-displacement curves were recorded at a crosshead rate of 2mm min^{-1} and two specimens (ie. 8 tests) were used to determine each transition temperature.

Grain boundary compositions were measured by AES using specimens machined from the transition temperature specimens. About 10 areas of each fracture surface were analysed and the proportions of intergranular fracture were determined by subsequent SEM examination.

7.3. Results

Mechanical Tests

The transition temperatures of the six steels, as a function of aging time, are shown in Figure 7.1. It is clear that both Mn and P have pronounced effects on the susceptibility of the steels. Steel 7+Mn is the most susceptible steel and even at zero aging time appreciable embrittlement is observed. The initial embrittlement kinetics of this material are very rapid (compared with Steel 7), but there is also a slow increase in transition temperature over longer aging times.

From the results in Figure 7.1, the change in transition temperature, ΔTT, produced by aging for 300hr, can be obtained. This parameter is shown in Figures 7.2(a-b), plotted as a function of either bulk P or Mn content. Embrittlement present prior to aging, which must result from a stage in the preceding heat treatment, is not included in these Figures.

The variations in VPN (20kg) hardness with aging time are shown in Figure 7.3. Each result is the mean of five measurements. The results show that hardness differences between the steels and hardness changes with aging time are both small.

Fracture Surface Examination (SEM)

Selected fractures from above and below the energy transition were examined by SEM. In all cases the high energy fracture mode was transgranular microvoid coalescence.

The low energy fractures varied with steel composition and aging time from 100% quasi-cleavage (QC) to 100% intergranular cleavage (IGC). In general, the proportion of IGC increased with transition temperature, and in all Steels, except 5 and 6, aging for times over 5hr produced fractures that were 80-100%IGC. Typical fractures in Steels 5 and 5+Mn are shown in Figures 7.4(a-d); after 300hr aging the fracture mode in Steel 5 was <5%IGC (ie. >95%QC). Representative fractures in Steels 6 and 6+Mn, after short- and long-term aging, are given in Figures 7.5(a-d), and in Figures 7.6(a-d) the fracture modes for Steels 7 and 7+Mn are shown.

The energy level of 4J, chosen to define the transition temperature, corresponded to fracture appearances that were quasi- or intergranular cleavage.

Fracture Surface Analysis (AES)

Specimens from the five most susceptible steels were examined by AES. The AES results, as a function of aging time, are shown in Figures 7.7-7.11. Peak-heights for P and Ni have been weighted for the proportions of intergranular fracture (which are given in Table 7.2, together with the numerical AES data). Apart from Steel 6, all AES specimens showed high proportions of intergranular cleavage (>75%), so that any errors arising from weighting are small.

The main solute elements detected on the fracture surfaces were P, Ni Cr and C. In addition, the usual O and small S peaks were present; no other impurity elements were observed. A detailed examination showed that Mn was also present on the fracture surfaces of the Ni-Cr-Mn steels, but the peaks were very small and approached the limit of detection by AES. It seems that in these steels the Mn-540eV peak may be obscured by the larger Cr-530eV and Fe-550eV peaks (previously reported AES studies of Mn segregation in temper embrittlement have used Cr-free 2%Mn steels [36,90]). A typical spectrum for Steel 7+Mn is shown in Figure 7.12.

Figures 7.7-7.11 show that the P segregation levels increase with bulk content in a similar manner to that described in Chapter 5 for AISI

3340 steel. It seems that Mn does not greatly influence the P levels and this is rather surprising in view of the mechanical test results (Figure 7.1). The main features of this effect are summarized in Figure 7.13, which shows the transition temperatures of the Ni-Cr and Ni-Cr-Mn steels (in material aged for 300hr), as a function of P monolayer coverage. At constant P coverage, the transition temperatures of the Ni-Cr-Mn steels are ∿125C higher than those of the Ni-Cr steels (for P coverages of 0.1-0.3 monolayers).

Segregation profiles were determined by alternate ion sputtering and AES analysis of the fracture surfaces. The profiles showed that in both the Ni-Cr and Ni-Cr-Mn steels, the majority of the P was contained within the first 1-2 atom layers, and hence that P was present as a solute segregant. As observed in the steels in Chapter 5, Ni showed a more gradual segregation profile, and no measurable Cr segregation was found. A segregation profile in Steel 7+Mn, for an aging treatment of 20hr at 480C, is given in Figure 7.14. The peak-heights are not weighted, but the fracture is 98% intergranular cleavage (Table 7.2).

7.4. Discussion and Conclusions

The main points from the mechanical tests (Figures 7.1 and 7.2) are:

i) At constant bulk P content, Ni-Cr-0.6%Mn steels are considerably more susceptible to temper embrittlement than Mn-free Ni-Cr steels. It is also noticeable that the effect of Mn on susceptibility seems to increase with P content (or alternatively, with transition temperature).

ii) Mn accelerates the temper embrittlement kinetics. This is shown most clearly in Steels 7 and 7+Mn where, during the first 5hr at 480C, the transition temperatures increased by 16C and 107C, respectively.

iii) The more susceptible steels embrittle significantly during tempering (625C/1hr). This is apparent from the zero-time transition temperatures in Figure 7.1.

The AES results (Table 7.2) show that, within experimental error, Mn does not measurably enhance the P segregation levels. A comparison of the segregation levels in Steels 7 and 7+Mn (eg. Figure 7.13) indicates that the mean P level is slightly higher in Steel 7+Mn, but this value is still well within the standard deviation of the results for Steel 7. These results show that the effect of Mn cannot be explained in terms of

increased P segregation, and it is therefore necessary to consider the alternative ways in which Mn might affect susceptibility to temper embrittlement.

Other studies of P and Sb segregation in Ni-Cr steels {34,39,114} suggest that the primary factors controlling the degree of intergranular embrittlement (as measured by a transition temperature test) are:

i) The matrix hardness or yield stress
ii) The prior austenite grain size
iii) The grain boundary composition

The experimental evidence suggests that Mn does not significantly affect the first or second factors above. Although Mn is a moderate solid-solution hardening element in pure Fe {121}, Figure 7.3 shows that in alloy steels, where strong hardening elements are present (ie. Cr and C), small additions of Mn make little contribution to the hardness. From studies of hardness effects in Ni-Cr-P steels {39} it is apparent that any hardness differences in the present steels are too small to satisfactorily explain the observations. The SEM fractographs in Figures 7.4-7.6 show that the embrittled steels have very similar prior austenite grain sizes (this was supported by examining lower magnification fractographs). Thus the effect of Mn cannot be attributed to a change in austenite grain size (ie. to a general increase in austenite grain size). On this basis it seems reasonable to propose that the main effect of Mn is to alter the chemical composition of the grain boundary.

Evidence supporting this hypothesis can be obtained by examining some of the individual results. Steels 5+Mn and 6 provide a suitable comparison between the Mn-bearing and Mn-free steels; the AES and mechanical test results are:

Steel	P coverage (m/l)	TT(C)	Hardness (VPN)
5+Mn (aged 300hr)	0.032 $\pm$ 0.007	-55 $\pm$ 10	268 $\pm$ 3
6 (aged 300hr)	0.15 $\pm$ 0.03	-85 $\pm$ 10	287 $\pm$ 3

Steel 5+Mn has a lower hardness and a much lower P coverage, but a higher transition temperature. The fracture modes for the two steels, at temperatures just below the energy transition, are given in Figures 7.4(d) (Steel 5+Mn) and 7.5(b) (Steel 6). It is clear that the higher transition

temperature of Steel 5+Mn is associated with a greater tendency for fracture to occur by intergranular cleavage. This loss in intergranular cohesion implies that the chemical composition of the grain boundary is changed by the presence of Mn in the steel. As shown in Figure 7.13, the effects observed in these two steels are typical of the general differences in behaviour between the Ni-Cr and Ni-Cr-Mn steels.

The AES results indicate that there are no extraneous elements on the grain boundaries of the Ni-Cr-Mn steels. Since the common impurity elements (Sb, Sn, N, etc.) are expected to be more readily detected than Mn (as discussed previously), the inferior properties of the Ni-Cr-Mn steels can only be ascribed to low levels of Mn segregation.

The suggested interpretation of the mechanical test results is that Mn segregates within the temper embrittlement range and is inherently embrittling. The ability of Mn to segregate in temper embrittled steels has been shown in other experimental work {36,37,90}, and it has been suggested that in unalloyed Fe, Mn will have a free energy of segregation of about $-5.2 kJ\ mol^{-1}$ {46,47}. As discussed previously (in Chapter 3), alloying elements such as Cr will tend to increase, rather than decrease, Mn segregation in Fe. The inherent embrittling effect of Mn is in agreement with previous studies of high-purity Ni-Cr-Mn {23,40} and Mn {21} steels.

The Guttmann theory for ternary Fe-Mn-X systems suggests that Mn will interact attractively with impurities such as P, Sb and Sn; this has been shown to be true for Mn-Sb steels {46,47}. The absence of a strong Mn-P interaction in the Ni-Cr-Mn-P steels cannot be interpreted in detail because at present there is no equivalent theory for more complex systems. The Cr-P, Mn-P and Fe-P interactions are all expected to be strong {47,99}, and the relatively low bulk concentration of Mn could possibly explain the lack of an appreciable effect of Mn on P segregation.

Finally, it should be mentioned that the P segregation levels determined by Mulford {39}, for 3.5Ni-1.7Cr steels (Chapter 5, Figure 5.13), appear to be higher than those observed in the 2.5Ni-1.4Cr steels. The approximate value of ΔG_P obtained from the present investigation is $-45.5 kJ\ mol^{-1}$ (compared with $\sim -52 kJ\ mol^{-1}$ for the results in Figure 5.13). Alloy content (Ni and Cr) seems to be responsible for the difference in ΔG_P, but confirmation of this effect is required.

Conclusions

The main conclusions are:

i) The susceptibility of Ni-Cr steels to temper embrittlement increases with both P and Mn bulk content. After tempering for 1hr at 625C, Mn-free steel containing 200ppm P shows a rise in transition temperature of ∿100C during aging at 480C. A similar steel containing 0.6%Mn and 200ppm P shows a rise in transition temperature of >200C.

ii) Observations of the effect of Mn on the transition temperatures and fracture modes indicate that the embrittlement induced by Mn is primarily due to a change in the grain boundary composition.

iii) AES studies of Ni-Cr and Ni-Cr-0.6%Mn steels show that Mn does not measurably enhance P segregation in Ni-Cr steels (for P contents up to 200ppm). Apart from low levels of Mn segregation, just above the AES detection limit, the grain boundary compositions appear to be similar in both types of steel.

iv) The inferior mechanical properties of the Ni-Cr-0.6%Mn steels are attributed to Mn segregation and it is suggested that Mn should be considered an embrittling element in Ni-Cr steels.

Steel	C	Ni	Cr	Mn	P	S
5	0.30	2.50	1.37	0.01	0.001	0.003
5+Mn	(0.30)	(2.50)	(1.37)	0.57	(0.001)	(0.003)
6	0.35	2.61	1.47	0.005	0.007	n.d.*
6+Mn	0.30	2.54	1.39	0.58	0.007	n.d.
7	0.28	2.54	1.41	0.005	0.021	n.d.
7+Mn	0.25	2.49	1.36	0.58	0.020	n.d.

* not determined

Table 7.1. Chemical compositions (wt%) of the steels used to study Mn and P effects in temper embrittlement (expected values are shown in parentheses). The residual impurities in Steel 5 are given in Table 3.2.

Aged	%IG	P-120eV	C-270eV	Cr-489eV	Ni-848eV
Steel 5+Mn					
100hr	95	2.41±0.5(11)	11.55±4.1(11)	3.55±0.3(11)	5.15±0.5(11)
300hr	95	2.87±0.7(12)	13.46±1.5(12)	3.88±0.5(12)	5.22±0.6(12)
Steel 6					
5hr	<2	0.67±0.2(6)	6.17±1.9(6)	2.05±0.6(6)	3.03±0.3(6)
20hr	30	7.68±3.8(7)	6.89±2.1(7)	2.27±0.3(6)	5.55±0.9(7)
300hr	68	13.22±3.1(9)	14.89±2.3(9)	3.52±0.4(9)	5.28±0.3(9)
Steel 6+Mn					
5hr	88	4.30±0.9(12)	11.58±1.4(10)	5.33±0.9(12)	5.06±0.3(12)
20hr	93	8.29±1.3(12)	12.21±1.8(12)	3.40±0.4(11)	4.98±1.7(12)
100hr	95	10.13±1.4(11)	11.4±1.2(11)	3.80±0.5(10)	5.88±0.4(11)
300hr	94	11.35±2.0(12)	8.75±1.5(12)	3.62±1.2(11)	6.00±0.7(12)
Steel 7					
20hr	82	17.96±6.0(11)	8.36±2.6(11)	2.97±0.4(11)	5.03±0.8(11)
100hr	96	22.11±5.4(11)	8.65±1.3(11)	3.91±0.4(10)	5.31±0.4(11)
300hr	95	25.18±4.1(12)	8.86±1.1(12)	4.13±0.2(11)	5.65±0.5(12)
Steel 7+Mn					
0hr	76	8.37±1.9(10)	10.39±2.1(9)	3.16±0.5(10)	4.43±0.7(10)
5hr	97	17.19±1.3(9)	8.61±1.2(9)	3.26±0.3(9)	5.31±0.3(9)
20hr	98	25.51±2.8(11)	9.45±1.0(11)	3.39±0.3(11)	6.14±0.2(11)
100hr	96	30.79±4.1(9)	10.67±1.7(9)	4.00±0.3(9)	6.77±0.4(9)
300hr	97	27.06±6.8(12)	10.50±2.8(12)	4.50±1.0(11)	7.05±1.0(12)

Table 7.2. AES results for the Mn-P Steels. Peak-heights for P and Ni have been weighted (except for Steel 6, aged 5hr).

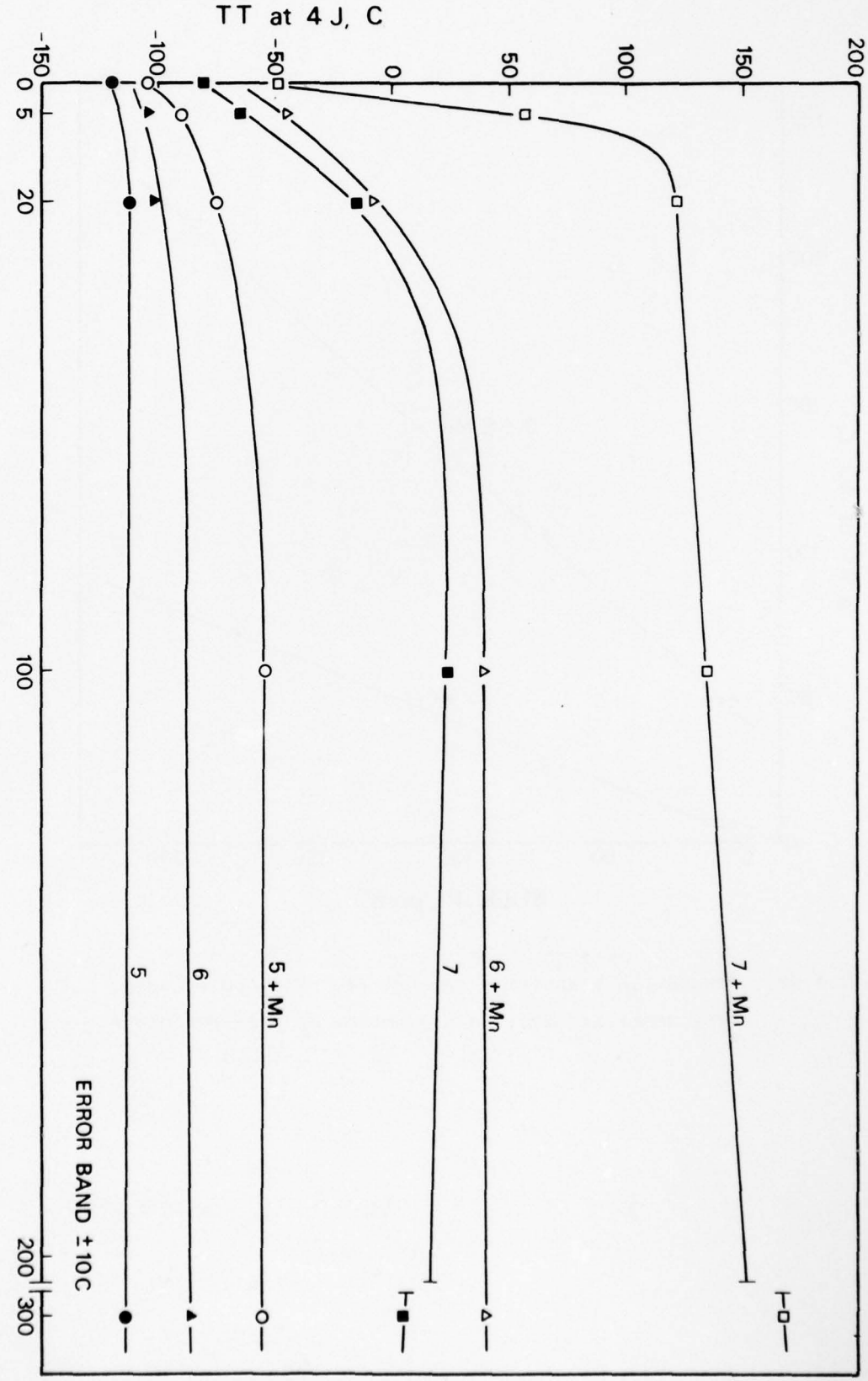

Figure 7.1. Variation in transition temperature with aging time at 480C.

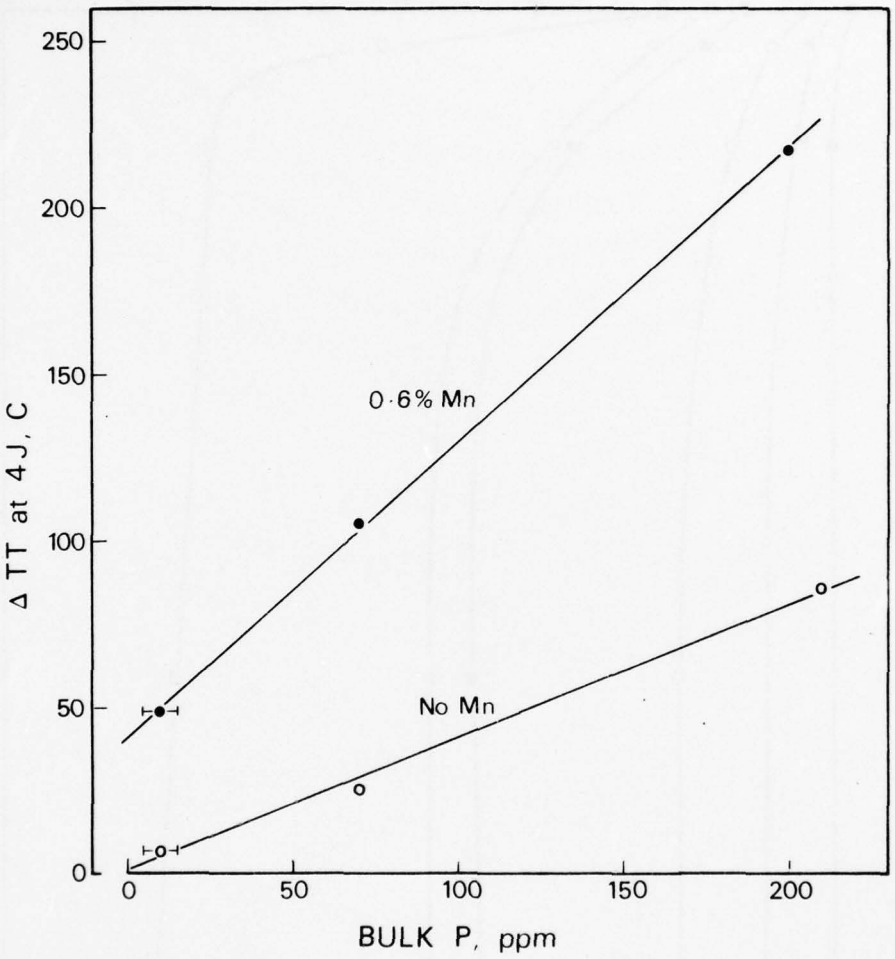

Figure 7.2(a). Change in transition temperature produced by aging for 300hr at 480C, as a function of bulk P content.

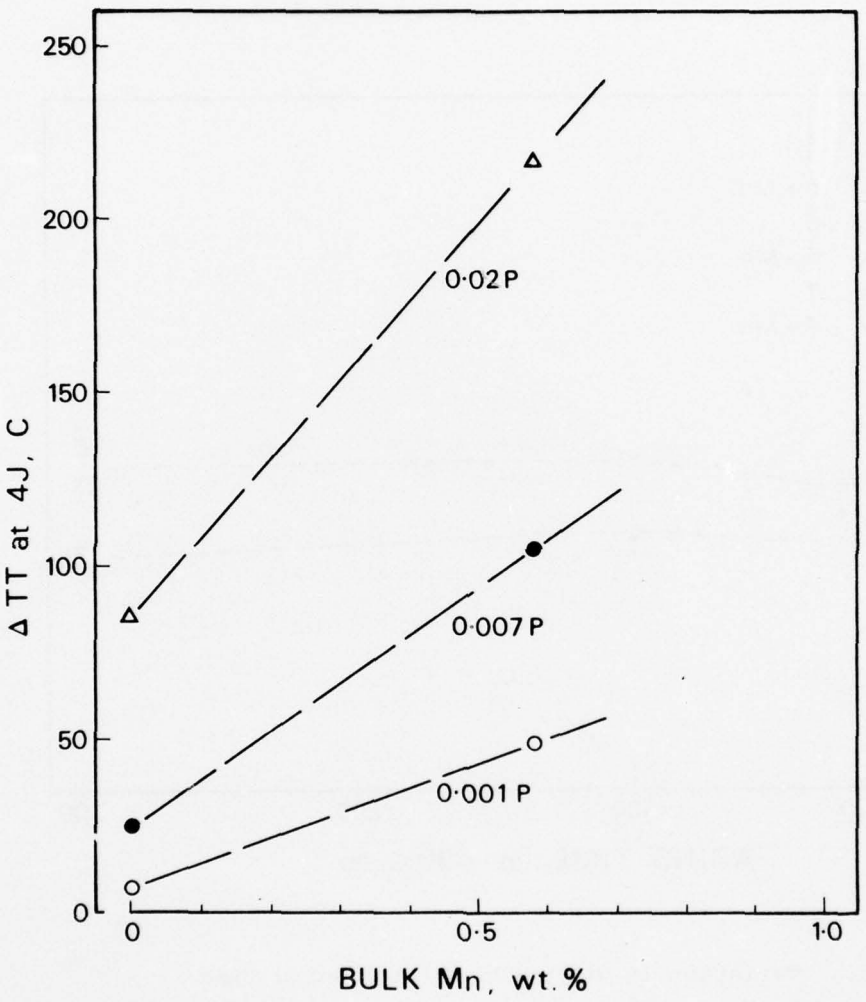

Figure 7.2(b). Change in transition temperature produced by aging for 300hr at 480C, as a function of bulk Mn content.

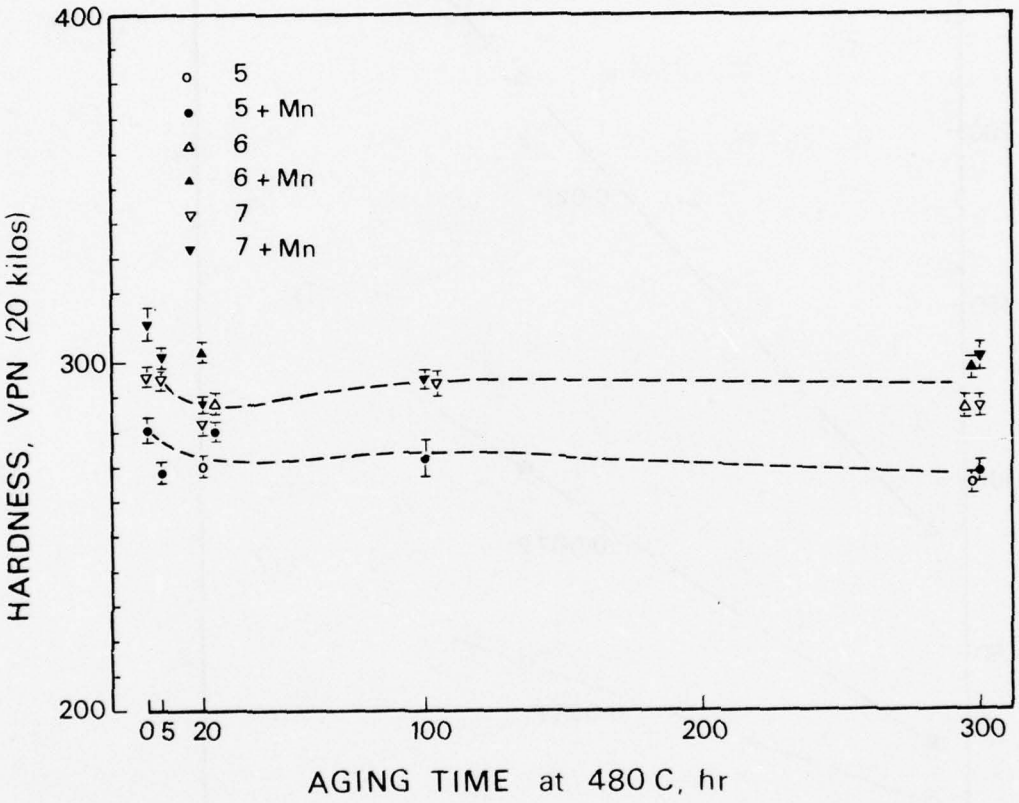

Figure 7.3. Variation in VPN hardness with aging time.

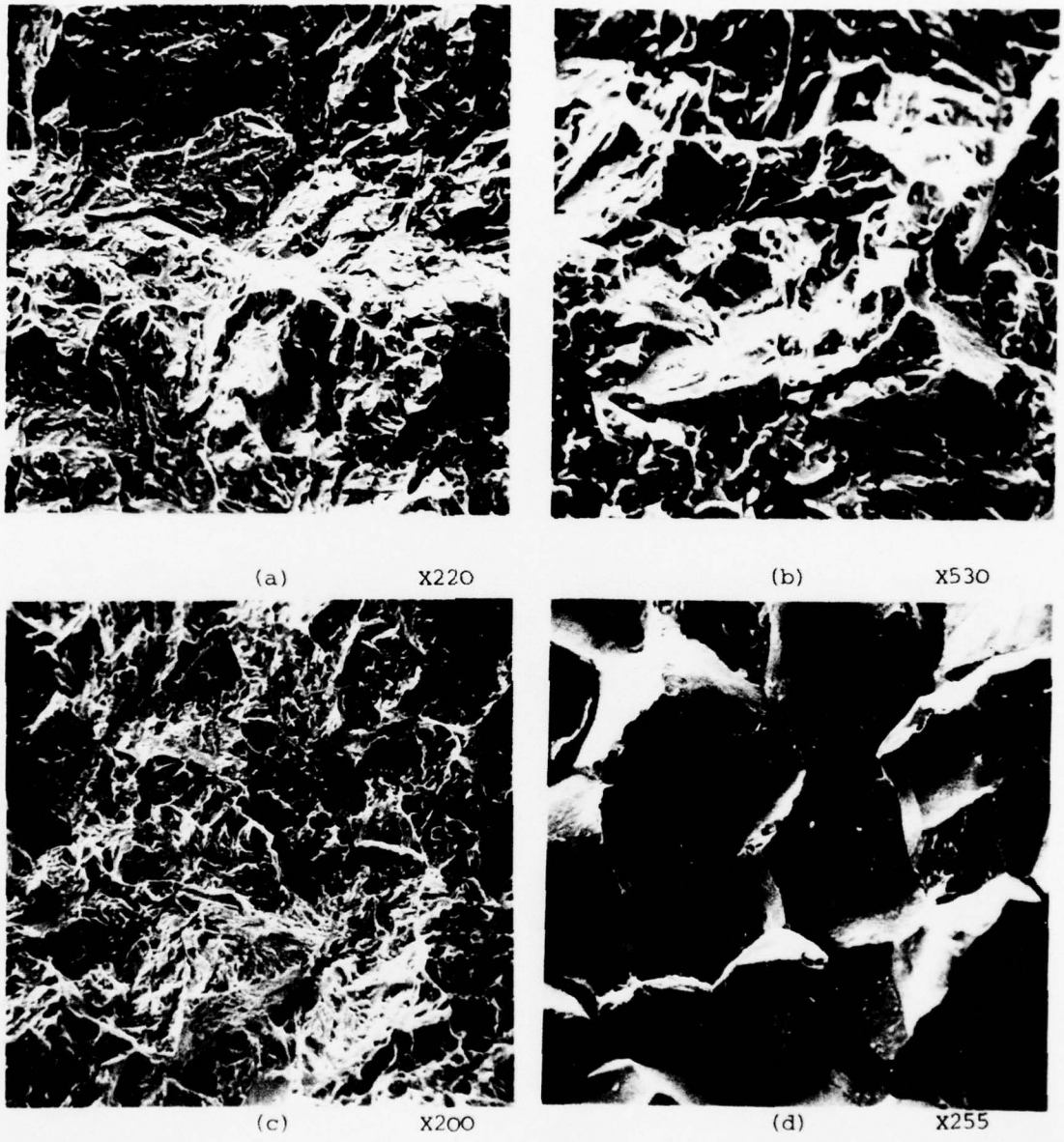

Figure 7.4. Brittle fracture modes in Steels 5 and 5+Mn; (a) Steel 5 before aging, tested at -130C; (b) Steel 5 aged 300hr, tested at -134C; (c) Steel 5+Mn before aging, tested at -117C; (d) Steel 5+Mn aged 300hr, tested at -59C.

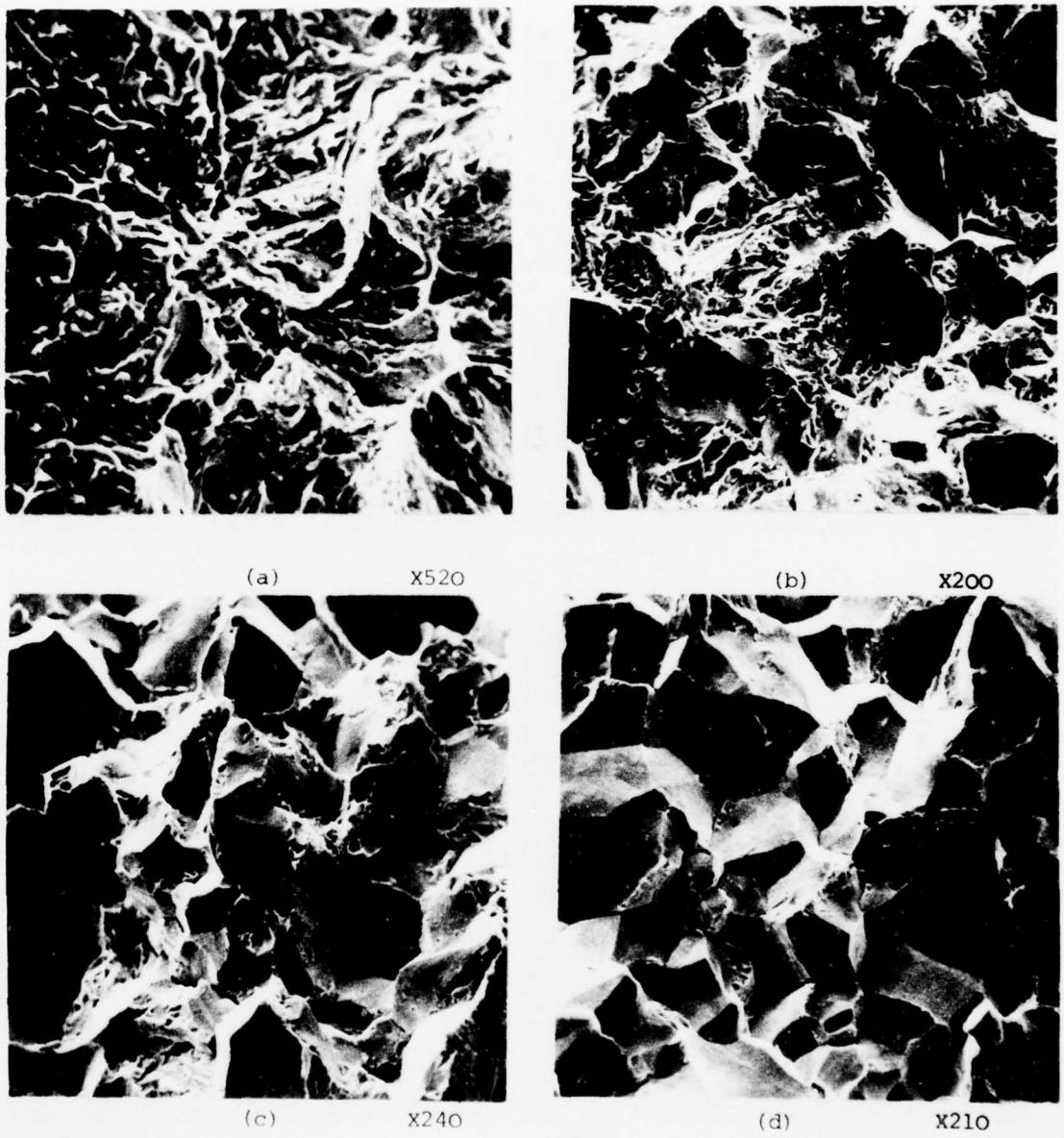

Figure 7.5. Brittle fracture modes in Steels 6 and 6+Mn; (a) Steel 6 aged 5hr, tested at -120C; (b) Steel 6 aged 300hr, tested at -95C; (c) Steel 6+Mn aged 5hr, tested at -58C; (d) Steel 6+Mn aged 100hr, tested at 17C.

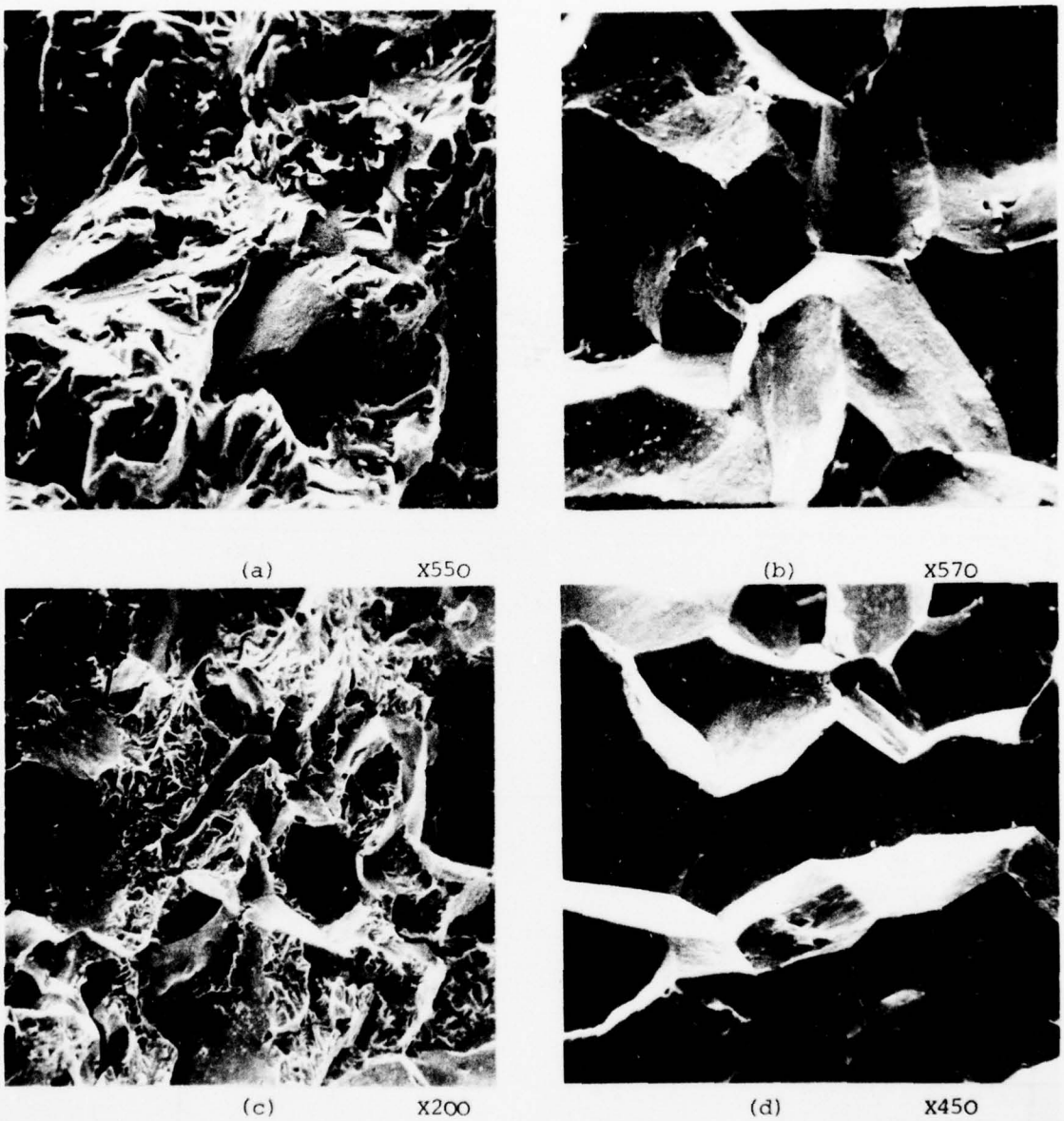

Figure 7.6. Brittle fracture modes in Steels 7 and 7+Mn; (a) Steel 7 before aging, tested at -108C; (b) Steel 7 aged 100hr, tested at -57C; (c) Steel 7+Mn before aging, tested at -89C; (d) Steel 7+Mn aged 300hr, tested at 133C.

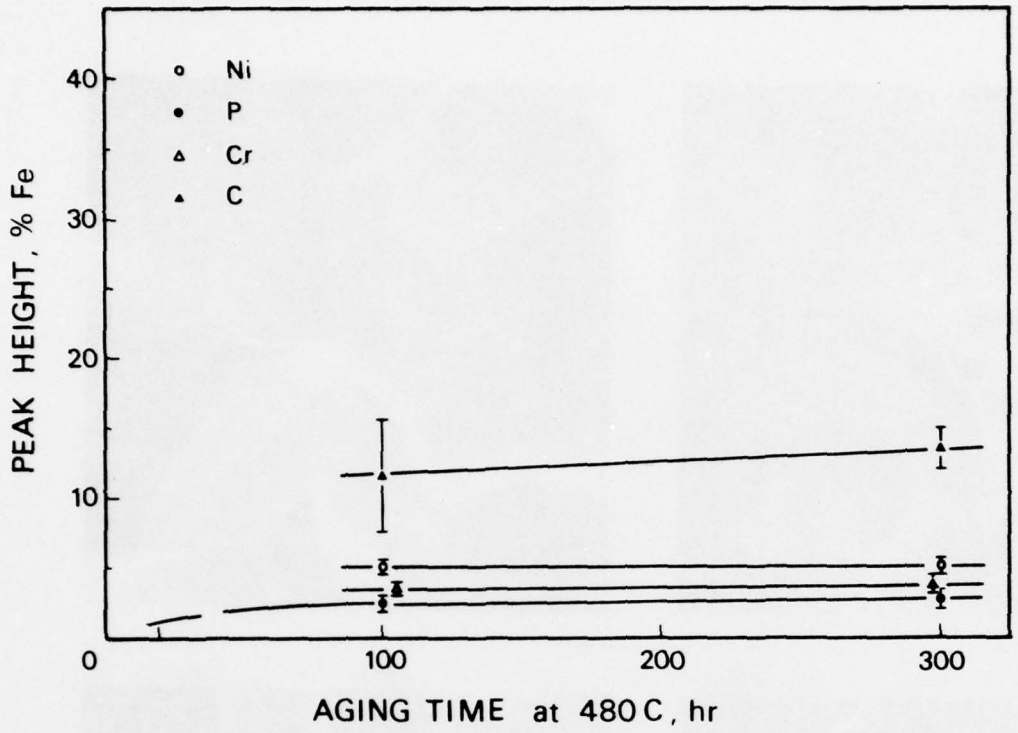

Figure 7.7. Auger peak-heights for Steel 5+Mn.

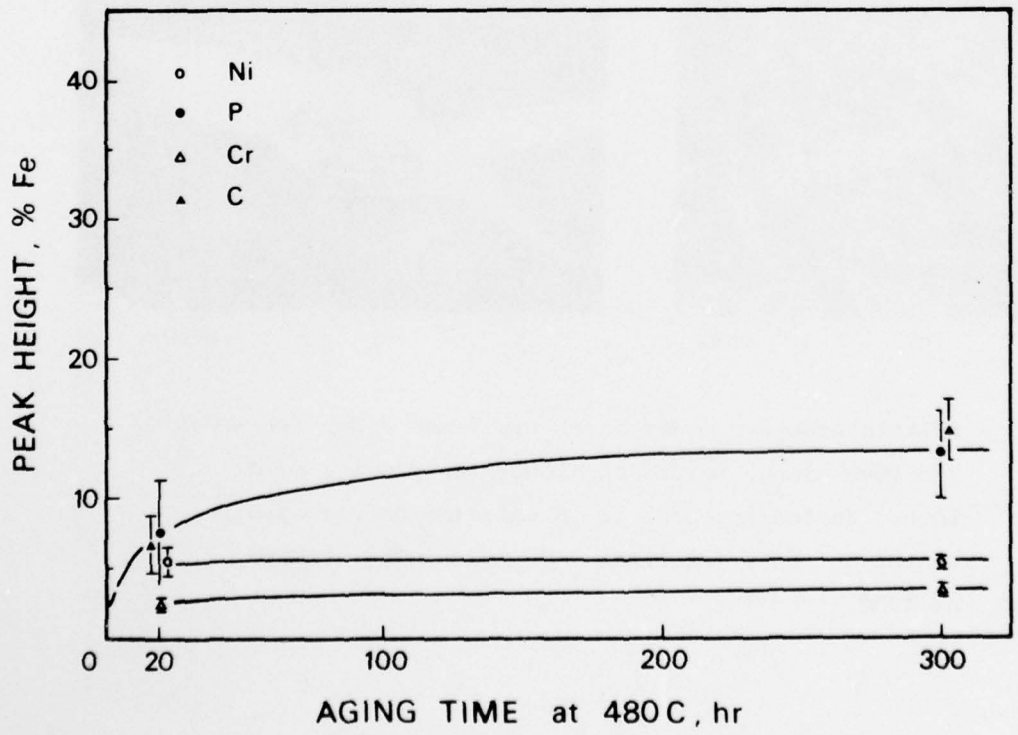

Figure 7.8. Auger peak-heights for Steel 6.

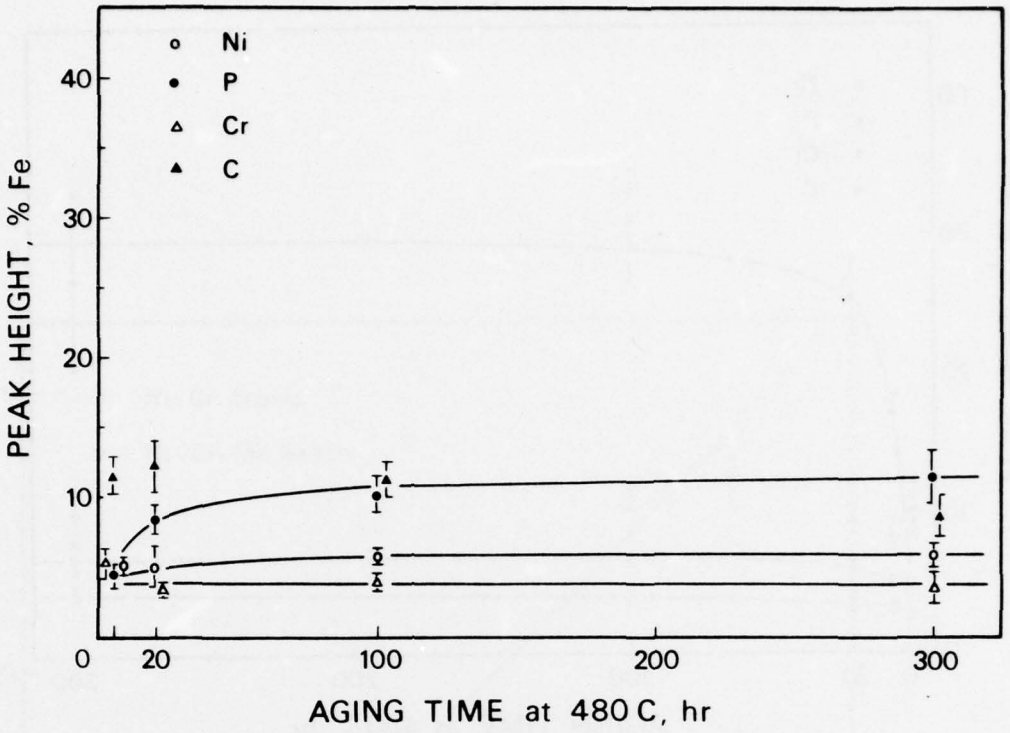

Figure 7.9. Auger peak-heights for Steel 6+Mn.

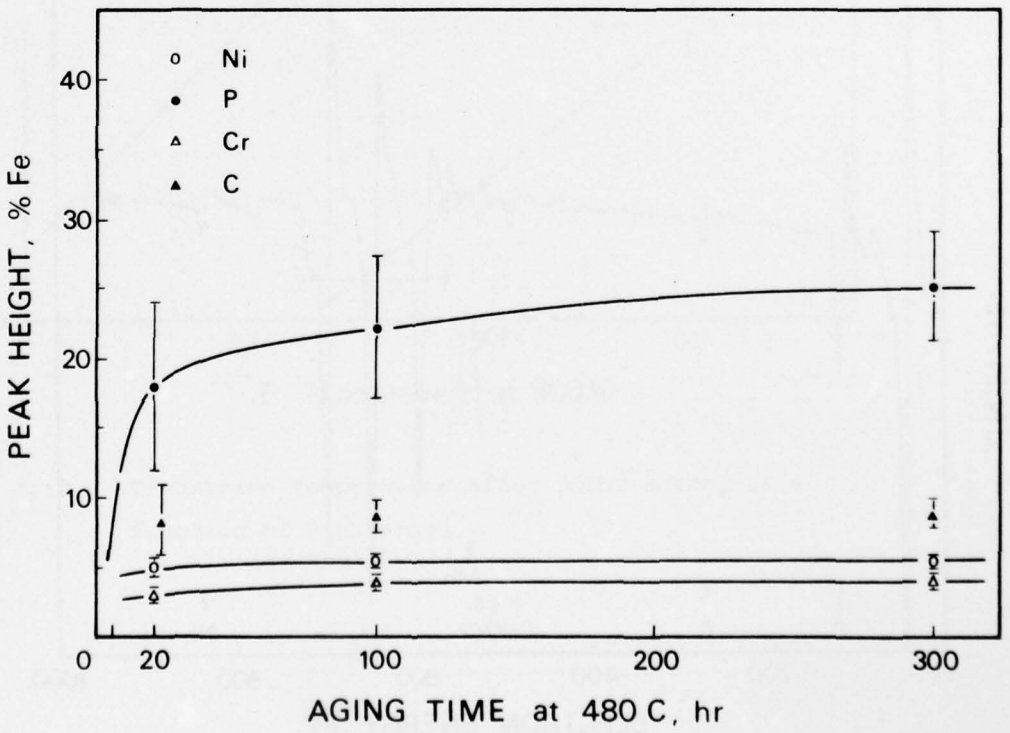

Figure 7.10. Auger peak-heights for Steel 7.

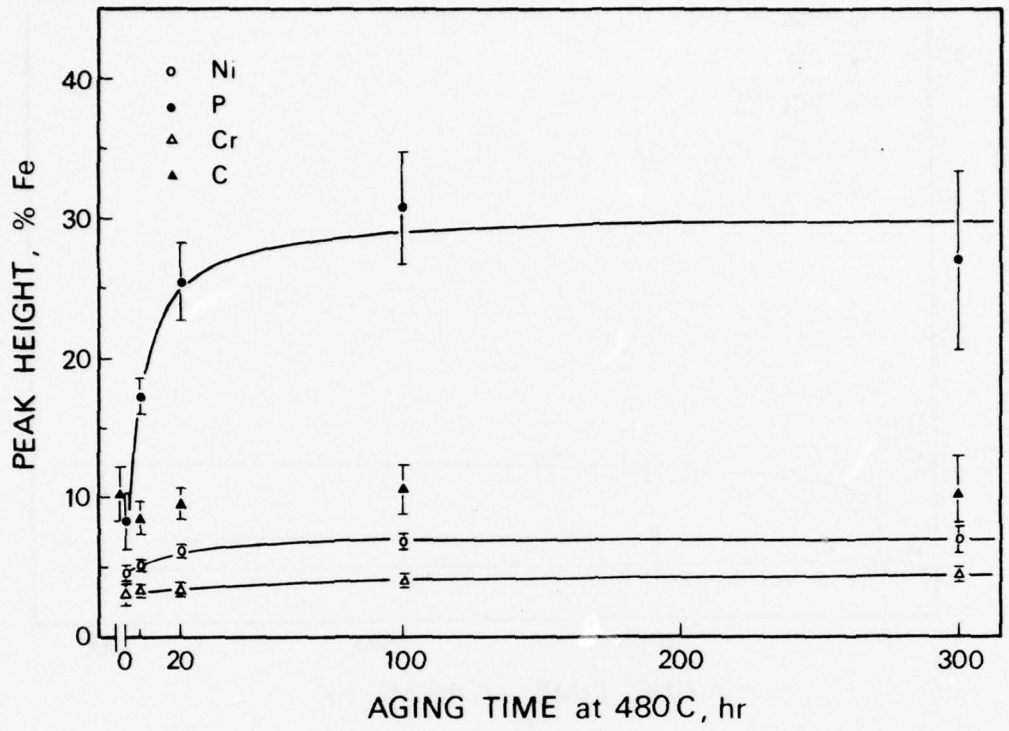

Figure 7.11. Auger peak-heights for Steel 7+Mn.

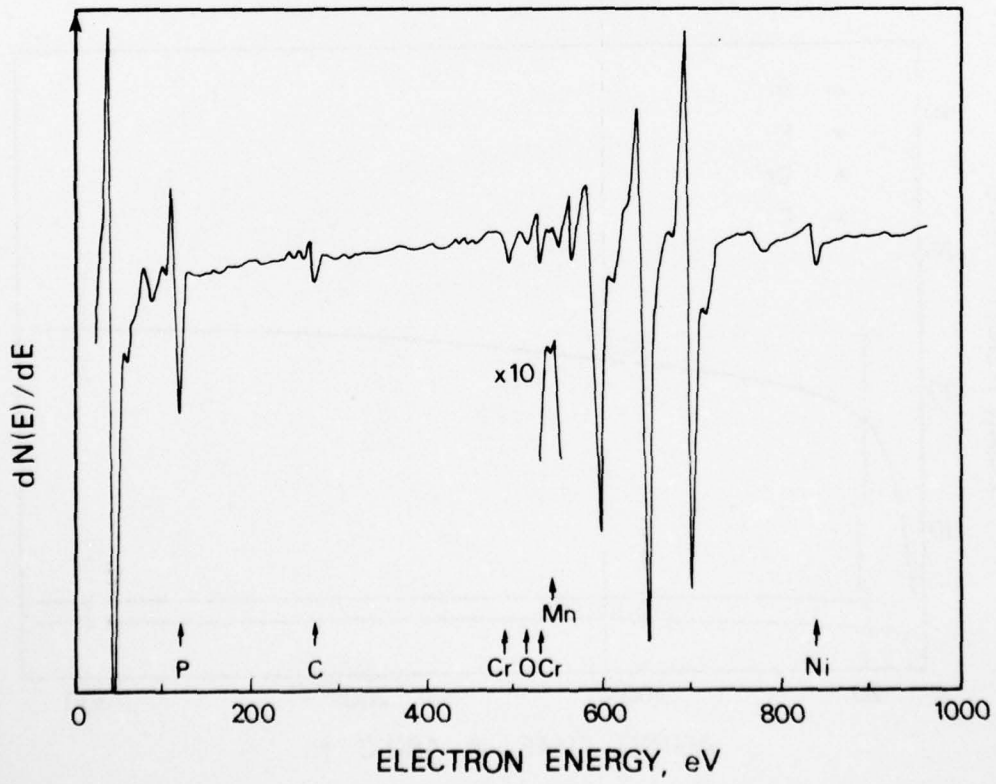

Figure 7.12. Example of Auger spectrum from Steel 7+Mn (specimen aged for 300hr).

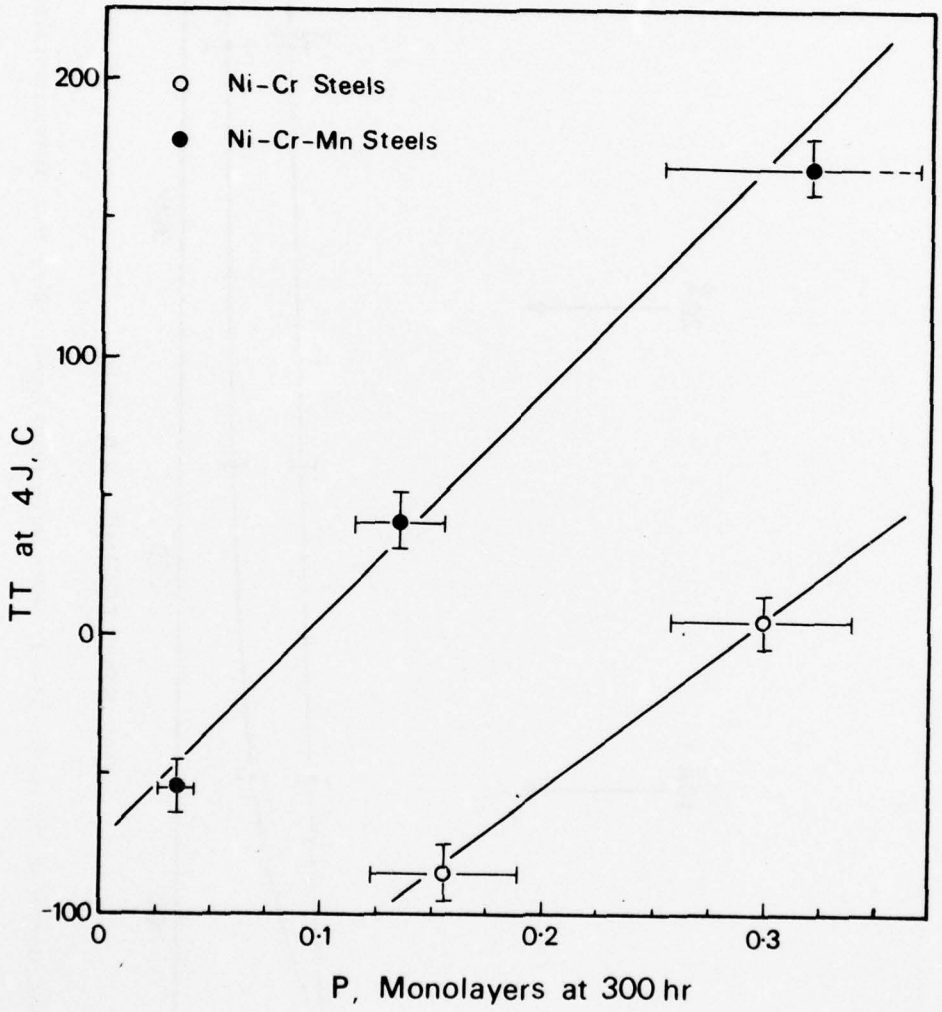

Figure 7.13. Transition temperature after 300hr aging, as a function of P coverage.

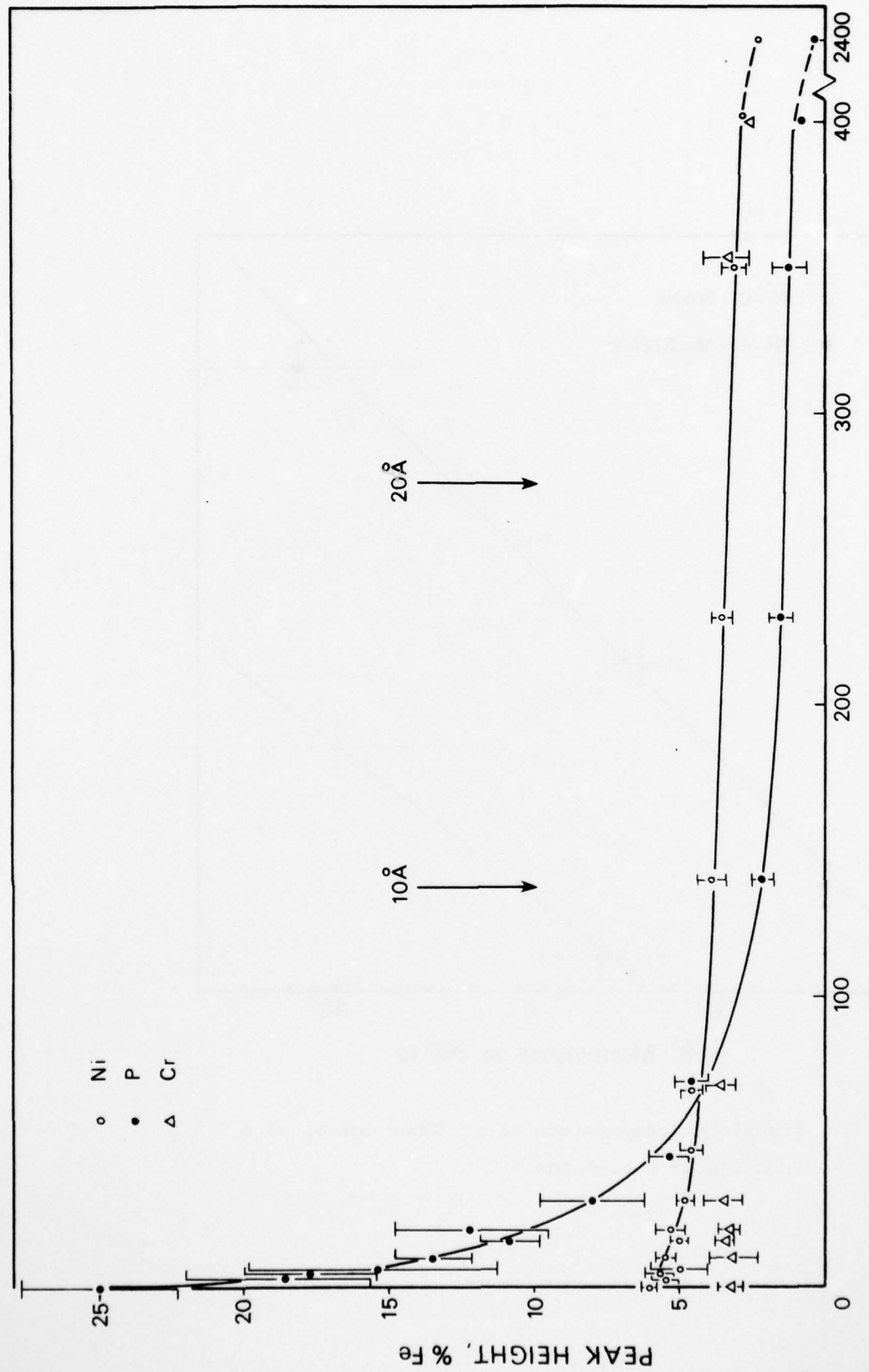

Figure 7.14. Segregant depth profile in Steel 7+Mn (specimen aged 20hr, 98% intergranular cleavage).

CHAPTER 8

CONCLUDING REMARKS AND RECOMMENDATIONS FOR FURTHER RESEARCH

It is now established that the austenitizing cycle can result in P segregation at austenite grain boundaries in Ni-Cr and Ni-Cr-Mn steels. For typical austenitizing treatments, the P enrichment ratio measured in steels of high bulk P content is in the range 100-200; this indicates that the grain boundary P coverage will be ~0.02-0.04 monolayers in a commercial steel containing 100ppm P. Bearing in mind that steels of high yield stress are particularly susceptible to embrittlement, this low P coverage is possibly sufficient to explain intergranular quench cracking, observed in steels of medium and high carbon content (as discussed in Section 1.3, quench cracking is largely confined to higher carbon contents, where crack nuclei are expected to be present in the microstructure). This coverage approaches the detection limit for surface analysis and it seems that P segregation in austenite cannot be reliably studied using commercial bulk concentrations (eg. 100ppm). Important areas for future research are, (i) the influence of cooling rate on P segregation levels, (ii) confirmation of the effect of Mn on the temperature dependence of P segregation, and (iii) the role of N in austenitic segregation.

In commercial purity Ni-Cr steels, light tempering at 350C produces an increase in transition temperature and an increased tendency for intergranular cleavage fractures. However AES analyses confirm that there is no strong impurity segregation associated with 350C embrittlement. There are two factors to be considered; first, the high yield stress imparts a high degree of susceptibility, so that low segregation levels have an appreciable embrittling effect; second, the embrittlement mechanism (the precipitation of Fe_3C platelets) either produces low segregation levels (carbide rejection), or facilitates fracture along previously segregated boundaries (austenitic segregation). If it is assumed that S and N are eliminated from solid solution (as MnS, and AlN or SiN), then P seems to be the main impurity responsible. The experimental evidence supports the view that P is involved; AES analyses of commercial steels show P on the grain boundaries and experiments with high-purity steels show that P additions produce

intergranular fractures after tempering at 350C. Unfortunately the low coverages do not enable the effects of austenitic segregation to be confidently separated from those of carbide rejection. However, since the P enrichment ratio in austenite is ∿150 , any carbide rejection must be assisted by austenitic segregation and it seems probable that both processes contribute to 350C embrittlement. There is some evidence that plain carbon steels are less susceptible to 350C embrittlement {122}, and a study of the effects of alloy content may prove to be worthwhile.

Overheating is characterised by ductile intergranular facets which result from a grain boundary MnS precipitate. In susceptible steels the principal factors controlling overheating are the austenitizing temperature and the subsequent cooling rate. It seems that commercial cooling rates will generally be too slow to prevent appreciable grain boundary precipitation, but variations in cooling rate may still affect the occurrence of overheating, mainly by altering the precipitate morphology. In materials subjected to high austeniti ing treatments, sulphide modification by elements such as cerium appears to be a satisfactory method of eliminating overheating {123}. An additional benefit of sulphide modification is that treated steels generally show improved directional properties {124}.

The present investigation has concentrated largely on temper embrittlement and although the general understanding of the problem has been assisted by the Guttmann analysis there are still many unanswered questions. The segregation of Sb and P in Ni-Cr steels can now be qualitatively explained and certain patterns are emerging which distinguish metalloid impurities from nonmetallic impurities. Examples of this behaviour are shown below for four of the main impurities:

Impurity	P	S	Sb	Sn
Type	Nonmetals		Metalloids	
Segregation in Fe	McLean (1m/1 or less)		BET (multilayer)	
Atom size (Fe units)	1.05	1.17	1.37	1.32
Chemical interaction with Fe	S	S	W	W
Effect of alloying elements on segregation	W	W	S	S

S-strong, W-weak

Two common impurities not included are As and N, however As is not strongly embrittling {27} and very little is known about As segregation. Nitrogen appears to differ from P and S in that it has only a weak interaction with Fe and thus alloying elements may have a strong effect on N segregation {99}.

This investigation has not determined the effects of austenite grain size in relation to temper embrittlement, but it can be shown by an elementary calculation that the total segregated solute is negligible compared with that retained in the bulk. Thus typical grain size variations should not affect the solute coverage (by bulk depletion). It seems that the influence of grain size on mechanical properties arises from changes in the mechanics of fracture, but this is clearly an effect which warrants investigation.

Other suggestions for further research are:

(i) A study of the mechanism by which impurity elements reduce interfacial cohesion; the physical nature of this effect is not understood.

(ii) A determination of the atomic arrangement of impurities and alloying elements segregated at interfaces and free surfaces. This could possibly be accomplished by LEED and ESCA studies which provide information on the crystal structure and chemical bonding at surfaces.

(iii) Determinations of thermodynamic segregation data are required for binary and ternary systems such as Fe-Sb, Fe-P, Fe-Sb-P, etc. This would greatly assist in the interpretation of segregation effects in more complex systems such as commercial steels.

(iv) Studies of the effects of Mo, Mn and N are required; for example, a study of the effect of Mn in Fe-C-Mn and Fe-C-Ni-Mn alloys should clarify the role of Mn in temper embrittlement. The effects of Mo and Mn on P segregation should be determined in basic Fe-C alloys.

(v) Finally, progress achieved in elementary studies using transition temperature measurement should be extended into practical fields. This will involve K_{IC} and/or COD testing over a range of temperatures.

AD-A048 448 CAMBRIDGE UNIV (ENGLAND) DEPT OF METALLURGY AND MAT--ETC F/G 11/6
SEGREGATION EFFECTS AND THE TOUGHNESS OF HIGH-STRENGTH STEELS.(U)
JUN 77 J Q CLAYTON, J F KNOTT DAJA37-74-C-1309

UNCLASSIFIED NL

3 OF 3
ADA048448

END
DATE FILMED
2-78
DDC

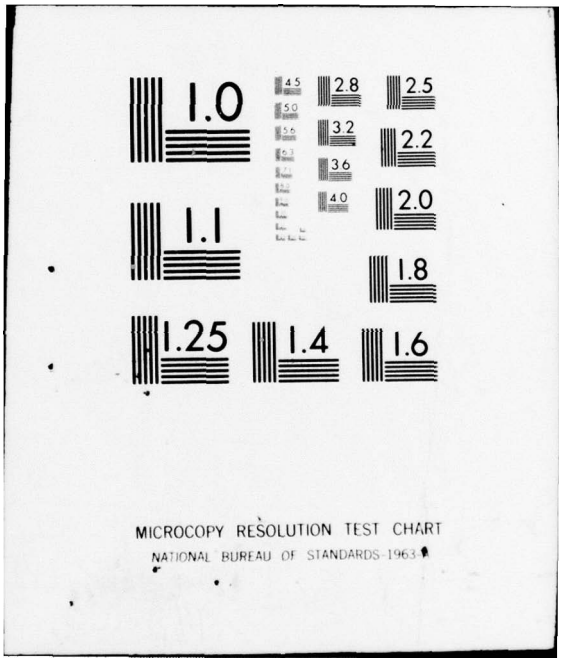
1.0
1.1
1.25
1.4
1.6
1.8
2.0
2.2
2.5
2.8
3.2
3.6
4.0
4.5
5.0
5.6
6.3
MICROCOPY RESOLUTION TEST CHART
NATIONAL BUREAU OF STANDARDS-1963-A

ACKNOWLEDGEMENTS

The authors are indebted to; Professor C.J. McMahon, Jr., (University of Pennsylvania) for valuable discussions and for making Auger facilities available; Dr. H.C. Feng (University of Pennsylvania) and Dr. G.T. Burstein for experimental assistance with the Auger spectroscopy and also for contributing by way of discussion; the Department technicians for their help with apparatus and machining, and particularly Mr. J. Leader for the preparation of laboratory melts.

Appreciation is also extended to Professor R.W.K. Honeycombe for the provision of laboratory facilities, and Dr. D. Elliott (BISRA), Dr. I. Milne (CERL) and Mr. H. Suzuki (Nippon Steel Corp., Japan), for kindly supplying many of the materials used in this work.

REFERENCES

{1} R.O. Ritchie and J.F. Knott : Acta Met., 1973, 21, p.639.

{2} R.O. Ritchie and J.F. Knott : Mater. Sci. Eng., 1974, 14, p.7.

{3} R.O. Ritchie and J.F. Knott : Met. Trans., 1974, 5, p.782.

{4} C.J. McMahon, K. Yoshino and H.C. Feng : Intnl. Conf. on Stress Corrosion Cracking and Hydrogen Embrittlement in Steels, Unieux-Firminy, June, 1973.

{5} K. Yoshino and C.J. McMahon : Met. Trans., 1974, 5, p.363.

{6} R.P. Harrison, D. de G. Jones and D.V. Thornton : Conf. on Mechanics and Mechanisms of Crack Growth, Cambridge 1973.

{7} R. Bruscato : Welding J. Res. Suppl., 1970, 49, p.148S.

{8} H.R. Tipler : Intnl. Conf. on Props. of Heat Resistant Steels, Dusseldorf, May, 1972.

{9} H. Jolivet and G. Vidal : Rev. Met., 1944, 41, p.387.

{10} J.H. Hollomon : Trans. ASM, 1946, 36, p.473.

{11} R.H. Greaves and J.A. Jones : JISI, 1925, 111, p.231.

{12} R.H. Greaves and J.A. Jones : ibid., 1920, 102, p.171.

{13} B.C. Woodfine : ibid., 1953, 173, p.229.

{14} D. McLean and L. Northcott : ibid., 1948, 158, p.169.

{15} B.C. Woodfine : ibid., 1953, 173, p.240.

{16} M. Szczepanski : The Brittleness of Steel, Publ. John Wiley and Sons, 1963, p.325.

{17} M. Baeyertz, W.F. Craig and J.P. Sheehan : Trans. AIMME, 1949, 185, p.535.

{18} M. Baeyertz, W.F. Craig and J.P. Sheehan : ibid., 1950, 188, p.389.

{19} Joint Discussion on Temper Brittleness : JISI, 1953, 174, p.358.

{20} J.B. Cohen, A. Hurlich and M. Jacobson : Trans. ASM, 1947, 39, p.109.

{21} A. Preece and R.D. Carter : JISI, 1953, 173, p.387.

{22} K. Balajiva, R.M. Cook and D.K. Worn : Nature, 1956, 178, p.433.

{23} W. Steven and K. Balajiva : JISI, 1959, 193, p.141.

{24} J.R. Low : Frac. Eng. Mat., ASM, 1964, p.127.

{25} P.L. Gruzin and V.V. Mural : Fiz. Metal. Metalloved., 1963, 16, p.551.

{26} P.L. Gruzin and V.V. Mural : ibid., 1964, 17, p.384.

{27} J.R. Low, D.F. Stein, A.M. Turkalo and R.P. Laforce : Trans. TMS AIME, 1968, 242, p.14.

{28} C.J. McMahon : ASTM STP, 1968, 407, p.127.

{29} R.G.C. Hill, J.W. Martin : Metal Treatment and Drop Forging, August 1962, p.301.

{30} P.A. Restaino, C.J. McMahon : Trans. ASM, 1967, 60, p.699.

{31} H.L. Marcus, P.W. Palmberg : Trans. TMS AIME, 1969, 245, p.1664.

{32} J.R. Low, C.L. Smith : Carnegie-Mellon University, Report No. 031-727-3, 1971, (also Met. Trans. 1974, 5, p.279).

{33} J.R. Low, C.L. Smith and F.W. Verdi : Carnegie-Mellon University, Report No. 031-727-4, 1972.

{34} R. Viswanathan : Met. Trans., 1971, 2, p.809.

{35} M. Guttmann and P. Krahe : Mem. Sci. Rev. Met., 1973, 70, p.657.

{36} P.R. Krahe and M. Guttmann : Scripta Met., 1973, 7, p.387.

{37} M. Guttmann, P.R. Krahe, F. Abel, G. Amsel, M. Bruneaux and C. Cohen : Met. Trans., 1974, 5, p.167.

{38} Ye. E. Glikman and Yu. I. Cherpakov : Fiz. Metal. Metalloved., 1972, 34, p.90.

{39} R. Mulford : Ph.D. Thesis, Univ. of Pennsylvania, October 1974.

{40} B.J. Schulz and C.J. McMahon : ASTM STP, 1972, 499, p.104.

{41} J.R. Rellick and C.J. McMahon : Met. Trans., 1974, 5, p.2439.

{42} C.J. McMahon, E. Furubayashi, H. Ohtani, and H.C. Feng : Acta Met., 1976, 24, p.695.

{43} M. Nageswararao, C.J. McMahon and H. Herman : Met. Trans., 1974, 5, p.1061.

{44} C.J. McMahon : Proc. Fourth Bolton Landing Conference on Grain Boundaries in Engineering Materials (June 1974), Claitors Publ. Divn., Baton Rouge, 1975, p.525.

{45} H. Ohtani, H.C. Feng and C.J. McMahon : Met. Trans. A, 1976, 7A, p.87.

{46} M. Guttmann : Ph.D. Thesis, Univ. of Paris, 1974.

{47} M. Guttmann : Surface Sci., 1975, 53, p.213.

{48} R.L. Rickett and J.M. Hodge : Proc. ASTM, 1951, 51, p.931.

{49} L.J. Klingler, W.J. Barnett, R.P. Frohmberg and A.R. Troiano: Trans. ASM, 1954, 46, p.1557.

{50} J.M. Capus : JISI, 1963, 201, p.53.

{51} B.S. Lement, B.L. Averbach and M. Cohen : Trans. ASM, 1954, 46, p.851.

{52} L.S. Castleman, B.L. Averbach and M. Cohen : ibid., 1952, 44, p.240.

{53} H. Schrader, H.J. Wiester and H. Siepmann : Archiv Eisenhüt., 1950, 21, p.21.

{54} G.R. Speich : Trans. TMS AIME, 1969, 245, p.2553.

{55} G.R. Speich and W.C. Leslie : Met. Trans., 1972, 3, p.1043.

{56} J.M. Capus : Rev. Met., 1959, 56, p.181.

{57} J.M. Capus and G. Mayer : Metallurgia, 1960, 62, p.133.

{58} E.B. Kula and A.A. Anctil : Jnl. of Mats., 1969, 4, p.817.

{59} G.A. Bruggeman and J.A. Roberts : Met. Trans. A, 1975, 7A, p.755.

{60} P.G. Shewmon : Transformations in Metals, Publ. McGraw-Hill Book Co., 1969.

{61} C.J. McMahon, J.R. Rellick and B.J. Schulz : Proc. Int. Conf. on Fracture, 1969, Paper 23, p.278.

{62} G. Krauss and A.R. Marder : Met. Trans., 1971, 2, p.2343.

{63} A.R. Marder, A.O. Benscoter and G. Krauss : ibid., 1970, 1, p.1545.

{64} G.D. Joy and J. Nutting : The Effect of Second Phase Particles on the Mechanical Properties of Steels, ISI, 1972, Paper 12.

{65} I.S. Brammar : JISI, 1963, 201, p.752.

{66} B.J. Schulz and C.J. McMahon : Met. Trans., 1973, 4, p.2485.

{67} A.H. Bodimeade, R.N. O'Brien, D.H. Jack and J. Nutting : Proc. Conf. on the Effects of Inclusions on the Mechanical Properties of Steels, Leeds, 1974, Paper 17.

{68} R.N. O'Brien, D.H. Jack and J. Nutting : Proc. Conf. on Grain Boundaries (Inst. of Metallurgists), Jersey, 1976, p.B16.

{69} E.T. Turkdogan, S. Ignatowicz and J. Pearson : JISI, 1955, 180, p.349.

{70} J.R. Brown : ibid., 1967, 154, p.154.

{71} T.J. Baker and R. Johnson : ibid., 1973, 211, p.783.

{72} J.M. Capus : ibid., 1962, 200, p.922.

{73} V.F. Zackay, E.R. Parker and W.E. Wood : Proc. Third Int. Conf. on Strength of Metals and Alloys, Cambridge, 1973, Vol. 1, p.175.

{74} G.Y. Lai, W.E. Wood, R.A. Clark, V.F. Zackay and E.R. Parker : Met. Trans., 1974, 5, p.1663.

{75} P. Auger : J. Phys. Radium, 1925, 6, p.205.

{76} J.J. Lander : Phys. Rev., 1953, 91, p.1382.

{77} L.A. Harris : J. Appl. Phys., 1968, 39, p.1419.

{78} L.A. Harris : ibid., 1968, 39, p.1428.

{79} P.W. Palmberg, G.K. Bohn and J.C. Tracy : Appl. Phys. Letters, 1969, 15, p.254.

{80} C.C. Chang : Surface Sci., 1971, 25, p.53.

{81} G. Ertl and J. Küppers : Low Energy Electrons and Surface Chemistry (Monograms of Modern Chemistry, V.4), Publ. Verlag Chemie, Germany, 1974.

{82} R.E. Weber and W.T. Peria : J. Appl. Phys., 1967, 38, p.4355.

{83} M.P. Seah : Surface Sci., 1973, 40, p.595.

{84} H.G. Suzuki : M.Sc. Thesis, Univ. of Pennsylvania, 1974.

{85} C.J. Powell : Surface Sci., 1974, 44, p.29.

{86} H.W. King : J. Mater. Sci., 1966, 1, p.79.

{87} M.P. Seah : Surface Sci., 1975, 53, p.168.

{88} M.P. Seah and E.D. Hondros : Proc. R. Soc. Lond., 1973, A335, p.191.

{89} E.D. Hondros : Proc. Interfaces Conf. Melbourne, (Publ. Butterworths London, 1969), p.77.

{90} T. Inoue, K. Yamamoto and S. Sekiguchi : Trans. Iron Steel Inst. Japan, 1974, 14, p.372.

{91} G. Clark, R.O. Ritchie and J.F. Knott : Nature, 1972, 239, p.104.

{92} P.G. Winchell and M. Cohen : Trans. ASM, 1962, 55, p.347.

{93} A.J. McEvily, R.C. Ku and T.L. Johnston : Trans. TMS AIME, 1966, 236, p.108 (and discussion p.1387).

{94} G.S. Ansell and E.M. Breinan : Trans. ASM, 1965, 58, p.110.

{95} V.V. Mural and P.L. Gruzin : Fiz. Metal. Metalloved, 1964, 17, p.792.

{96} R.V. Ramasubramanian and D.F. Stein : Met. Trans., 1973, 4, p.1735.

{97} D. McLean : Grain Boundaries in Metals (Publ. Oxford Univ. Press, London), 1957, p.133.

{98} H. Kaneko, T. Nishizawa, K. Tamaki and A. Tanifuji : J. Japan Inst. Metals, 1965, 29, p.166.

{99} M. Guttmann : Met. Sci., 1976, 10, p.337.

{100} M. Hansen, R.P. Elliott and K. Anderko : Constitution of Binary Alloys (McGraw-Hill, New York) Vol. 3, 1969.

{101} G. Kirchner and B. Uhrenius : Acta Met., 1974, 22, p.523.

{102} British Standards Institute, DD3, 1971.

{103} J.Q. Clayton and J.F. Knott : Met. Sci., 1976, 10, p.63.

{104} J.R. Rice : Third Intnl. Congress on Fracture, Munich, 1973 (Paper I-441), and D.M. Tracey : Ph.D. Thesis, Brown Univ., 1973.

{105} The Mechanical Properties of Nickel Alloy Steels, International Nickel Co. (Mond), 1963, p.30.

{106} R.O. Ritchie, B. Francis and W.L. Server : Met. Trans. A, 1976, 7A, p.831.

{107} Quenching and Martempering, Publ. ASM, 1964.

{108} J. Askill : Tracer Diffusion Data for Metals Alloys and Simple Oxides (IFI/Plenum Data Corporation), 1970, p.47.

{109} J. Crank : The Mathematics of Diffusion (Oxford Univ. Press, 1957), p.31.

{110} D. Gnanamuthu, T.Z. Kattamis, M.C. Flemings and R. Mehrabian : Met. Trans., 1974, 5, p.2557.

{111} N.G. Ainslie, R.E. Hoffman and A.U. Seybolt : Acta Met., 1960, 8, p.523, (2 papers).

{112} D. McLean : Grain Boundaries in Metals (Publ. Oxford Univ. Press, London), 1957, p.118.

{113} M.P. Seah and C. Lea : Phil. Mag., 1975, 31, p.627.

{114} R.A. Mulford, C.J. McMahon, D.P. Pope and H.C. Feng : to be published.

{115} E.A. Guggenheim : Thermodynamics, Publ. North-Holland Co., 1967, p.48.

{116} E.D. Hondros and D. McLean : Monograph No. 28 (Society of Chemical Industry, London), 1968.

{117} C.A. Shell and J.C. Riviere : Surface Sci., 1973, 40, p.149.

{118} J.J. Burton, C.R. Helms and R.S. Polizzotti : Corporate Research Laboratories Report No. CRL.55P.75, 1975.

{119} C. Lea and M.P. Seah : Proc. Interdisciplinary Surface Science Meeting (Inst. of Phys.), Warwick, 1975.

{120} C. Lea and M.P. Seah : Phil. Mag., to be published.

{121} W.C. Leslie : Met. Trans., 1972, 3, p.5.

{122} J.E. King, R.F. Smith and J.F. Knott : Proc. Fourth Int. Conf. Fracture, Waterloo, June 1977.

{123} D.R. Glue, C.H. Jones and H.K.M. Lloyd : Met. Techn., Sept. 1975, p.416.

{124} J.Q. Clayton and J.F. Knott : to be published.